Universität Stuttgart

Institut für Wasser- und Umweltsystemmodellierung

Mitteilungen

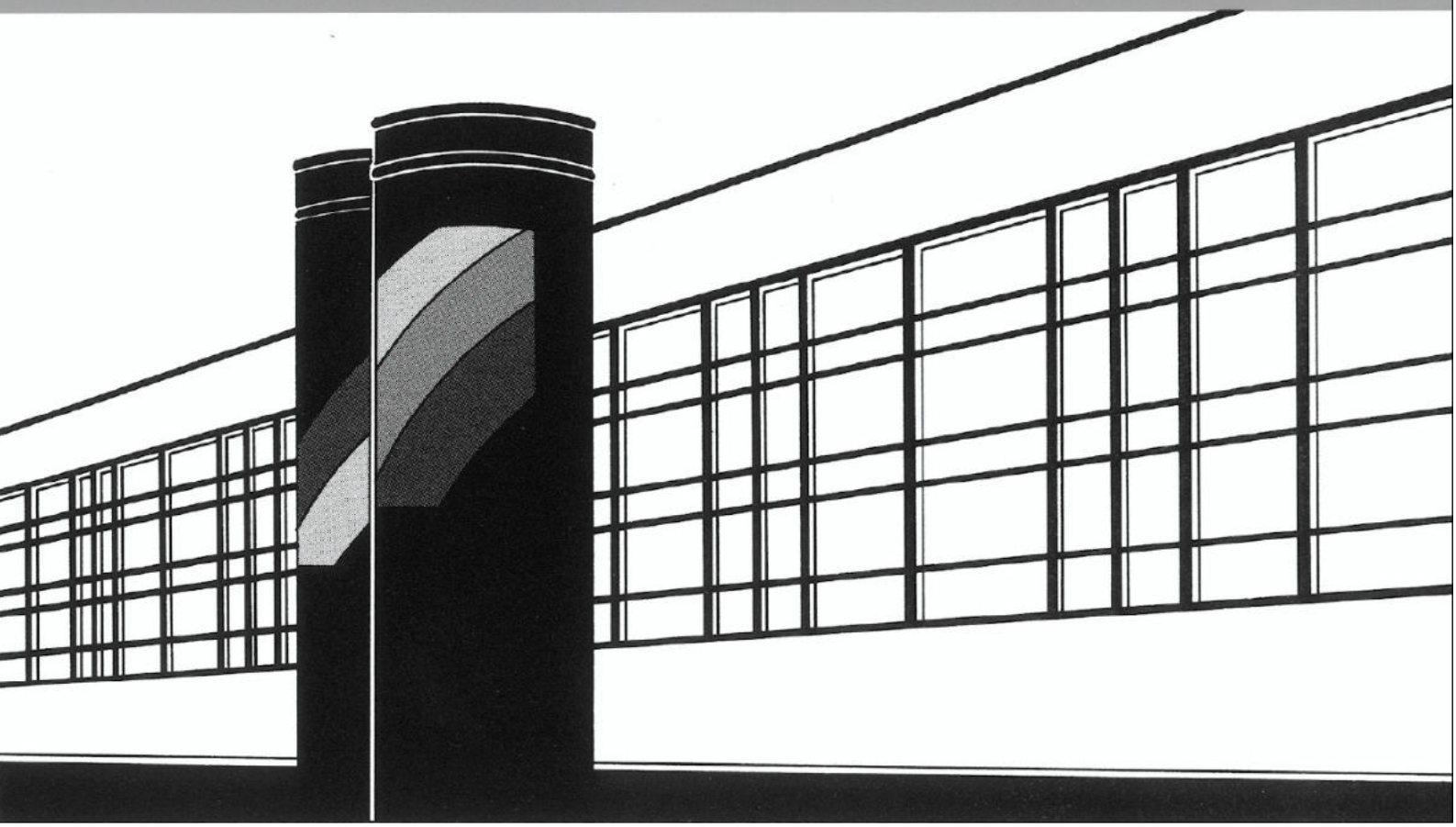

Heft 276 Lydia Seitz

Development of new methods to apply a multi-parameter approach – A first step towards the determination of colmation

Development of new methods to apply a multi-parameter approach – A first step towards the determination of colmation

von der Fakultät Bau- und Umweltingenieurwissenschaften der Universität Stuttgart zur Erlangung der Würde eines Doktor-Ingenieurs (Dr.-Ing.) genehmigte Abhandlung

vorgelegt von

Lydia Seitz

aus St. Georgen, Deutschland

Hauptberichter:	Prof. Dr.-Ing. Silke Wieprecht
Mitberichter:	Prof. Dr.-Ing. Holger Steeb

Tag der mündlichen Prüfung: 29.07.2020

Institut für Wasser- und Umweltsystemmodellierung
der Universität Stuttgart
2020

Heft 276

Development of new methods to apply a multi-parameter approach – A first step towards the determination of colmation

von
Dr.-Ing.
Lydia Seitz

Eigenverlag des Instituts für Wasser- und Umweltsystemmodellierung
der Universität Stuttgart

D93 Development of new methods to apply a multi-parameter approach – A first step towards the determination of colmation

Bibliografische Information der Deutschen Nationalbibliothek
Die Deutsche Nationalbibliothek verzeichnet diese Publikation in der Deutschen Nationalbibliografie; detaillierte bibliografische Daten sind im Internet über http://www.d-nb.de abrufbar

Seitz, Lydia:
Development of new methods to apply a multi-parameter approach – A first step towards the determination of colmation, Universität Stuttgart. - Stuttgart: Institut für Wasser- und Umweltsystemmodellierung, 2020

(Mitteilungen Institut für Wasser- und Umweltsystemmodellierung, Universität Stuttgart: H. 276)
Zugl.: Stuttgart, Univ., Diss., 2020
ISBN 978-3-942036-80-1

NE: Institut für Wasser- und Umweltsystemmodellierung <Stuttgart>: Mitteilungen

Herausgegeben 2020 vom Eigenverlag des Instituts für Wasser- und Umweltsystem-modellierung

Druck: DCC Kästl e.K., Ostfildern

Acknowledgment

First of all, I would like to express my gratitude to my supervisor and examiner Prof. Dr.-Ing. Silke Wieprecht, chair of the Department of Hydraulic Engineering and Water Resources Management of the Institute for Modelling Hydraulic and Environmental Systems (IWS) at the University of Stuttgart for her outstanding supervision and motivating attitude during my time at IWS and during the time I have been working on my dissertation. I would like to thank her for her support and giving me the freedom to realize my own ideas.

Further, a special thank you goes to Prof. Dr.-Ing. Holger Steeb, head of the Institute of Applied Mechanics at the University of Stuttgart as co-supervisor of my thesis. I benefited from numerous discussions particularly coming from another field of interest.

A very warm thank you to Prof. Dr.-Ing. Markus Noack, head of the Department of Hydraulic Engineering and Water Resources Management at the University of Applied Sciences at Karlsruhe for supervising my dissertation and introducing me to the fascinating field of colmation. Without his encouragement, support, and fruitful discussions this thesis would not have been realizable. I greatly enjoyed his company and discussions.

I am also grateful to my colleagues at the Institute for Modelling Hydraulic and Environmental Systems for having a pleasurable time in a friendly atmosphere leading to many fruitful discussions. Especially mentioned are the employees of the Hydraulic Laboratory who greatly supported me during my laboratory experiments and who provided specific field equipment.

There are many student assistants who supported me during field work and laboratory experiments mostly under extremely harsh conditions. I could not have done all of this without your everlasting power of support.

Finally, I want to express my gratitude to my family and especially to my husband Christian for their unconditional support, patience, and encouragement.

Table of content

List of Figures

List of Tables

Abbreviations

The following abbreviations are used in this thesis:

CO_2	Carbon dioxide
CS	Coarse sand
DEM	Digital elevation model
DO	Dissolved oxygen
FS	Fine sand
G	Gravel
HZ	Hyporheic zone
IDOS	Intragravel dissolved oxygen saturatio
IGDO	intragravel dissolved oxygen concentration
K1 – K9	Simple geometric bodies no 1-9
L1 – L5	Layer experiment for the VertiCo method no. 1 - 5
LAWA	Working Group on water issue for the Federal States and the Federal Government (Dt: Bund/Länder Arbeitsgemeinschaft Wasser)
MIB	Macroinvertebrate
O_2	Oxygen
Px	Preliminary experiments no. x
SedSa 1 and SedSa 2	Artificial sediment sample
SF	Shape factor
SfM-MVS	Structure from Motion with Multi View Stereo
UAV	Unmanned airborne vehicles
V1-V3	Version 1 -3 of MODFLOW groundwater model
WFD	EU Water Framework Directive
WL	Water level experiment
WRM	Water replacement method

Notation

The following symbols are used in this thesis:

a	[s/m]	Fochheimer coefficient
b	[s²/m²]	Forchheimer coefficient
C	[-]	Hazen constant factor
CK-C	[-]	Kozeny-Carman empirical coefficient
D	[m]	diameter of pipe
D_{ci}	[mm]	Center of class in φ-units of ith size class
D_m	[mm]	Median grain diameter
D_{max}	[mm]	Maximum grain size
D_x	[mm]	Grain diameter, where x percent is finder
e	[-]	void ratio
f_i	[%]	fraction of sediments in size class i
FI	[-]	Fredle index
$FSA_{<x\ mm}$	[%]	Fine sediment amount below x mm
g	[m/s²]	Acceleration of gravity
H	[m]	Distance from sediment surfarce to top of standpipe
h	[m]	Water level
H_0	[m]	water level at t0
H_1	[m]	water level at t1
h_k	[m]	Colmation depth
i	[-]	Hydraulic gradient
I_0	[mm]	Intersept
k_f	[m/s]	Hydraulic conductivity
k_h	[m/s]	horizontal hydraulic conductivity
k_v	[m/s]	Vertical hydraulic conductivity
L	[m]	length of the pipe within the streambed
L_e	[m]	Length of the well screen
m	[-]	Isotropic transformation ration
m_i	[kg]	Weight of particles retained for ith size class
MQ	[m³/s]	Annual averaged discharge
ms	[kg]	Mass of sediment sample

m_{tot}	[kg]	Total weight of particles per sample
n	[-]	Porosity
n_{SfM}	[-]	Porosity based on SfM method
n_{WRM}	[-]	Porosity based on WEM method
Q	[m³/s]	Discharge
R^2	[-]	Correlation coefficient
r_c	[m]	Inside radius of standpipe
R_e	[m]	Effective radius of well over which head loss is dissipated
Re	[-]	Reynolds number
r_w	[m]	Radial distance between undisturbed aquifer and well center
S_0	[1/cm]	specific surface area per unit volume of particles
SO	[-]	Sorting index
SR	[ml/s]	Slurping rate
T	[°C]	Temperature
v	[m/s]	Velocity
V_{cal}	[ml]	Calculated Volume
v_f	[ml]	Specific flow
V_p	[ml]	Pore volume
V_{se}	[ml]	Volume of sediment
V_{SfM}	[ml]	Volume based on SfM method
V_{tot}	[ml]	Total sample volume
V_{WRM}	[ml]	Volume based on WRM method
X	[m/ml]	Constant factor for slurping rate [m/ml]
y_0	[-]	Normalized displacement time --> 0
y_t	[-]	Normalized displacement time --> t
γ	[-]	unit weight of permanent
Δt	[s]	Time difference
μ	[kg/ms]	Dynamic viscosity of permanent
ν	[m²/s]	Kinematic viscosity
σ_g	[mm]	Geometric standard deviation
φ_i	[-]	characteristic sediment diameter for size class i, expressed on the φ-scale

Abstract

Colmation is defined as the infiltration and deposition of fine sediments into the riverbed, which clogs the pore space and reduces exchange processes of oxygen-rich and nutrient-rich surface water into the hyporheic zone. This negatively affects the reproduction cycle of gravel spawning fish and the habitat quality of aquatic organisms such as macroinvertebrates. Colmation is a naturally occurring process that is enhanced by anthropogenic activities. Over the past decades, numerous studies have focused on this topic, where, among other factors, the main influencing factors have been investigated. However, there are still various knowledge gaps in this field of research. So far, there is no standardized method to determine colmation. Existing methods are based on qualitative and subjective methods, such as mapping of colmation, which result in possible observer bias and whose results are not transferable to other rivers. Quantitative methods, such as the determination of the fine sediment fraction, are based on only a single parameter and cannot adequately describe the complex processes of colmation. The aim of this study is to close knowledge gaps in the field of colmation and especially in the determination of colmation. A multi-parameter approach is developed based on the following four parameters: sediment characteristics, intragravel dissolved oxygen saturation, porosity and hydraulic conductivity. In order to obtain more detailed information about the complex processes of colmation the parameters used in the multi-parameter approach are measured in a vertical profile. This enables the detection and localization of colmation layers in the riverbed. For the determination of the sediment characteristics as well as the intragravel dissolved oxygen saturation, already existing methods are used, which only need to be modified insignificantly. For the determination of porosity and hydraulic conductivity new methods are developed since existing methods are not suitable for measurements in a gravel riverbed. The development and verification of these two methods as well as the tests of applicability of the multi-parameter approach in a field campaign is the focus of this work.

For the determination of porosity, a photogrammetric approach (SfM-MVS) is developed, where a 3D model of a frozen sediment sample is created from 2D images of a sediment sample. After thawing the sample, the sediment volume is determined by applying the water replacement method enabling the determination of porosity. In order to verify the newly developed method, laboratory tests are carried out in which the total volume of simple geometric bodies as well as of different sediment samples is determined and compared with the total volume of sediment samples determined with the commonly used water replacement method. The results show that both methods perform well in determining porosity. The water replacement method leads to a systematic error where the porosities are on average smaller than the porosities determined by the photogrammetric approach. This is due to the melting of the pore water during the procedure and the immersion of the sample in water. The results also show that the photogrammetric approach provides reproducible and accurate results, is inexpensive to implement; since almost no additional equipment is required during the field measurement and the sample remains intact during the image acquisition.

Numerous methods for determining hydraulic conductivity already exist. However, these are only suitable for soils and fine materials such as sand, silt and clay and cannot be applied on

coarse gravel riverbed. Therefore, a robust method for determining hydraulic conductivity is developed, which can be used to measure a vertical profile. Based on the slurping method developed by Terhune (1958), a new method is developed in which vertical profiles of hydraulic conductivity are measured by using a double packer and a perforated standpipe. The measurements result in a slurping rate, which in a further step needs to be converted into hydraulic conductivities. For this purpose, a MODFLOW groundwater model is developed, which estimates the hydraulic conductivity based on the measured slurping rates and considering the respective hydraulic conditions. This model applies the Forchheimer equation, which is used for higher flow velocities, where the Darcy Law is not valid anymore. Various preliminary experiments and laboratory experiments are carried out to test and verify the new method. Sediments with different hydraulic conductivities are used in the laboratory experiments. The results show that the VertiCo method performs well in distinguishing between different materials and is able to detect thin layers with reduced hydraulic conductivity. The simulated hydraulic conductivities agree well to the hydraulic conductivities measured in the laboratory constant head tests. The VertiCo method offers a vertical resolution of 3 cm steps and has the advantage that further parameters, such as intragravel dissolved oxygen saturation or other water related parameters, can be determined. The standpipes can remain in the riverbed enabling long time measurements without disturbing the riverbed periodically. The VertiCo method is an excellent method to determine colmation.

In a further step the developed multi-parameter approach is applied in a field campaign including the newly developed methods. A total of eight rivers is investigated, which differ in hydrological and morphological characteristics. The results show that the multi-parameter approach is robust for gravel riverbeds and can be applied in the field. The obtained vertical profiles of hydraulic conductivity and intragravel dissolved oxygen saturation are evaluated and analyzed with the point measurements of porosity and sediment characteristics. It is shown that in some cases there is a strong correlation between hydraulic conductivity and dissolved oxygen, but this is overlapped by other factors such as biological oxygen consumption or exfiltrating groundwater conditions. The comparison with the other parameters is not quite as clear-cut. However, there is the problem that vertical profiles are compared with depth-integrated data. It is recommended for future research to develop a method to determine porosity and sediment characteristics with a vertical resolution. In summary, the multi-parameter approach is a good method to determine colmation quantitatively and qualitatively.

In order to establish an evaluation for colmation, it is recommended to consider the multi-parameter approach from an ecological point of view. Macroinvertebrate sampling, or the analysis of reproduction condition of gravel spawning fish should be included and measured simultaneously to the multi-parameter approach. Thus, thresholds based on ecological aspects can be derived.

Zusammenfassung

Kolmation beschreibt das Infiltrieren und Absetzen von Feinsedimenten in die Gewässersohle, welche dadurch verstopft und Austauschprozesse von sauerstoffreichem und nährstoffreichem Oberflächenwasser ins hyporheische Interstitial vermindert. Dies hat negative Auswirkungen auf den Reproduktionszyklus von kieslaichenden Fischen sowie auf den Lebensraum von aquatischen Lebewesen wie Makrozoobenthos. Kolmation ist ein natürlicher Prozess, der durch menschliche Eingriffe aus dem Einzugsgebiet verstärkt wird. In den vergangenen Jahrzehnten haben sich zahlreiche Forschungsstudien mit diesem Thema beschäftigt und dabei unter anderem die maßgeblichen Einflussfaktoren untersucht. Trotz intensiver Studien bestehen noch diverse Wissenslücken in diesem Bereich. Bislang gibt kein standardisiertes Verfahren, welches zur Messung von Kolmation angewandt werden kann. Bestehende Methoden basieren größtenteils auf qualitativen und subjektiven Verfahren, wie z. B. Kartierung von Kolmation, welche einen großen Beobachterfehler bergen und deren Ergebnisse nicht auf andere Flüsse übertragbar sind. Quantitative Verfahren, wie z.B. die Bestimmung des Feinsedimentanteils, basieren nur auf einem einzelnen Parameter und können die komplexen Prozesse der Kolmation nur unzureichend beschreiben. Ziel dieser Studie ist es Wissenslücken im Bereich der Kolmation und speziell im Bereich der Bestimmung von Kolmation zu schließen. Es wird ein multi-Parameter Ansatz entwickelt, der auf den folgenden vier Parametern aufbaut: Sedimentcharakteristik, Gelöstsauerstoff im Interstitial, Porosität und hydraulische Leitfähigkeit. Dabei sollen so viele Parameter wie möglich in einem vertikalen Profil gemessen werden. Dies ermöglicht eine genauere Darstellung von Kolmationsprozessen in der Gewässersohle und ermöglicht die genaue Lokalisierung von Kolmationshorizonten. Für die Bestimmung der Sedimentcharakteristik sowie des Gelöstsauerstoffes werden bereits bestehende Verfahren zum Einsatz gebracht, die nur unwesentlich modifiziert werden müssen. Für die Bestimmung der Porosität und der hydraulischen Leitfähigkeit müssen neue Methoden entwickelt werden, da die bestehenden Methoden nicht für Messungen in kiesigen Flüssen geeignet sind, oder da eine zerstörungsfreie Bestimmung nicht möglich ist. Die Entwicklung und Verifizierung dieser beider Methoden sowie die Erprobung des multi-Parameter Ansatzes stellt den Fokus dieser Arbeit dar.

Für die Bestimmung der Porosität wird ein photogrammetrischer Ansatz (SfM-MVS) entwickelt, bei dem ein 3D-Modell einer gefrorenen Sedimentprobe (freeze-core Probe) aus unterschiedlichen Fotos der Probe erstellt wird. Dadurch kann, nach Auftauen der Probe, das Sedimentvolumen mittels Wasserverdrängungsmethode ermittelt und anschließend die Porosität bestimmt werden. Um die neu entwickelte Methode zu verifizieren werden Laborversuche durchgeführt, in denen das Gesamtvolumen von einfachen geometrischen Körpern sowie von verschiedenen Sedimentproben bestimmt wird und mit den Gesamtvolumina von Sedimentproben verglichen wird, die mit der herkömmlichen Wasserverdrängungsmethode bestimmt werden. Die Ergebnisse zeigen, dass beide Methoden genaue Ergebnisse bei der Bestimmung der Porosität ergeben. Die Wasserverdrängungsmethode führt zu einem systematischen Fehler, bei dem die Porositäten durchschnittlich kleiner sind als die Porositäten, die mittels photogrammetrischen Ansatzes bestimmt werden. Dies ist auf das Schmelzen des Porenwassers während der Versuchsdurchführung und das Eintauchen der Probe in Wasser

zurückzuführen. Die Ergebnisse zeigen weiterhin, dass der photogrammetrische Ansatz reproduzierbare und genaue Ergebnisse liefert, kostengünstig umzusetzen ist, da nahezu kein weiteres Equipment während der Feldmessung notwendig ist und die Probe während des Fotografierens intakt bleibt.

Es gibt bereits zahlreiche Methoden zur Bestimmung der hydraulischen Leitfähigkeit. Diese sind allerding für Böden und feine Materialien wie Sand, Schluff und Ton ausgelegt und können in groben kiesigen Gewässersohlen nicht angewandt werden. Aus diesem Grund wird eine robuste Methode zur Bestimmung der hydraulischen Leitfähigkeit entwickelt, mit der ein vertikales Profil gemessen werden kann. Ausgehend der Schlürfmethode von Terhune (1958) wird eine neue Methode entwickelt, bei dem durch die Verwendung eines Doppelpackers und eines perforierten Standrohres vertikale Messungen durchgeführt werden. Die Messungen liefern eine sogenannte Schlürfrate, die in einem weiteren Schritt in hydraulische Leitfähigkeiten umgerechnet werden. Hierfür wird ein MODFLOW Grundwassermodell erstellt, welches die hydraulische Leitfähigkeit unter Berücksichtigung der gemessenen Schlürfrate und den hydraulischen Randbedingungen abschätzt. Dieses Modell wendet die Forchheimer Gleichung an, die bei größeren Fließgeschwindigkeiten zum Einsatz kommt, in Bereichen außerhalb der Darcy Strömung. Mit Hilfe der neu entwickelten Methode können vertikale Profile von hydraulischen Durchlässigkeiten bestimmt werden, weshalb sie im weiteren Verlauf VertiCo genannt wird. Es werden verschiedene Vorstudien und Laborexperimente durchgeführt, um die Methode zu testen und zu verifizieren. Dabei werden Materialien mit verschiedenen hydraulischen Durchlässigkeiten verwendet. Die Ergebnisse zeigen, dass die VertiCo Methode sehr gut geeignet ist, um Materialien mit unterschiedlichen Durchlässigkeiten zu unterscheiden und eingebaute Schichten mit reduzierten Durchlässigkeiten zu detektieren. Die berechneten hydraulischen Durchlässigkeiten passen gut zu den Durchlässigkeiten, die in Säulenversuchen im Labor gemessen wurden. Die VertiCo Methode bietet eine vertikale Auflösung von 3 cm Schritten und hat zudem den Vorteil, dass weitere Parameter, wie z.B. Gelöstsauerstoff im Interstitial oder andere Wasserparameter bestimmt werden können. Die Standrohre können im Gewässerbett verbleiben und bieten die Möglichkeit einer Zeitreihenmessung, ohne vermehrt Störungen in der Gewässersohle hervorrufen zu müssen. Die VertiCo Methode ist eine ausgezeichnete Methode, die zur Bestimmung von Kolmation eingesetzt werden kann.

In einem weiteren Schritt wird der entwickelt multi-Parameter Ansatz mit den neu entwickelten Methoden in Feldeinsätzen erprobt. Es werden insgesamt acht Flüsse beprobt, die unterschiedliche hydrologische und morphologische Charakteristiken aufweisen. Die Ergebnisse zeigen, dass der multi-Parameter Ansatz robust für kiesige Gewässersohlen ist und gut im Feld angewandt werden kann. Die gewonnenen vertikalen Profile von hydraulischer Leitfähigkeit und Gelöstsauerstoff werden mit tiefengemittelten Punktmessungen von Porosität und Sedimentcharakteristik ausgewertet und analysiert. Es zeigt sich, dass teilweise eine starke Korrelation zwischen hydraulischer Leitfähigkeit und Gelöstsauerstoff herrscht, diese wird jedoch durch andere Faktoren wie biologische Sauerstoffzehrung oder wechselnde Grundwasserstände überlappt. Der Vergleich zu den anderen Parametern ist nicht ganz so eindeutig. Hierbei besteht allerdings auch die Problematik, dass vertikale Profile mit Punktmessungen verglichen werden. Zusammenfassend kann man sagen, dass der multi-

Parameter Ansatz eine gute Methode darstellt, um Kolmation quantitative und qualitativ bestimmen zu können. Für weitere Studien wird empfohlen eine Methode zu entwickeln, um Porosität und die Sedimentcharakteristik ebenfalls über die Tiefe aufgelöst darzustellen. Dies ermöglicht eine genauere Betrachtung der Kolmation. Um eine Bewertung in Form von einer Bewertungsskala zu erstellen, wird empfohlen den multi-Parameter Ansatz nicht ausschließlich unter sedimentologischen Gesichtspunkten zu betrachten, da die sich daraus ergebenen Grenzwerte meist willkürlich gewählt sich. Eine gekoppelte Betrachtung unter Berücksichtigung von ökologischen Gesichtspunkten wird empfohlen. Dabei werden neben dem multi-Parameter Ansatz weitere ökologische Daten, wie z.B. Makrozoobenthos Beprobung durchgeführt. Eine weitere Möglichkeit ist es den multi-Parameter Ansatz mit Daten zur Reproduktionsbedingungen von kieslaichenden Fischen in Verbindung zu bringen und dadurch mögliche Grenzwerte abzuleiten.

1. INTRODUCTION

1.1 Motivation

Rivers are dynamically connected to the groundwater and surrounding riparian areas through the hyporheic zone (HZ). This transition zone is characterized by high physical and chemical gradients (Boulton et al. 1998) and it is known for its richness in biodiversity (Tonina and Buffington 2009). Pressure variations along the riverbed as it occurs at riffle/pool sequences are the main driver for hyporheic flow. Bedforms such as riffles interact with the river flow, resulting in a modification of water depth and flow direction. Due to these changes, high-pressure zones are generated upstream of the riffle crest, where in-stream water is driven into the sediment (downwelling conditions, Tonina 2005). A complimentary low-pressure zone occurs on the downstream side of the riffle, due to the shallow water and the higher flow velocities, where water from the sediment re-enters the river flow (upwelling conditions. Tonina 2005). The intense gradients within the HZ are mainly due to differences between these two environments (surface water and groundwater). Surface water is characterized by its currents, turbulent flow, change from daylight and night, oxygen richness, and in general high dynamics regarding sediment and nutrient transport. In contrast, groundwater is characterized by permanent darkness, laminar flow, long water residence time, low oxygen concentration, and low dynamics regarding nutrients transport with only few changes in sediment structure (Boulton et al. 1998).The significance of HZ to river ecology lies in the hyporheic exchange of nutrients and oxygen transport from the surface water into the HZ. Some aquatic organisms are affected directly by surface water – groundwater exchange for example regarding supplying dissolved oxygen and nutrients to hyporheic microbes, macroinvertebrates, and macrophytes, whereas other organisms are affected indirectly such as sustaining fish species with high trophic-level, which feed on hyporheic macroinvertebrates (Boano et al. 2014). Especially the oxygen transport is a key factor for the reproduction cycle of gravel spawning fish where reduced intragravel oxygen content increases mortality in eggs from gravel spawning fish such as salmonids. An essential requirement for oxygen exchange in the HZ is a “clean” riverbed with high hydraulic conductivity. The process of sediment deposition, infiltration and accumulation of fine sediments in gravel riverbeds is defined as colmation and it significantly reduces the exchange processes of dissolved oxygen in interstitial habitats resulting in strong negative impacts on the macro-invertebrates and the reproduction cycle of gravel spawning fish (Jones et al. 2012). A large number of research have been conducted about the highly complex processes of colmation (Schaelchli 1993; Brunke and Gonser 1997; Wharton et al. 2017). However, there is still a lack of understanding. Monitoring and measuring the extend of colmation over spatial and temporal scales improves the understanding of such complex processes, enabling the development of solutions to reduce or even prevent colmation effects or develop measures for enhancing natural occurring decolmation (remobilization of fine sediments during high flow events). So far, there is no parameter to describe colmation qualitatively or quantitatively. The existing methods to determine colmation are commonly based on the analysis of fine sediment content or on hydraulic conductivity. However, these single-parameter approaches fail to assess the complexity of colmation, which illustrates the

need for a new method. Following this motivation, the thesis intends to develop a new methods to determine colmation in rivers based on a multi-parameter approach.

1.2 Objectives

A multi-parameter approach is developed in this study in order to reduce the lack of knowledge regarding colmation. This is a first step towards an innovative approach to determine infiltration processes in the hyporheic zone. To address the challenging goal of this thesis new methods are demanded in order to measure the describing parameter of colmation in a vertical profile. The vertical profile is required to evaluate the complex processes of colmation and further to detect the location of colmation within the riverbed.

The following objectives can be formulated to achieve the challenging goals of this study:

1. Development of a new approach to determine porosity of riverbed sediment

Existing methods for determining porosity of frozen sediment samples such as the water replacement method (WRM) determines the total volume of the frozen samples and thus require additional material, which needs to be brought to the field. During measurement the samples start to melt which leads to partial destruction of the samples, especially of the grain structure. A new method is required which leaves the sample non-destructive. A photogrammetric approach called Structure from Motion with Multi-View Stereo (SfM-MVS) is presented in this thesis to determine the total volume of a frozen sediment samples based on the generation of 3D models using 2D images. In order to investigate the capability of SfM-MVS for porosity measurements, different assessments and laboratory experiments are conducted:

a) Preliminary study: determination of the accuracy of volume measurements for simple geometric bodies with known geometry.

b) Identification of the overall accuracy of porosity measurements for various homogeneous sediments, artificial mixed sediments, and natural sediment samples.

c) Comparison of the measured porosity values based on SfM-MVS with porosity values calculated from mathematical predictors in literature and evaluation of the general performance of mathematical predictors.

The volumes and porosities obtained in a) and b) are also compared to the most commonly applied WRM.

2. Development of a new method to determine hydraulic conductivity of gravel riverbed in a vertical profile

Many different techniques exist to determine the hydraulic conductivity of soils and riverbeds. However, due to coarse material and high hydraulic conductivities in gravel riverbeds, these methods are not practicable in these rivers. Further, a high resolution is required to investigate colmation. This requires the measurement of a vertical profile, which provides high spatial

resolution and thus can detect possible colmation horizons. In this thesis a new approach to determine **vert**ical profile of hydraulic **co**nductivity (VertiCo) is presented. In this approach the newly developed VertiCo method is used to determine slurping rates and later transfer them into hydraulic conductivities by using a numerical MODFLOW groundwater model. Different laboratory experiments are required to assess the applicability and accuracy of the VertiCo method and the used groundwater model:

a) Preliminary experiments: Assessment of reproducibility and the capability to differentiate between sediment characteristics.

b) Laboratory experiments: i) Investigation of varying hydraulic heads on slurping rate by varying water level and sediment depth. ii) Assessment of a relation between slurping rate and hydraulic conductivity of different sediment mixtures. iii) Capability of detecting layer with lower hydraulic conductivity

The hydraulic conductivities obtained from the groundwater model are further compared to hydraulic conductivities from laboratory experiments, which are determined with the commonly used constant head tests.

3. Develop and apply multi-parameter approach in the field

The outcomes from first and second objective are transferred into a multi-parameter approach. A measuring procedure is set-up for the four parameters *porosity*, *hydraulic conductivity*, *intragravel dissolved oxygen saturation* and *grain size characteristics*. The approach is tested in the field in different rivers with varying hydraulic and sedimentological conditions. The gathered data sets from the field measurements are assessed regarding the relations between the four parameters and the capability of determining colmation. The overall applicability of the multi-parameter approach is further discussed.

1.3 Structure of work

This section outlines the structure of the thesis in order to provide an understanding of the workflow and the different topics within this thesis. The thesis consists of eight chapters. The motivation and objectives are given in the first chapter. The second chapter summarizes the basic information about colmation, the physical processes of colmation and basics about the four parameters used in the multi-parameter approach to describe colmation. General measuring methods for determining these four parameters are presented in the third chapter. In the fourth chapter the applied methods for measurement of intragravel dissolved oxygen saturation and grain size analysis as well as the method description and the laboratory experiments for the two newly developed methods for *porosity determination based on a photogrammetric approach* and the *determination of hydraulic conductivity using the VertiCo method* are explained in detail followed by the measuring procedure for the application of the multi-parameter approach in the field. The results and discussions are covered from chapter five to chapter seven. In chapter five the results from the laboratory experiments of the porosity determination as well as the corresponding discussion is presented. The results from the laboratory experiments from the

VertiCo method followed by the discussion and the comparison to the simulated results of the ground water model are presented in the sixth chapter. The seventh chapter presents the results from the application of the multi-parameter approach in the field and a detailed analysis and discussion of the data obtained in the field. This thesis is finalized in the eighth chapter with an overall conclusion of the multi-parameter approach especially, the two newly developed methods and the capability to determine colmation are discussed. Further, future research is discussed in this chapter.

2. LITERATURE REVIEW - BASICS

2.1 Ecological aspects

2.1.1 Life cycle of gravel spawning fish

Sediment of riverbeds and the amount of fine sediments have a high ecological impact on aquatic life (see chapter 2.2.3). Especially anadromous salmonids like Atlantic salmon (*Salmo salar*) and brown trout (*salmo trutta*) as well as indigenous rheophil gravel spawning fish such as barbel (*Barbus barbus*) and grayling (*Thymallus thymallus*) are affected from sediment quality in different life stages. Since these fish have narrow habitat requirements in their juvenile riverine freshwater habitats (Schiemer et al. 2003) they can also be considered as ecological indicator. These habitat requirements are not fix; they change according to each life stage. In order to demonstrate the importance of sediment quality to the single life stages the life-cycle and its corresponding habitat requirements of Atlantic salmon and brown trout is briefly explained in the following section (Figure 2.1). Atlantic salmon and brown trout is chosen over barbel and grayling since a lot of information can be found in literature (Crisp and Carling 1989; Crisp 1993; Kondolf and Wolman 1993; Crisp 1996; Armstrong et al. 2003; Jonsson and Jonsson 2011). However, barbel and grayling also have high habitat requirements, especially in the juvenile development.

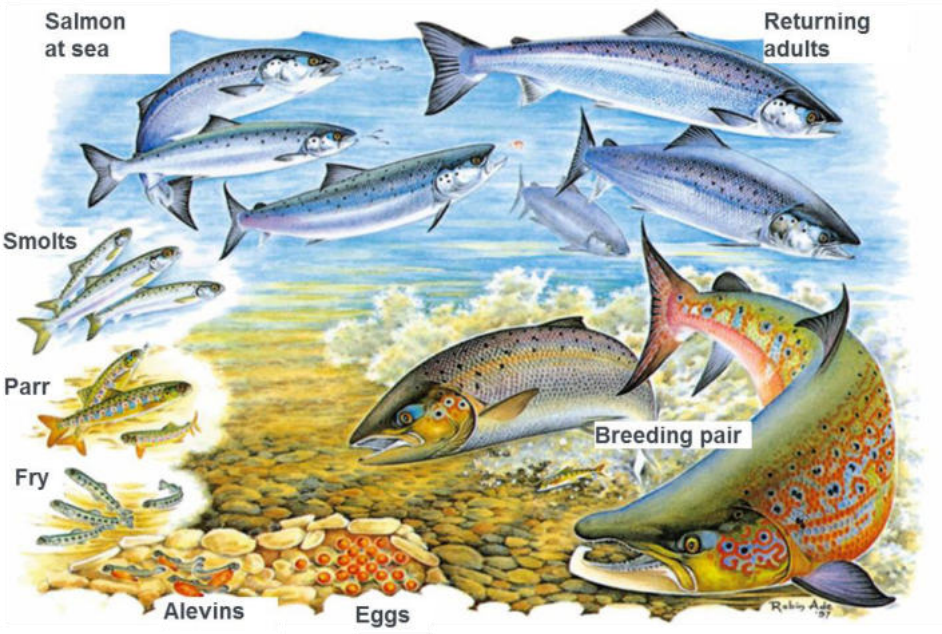

Figure 2.1: Life cycle of Atlantic salmon (salmo salar) (modified from (NASCO 2018).

The life cycle of Atlantic salmon is shown exemplary in Figure 2.1. Spawning time for Atlantic salmon and brown trout is in autumn or winter (Jonsson and Jonsson 2011) whereas trout tend to spawn earlier compared to salmon and move further to small headwaters (Armstrong et al. 2003).

Females dig one or more egg pockets forming a redd (Armstrong et al. 2003) and construct commonly one redd per season even though she may construct more than one redd (Crisp and Carling 1989). Typical spawning grounds can be found at positions with high hydraulic gradients to ensure sufficient interstitial flow for the incubation period (Gibson 1993; Crisp 1996; Kondolf 2000). Groundwater seepage rate and direction, hyporheic flow and oxygen concentration seems to be common indicators for female site selection. These areas can be found e.g. at the tails of pools. After a suitable redd site is selected, female fish beat the gravel with their body and tail for excavating the nests. Larger fish can move coarser particles, which can reach up to 10 % of their body length (Kondolf and Wolman 1993).For digging the nests they turn on one of their sides and beat the gravel with rapid movements of their body and tail (Jonsson and Jonsson 2011). This causes a depression, commonly called pit where the eggs finally will be deposited (Crisp and Carling 1989; Jonsson and Jonsson 2011). The female salmons releases 1600-1800 large eggs per kg fish which is a rather small amount of eggs compared to other fish species (Armstrong et al. 2003). The eggs will be covered with sediment subsequent the fertilization. The procedure of egg deposition and coverage of the eggs can be repeated on one redd for several times. During the embryonic development a high concentration of dissolved oxygen is needed to supply the embryos with sufficient amount of oxygen since the transfer from oxygen into the eggs is achieved with diffusion. This is only guaranteed with a large hydraulic conductivity and thus a sufficient interstitial flow. Embryos are attached to a yolk sac which guarantees the internal feeding.

They hatch in spring time after embryonic development happen during winter. Young fish which are still attached to the yolk sac are called alevins. The incubation time depends mainly on the water temperature but can be influenced by environmental stresses like low oxygen levels and mechanical disturbance (Hayes 1949; Jonsson and Jonsson 2011). Approximately the first month after hatching, alevins stay in the gravel until the yolk is almost consumed and they switch to external feeding. This phase is also influenced by the temperature where a decrease in water temperature increases the alevin stage (Jonsson and Jonsson 2011). Here, a high hydraulic conductivity is required for transportation of dissolved oxygen into the sediments and transportation of metabolic waste out of the sediment. The alevins emerge upwards from the gravel substratum into the open water column. However, most of their time is spend in the gravel in order to hide from predators, just leaving the shelter for feeding. Large pores are required first to enable upward migration and second to serve as shelter (Jonsson and Jonsson 2011).

Starting to feed tiny water organisms fry live in the first summer. In this time, they use large pores as shelters to hide from predators and to protect from high flows. After the first summer young fish are called parr as long as they live in freshwater before migrating to the sea. This phase lasts for 0 – eight years depending on water temperature and food availability. They can inhabit still and running waters and feed mostly from drifting insects' larvae, molluscs and crustaceans (Jonsson and Jonsson 2011).

Smoltification starts at a body length of approximately 15 cm and salmon smolts migrate during springtime into the sea. This is the first life stage where sediment quality, pore size and pore

availability become minor important. After one to four sea winters adult Atlantic salmon return to their home rivers for spawning. In contrast to Atlantic salmon, anadromous brown trout often return to their home river in the same year either for spawning or as immature fish for wintering (Jonsson and Jonsson 2011). Unlike to the Pacific salmon both Atlantic salmon and brown trout survive upstream migration and reproduction and can spawn again. Atlantic salmon commonly spawns every two years whereas brown trout commonly spawns every year (Jonsson and Jonsson 2009).

Especially the young life stages which ensure species survival depends on sediment quality and flow characteristics. The number of returning fish for spawning is strongly related to survival in the early life stages. Beside mortality of smolts in the sea from predators or parasitic infestation, the riverine habitat quality such as open pore space and a sufficient interstitial flow are crucial factors for the survival of anadromous salmonids. Both parameters, pore space and interstitial flow significantly influence the oxygen exchange into the hyporheic zone. Limiting oxygen transport leads to an increased mortality rate during the reproduction phase.

2.1.2 Oxygen consumption of different life stages and critical thresholds

The previous chapter (2.1.1) showed that the availability of oxygen within the gravel bed has been identified (amongst others) as an important factor limiting the survival of salmonid embryos (Greig et al. 2007). The oxygen consumption is not constant over time, but changes with development stage and physical activity (Lindroth 1942; Rombough 1988; Greig et al. 2007). In general a constant increase of oxygen consumption prior to hatching can be observed with increasing development time (see part (a) in Figure 2.2; Lindroth 1942; Crisp 1981; Rombough 1988; Greig et al. 2007). Greig et al. (2007) further observed a first peak of oxygen consumption directly after fertilization which is caused by proliferation of the blastodisc. A second peak occurs at hatching (part (b) in Figure 2.2) followed by a sudden decrease of oxygen consumption (part (c) in Figure 2.2). However, the general oxygen consumption after hatching is higher compared to the egg stage since metabolic activity is also higher (Greig et al. 2007). The peak during hatching can be explained be the exertion of breaking free from the egg (Greig et al. 2007). Rombough (1988) reports oxygen consumption after fertilization of less than 1 mg/l, 7.5 – 9.7 mg/l for hatching and a decline to finally 2.3 – 4.8mg/l. Based on the data from Figure 2.2 hatching is the most sensitive stage for survival.

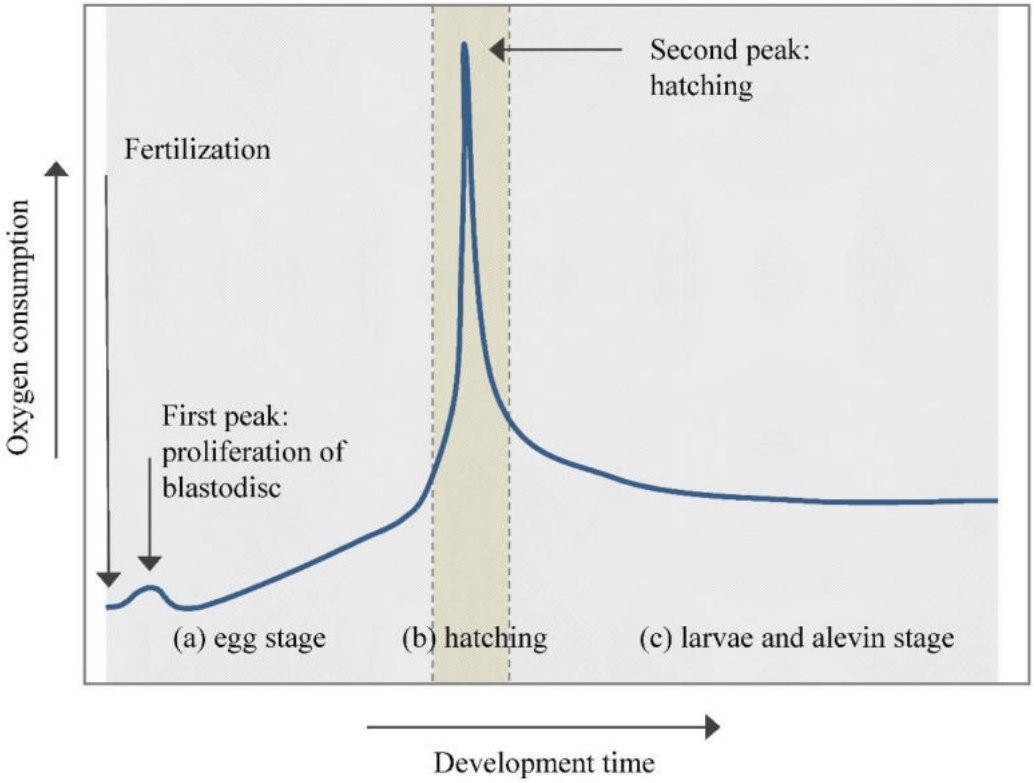

Figure 2.2: Oxygen consumption for gravel spawning fish for different life stage: (a) egg stage – fertilization to hatch (b) hatching (c) hatching to larvae stage (modified from Lindroth 1942, Hayes et al. 1951 and Greig et al. 2007).

Oxygen consumption and thresholds

The intragravel dissolved oxygen concentration (IGDO) is controlled by the oxygen content of the surface water and the ground water, respectively. Oxygen is transferred into the water by mixing due to turbulences. Most rivers have an oxygen concentration close to saturation (depending on temperature, Cardenas et al. 2016). Oxygen consumption in the riverbed can be composed of different driving forces. The main part is the biological oxygen demand (BOD). Micro-organisms use organic material as energy source which consumes oxygen in a carbon oxidation process. And this process is in direct competition with oxygen supply for reproduction process.

Surface oxygen concentration is highly depending on the temperature, light conditions, turbulences which leads to mixing of water and fresh air. Thus, oxygen concentration of the surface water and the residence time of water in the hyporheic interstitial affect the concentration of IGDO.

An insufficient amount of IGDO can have negative effects on embryonic development of gravel spawning fish and other life stage of salmonids. Greig et al. (2005) for example reports decreasing embryonic O_2 consumption with the addition of clay to the water and the resulting thin film of sediment across the egg surface. Egg consumption was reduced on 41 % (on

average) for the addition of 0.3 g of clay and to a reduction of 96 % for the 0.5 g addition compared to the sediment free condition. The clay reduces O_2 availability and restricting O_2 consumption by incubating embryos. Furthermore, clay blocks the pore space of the egg, restricting the transport of O_2 across the eggs chorion (Greig et al. 2005). Rubin and Glimsater (1996) found in their study that IGDO was the major parameter which influenced the egg-to-fry survival up to hatching for sea trout.

Information about egg-to-fry survival in natural redds are scarce since the number of salmonid eggs deposited in the reeds are not exactly known (Ingendahl 2001). However, many studies have been conducted to investigate the effect of varying oxygen concentrations on the egg-to-fry survival in artificial reeds either in laboratory studies or in field experiments. Different thresholds can be found in literature, which describes the embryonic survival or the mortality rate according to a certain O_2 concentration as summarized in Table 2.1. The summary shows that the thresholds differ widely between species. Rubin and Glimsater (1996) explain possible discrepancy between species with variations in egg size, degree of carotenoid pigmentations, importance of the network of capillaries covering the yolk sac and spawning habitat. Furthermore, they found that lethal values obtained from laboratory studies are generally lower compared to values obtained from experiments in rivers.

Table 2.1: Thresholds for survival of salmonids eggs based on literature.

Reference	Species	Experimental principle	Concentration	Comments
Greig et al. (2005)	Atlantic salmon *Salmo salar*	Nature	2-7 mg/l	Considered as critical for embryonic survival
Ingendahl (2001)	Sea trout	Nature	7 mg/l	Critical threshold for egg-to-fry survival
Crisp (1996)	*Oncorhynchus mykiss* *Oncorhynchus nerka*	Based on literature data	> 7mg/l	General threshold to allow a high rate of egg survival
Gibson (1993)	-	-	> 5 mg/l	General threshold during incubation
Rubin and Glimsater (1996)	Sea trout *Salmo trutta L.*	Nature	10 mg/l 10 mg 10 mg/l/l	Lethal limit for eyed stage of sea trout *Salmo trutta* L. Threshold for survival to hatching Threshold for survival to emergence
Phillips and Campell (1962)*	Coho salmon	Nature	8 mg/l	Lethal concentration
Phillips and Campell (1962)*	Steelhead trout	Nature	7 mg/l	Lethal concentration
Smirnov (1975)*	Pink salmon *O. gorbuscha*	Nature	3 – 4 mg/l	50 % of mortality
Scrivener (1988)*	Chum salmon	Nature	4.6 mg/l	Lethal concentration
Heywood and Walling (2007)		Nature	4- 5 mg/l	76-100 % of mortality

* In Rubin and Glimsater (1996)

2.2 Colmation

Colmation is one of the main threads for the reproduction of gravel spawning fish. In order to develop solutions to reduce or prevent colmation, a deep understanding of the complex relationship of colmation is required. The following chapter introduces the basics of colmation, the physics of the process, existing assessment methods as well as impact of colmation.

Fine sediments are naturally occurring in rivers and are part of natural substratum composition. A lot of influencing factors lead to varying types and amount of fines. The amount of fine particles naturally increases with the length of the river. Upper reaches usually contain less fines

since it will be transported downstream whereas lower reaches contain more fines. Due to the reduced slope at downstream reaches fine sediments tend to accumulate in these regions and will not be transported further (Thurmann and Zumbroich 2013). Fine sediments in general have no negative effects on the aquatic environment. However, increased amount of fines its deposition into the hyporheic interstitial and the alteration in the natural flow regime due to anthropogenic activities can lead to negative environmental effects.

2.2.1 Basics about colmation

Colmation is defined as a process in which suspended solids infiltrate and deposit in the riverbed and clog the pore space leading to a reduction of pore volume, consolidation of porous medium and a reduction of hydraulic conductivity (Beyer and Banscher 1975; Banscher 1976; Cunningham et al. 1987; Schaelchli 1993).

Terms like embeddedness, siltation and clogging of a riverbed can also be found synonymously in literature (e.g. Sylte and Fischenich 2002). Some of these terms do have slightly different definitions such as embeddedness which is described the degree to which a big particle is surrounded (embedded) by small particles (Bunte and Abt 2001). The term embeddedness refers mostly to fisheries biologists to quantify the abundance of fine sediment in a streambed (Bunte and Abt 2001). In this study the term colmation will be used according to the definition mentioned above.
Suspended solids can deposit on the riverbed due to low flow conditions and form a sealing layer on top of the riverbed (gravitational settling). The deposit is referred to as outer colmation (Banscher 1976; Schaelchli 1993). In this case the underlying pore space is not clogged. Due to a hydraulic gradient or turbulence flow conditions, suspended solids can infiltrate into the riverbed and settle in the hyporheic interstitial (transport based on interstitial flow). This is called inner colmation resulting in the formation of a colmation horizon. Biological colmation results due to the colonization of organism or due to deposition of organic material (Schaelchli 1993). According to (Banscher 1976) especially diatom can build a high filter resistance. Biological colmation is of greater concern in eutrophicated rivers where less sediment transport occurs.

Pertaining to the aim of this study, outer and biological colmation will not be taken into consideration. In the following chapters the term colmation only refers to inner colmation.

Cause of colmation

Colmation is caused by fine sediments, which infiltrate the river from the surrounding catchment and which are eroded and transported from the upstream river section. Colmation is a naturally occurring process which can be enhanced from anthropogenic activities such as intensified agricultural land use, construction and deforestation (Frostick et al. 1984; Owens et al. 2005). Owens (2005) reports that the changes in bed sediment quality was often associated with a change in land use. Land use changes and agricultural activities alter the riverbed quality on the long term whereas construction and deforestation can lead to only short-term effects.

Another substantial anthropogenic activity belongs to dam operations including discharge regulation and artificial sediment flushing. These activities change the natural dynamical flow regime leading to a lack of peak flows and natural bed alteration preventing flushing of fine sediments from the riverbed and thus resulting in a non-natural accumulation of fine sediments (Kondolf et al. 2014).

Structure of riverbeds

Schaelchli (1993) describes three different layers of a riverbed which develop during the process of colmation (Figure 2.3). The first layer is the armour layer, which develops on top of the riverbed. The armour layer is characterized by coarse material which is resistant against high flow conditions. Fine particles in this layer are already washed out. The filter layer and finally the subsurface layer follow the armour layer. In case of no colmation the filter layer corresponds to the subsurface layer. Fine sediments flow through the armour layer and infiltrate into the filter layer where they preferable deposit. The boundary between armour layer and filter layer acts as interface between coarse substrate and fine substrate and form a thin colmation layer. The filter layer is characterized by a lower porosity and lower hydraulic conductivity compared to the subsurface layer. In case of very fine sediments as suspended load and a coarse filter layer, fine sediments might infiltrate into the subsurface layer.

Schaelchli (1993) observed a locally occurring phenomenon in which a fourth layer, called skeleton, develops. This layer develops below the armour layer and is as coarse as the armour layer. Due to the turbulences in this layer, no deposition takes place and it can be seen as an extension from the armour layer.

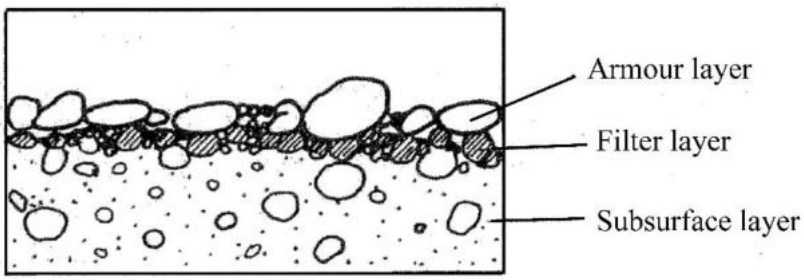

Figure 2.3: Structure of riverbed including armour layer, filter layer and subsurface layer (Schaelchli 1993).

Colmation process – temporal and spatial scales

The process of colmation can be separated into three temporal phases (Schaelchli 1993). Figure 2.4a shows an initial clean gravel riverbed without colmation. In the first phase bigger particles such as sand is the dominating particle size by bridging or depositing into big pores and dead ends (Figure 2.4b) (Schaelchli 1993; S. Gibson et al. 2009; 2010). In this phase smaller particles do not play an important role since they are not filtered and infiltrate deeper into the riverbed. The bridging and depositing process takes place in the upper part of the filter and the armour

layer. It may reduce the porosity significantly; however, the hydraulic conductivity is not strongly influenced. In the second phase median coarse particles play the dominant role clogging the fine pores by sieve-infiltration and interception (Figure 2.4c). In this phase the hydraulic conductivity reduces markedly. In the third phase the finest fractions play the dominant role since coarse and medium particles are prevented from infiltrating deeper into the interstitial space. In this phase the hydraulic conductivity reduces markedly. In the third phase the finest fractions play the dominant role since coarse and medium particles cannot infiltrate any more. Pores are fully clogged and filter velocity further decreases, which in turn prevent other fine particles from infiltrating into the filter layer (Frostick and Reid 1984; Lisle 1989; Schaelchli 1993; Cui et al. 2009). Quasi steady conditions are reached until increase discharge washes out fine particles and initiates bed load transport.

These phases are dependent on the availability of the three particle classes. In case of low flow conditions or the lack of sand, the first phase can be omitted, and fine sediments can infiltrate deeper into the riverbed.

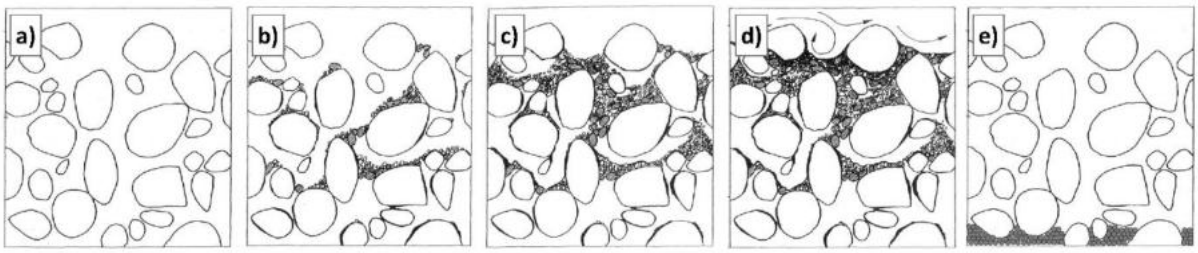

Figure 2.4: Developing infiltration and accumulation processes of fine sediments into gravel structure. a) no colmation: initial state; b) first phase: bridging process with coarse particles; c) second phase: clogging of pore space with finer material; d) third phase: complete colmation.; e) unimpeded static percolation (modified from Schaelchli (1993)

Colmation processes occur heterogeneously in the riverbed since fine sediments are delivered preferentially as suspended load and through the hyporheic interstitial (Boano et al. 2014). Heterogeneities in colmation processes can also reach different scales of bed forms since the deposited fine sediments produce distinct patterns and suspended fine particles tent to follow pore water flow paths. In a longitudinal scale, pool and riffle sequences are characterized by different interstitial flow directions and have therefore different conditions of clogging. At the end of a pool for example (position A in Figure 2.5) infiltrating conditions enhance colmation due to increased interstitial flow. Contrasting to this, colmation is prevented at a riffle sequence (position B in Figure 2.5) due to exfiltration conditions. Colmation processes also follow a temporal variance since it might increase over time and create new flow paths based on formerly clogged paths on one hand. On the other hand colmation might change due to changing discharge conditions and bed load movements (Schaelchli 1993; Brunke and Gonser 1997). High discharges can alter the riverbed and reverse colmation effects by flushing out fine sediments. During a decolmation experiment of Blaschke et al. (2002), a formation of a new colmation layer within short time is observed. The formation is explained by the high discharge of the river and the theory was established that high discharge enhances colmation processes. This is also supported by the study of Frostick et al. (1984).

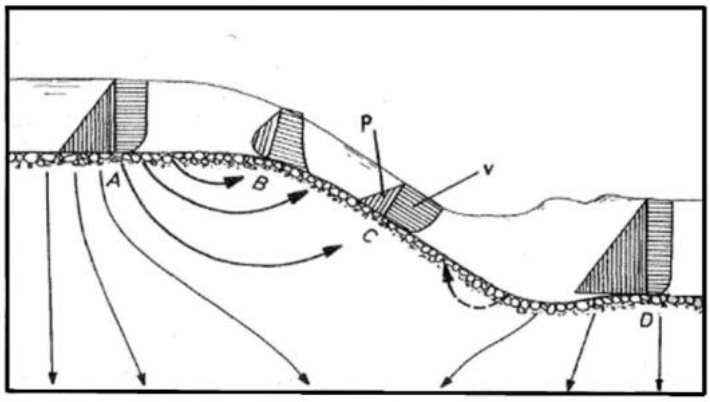

Figure 2.5: Vertical pressure and velocity distribution in a riffle-pool sequence including interstitial flow path in the riverbed (Schaelchli 1993).

Theory of infiltration depth

Einstein (1968) observes unimpeded static percolation in his laboratory experiments where the fine sediments filled the gravel bed flume from the bottom up (Figure 2.4e). This phenomenon is also observed from Diplas und Parker (1992) and Lunt und Bridge (2007). However, this phenomenon is unlikely in natural systems (Diplas and Parker 1992) since the fine sediments need to be much smaller compared to the riverbed sediment (Bunte and Abt 2001). Gibson et al. (2009, 2010) establishes a threshold to differentiate between unimpeded static percolation and the formation of a bridging layer close to the surface. The threshold is given with the $d_{15-gravel}/d_{85-sand}$ ratio of 12 to 14 where an exceeding of the threshold leads to a bottom up filling of the gravel bed. Ratios below the threshold lead to a near surface colmation layer.

According to Schaelchli (1993) colmation forms a small horizon where the depth can be estimated based on the grain size distribution (Schaelchli 1993; Blaschke et al. 2002; 2003). Based on observations from laboratory experiments from Schaelchli (1993), Blaschke et al. (2002, 2003) and, Gibson et al. (2009), the colmation depth h_k [m] can be estimated based on the certain grain size diameter such as the median grain size d_m [m]. Table 2.2 summarizes equations found in literature to estimate colmation depth based on the grain size. Most approaches only consider the grain size of the riverbed material. However, Gibson et al. (2009) found that the infiltration depth also highly depends on the grain size of the intruding material where finer sediments are introduced deeper in the riverbed.

Table 2.2: Summary of colmation depths found in literature

Colmation depth	No. of equation	Reference
$h_k = 3d_m + 0.01$	(2.1)	Schaelchli (1993)
$h_k = 2.5 - 5d_{90}$	(2.2)	Beschta and Jackson (1979)
$h_k = 3d_{90}$	(2.3)	(Diplas 1986)
$h_k = 2.6d_{90}$	(2.4)	Lisle (1989)

Influencing parameter

Different studies are found in literature evaluating the influencing parameters of colmation (Schaelchli 1993; Rehg et al. 2005; Fries and Taghon 2010; Gibson et al. 2009). Since some of the studies are conducted in the laboratory (Beyer and Banscher 1975; Banscher 1976; Schaelchli 1993), where also boundary conditions vary from each other and some are based on field investigations (Frostick et al. 1984) the observations vary widely from each other.

Generally, colmation is influenced by a variety of temporal and spatial varying factors (Schaelchli 1993) which are controlled by larger scale patterns (Boano et al. 2014). Most of the influencing factors interact with each other and influence colmation and can only be described qualitatively.

The following factors can influence colmation, however, the extent to which these factors influence colmation are not yet investigated for all factors.

- Hydraulic factors: shear stress representing flow conditions, turbulences, hydraulic gradient (amount and direction), suspended load and grain size distribution of suspended load (sink velocity) (Beyer and Banscher 1975; Banscher 1976; Schaelchli 1993; Brunke and Gonser 1997).
- Morphological factors: Riffle / pool sequences; hiding / exposure
- Geohydraulic factors: filter conditions and filter velocity represented by the grain size distribution of the gravel bed, pore geometry and hydraulic conductivity (Beyer and Banscher 1975).
- Biological factors: eutrophication, light conditions, temperature (Beyer and Banscher 1975), development of a biological layer with adhesive capacities (Brunke and Gonser 1997).

Bed load transport is observed to prevent colmation since fine sediments are not able to infiltrate into the riverbed (Rehg et al. 2005). With increasing bed shear stress infiltrating fine sediments is reduced (Gibson et al. 2009).

2.2.2 Assessment of colmation

Colmation is a highly complex process which cannot be explained by a simple calculation approach. Nevertheless, several studies can be found in literature, which assess colmation or infiltration processes in different ways (Schaelchli 1992; Beschta and Jackson 1978; Packman et al. 2004; Frostick, and Reid 1984). In general, it can be distinguished between laboratory experiments, investigations in rivers (field measurements/experiments) and mathematical models. Laboratory experiments can simplify complex systems such as infiltration processes for example by using uniform material as bed material and as infiltrating material. Different parameters can be varied in the laboratory to focus on specific results. However, these results cannot be directly compared and transferred to outcomes of field experiments where natural systems are investigated. A wide range of studies have been published recently that present mathematical models to assess or predict colmation (Brunke 1999; Ren and Packman 2004; Cui et al. 2009; Fox 2016). In the following section different experimental methods for determination colmation in the field are introduced. Their advantages and disadvantages are further discussed. Laboratory experiments and mathematical models will not be discussed further here since these topics are beyond the scope of this study.

Field based experimental methods

There is a high variety of different parameter or methods to assess colmation (Seitz et al. 2019). An online survey about colmation is conducted where people who are working with colmation regularly are asked about general knowledge of colmation. One of the questions is “Which methods are suitable to assess colmation?”. In total 35 different methods are given in this survey which shows that there is no universal method for assessing colmation (Seitz et al. 2019, Lenz 2018). Most of the named methods are related to sediment sampling, sediment traps, visual methods such as mapping, measurements of hydraulic conductivity or tracer tests. Some mentioned methods are more indirect measurements such as the egg-to-fry survival of salmonids or the concentration of dissolved oxygen in the hyporheic zone. Table 2.3 gives a brief overview of the most common experimental methods, which are also explained in the following section. The methods are distinguished into qualitative and quantitative methods.

Table 2.3: Summary of methods to assess colmation.

Method	Parameter	Reference
Qualitative methods		
Visual mapping	Visible amount of fine particles; visible pore space, degree of pore clogging	Schaelchli (2002); Descloux et al. (2010a); Platts et al. (1983)
Kick tests (Dt: Stiefelprobe)	Assessment of penetration resistance (bar or boots) and observation of sediment plume	Schaelchli (2002); Thurmann and Zumbroich (2013)
Wooden sticks	Assessment of oxygenated conditions using wooden sticks	Marmonier et al. (2004)
Shelter availability	Measurement of shelter depth using small rubber tubes	Finstad et al. (2007)
Quantitative methods		
Sediment samples using freeze-core or freeze-panel technique	Analysis of grain size distribution and amount of fine sediments	Bunte and Abt (2001)
Sediment traps and sediment buckets	Analysis of infiltrating sediments in a certain time interval.	Frostick et al. (1984); Mahoney and Erman (1984); Lachance and Dubé (2004); Heywood and Walling (2007); Franssen (2014)
Tracer tests	Residual time of tracer in hyporheic interstitial and thus hydraulic conductivity	Packman and MacKay (2003; Packman et al. (2004)
Mark IV Standpipe	Hydraulic conductivity	Terhune (1958), (Gustafson-Greenwood and Moring 1991)
Kolmameter®	Hydraulic conductivity	Zumbroich and Hahn (2018)

Qualitative methods

Visual observation and mapping

A common way to estimate the degree of colmation is based on visual mapping of the riverbed since it is a simple method and does not require any special equipment (Descloux et al. 2010b). Schaelchli (2002) developed a mapping method in which the degree of inner colmation can be estimated. Therefore, gravel bars, river banks or any other non-wetted area are assessed by removing the top layer and evaluating the underlying material (Figure 2.6). The exposed underlying material is assessed based on three different indicators which describe 1) the composition of underlying material, especially the amount of cohesive particles in the bed material, 2) the availability and distribution of big and small pores and 3) the compaction of the riverbed material. The subsurface material can be distinguished into five classes ranging from no colmation (class 1) to very strong colmation (class 5) (Table 2.4). Decisive for the assignment to a class is the visible amount of the different grain fractions below the top layer. The amount of cohesive particles plays an important role for the colmation. Additional observation of the river and the evaluation of morphological conditions (channelization, bank protection, hydraulic structures etc.) are added to the assessment. Outer colmation is not considered in this evaluation system. This method cannot be applied in cases without any dry area. However, it could be transferred to wetted areas, resulting in higher uncertainties.

Table 2.4: Classification of inner colmation according to Schaelchli (2002).

Class	Evaluation	Indicator
1	No colmation	Coarse-grained substrate
		Few sand depositions, no cohesive deposition
		Dominating pore space is coarse-grained
2	Weak colmation	Loose substrate with a wide grading (pebble, gravel, sand)
		No visible deposition of cohesive particles
		Pore space coarse to fine-grained
3	Moderate colmation	Substrate slightly compacted
		Pore space approx. 1/4 filled with cohesive particles; the remaining material mainly sand but also gravel and pebbles
		Pore space mainly fine-grained, for cohesive deposits no pores are visible
4	Strong colmation	Substrate is clearly compacted
		Pore space filled about half with cohesive fine particles, remaining material mainly sand
		Pore space with fine pores visible locally
5	Complete colmation	Substrate is heavily compacted
		Pore space completely filled with cohesive fine particles
		No visible pore space

In order to apply this method to outer colmation Schaelchli (2002) recommends focusing on (a) the ratio of coverage (comparing to the total observation section) and the thickness of the deposition, (b) the composition of the deposition especially regarding the amount of clay and (c) estimating the potential of remobilization. Figure 2.6 shows examples of the five different colmation classes ranging from no colmation (Figure 2.6 a) to complete colmation (Figure 2.6 e).

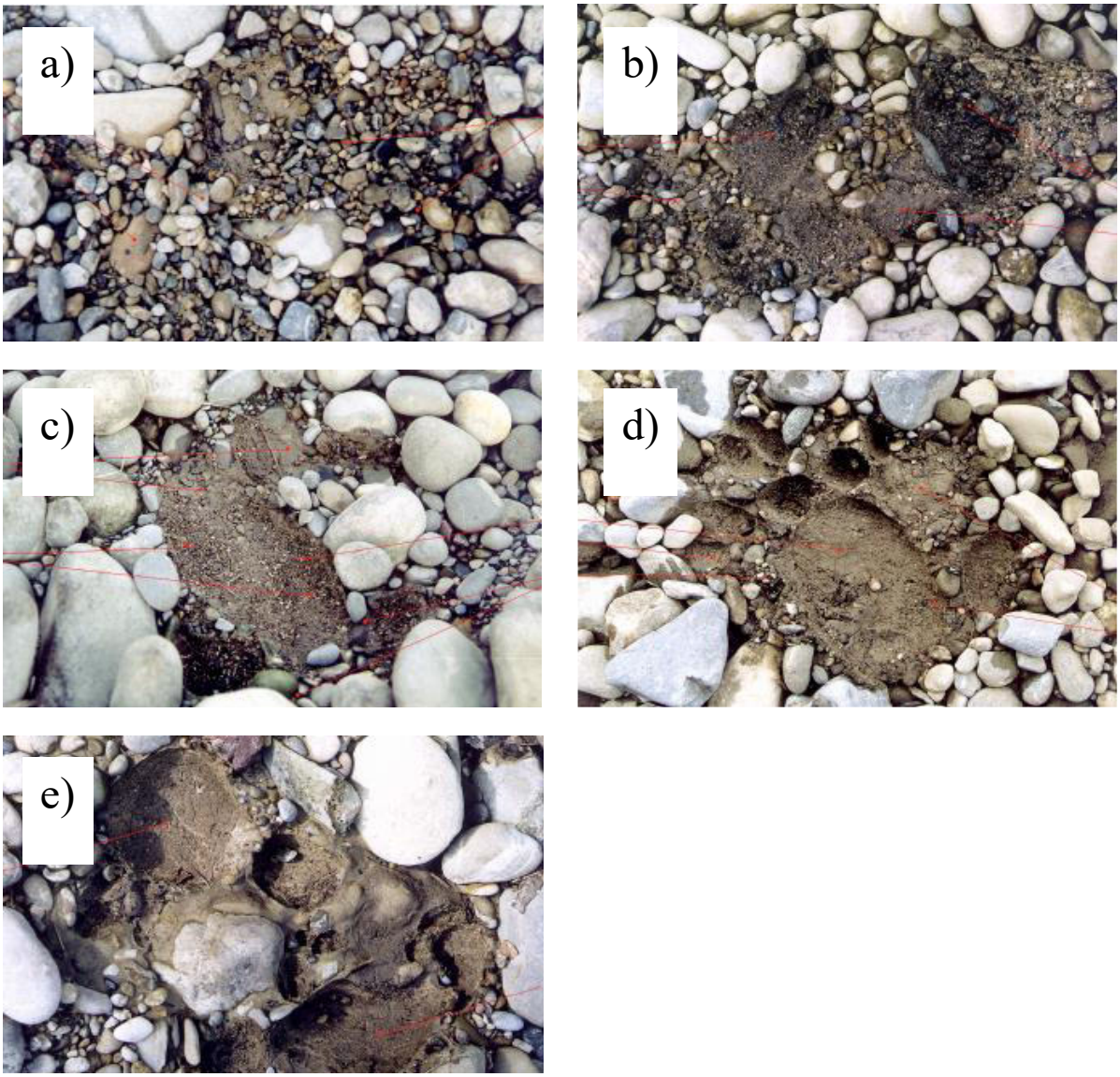

Figure 2.6: Image of the five different classes of colmation: a) no colmation, b) weak colmation, c) moderate colmation, d) strong colmation and e) complete colmation.

Kick test

For conducting the kick test a small area of the riverbed is disturbed with a spade or with boots by whirling up the top layer of the riverbed. Firstly, the penetration resistance of the gravel to enter the spade or boots and secondly, the re-suspending sediment plume from the disturbed area is evaluated (Thurmann and Zumbroich 2013). This method is limited to low discharge

and low turbidity. It is difficult to compare results from different rivers with varying flow velocity and turbulences.

Wooden sticks

A simple, cheap and easy method to determine the oxygenated conditions in the sediment is introduced from Marmonier et al. (2004), where wooden sticks are placed into the riverbed for several weeks and removed after a time period of four weeks. When the color of the wooden sticks changes from brown to dark grey or black, hypoxic or even anoxic conditions can be assumed. This change can somehow be correlated to sediment conditions like colmation. However, it can only give a very brief insight of the ecological condition and there is no relation established in the existing literature connecting the anoxic conditions to sediment characteristics by now.

Shelter availability according to Finstad et al. (2007)

The measurement of shelter availability is an indirect measuring method for colmation. The availably of shelter for juvenile fish is a sign for good gravel conditions. In order to measure the shelter depth a small rubber tube is marked at certain depths to indicate different categories of shelter depth. The rubber tube is then plunged into the voids of the sediment particles without moving them on an area of 0.5 m x 0.5 m of the riverbed (Finstad et al. 2007).

Quantitative methods

Sediment samples and grain size analysis

Sediment sampling using the freeze core or freeze panel technique is a common method used for investigations about colmation (see chapter 2.3.1) (Carling and Reader 1982; Bunte and Abt 2001). The advantage of both methods is that no fine sediments are washed out during retrieving, the sample can be assumed as undisturbed and the natural structure remains intact. The freeze core technique provides detailed information about the grain size distribution over depth and also regarding the vertical stratification. In contrast to this the freeze panel technique gives detailed information about the top layer of the riverbed which is often not included into the freeze core technique. Both methods combined allow a proper assessment deposited fine sediments. The grain size analysis is used to assess the amount of fine sediments which are commonly below 1 mm or 2 mm (Beschta and Jackson 1978; Petts 1988). The natural and current state of a riverbed can be assessed with this method. A further application is to clean parts of the riverbed a certain time before applying the freeze core or freeze panel technique in order to investigate the reinfiltration of fine sediments as it has been done in some studies for evaluating salmonid redds (Franssen et al. 2014). An important point to consider is that the natural amount of fine sediments varies for each river according to the surrounding geomorphological conditions. Therefore, a universal threshold for amount of fine sediments cannot be established. In order to evaluate colmation based on amounts of fine sediments a reference reach is required.

Sediment traps and sediment buckets

Sediment traps (e.g. Frostick and Reid 1984; Mahoney and Erman 1984) and sediment buckets (Lachance and Dubé 2004) are a simple way to estimate the amount of infiltrated fine sediments over a given period of time. They are filled with clean material, installed into the riverbed and remain installed for a certain time assessing the infiltrated fines in a certain time (Frostick and Reid 1984). A similar method is to manually disturb a specific area upstream of the traps collecting the eroded material in the traps resulting in a sediment index for the trapped material as conducted in the study from Mahoney and Erman (1984).

Tracer test

General exchange processes within the hyporheic zone can be evaluated using tracer tests (Packman and MacKay, 2003; Packman et al. 2004). Applying this method a tracer (e.g. Rhodamine WT dye; Wondzell and Swanson 1996) is injected into the hyporheic zone. Depending of the aim of the study one or more samples at a downstream area are extracted to measure the arrival time and concentration of the tracer plume (Wondzell and Swanson 1996). This allows the analysis of preferred flow paths in the hyporheic zone and the hydraulic conductivity of the riverbed material which can be used to assess colmation processes.

Mark IV Standpipe

The Mark IV Standpipe, introduced from Terhune (1958) is a method to assess the hydraulic conductivity of a riverbed. Due to the pore reducing process of colmation, it also reduces the hydraulic conductivity. Thus hydraulic conductivity can also be a parameter to assess colmation since an increase in the proportion of fine sediments results in the reduction of hydraulic conductivity (Descloux et al. 2010a; Datry et al. 2015). The Mark IV Standpipe is a standpipe with a filter close to the tip, which is driven into the sediment at a certain depth. Water is pumped out of the filter using a vacuum pump with a hydraulic head of 0.025 m. The amount of extracted water is measured. This discharge is later correlated to hydraulic conductivities. Therefore, the method is applied in the laboratory using different materials with known hydraulic conductivity (Terhune 1958).

Kolmameter® according to Zumbroich and Hahn (2018)

A new method is the Kolmameter® developed from Zumbroich and Hahn (2018) which measures the effective level of permeability. Water is injection into the hyporheic zone under constant pressure and the leakage resistance due to the surrounding material is measured. Whereas coarse material shows less leakage resistance there will be a much higher leakage resistance in clogged riverbeds since the available pore space is reduced.

2.2.3 Impact of colmation

Colmation is known to have a severe ecological impact. However, beside the ecological impact it also influences socioeconomics such as the reduction of riverbed infiltration and different hydromophological aspects. In the following chapter the impact of colmation on the different field is describes. Since the focus in this study are ecological aspects of colmation this will also be the focus in this chapter.

Ecological impact of colmation

Some ecological impacts of colmation are already mentioned in the sections above. However, this section gives a detailed overview on how colmation affects the reproduction of gravel spawning fish and other aquatic organism such as macroinvertebrates. It affects the whole life cycles of gravel spawning fish during different life stages. Both habitat quality and reproduction success are interrupted or disturbed by the infiltration process.

Impact on the reproduction period of gravel spawning fish

In the first place colmation can cause the loss of physical spawning habitat. Gravel spawning fish are known to only select spawning areas with higher flow velocities, coarse substrate and low amount of fine sediment to ensure high oxygen consumption during incubation phase (Bernier-Bourgault and Magnan 2002). If this condition is not available, female will not start with redd construction. It may also hinder female fish to move gravel and stones for digging the redd since the riverbed is highly solidified due to increased fine sediment amounts (Kondolf et al. 2008).

In case of successful egg deposition colmation can occur during incubation phase limiting the survival rate of embryos (Franssen et al. 2014). By reducing porosity and hydraulic conductivity exchange processes within the hyporheic zone are limited (Argent and Flebbe 1999; Greig et al. 2005; Sear et al. 2008). This leads to reduced oxygen availability for embryos and in case the oxygen concentration drops below a critical limit increased mortality of embryos occur. Furthermore toxic metabolic waste is not transported out of the redd (Dumas and Marty 2006). Fine sediment can also lead to physical abrasion of the embryos (Heywood and Walling 2007).

Sear et al. (2008) hypothesize that finer silt and clay fractions affect the survival of the incubating embryos whereas the coarser fractions influence the emergence of alevins by blocking the pore space. Thus, the clogged pore space prevents fry from emerge from the gravel bed (Chapman 1988; Heywood and Walling 2007). This blocking can be caused by either two ways. It can be caused by occlusion of pathways through the intragravel pore space (inner colmation) or by forming a thick impenetrable layer of fine sediment on the riverbed surface (outer colmation) (Gustafson-Greenwood and Moring 1991; Kondolf 2000; Sear et al. 2008). After successful incubation phase alevin start to emergence to the riverbed surface and live between the gravels of the riverbed surface. By clogging the intragravel pore space alevin lose shelter possibilities against predators and may be drifted away during high flow events due to

missing shelter. Finstad et al. (2007) further observed a significantly improved juvenile salmon performance with increasing shelter availability. Another important factor is the limited food availability caused by the reduced pore space.

Regarding the size fraction of fine sediments responsible for negative effects on egg survival Zimmermann und Lapointe (2005) state the importance of sandy fractions within fine sediments due to its capability of trapping silt and clay within the egg zone. Their experiments show that clay could only be trapped with a certain amount of sand fractions in the gravel framework. Kondolf et al. (2008) report the reduced exchange rate of dissolved oxygen into intragravel pore space due to increasing clay content and the increased rate of egg mortality, whereas Greig et al. (2007) reports high rates of egg survival in the absence of clay/silt and in presence of high rates of sand. Further, Crisp (1993) reported that increased sand fractions prevent alevins from emergence, resulting in entombment. This result was also confirmed by the observations of Gibson (1993). It can be concluded that both fractions, clay/silt and sand need to be considered when evaluating sedimentological conditions of redds. As a result, catchments producing clay/silt and sand fractions might have a higher risk to affect salmonids (Sear et al. 2016).

Several studies have been conducted within the last decades investigating the effect of fine sediment intrusion and the survival of fish egg (Chapman 1988; Ingendahl 2001). In general increasing mortality and reducing egg-to-fry survival can be observed with increasing amount of fine sediments (Ingendahl 2001; Franssen et al. 2014). However, most of the studies do not observe any linear relation. (Sear et al. 2016). Argent and Flebbe (1999) observe 90% reduction of survival brook trout eggs during laboratory flume experiments for an increase of fine sediments (0.43mm-0.85mm) from 0 to 25 %. Tappel and Bjornn (1983) establish a relationship between survival predictions of chinook salmon embryos and different rates of fine sediments (Figure 2.7). Crisp (1996) observes higher survival rates in gravel without fines sediments. However, several thresholds observed in laboratory or field studies can be found. Table 2.5 summarizes the amount of fine sediments for different fractions and the corresponding observed rate of mortality.

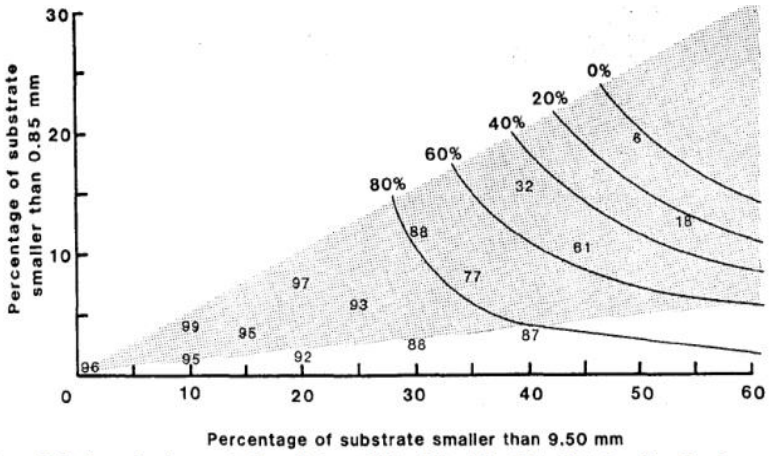

Figure 2.7: Isolines showing survival predictions for chinook salmon embryos unter different sediment conditions. scattered numbers are percent survival values from laboratory tests (Tappel and Bjornn, 1983).

Table 2.5: Thresholds regarding the mortality of salmonid eggs in relation to fine sediment rates.

Reference	FSA < 2 mm (%)	FSA <1 mm (%)	FSA < 0.85 mm (%)
Crisp and Carling (1989)		8-12	
Milan et al. (2000)		14	
Soulsby et al. (2001)	23		
Ottaway et al. (1981)	10		
Heywood and Walling (2007)	9 (50 % mortality)	8 (50% mortality)	
Heywood and Walling (2007)	14 (100 % mortality)	12 (100% mortality)	
Hausle (1973)	0 (0% mortality)		
Hausle (1973)	10 (50% mortality)		
Hausle (1973)	20 (90% mortality)		
Argent and Flebbe 1999)			20 (57 % mortality)
Reiser and White (1988)			0 (37 % mortality)
Reiser and White (1988)			10 (90 % mortality)
Reiser and White (1988)			20 (98 % mortality)
Petts (1988)	20-26		
Sear (1993)			4

Table 2.5 shows that the range of observed fine sediment rates vary highly and that the complexity of salmonid redds can not be reduced to a single parameter. Furthermore, the rate of fine sediment is highly dependent on the samples mass and the maximum grain included in the investigated samples. Heywood and Walling (2007) conclude that there will not be a universal applicable threshold level of fine sediment in redd gravel. They recommend assessing the overall textural composition (dg, FI, SO) in order to evaluate incubating conditions than the relative proportion of fine sediment within the redd. There is no single parameter that can fully represent the gravel size distribution for evaluating redd construction, embryo incubation and fry emergence (Kondolf 2000). For each life stage the role of fine sediments plays a different role and thus the relevant size attributes differ (Kondolf 2000).

Impact on macroinvertebrates

Colmation processes not only influences different life stage of gravel spawning fish it also affects habitat conditions of macroinvertebrates (MIB). Since MIB is an important food source for fish such as gravel spawning fish the appearance of MIB also influences fish habitat conditions (Duan et al. 2009).

The tight packing of riverbed decreases the size of interstitial pore space for MIB, reduces the availability of oxygen, limiting the trapping of organic detritus and thus resulting in a decrease in the heterogeneity of the substrate and of the resulting heterogeneity of habitats (Gayraud and Philippe 2003; Bo et al. 2007; Descloux et al. 2013). It further impedes the vertical migration of MIB. Several studies observed a decrease of MIB density and a decrease in species richness with increasing fine sediment content (Sear 1993; Rabeni 1997; Bo et al. 2007; Buendia et al. 2013). Angradi (1999) observed a reduction of MIB densities by a factor of two with increasing

rates of fine sediments form 0 to 30 %. Gayraud and Philippe (2003) and Maridet et al. (1992) found a positive relation between MIB density and effective porosity.

The influence of colmation processes can further be observed in the taxonomical, ecological and functional composition of benthic and interstitial/hyporheic assemblages (Bo et al. 2007). Benthic organisms live on the riverbed gravel whereas interstitial or hyporheic organisms inhabit the hyporheic zone down to 30 – 45 cm (max observed 70 cm) (Richards and Bacon 1994).

The feeding groups of benthic organisms are affected by colmation processes in a way that filter-feeders and scrapers change towards deposit feeders (Descloux et al. 2013). Benthic densities can be reduced by a factor of three in heavily colmated reaches. Percentage of Diptera, Crustaceans, Harpaciticoida and Cyclopoida were found to be significantly higher in lightly colmated reaches than in heavily colmated ones (Descloux et al. 2013). Other organisms such as Ephemeroptera, Plecoptera, Trichoptera which are commonly inhabit cobbles, gravel and moss-covered bedrock are reduced due increased fine sediments (Duan et al. 2009).

While benthic organisms and their reaction on colmation is well studied there are only few studies regarding hyporheic organisms (Descloux 2013). Weigelhofer und Waringer (2003) find a significant decline in densities of hyporheic Gammaridae, Ephemeroptera, Plecoptera, Trichoptera and Sialidae under clogged riverbed conditions.

A few studies report that some groups can benefit from the changing conditions since competition against other groups is reduced. While the percentage of organisms with a high oxygen demand is commonly reduced with increasing fine sediment content Bo et al. (2007) and Descloux et al. (2013) observe increasing densities of Oligochaeta, Rhithrogena spp. and Baetidae in heavily clogged areas.

Impact on riverbank infiltration

In many areas the natural ground water resources do not meet the increasing water needs of the population, agriculture and industry (Beyer and Banscher 1975). The direct use of surface water from rivers and lakes requires intensive treatment of the raw water, which is associated with high investment and operating costs, due to the often heavy pollution of the water bodies. The infiltration of surface water into groundwater through the operation of bank filtration is in many cases an efficient way of making advantageous use of the naturally existing filter and reactor effect of the aquifers to improve the water quality (Beyer and Banscher 1975; Goldschneider et al. 2007). In 2003 16 % of the drinking water supply in Germany (more than 300 water works) is produced from river bank filtration (Schmidt et al. 2003). In order to guarantee a high water quality a retention time of the surface water in the ground water aquifer is required. Schubert (2002) reports a retention time of at least three weeks. During this retention time biodegradation of nutrients from the surface water occur, as well as the removal of bacteria, viruses and parasites. A further advantage of the high retention time is that fluctuations in temperature are balanced (Schubert 2002).

Due to the increased hydraulic seepage during the well operation and the transport of suspended sediments in the surface water colmation is likely to occur along the river bank reducing the hydraulic conductivity of the riverbed and thus limiting the rate and the volume of water production (Beyer and Banscher 1975; Hiscock and Grischek 2002; Goldschneider et al. 2007; Pholkern et al. 2015; Ulrich et al. 2015). Beside the fact that colmation limits the rate of water production it might also be a desirable effect in terms of drinking water production in case of flood events and the transportation of possible pollutions due to the sealing effect of the colmation layer. It might also increase the natural self-cleaning effect due to increased retention time (Goldschneider et al. 2007).

Hydromorphological aspects

Even colmation usually takes place in the subsurface layer of the riverbed it might lead to alteration of hydraulic conditions. When filling up the pore space between coarser grains the effective roughness of the bed is reduced (Barzilai et al. 2013). This in turn affects the relationship between discharge and flow depth, leading to higher flow velocities and subsequently to lower water depths.

Colmation not only influences the hydraulic conditions of a river it also affects some morphological mechanisms. Due to the pore filling process the packing density of the riverbed is increased hampering coarse material to be moved. Additionally, hiding effects caused by coarse material reduces the erosion of fine material. The combination of both effects results in an increase of critical bed shear stress for incipient motion (Wilcock 1988; Wilcock and Kenworthy 2002). On the other hand (Barzilai et al. (2013) report possible enhancement of the mobilization of protruding grains due to the higher near bed velocities caused by the decreased effective bed roughness. Therefore, colmation affects sediment transport mechanisms in different ways and cannot be generalized.

2.3 Towards a multi-parameter approach

Chapter 2.2.2 summarizes the existing assessment methods for colmation. However, these methods fail to describe colmation sufficiently since only a single parameter is commonly applied. This thesis intends to develop a multi-parameter approach to determine colmation with a high degree of accuracy. Therefore, based on the literature review (see chapter 2.2.1) and the existing assessment methods (chapter 2.2.2) four parameter are identified and integrated in a multi-parameter approach. Each parameter is described in detail in the following chapter. The general basics of each parameter is described followed by possible determination or sampling methods.

The four parameters included in the multi-parameter approach are the following:

- Grain size distribution / sediment characteristics
- Intragravel dissolved oxygen saturation

- Porosity
- Hydraulic conductivity

Grain size distribution provides an overview on the general composition of the riverbed material and its fine sediment content. Several statistical parameters can be derived from the grain size distribution for further analysis (Kondolf 2000).

Intragravel dissolved oxygen saturation (IDOS) is one of the main limiting factors for salmonid reproduction and egg survival and is therefore an important parameter to link colmation to ecological conditions. However, it has to be considered that IDOS can also be influenced by oxygen-consuming degradation as well as upwelling or downwelling effects.

Porosity does not contribute to a value for the general pore size, but it provides an estimation about the available pore space. However, it can only be analyzed together with other values since a high porosity can also result from uniform material with a high pore space. Sand for example can reach porosity up to 45% but the pore space is too small as habitat for juvenile fish.

Hydraulic conductivity seems to be the most important parameter to describe colmation since it directly represents the ability of water being transported into the hyporheic interstitial allowing exchange processes. A reduction in hydraulic conductivity means that less oxygen rich water or nutrients from the surface can be transported into the hyporheic interstitial and therefore limiting the survival rate for incubating fish.

2.3.1 Grain size distribution

Grain size analysis commonly means the analysis of grain size, particle shape, particle density and bulk density. Particles can also be described in the sense terms of mineralogy, color, concentration in the water column and orientation and degree of compactions in the bed (Gordon et al. 2004); however, the size and the shape are chiefly used. Additionally, parameters might be important depending on the question and the problem. The following chapter focuses mainly on grain size analysis and particle shape.

The Φ-scale and sieve analysis

The frequency distribution of particles per size class tends to follow approximately a lognormal distribution (Bunte and Abt 2001). As a consequence, the arithmetic mean diameter and the arithmetic median particles size are not the same. The mean diameter is usually larger than the median diameter (Bunte and Abt 2001). In case of a truly logarithmic distribution a log transformation of particle-size units would produce a normal distribution. (Krumbein 1938) expressed particle size D as the negative logarithm to the base of 2 and called the result the Φ-scale.

$$\Phi = -log_2(D_i) = -\frac{\log(D_i)}{\log(2)} \qquad (2.5)$$

Using the Φ-scale leads to negative values for particles sizes smaller than 1 mm (Table 2.6). This feature is convenient for studies that focus on gravel and bigger sediments (Bunte and Abt 2001). For studies where sand and smaller sediments are in the focus the ψ-scale is more convenient since the negative value from the Φ-scale are used and thus leading to positive values for particle sizes smaller than 1 mm (see Eq. (2.6).

$$\psi = -\Phi = log_2(D_i) = \frac{\log(D_i)}{\log(2)} \qquad (2.6)$$

In order to analyze sediments according to their size distributions particles are grouped into classes with different sizes. These classes mainly correspond to the size of sieve openings (Bunte and Abt 2001). According to Wentworth (1922) sediments can be classified into six major categories: boulders, cobbles, gravel, sand, silt and clay as displayed in Table 2.6. The frequency of particles per size class in fluvial gravel tend to be approximately logarithmically distributed if particles size-classes progress in a linear scale (10, 20, 30mm) (Bunte and Abt 2001). In order to obtain an approximately normal distribution of particle sizes, particles-size classes were made to increase by a factor of 2 (Wentworth scale). Thus, particles sizes in units of mm double in consecutively larger size classes (see Table 2.6) (Bunte and Abt 2001; Blott and Pye 2001).

Table 2.6: Wentworth scale including separation into mm, φ-scale as well as ψ-scale (Wentworth 1922).

Particle size discription			mm	$\varphi = -\log_2$	$\psi = \log_2$
Boulder	very large		4096	-12	12
	large		2048	-11	11
	medium		1024	-10	10
	small		512	-9	9
Cobble	large		256	-8	8
	small		128	-7	7
Gravel	very coarse	Pebble	65	-6	6
	coarse		32	-5	5
	medium		16	-4	4
	fine		8	-3	3
	very fine	Granule	4	-2	2
Sand	very coarse		2	-1	1
	coarse		1	0	0
	medium		0.5	1	-1
	fine		0.25	2	-2
	very fine		0.125	3	-3
Silt			0.063	4	-4
Clay			0.0039	8	-8
			0.00024	12	-12

Presentation of sieve curves and statistical analysis from grain size distribution

To visualize the particle size distribution from sediment samples the so-called sieve curve or gradation curve is plotted based on the cumulative particle size-distribution on the abscissa and the percent finer by weight on the ordinate. Figure 2.8 shows an exemplary sieve curve including the frequency distribution. The x-axis is commonly expressed in a logarithmic scale if particle size is expressed in mm. If particle size is expressed in Φ- or ψ-units, the x-axis is kept linear as shown in Figure 2.8 (Bunte and Abt 2001).

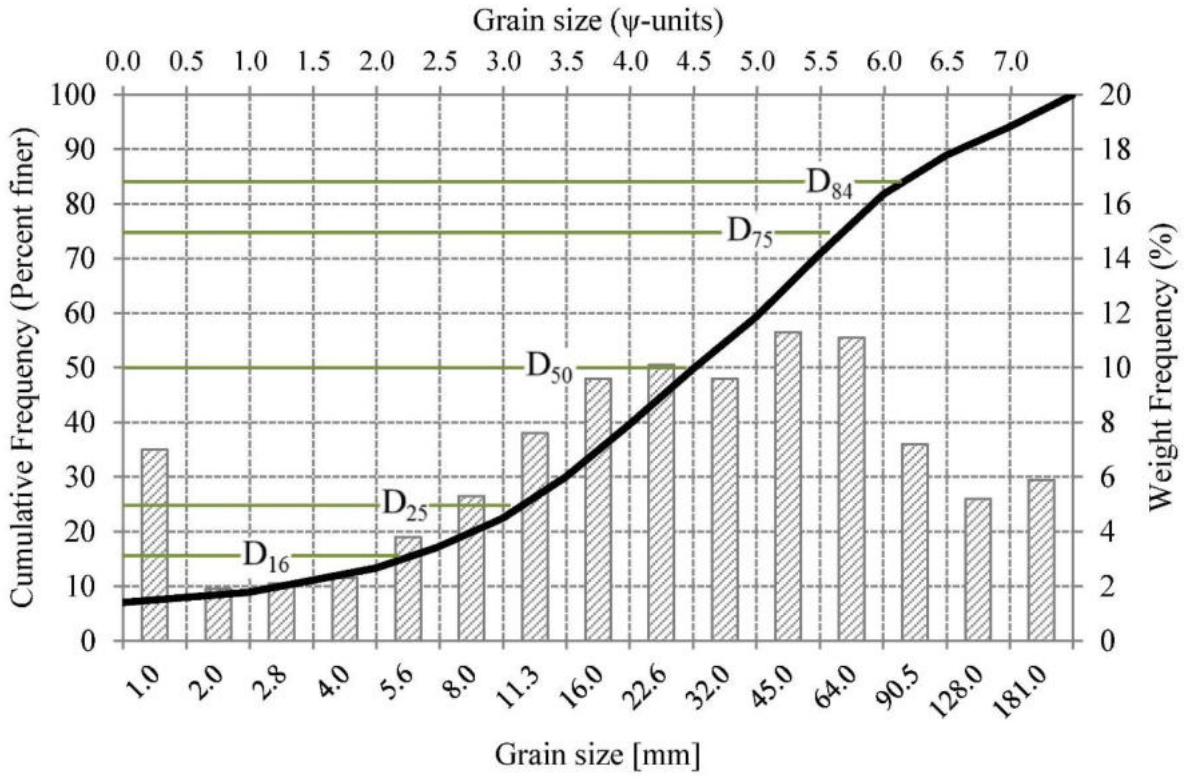

Figure 2.8: Exemplary sieve cure including frequency distribution, ψ-scale and the weight frequency (modified from Bunte and Abt 2001).

Displaying several grain size distributions a sieve curve diagram might be too confusing since different lines are overlapping. In this case a box-plot diagram is recommended as shown in Figure 2.9. A box plot diagram has the advantage of no crossing lines so that a large number of different grain size distributions can be displayed in one figure.

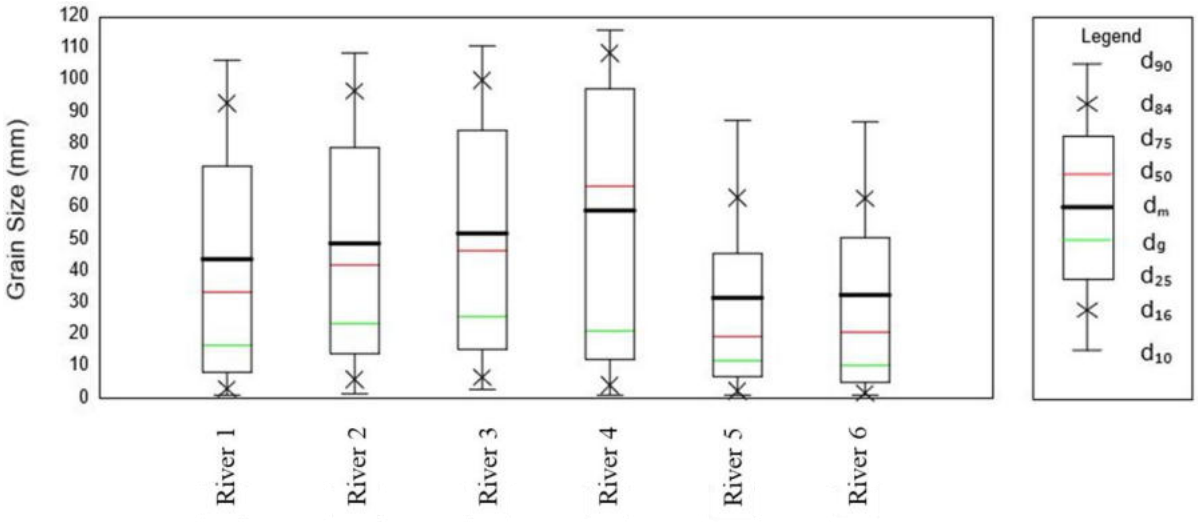

Figure 2.9: Single variable statistics of different mixtures (Boxplot diagram) without crossing lines (modified from Kondolf 2000).

In order to compare different sediment samples and sediment mixtures and to derive statistical parameters to describe the sediment composition several percentile values can be derived from the grain size distribution. A percentile is a grain size diameter indicated by the cumulative distribution curve for particular percent finer value. For example the D_{16} is the diameter where 16% of the whole sample is finer. In fact, each percentile between 1 and 100 can be used for comparing sediment mixtures, however, in literature customarily the particle sizes of the D_{50}, D_{25}, D_{75}, D_{16}, D_{84}, D_5 and D_{95} are used (Bunte and Abt 2001). Based on the percentiles other statistical parameter can be derived. Bunte and Abt (2001) provide an overview of the most common statistical parameter such as skewness, sorting coefficient and geometric standard deviation. Lotspeich and Everest (1981) further introduced the Fredle-Index as coefficient to characterize interstitial habitat conditions. Table 2.7 provides an overview of the indices and coefficients in evaluating sediment characteristics in this study.

Since natural riverbed compositions show wide variations of their grain size distribution and spatial variation in horizontal and vertical direction a single parameter is not sufficient to describe riverbed characteristics (Crisp and Carling 1989).

Table 2.7: Sediment indices to evaluate substrate characteristics

Variable	Abbreviation	Expression/formula	Equation ID
Mean particles size of a distribution [mm]	D_m	$D_m = \frac{1}{m_{tot}} \sum_{i=1}^{n} (D_{ci} \cdot m_i)$	2.7
Geometric mean diameter [mm]	D_G	$D_g = \sqrt{D_{16} \cdot D_{84}}$	2.8
Percentiles	D_X	D_5, D_{10}, D_{16}, …. D_{84}, D_{95}	-
Sorting coefficient	SO	$SO = \sqrt{\frac{D_{84}}{D_{16}}}$	2.9
Geometric standard deviation	σ_G	$\sigma_G = \sqrt{\sum f_i \, (\varphi_i - \sum f_i \varphi_i)^2}$	2.10
Uniformity coefficient	C_U	$C_U = \frac{D_{60}}{D_{10}}$	2.11
Percentage of fines	AFS<2mm AFS<1mm AFS<0.5mm	-	-
Fredle-Index	FI	$FI = \frac{D_G}{SO}$	2.12

The following abbreviations are used in Table 2.7

D_{ci}	Center of class in φ-units of ith size class
m_i	Weight of particles retained for ith size class
m_{tot}	Total weight of particles per sample
f_i	fraction of sediments in size class *i*
φ_i	characteristic sediment diameter for size class *i*, expressed on the φ-scale

Methods for sediment sampling

To obtain detailed information about the sediment composition of a riverbed, samples must be taken undisturbed without losing certain particles sizes (Thoms 1992). Bunte and Abt (2001) provide a detailed collection of different procedures for sediment sampling under submerged conditions.

Shovel sampling

Shovel sampling is a very simple method for sediment sampling which does not need too specific equipment. This method is not time consuming and can be applied at remote areas. However, when taking the sample under water fine sediments are going to be washed out causing a unrepresentative sample that is biased against fines (Bunte and Abt 2001). It is therefore recommended to only apply the shovel method in low flowing areas to reduce the loss of fines. The riverbed can be removed in different layers (top layer/armour layer and subsurface layer) but possible stratifications of the riverbed cannot be detected visually before sample taking. A possibility to overcome the problematic with washing out the fines is to install an underwater storage box with a mesh-bag cover for collecting all the washed out fine sediments.

Grab sampler / Van Veen Grab sampler

A grab sampler has a predefined sampling volume which can be filled with an automatically closing mechanism so that it can also be applied in non-wadable areas. They have been developed for sandy streams. However, the device might not close properly in case of coarser grains wedging in the closing mechanism resulting in a gap where fine sediments can be washed out. Thus, it is not suitable for gravel riverbeds (Bunte and Abt 2001).

Pipe sampler McNeil sampler

The McNeil sampler consists out of two pipes as shown in Figure 2.10. The smaller pipe is driven into the riverbed down to the required sampling depth. The material is removed from the inner pipe into a separated bucket or bag. Fine sediments which cannot be manually removed from the inner pipe accumulate in the outer pipe and can later be added to the original samples. This overcomes the problem of washing out fines. However, it works best in sandy or medium gravel streams since it might be not suitable to introduce the device into a riverbed consisting of coarse gravel and big stones.

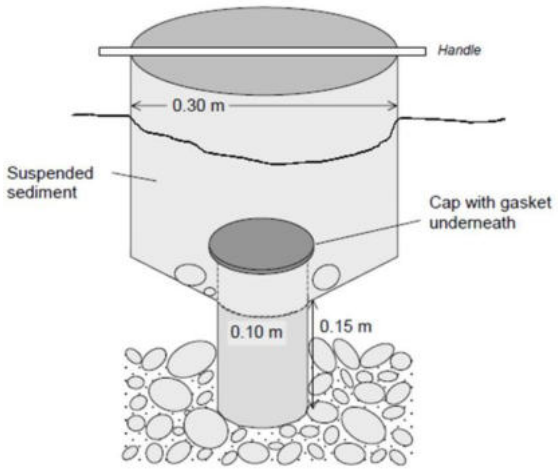

Figure 2.10: McNeil sampler showing two pipes, a handle for removing and a cap to keep suspended solids inside the device (Bunte and Abt 2001).

Freeze-core and Freeze-plate

The freeze-core and freeze-plate technique ensures a minimal loss of fine sediments during sampling and remains the natural structure of the riverbed intact (Carling and Reader 1981). The freeze-core technique used a core which is driven into the riverbed and filled with liquid nitrogen to freeze the surrounding area including all grains in the close vicinity of the core. A solid frozen sample can then be removed where possible stratifications of the grain size composition are visually detectable. This method provides detailed information about the grain size distribution over depth regarding a vertical stratification. In contrast to this the freeze-panel technique uses a plate which is placed on the riverbed, freezes the top layer of the riverbed and provides detailed information about the top layer. The combination of both methods allows a prober assessment of the riverbed characteristics. However, it should be mentioned that this method is expensive concerning acquisition costs and since the equipment is rather heavy it might be difficult to apply in hardly accessible reaches.

Representative sample mass

The decision which method to use depends on several factors such as the expected grain size of the sample, the required accuracy, the time and financial budget of the project and the accessibility of the river reach. For gravel riverbeds most sampling methods are biased towards coarse material since the sample mass is not sufficient to represent coarse particles correctly (Thoms 1992). In case of a non-representative sample volume one big stone included into the sample highly influences the grain size distribution and especially the percentage of fine sediments. In literature several studies can be found where large fractions are excluded from the analysis (Ingendahl 2001). This leads to an artificial overestimation of fine fractions.

In literature several criteria for the required sample mass can be found (De Vries 1970; DIN18123 1983; Church et al. 1987). For example Church et al. (1987) presented a criterion for sample mass for different amounts of the largest particle size whereas De Vries (1970) established different criteria for high, normal and low precisions Table 2.8.

Table 2.8: Comparison of different criteria from literature to define the minimal samples mass for representative sediment sampling.

Reference	Precision	Equation
De Vries (1970)	High precision	$m_s = 26{,}500{,}000 \cdot D_{max}^3$
De Vries (1970)	Normal precision	$m_s = 2{,}650{,}000 \cdot D_{max}^3$
De Vries (1970)	Low precision	$m_s = 265{,}000 \cdot D_{max}^3$
Church et al. (1987)	Normal precision	$m_s = 138{,}000 \cdot D_{max}^3$
Church et al. (1987)	D_{max} = 1 % m_s Low precision	$m_s = 27{,}751 \cdot D_{max}^3$
DIN (1983)	D_{max} = 5 % m_s German Standard	-

2.3.2 Porosity

The porosity of sediment samples of riverbed material is defined as the relation of pore volume to total volume and is a geomorphologic parameter to describe sediment characteristics. It is influenced by the size, distribution and shape of individual sediment grains (Fraser, 1935; Graton and Fraser, 1935).

During recent decades, porosity has been the focus of various studies (Carling and Reader, 1982; Yu and Standish, 1991; Wu and Wang, 2006; Wooster et al., 2008; Frings et al., 2011; Zou et al., 2011; Capece et al., 2014; Liang et al., 2015). The porosity *n* is calculated by the volumetric proportion of pore space and sediment volume:

$$n = \frac{V_P}{V_{tot}} = 1 - \frac{V_{tot} - V_{Se}}{V_{tot}} \tag{2.13}$$

with either a known pore volume V_P and total sample volume V_{tot} , or a known V_{tot} and the particle volume V_{Se}.

In principal, three options are available to assess the porosity of riverbed sediments: (i) in-situ field measurements, (ii) laboratory measurements or (iii) estimation based on mathematical predictors. All principals will be briefly described in the following sections.

Experimental methods to determine porosity in the laboratory and in the field

A common but time-consuming method to identify porosity on site or in the laboratory is the water replacement method (WRM, e.g., Frings et al., 2011; Bunte and Abt, 2001). One possible way to apply WRM can be found in the guidelines from the American Society of Testing and Materials (2004) in which the sediment is first removed from the location of interest, then the excavation is covered with a liner and filled with water. The amount of water used to fill the excavation gives V_{tot}. The extracted sediment is transported to the laboratory, dried and V_{Se} is determined using the WRM.

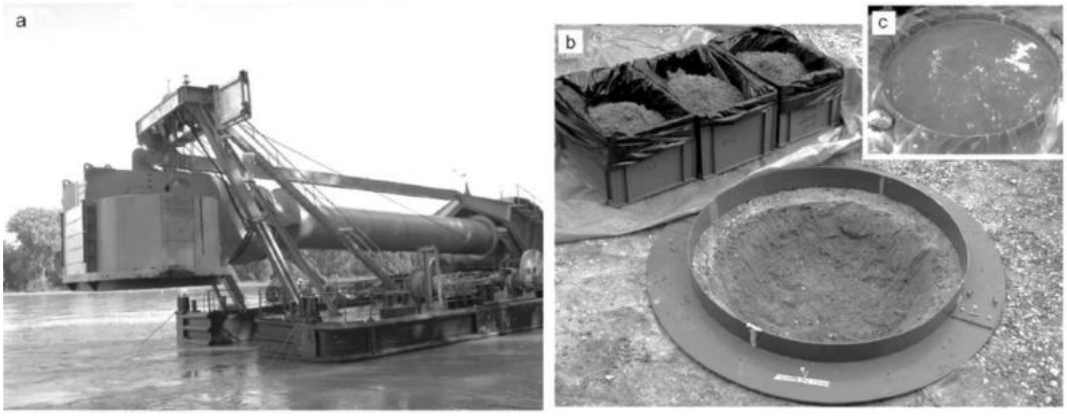

Figure 2.11: Example of application of water replacement method. Diving bell on the left picture; excavated hole and extracted sediment as well as covered excavation hole on the right picture.

To analyze the porosity of sediment samples in laboratories, several methods are available. Exemplary methods include the gas pycnometer, following Boyle´s Law of volume-pressure relationships, or the water desorption method (Klute, 1986). For the water desorption method, a saturated sample is drained stepwise and the water volume that is removed from the soil pores is measured, which enables porosity to be determined. Other methods are based on nuclear techniques, such as gamma-ray attenuation or computed tomography following the Beer-Lambert Law, where a gamma- or X-ray interacts with a material and the absorbed intensity of the gamma- or X-ray is transmitted (Pires and Pereira, 2014).

Mathematical predictors to determine porosity

Since in-situ measurements of porosity in the field and in the laboratory are time- and labor-intensive, several theoretical or mathematical equations have been developed to estimate porosity. Most of the mathematical predictors (Table 2.9) apply empirical relationships between porosity and the grain size distribution, where other controlling factors like grain shape, for example, are neglected (Frings et al., 2011). For these predictors, two approaches are available. The first uses the D_{50} as the characteristic parameter, while the second approach is based predominantly on the geometric standard deviation. Komura (1961) first established a relationship between the D_{50} and porosity using unconsolidated natural sediments from different Japanese rivers. The equation of Carling and Reader (1982) also employs a correlation ($r^2 = 0.9$; $p<0.001$) between the D_{50} and the porosity of poorly sorted, unconsolidated sediments. Wu and Wang (2006) used data based on studies found in the literature and data from different reservoirs in China (see CAHE Committee on Sedimentation, 1992). By modifying and adapting the approach of Komura (1963), a correlation with the D_{50} can be confirmed. The second approach uses the geometric standard deviation σ_g, which considers the whole grain size distribution instead of only one statistical parameter. The geometric standard deviation σ_g of the φ-scale is calculated via the method of moments 2.10, Frings et al., 2011):

Wooster et al. (2008) established a relation between the geometric standard deviation and the porosity using a power function ($r^2 = 0.85$, $p<0.001$). Frings et al. (2011) measured the porosity of sediment mixtures based on samples obtained from the field and the laboratory and established a multivariate regression function between the geometric standard deviation, the percentage of fines smaller than 0.5 mm ($f<0.5$) and the porosity ($r^2 = 0.71$). Beside mathematical predictors based on the grain size distribution, Yu and Standish (1991) established a linear-mixture packing model to estimate the porosity. Liang et al. (2015) developed a stochastic digital packing algorithm that considers controlling factors such as grain shape. Table 1 summarizes the mathematical predictors mentioned above, which are based on a relationship between porosity and the grain size distribution. Although mathematical predictors are easy to apply, it is widely recognized that they do not reproduce porosity very accurately (Frings et al. 2011), making direct measurements of porosity desirable.

Table 2.9: Mathematical predictors to estimate porosity based on a relationship between porosity and grain size.

Reference	Equation	No. of equation	Range of application
Komura (1961)	$n = 0.0864 D_{50}^{-0.21} + 0.245$ (D50 in cm)	2.14	$0.01 < D_{50} < 1000$ mm
Carling and Reader (1982)	$n = 0.4665 D_{50}^{-0.21} - 0.0333$	2.15	D = 2 – 1000 mm $5 < D_{50} < 200$ mm
Wu and Wang (2006)	$n = 0.13 + \frac{0.21}{(D_{50} + 0.002)^{0.21}}$	2.16	$10\text{-}3 < D_{50} < 100$ mm
Wooster et al. (2008)	$n = 0.621 \sigma_g^{-0.659}$	2.17	D = 0.075 – 22 mm $0.26 < \sigma_g < 1.80$
Frings et al. (2011)	$n = 0.353 - 0.068 \sigma_g + 0.219 f_{<0.5}$	2.18	D = 0.02 – 125 mm

2.3.3 Hydraulic conductivity

Basics of hydraulic conductivity

Hydraulic conductivity is described as the ease of water to flow through a porous medium (Terhune 1958; Alyamani and Şen 1993). In geotechnical engineering hydraulic conductivity is commonly replaced by permeability or permeability coefficient. However, this substitution is not correct since permeability (intrinsic permeability) [m²] is independent of the permeating fluid properties such as viscosity, whereas hydraulic conductivity [m/s] depends beside other factors on the permeating fluid.

According to Darcy´s Law the specific flow v_f through a porous medium of laminar flow is proportional to the hydraulic conductivity k_f and hydraulic gradient i as shown in equation (2.19).

$$v_f = -k_f \cdot i \qquad (2.19)$$

The flow follows the direction of decreasing head what is indicated with the negative sign in the equation. The hydraulic conductivity is affected by the temperature of the fluid, grain-size, grain shape, uniformity coefficient of grain size distribution, continuity of pore space and the packing of the porous medium (Fraser 1935). According to Hazen (1893) and Fraser (1935) the hydraulic conductivity is direct proportional linked with the temperature and increases the

hydraulic conductivity by a factor of 1.3 per 10°C increase of temperature. The grain size seems to be the most influencing sedimentological parameter since it directly affects the pore throat size which is interrelated with the shear resistance of the flow (Graton and Fraser 1935; Sperry and Peirce 1995). Additionally, the uniformity coefficient (Hazen 1893; Krumbein et al. 1943) and the grain shape (Sperry and Peirce 1995) influence the hydraulic conductivity to a certain extend. Krumbein et al. (1943) found in their experiments a proportional relation with sandy material between the hydraulic conductivity and the square of the mean diameter as well as the negative exponential of the logarithmic standard deviation.

In-situ measurements

Hydraulic conductivity is an important factor to describe habitat conditions of aquatic organisms since it influences exchange processes within the hyporheic interstitial. In-situ measurements are required to analyze the hydraulic conductivity in the field since a sediment extraction disturbs the natural structure and thus alter the hydraulic conductivity. Several methods can be found in literature which are suitable for in-situ measurements of hydraulic conductivity in saturated soils (e.g. Amoozegar and Warrick 1986). However, only a few methods are applicable for instream measurement of hydraulic conductivity in rivers. The presence of coarse gravel limits most methods. Commonly applied methods are the falling or constant head test, slug tests, permeameter test and standpipe test (Barnard and McBain 1994; Landon et al. 2001; Bouwer and Rice 1976; Terhune 1958; Hvorslev 1951; Genereux et al. 2008). In this section the different methods for in-situ measurements of hydraulic conductivity in riverbed materials are introduced and explained.

Falling head

A regular pipe is driven into the streambed to a required depth (Figure 2.12). The water level in the pipe is increased by adding a certain amount of water and the time is measured for the water level to sink to a lower level (Landon et al. 2001). Due to the increased hydraulic head the water flows through the sediment covered by the pipe and limited by the hydraulic conductivity of the sediments. This method can also by conducted as rising head by removing a certain amount of water until a certain water level and measure the time for the water level to rise. The vertical hydraulic conductivity kv can be analysed for this method using Darcy´s Law (Equation 2.20) or the approach according to Hvorslev (1951) (Equation (2.21).

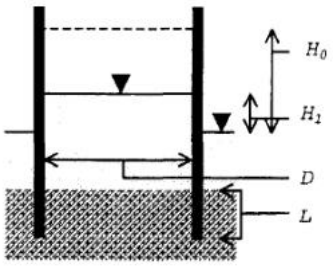

Figure 2.12: Falling head permeameter (Landon et al. 2001)

$$k_v = \frac{L}{t_1 - t_0} \ln \frac{H_0}{H_1} \quad (2.20)$$

$$k_v = \frac{\frac{\pi}{11}\frac{D}{m} + L}{t_1 - t_0} \ln \frac{H_0}{H_1} \quad (2.21)$$

k_v: Vertical hydraulic conductivity (m/s)
L: length of the pipe within the streambed (m)
D: diameter of pipe (m)
H_0: water level at t_0 (m)
H_1: water level at t_1 (m)

m: Isotropic transformation ration $m = \sqrt{k_h/k_v}$

Constant head

The set-up of the constant head is similar to the falling head method. A regular pipe is placed on the streambed and driven into a certain depth. Instead of adding a certain amount of water at once a constant flux is added into the pipe in order to keep a constant water head in the pipe (Figure 2.13). Measuring the flux enables the use of the Darcy equation (Equation

(2.22) for this method or the approach according to Hvorslev (1951) (Equation (2.24).

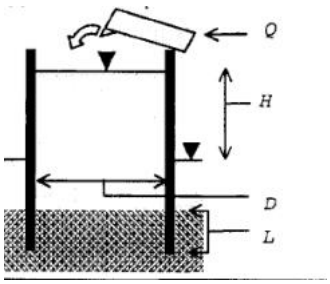

Figure 2.13: Set-up of a constant head test (Landon et al. 2001)

$$k_v = \frac{Q}{A_{xs}} \frac{L}{H} \quad (2.22)$$

$$A_{xs} = \frac{\pi D^2}{4} \quad (2.23)$$

$$k_v = \frac{4Q\left(\frac{\pi}{11}\frac{D}{m} + L\right)}{\pi D^2 H} \quad (2.24)$$

k_v: Vertical hydraulic conductivity (m/s)
Q: Flow rate (m³/d)
L: length of the pipe within the streambed (m)
Axs: Cross-sectional area of device (m²)
H: Water level (m)
D: diameter of pipe (m)

m: Isotropic transformation ration $m = \sqrt{k_h/k_v}$

For both methods, the constant head and the falling head test, the measuring depth can vary according to the scope of the investigation. Most depths found in literature vary between 10 and 50 cm (Datry et al. 2015; Ryan and Boufadel 2006; Chen 2004; Cardenas and Zlotnik 2003). The receiving k_f value for both methods is an integrative value over the sediment depth and does not consider heterogeneities within the length.

Slug test

Bouwer and Rice (1976) introduce the slug test as an alternative to the commonly applied pump test. Changing the water level in a well by suddenly removing a certain water volume the rate

of rise can be detected and the hydraulic conductivity can be determined. Instead of using a well a filter is driven into the riverbed for this method. The slug test equals the falling head method with the difference of using a filter instead of a pipe. This results in the determination of a horizontal hydraulic conductivity k_h instead of a vertical hydraulic conductivity k_v. The filter has a closed bottom and allows in- or exfiltration in horizontal direction.

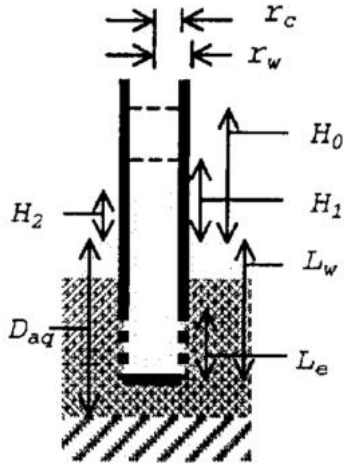

Figure 2.14: Set up of slug test in a riverbed (Landon et al. 2001)

$$k_h = \frac{r_c^2 \ln(R_e/r_w)}{2L_e} \frac{1}{\Delta t} \ln \frac{y_0}{y_t} \quad (2.25)$$

L_e: Length of the well screen (m)
Δt: Time difference (d)
y_0: Normalized displacement time 0 → H_1/H_0
y_t: Normalized displacement time t → H_2/H_0
k_h: horizontal hydraulic conductivity (m/s)
r_c: Inside radius of standpipe (m)
R_e: Effective radius of well over which head loss is dissipated (m)

r_w: Radial distance between undisturbed aquifer and well center (m)

Mark VI standpipe

The groundwater mark VI standpipe is introduced by Terhune (1958) as indirect measurement of hydraulic conductivity. Terhune (1958) uses a standpipe which is perforated of the lower part. After driving it into the gravel water is extracted from the pipe using a vacuum pump with a constant head of 2.54 cm (1 inch) and the flow rate is detected (Figure 2.15). Terhune (1958) verifies that the flow rate is direct proportional to the hydraulic conductivity. In order to transfer flow rates into hydraulic conductivities a calibration curve is required where known flow rates correspond to measured hydraulic conductivities as displayed in Figure 2.16. With this calibration curve in-situ measurements of flow rate can directly by transferred to hydraulic conductivities.

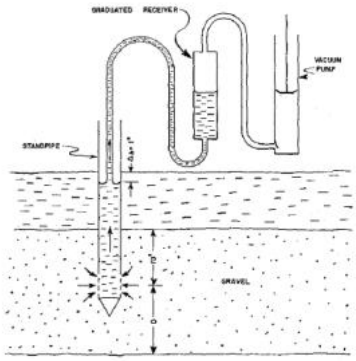

Figure 2.15: Set up of the standpipe apparatus and experiment (Terhune 1958).

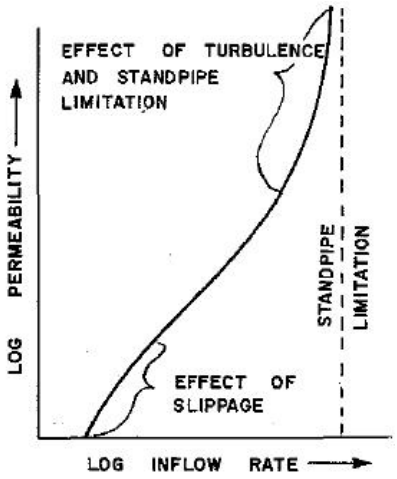

Figure 2.16: Hydraulic conductivity calibration curve (Terhune 1958).

Mathematical predictors to determine hydraulic conductivity

In-situ measurements are not always applicable since they are time and labor intensive and the river needs to be wadeable. Empirical and mathematical predictors can be applied to estimate the hydraulic conductivity based on the grain size distribution. This estimation expects a certain relation between the hydraulic conductivity and the grain size distribution (Alyamani and Şen 1993) which is expressed as a statistical variable of the grain size distribution.

Table 2.10 summarizes the most common mathematical predictors to estimate hydraulic conductivity based on the grain size distribution.

Table 2.10: Mathematical predictors to estimate hydraulic conductivity based on a relationship between k_f and grain size distribution.

Reference	Equation	No. of equation	Parameter
Hazen (1893)	$k_f = CD_{10}^2(0.7 + 0.03T)$*	2.26	k_f in m/day *C*: constant factor; commonly set to 1000 but can be adjusted D_{10}: diameter of which 10% of the sediment is finer [mm] *T*: Temperature in °C
Kozeny - Carman (1939)	$k_f = (\gamma/\mu)(1/C_{K-C})(1/S_0^2)[e^3/1+e]$	2.27	*γ: unit weight of permeant* *μ: viscosity of permeant* *CK-C: Kozeny-Carman empirical coefficient* *S0: specific surface area per unit volume of particles ~1/cm* *e: void ratio*
Carrier (2003) modified/simplified the Kozeny-Carman approach	$k_f = 1.99 \cdot 10^4 \left(100\%/\left(\sum[f_i/(D_{li}^{0.404} \cdot D_{si}^{0.595})]\right)\right)^2 (1/SF^2)[e^3/1+e]$	2.28	*f i5fraction of particles between two sieve sizes* *SF Shape Factor* *e: void ratio*
Alyamani and Şen (1993)	$k_f = 1300[I_0 + 0.025(D_{50} - D_{10})]^2$	2.29	*D10: diameter of which 10% of the sediment is finer [mm]* *D50: diameter of which 50% of the sediment is finer [mm]* *I0: Intercept [mm]*

* The term in the brackets turns 1 for 10°C

2.3.4 Intragravel dissolved oxygen saturation

Basics of dissolved oxygen

Dissolved oxygen refers to the amount of free (non-compounded or bonded) oxygen in water or other liquids. It affects especially aquatic organisms and represents an important parameter in assessing water quality and health of flora and fauna. Dissolved oxygen is used as respiration for fish and macroinvertebrates as well as aquatic plants and phytoplankton in case of no light for photosynthesis (Hitchman 1978).

The concentration of dissolved oxygen is depended on temperature, pressure and salinity. Increasing temperature leads to a decrease of oxygen solubility which can lead to a complete degassing at the boiling point of the water. Thus, cold water can hold higher concentrations of dissolved oxygen. Further, dissolved oxygen decreases with increasing level of salt but it increases with increasing pressure (atmospheric and hydrostatic pressure) (Hitchman 1978).

The amount of dissolved oxygen in natural waters is in a state of dynamic equilibrium. Bacteria and other aquatic species consume dissolved oxygen in an oxidation process. In order to regenerate the concentration of dissolved oxygen, aeration and photosynthesis is necessary (Hitchman 1978). Aeration is the most important process in rapid flowing streams whereas photosynthesis plays a dominant role in lakes. In streams daily fluctuation are not important since aeration is not dependent on sunlight or temperature whereas in lakes are considerable variations since oxygen production by photosynthesis happens during daylight and oxygen consumption is during night (Hitchman 1978).

Measurement of dissolved oxygen

There are three ways to measure dissolved oxygen in natural waters (Mitchell 2006). The first procedure, called Winkler Titration, is a destructive chemical titration where the water sample is mixed with manganous sulfate, potassium hydroxide and potassium iodide in order to form manganous hydroxide (Mitchell 2006). After some chemical reactions iodine is released free which is stoichiometrically equivalent to the dissolved oxygen and can be determined by titration with sodium thiosulfate. In anoxic conditions this method overpredicts DO values whereas it underpredicts in hyperoxic conditions.

The second method is the Clark Cell Electrode which is an amperometric sensor. Here, a two-electrode cell is filled with electrolyte solution and covered by a thin organic membrane (commonly Teflon). The electrode is place into the water and separated from the electrolyte solution by the membrane. Dissolved oxygen from the water can pass the membrane, travels into the chamber towards the cathode and electronically reduces at the cathode (Clark and Lyons 1962). The dissolved oxygen can then be calculated by measuring the current from the cathode as well as the sample temperature (Mitchell 2006). The oxygen consumption at the cathode which reduces the lifetime of the sensor and the diffusion dependence of oxygen through the membrane is a negative aspect of this method (Mitchell 2006). The third and the most recent

method is the luminescence-based Optode using a phase-modulation technique to measure oxygen-dependent luminescence quenching. The optodes sensor consists of a blue and red LEDs and a silicon photodetector (Figure 2.17, Mitchell 2006). The blue LED is used as stimulation and is sinusoidally modulated at a certain frequency. The resulting phase delay between the exciting blue LED signal and the detected red emission from the luminophor is inversely related to the amount of dissolved oxygen and can be detected. This method is highly temperature dependent so the temperature of water and the sensor needs to be measured (Mitchell 2006). It has the advantage of high sensor life and no oxygen consumption as well as non-destructive method over the other existing methods (Mitchell 2006).

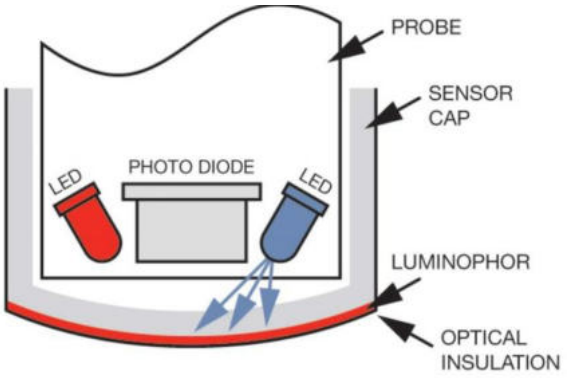

Figure 2.17: Scheme of a luminescence-based Optode for measurement of dissolved oxygen (Mitchell 2006)

2.4 Evaluation of existing assessment methods for determining colmation

There are many recent studies concerning the complex mechanism of colmation and the infiltration of fine sediments. However, there is still a lack of knowledge about natural clogging conditions (Datry et al. 2015). The previous chapter shows that different methods exist to assess colmation and infiltration processes. However, so far there is no standardized approach, which describes colmation sufficiently and there is no parameter agreed on which is suitable to determine colmation (Sennatt et al. 2006). Additionally, values and thresholds linking colmation to negative ecological impacts such as the impact on reproduction of gravel spawning fish are rare.

The qualitative methods such as mapping are highly subjective including a high observer bias increasing the uncertainties of the results (Schaelchli 2002; Thurmann and Zumbroich 2013). They also fail in terms of reproducibility among different investigators and the transferability of outcomes from one river to another is not guaranteed. These methods are further restricted to the riverbed surface and do not provide information about conditions of the subsurface layer where colmation takes place (Brunke 1999; Descloux et al. 2010b).Other single parameter methods such as sediment sampling fail to describe the complex process of colmation in one parameter (Nogaro et al. 2010). Sediment samples and its corresponding amount of fine sediments and infiltration rates do not necessarily assess colmation since the amount of fine sediment is highly related to the surrounding bed material; and infiltration rates do not provide information about the spatial distribution of the fine sediments.

A new method for assessing colmation is needed which is based on several parameter in order to describe colmation in a sufficient way. In this study a multi-parameter approach is introduced in which the four parameters provide detailed information on colmation.

Sediment sampling using the freeze-core technique is an already well-established method and can be applied in this study without severe modification. Also, the measurement of IDOS using an optical measuring device (optode) is an already well working method which does not need any modification. However, the literature research (see chapter 2.3.2 and 2.3.3) has shown that new methods are required in order to determine porosity and especially hydraulic conductivity in gravel riverbed.

The most common applied WRM for assessing the porosity using freeze-core samples result in a high loss of sediments during measurement. It further requires additional equipment such as a big tank and measuring devices such as ultrasonic sensor for measuring the change in water level require electrical power in the field. The tank to submerge the freeze-core sample should be as small as possible to accurately measure the difference in volume change. However, the volume of freeze-core samples cannot be predicted, and big stones can increase the diameter of a sample enormous so that the sample does not fit inside the tank anymore. Therefore, a new method is introduced which reduces the additional measuring equipment and keeping the effort in the field to a minimum.

Chapter 2.3.3 summarized the most common methods for determining the hydraulic conductivities. Most of the methods are developed for soil assessments but can also be applied to sandy bedded streams. However, in case of coarse gravel bedded river the existing methods fail to measure the hydraulic conductivity. For using a pipe for falling or constant head tests the required pipe diameter is dependent on the maximum grain which is given as $10*D_m$. This can result in a required diameter of up to 0.5 m for grains with a D_m of 50 mm. Depending on the hydraulic conductivity this in turn leads to a high flow rate for the constant head test which needs to be managed during field measurements. For the falling head test this means a high amount of water which needs to be added to the pipe. For high hydraulic conductivities, the water level change during the falling head test is fast so that the amount of uncertainties increases due to measuring errors. Further, the existing methods fail to locate the process of colmation. In order to sufficiently describe colmation a vertical resolution of the data is required. Therefore, an innovative method is introduced in this study to measure the hydraulic conductivity in a gravel bedded river and in a vertical profile. This enables the detection and location of colmation processes.

3. METHODS

In this study four different parameters are determined in order to assess colmation processes in riverbeds. The parameters *grain size distribution*, *porosity*, *concentration of dissolved oxygen* and *hydraulic conductivity* are chosen based on an intensive literature research to describe colmation effects. Since colmation takes place below the sediment surface a vertical resolution of single parameters is worthwhile to exactly detect the location of colmation horizon. Therefore, this study intends to develop new methods which on one hand are able to describe colmation and on the other hand are measured in a vertical profile allowing detailed information regarding colmation extend and colmation depth. Therefore, a new method for determining the hydraulic conductivity in a vertical profile is developed and tested in this study. Additionally, a new method to determine porosity based on a photogrammetric approach is developed and introduced in this study. Both newly developed methods as well as the existing methods to take sediment samples and to measure dissolved oxygen concentration is explained in detail in this chapter.

3.1 Sediment samples and grain size distribution

3.1.1 Sediment sampling with the freeze core technique

Sediment samples are taken with the freeze core technique as described in chapter 2.3.1. In this study the core is driven in the riverbed until a depth of 50 cm is reached. The core is flushed with liquid nitrogen for approximately 20 - 30 min (depending on outside and water temperature and grain size distribution) to ensure sufficient time for the sediment to be frozen. A tripod with a chain hoist is placed around the core and connected to it. The frozen sediment sample can finally be extracted using the chain hoist (Figure 3.1). The samples can be visually observed and in case of visible stratifications of the material the sediment samples are separated according to the stratification. The frozen sediment sample is further used for porosity analysis (see chapter 3.2) and transported to the laboratory afterwards. After thawing the sediment sample is dried and sieved in the laboratory for further analysis.

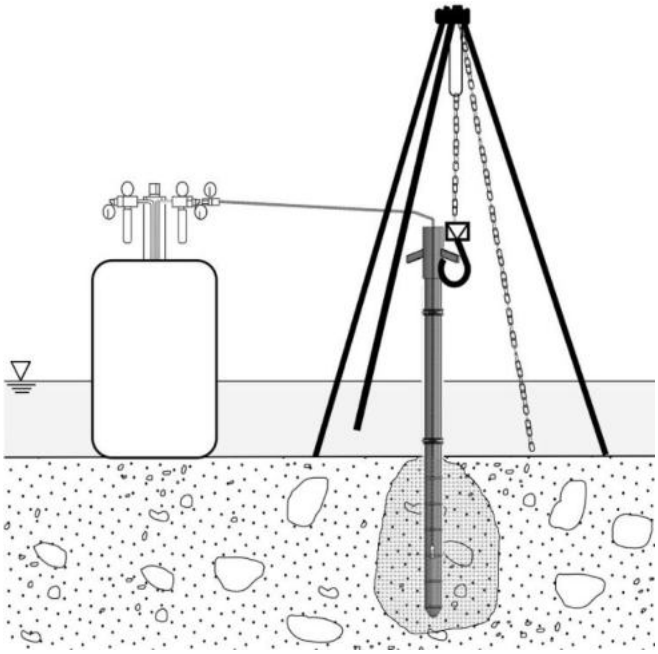

Figure 3.1: Sediment sampling using the freeze core technique showing the set-up in the river.

3.1.2 Grain size distribution

Sediment samples are dried in an oven with 105°C for 24 h (DIN 1996) to ensure that the pore water is fully dried. After drying the samples are dry sieved according to the Wentworth scale (Wentworth 1922, see chapter 2.3.1) in integral numbers of the φ scale (64 mm, 32 mm, 16 mm, 8 mm, 4 mm, 2 mm, 1 mm, 0.5 mm, 0.25 mm, 0.125 mm).

Based on the sieving results the frequency distribution and the cumulative sieving curve are derived. Further statistical parameter and percentiles such as the D_{10}, D_{16}, D_{25}, D_{50}, D_{60}, D_{75}, D_{84}, D_{90}, D_m, D_g and Skewness are derived from the sieving results. Based on the statistical parameter, indirect sediment related parameters such as the uniformity coefficient C_U, the geometric standard deviation σ_G, sorting index SO and the Fredle-index FI are further derived from the different percentiles. In a next step the grain size distribution and its deriving percentiles can be used to estimate porosity and hydraulic conductivity based on different empirical formulas as described in chapter 2.3.2.

3.2 Porosity using Structure from Motion with Multi View Stereo

The common method to determine porosity of riverbed sediments is the water replacement method (WRM) as described in chapter 2.3.2 (e.g. Frings et al. 2011). Since this method is labor intensive and requires special equipment like a diving bell when applied under water a new method is introduced in this study, which is based on a photogrammetric approach. A brief description of the operating principle of SfM-MVS is given in the following section followed by an introduction of the image acquisition and determination of the total volume of a sediment sample as well as a brief overview of the applied software.

SfM-MVS requires multiple overlapping photographs of an object from different perspectives (multiple viewpoints) to resolve a three-dimensional model of the object (e.g., Westoby et al., 2012).SfM-MVS photogrammetry can be performed with consumer-grade cameras, requires no expert supervision (Micheletti et al., 2015), and is therefore extensively employed in various fields of application (Westoboy et al., 2012; Eltner et al., 2016; Smith et al., 20162015) . Eltner et al. (2016) provides an overview of the merits and limits of SfM-MVS, including different fields of application such as the generation of digital elevation models (DEM) with unmanned airborne vehicles (UAV).SfM-MVS differs from traditional stereoscopic photogrammetry in that it automatically computes camera position and orientation (Snavely et al., 2008; Westoby et al., 2012). Overall, five steps are necessary to produce a high quality 3D model of an object or surface during the processing of digital images.

First, high resolution images must be acquired with sufficient overlap to generate a high-quality model. Second, the software detects features on overlapping images, which are invariant to scaling and rotation effects (e.g., Westoby et al., 2012). With a scale invariant feature transformation (SIFT, Lowe, 1999), the spatial relationship between the image location in a coordinate system is established (Micheletti et al., 2015). These ‘key points’ are detected for all images and are used to determine the exact camera position. A sparse point cloud (Figure 3.2a) consisting of tie points (points that tie one image to another) is created out of the key points by a sparse bundle adjustment (Snavely et al., 2008), resulting in their 3D location (Micheletti et al., 2015). In the third step, the sparse cloud is intensified by applying Multi View Stereo techniques (MVS, e.g., Furukawa and Ponce, 2010; Westoby et al., 2012; Micheletti et al., 2015), resulting in the dense point cloud (Figure 3.2b). The fourth step includes a triangulation of the dense cloud, which leads to the 3D-mesh of an object or a surface (Figure 3.2c and d). Finally, the pixel-based 3D model is transformed to a metric coordinate system using scale bars that are placed in the 3D model.

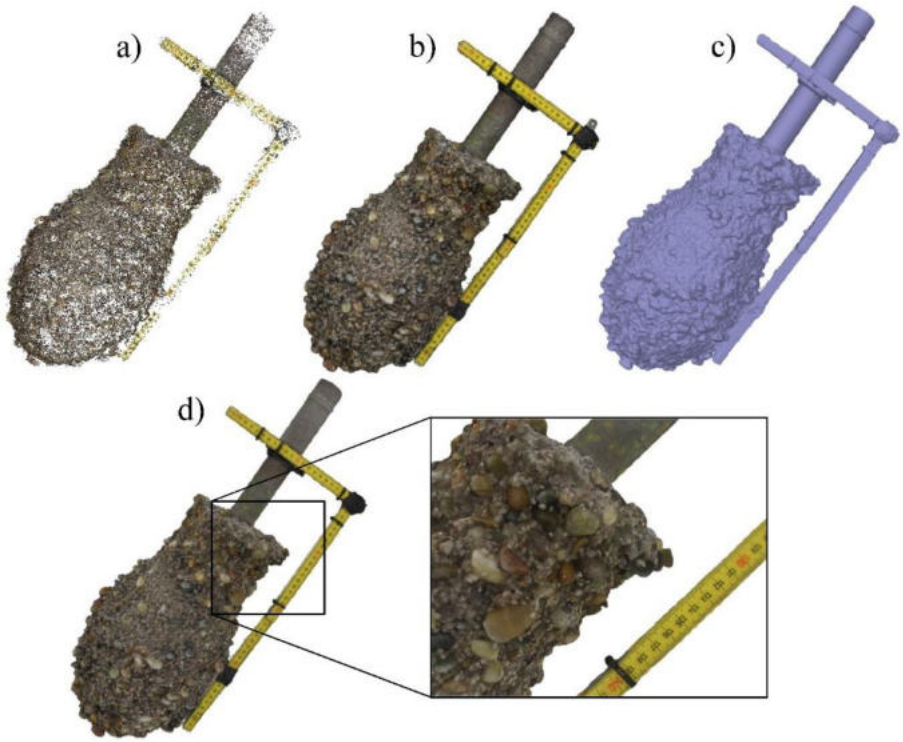

Figure 3.2: Five steps of the SfM-MVS procedure to create a detailed 3D model of a frozen sediment core including (a) sparse cloud, (b) *dense* cloud, (c) triangulated mesh, and (d) 3D model with texture including two scale bars for later transformation to a metric

3.2.1 Determination of V_{tot}

To ensure sufficient image acquisition, preliminary studies have been conducted to optimize the setup for image acquisition (Klopfer 2016). This also includes the development of a method to acquire images rapidly in order to avoid the melting of the frozen sediment sample. Initial tests show that rotating the sample instead of the camera during image acquisition produce higher model quality because lighting conditions remained constant. Therefore, the frozen sediment sample is fixed with V-clamps on a wooden frame in a horizontal position to enable rotation around the longitudinal axis of the core (Figure 3.3). Different camera positions and image quantities are tested to obtain the best model quality. Five camera positions are determined to produce the best results for a frozen sediment sample with an average length up to 0.5 m. Fewer camera positions result in reduced model quality since heterogeneities are not detected sufficiently, whereas increasing the number of camera positions does not significantly increase the accuracy of the model (Klopfer 2016). One position is located in front of the sample, while the other four positions are located at different angles along the axis of the sediment core to cover its heterogeneous topography (Figure 3.3). For each of the five camera positions, the sample is rotated after taking an image and approximately 20 images are taken at each position. This corresponds to a rotation angle of 18° for two consecutive images and guarantees sufficient image overlap. The procedure is repeated for all positions. Additional images of the scale bars that are required for a metric transformation are taken to improve the model quality, leading to a total of 100-120 images. It is determined that scale bars should be oriented in at least two

directions to increase precision (Klopfer, 2016) (Figure 3.3). These scale bars are firmly fixed on the core allowing the scale bars to rotate with the sample. The background in the sediment images can produce problems because it remains fixed while the sediment sample rotates, causing the program to detect features on the sample and on the background and preventing it from generating a 3D model. To avoid this issue the background of the sample is covered with white boards and the remaining background is masked in a post processing step in the software.

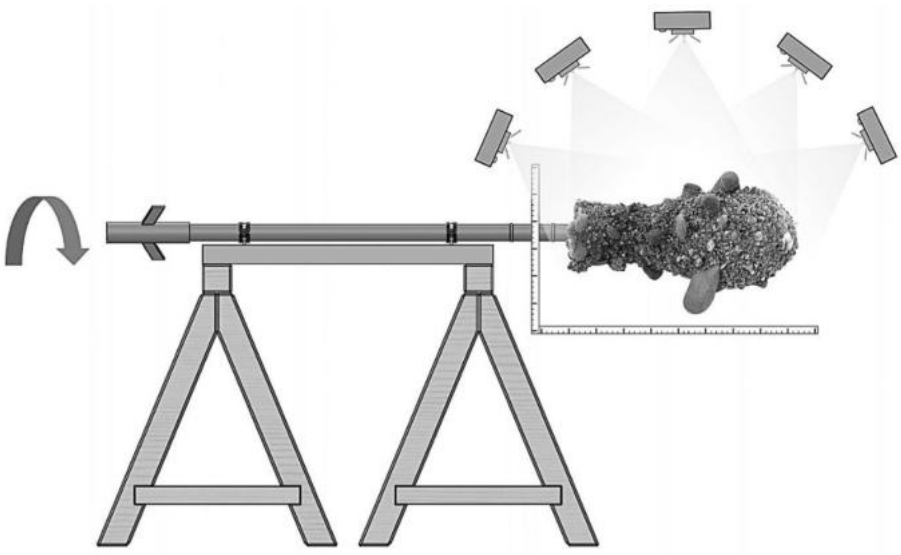

Figure 3.3: Experimental set-up for image acquisition of frozen sediment samples to apply SfM-MVS for determining the total volume of the sediment sample including the recommended five camera positions.

3.2.2 Software Photoscan (Agisoft)

The software Photoscan (Version 1.3.1) from Agisoft is used to generate the 3D-models in which V_{tot} is assessed. The set-up which is generally used in Photoscan is summarized in The *key point limit* and the *tie point limit* are adapted when necessary to improve the model quality. Other configurations are tested without showing high sensitivity to the variations and kept constant for the single steps.

Table 3.1: Set-up of parameters used in Photoscan (Version 1.31) for generation of the model

Workflow	Parameter	Setting
Align Photos		
	Generic preselection	Activated
	Reset current alignment	Activated
	Key point limit	0 or adapted according to the model
	Tie point limit	0 or adapted according to the model
	Constrain features by mask	Activated
	Adaptive camera model fitting	Activated
Build Dense Cloud		
	Quality	High
	Depth filtering	Mild
	Calculate point colors	Activated
Build Mesh		
	Surface type	Arbitrary (3D)
	Surface data	Dense Cloud
	Face count	Medium
	Interpolation	Enable (default)
	Calculate vertex colors	Activated
Build Texture		
	Mapping mode	Generic
	Blending mode	Mosaic (default)
	Texture size/count	4096*1
	Enable hole filling	Activated
	Enable ghosting filter	Deactivated

3.2.3 Determination of V_{Se} and porosity

The water replacement method (WRM) is used for the determination of V_{Se}. Therefore, the dried sediments are added to a water filled tank with a known cross sectional area and the rise in water level is detected using an ultrasonic sensor (Pepperl+Fuchs, UB500-18GM75-U-V15, resolution of 0.1 mm). In contrast to Equation (2.13, the porosity formula using freeze core samples is adapted to account for the volume expansion, when water is changing from the liquid to the solid phase. According to Kell (1975), the volume expands by 9.17 % from water to ice, which is considered for the porosity calculation in Equation (3.1.

$$n = 1 - \frac{V_{Se}}{V_{tot} - (V_{tot} - V_{Se})0.0917} \tag{3.1}$$

Where V_{tot} is the total volume of the sample and V_{Se} is the volume of the sediment.

3.3 In-situ measurement of slurping rates for determination of vertical profiles of hydraulic conductivity (VertiCo)

In this section a new method is introduced to measure in-situ **vert**ical profiles of hydraulic **co**nductivity (VertiCo) of riverbed sediments. The method is based on an existing method introduced from Terhune (Terhune 1958). The major difference to Terhunes (1958) Mark VI groundwater standpipe (see chapter 2.3.3) is the use of a deep double packer, enabling to vary the position within the standpipe and thus measure a vertical profile.

3.3.1 Equipment used for the VertiCo method

Standpipe

In order to conduct in-situ measurements of hydraulic conductivity a steel pipe is used as filter standpipe. After several optimization steps a final set up is developed which can be applied for fine and coarse sediments. The final steel pipe is 1.15 m long and has an outer and inner diameter of 45 mm and 35 mm, respectively. Perforations with 10.5 mm diameter are distributed longitudinal along the filter to allow for water infiltration into the filter (see Figure 3.4). There are two holes of the opposite of the filter with a longitudinal distance to the next position of approximately 3.0 cm. In total 15 positions can be measured with this standpipe with a resolution of 3.0 cm. The holes are covered with two different kind of metal mesh. The fine mesh (Figure 3.4d) prevents fine sediments from infiltrating into the standpipe. A coarser mesh is fixed on top of the fine mesh to prevent it from destruction during introduction, operation or removal of the riverbed. A tip is added to the filter allowing the filter to be hammered into the riverbed material. With this set-up the filter is robust against pounding it into the sediment and a vertical resolution of approximately 3.0 cm can be reached.

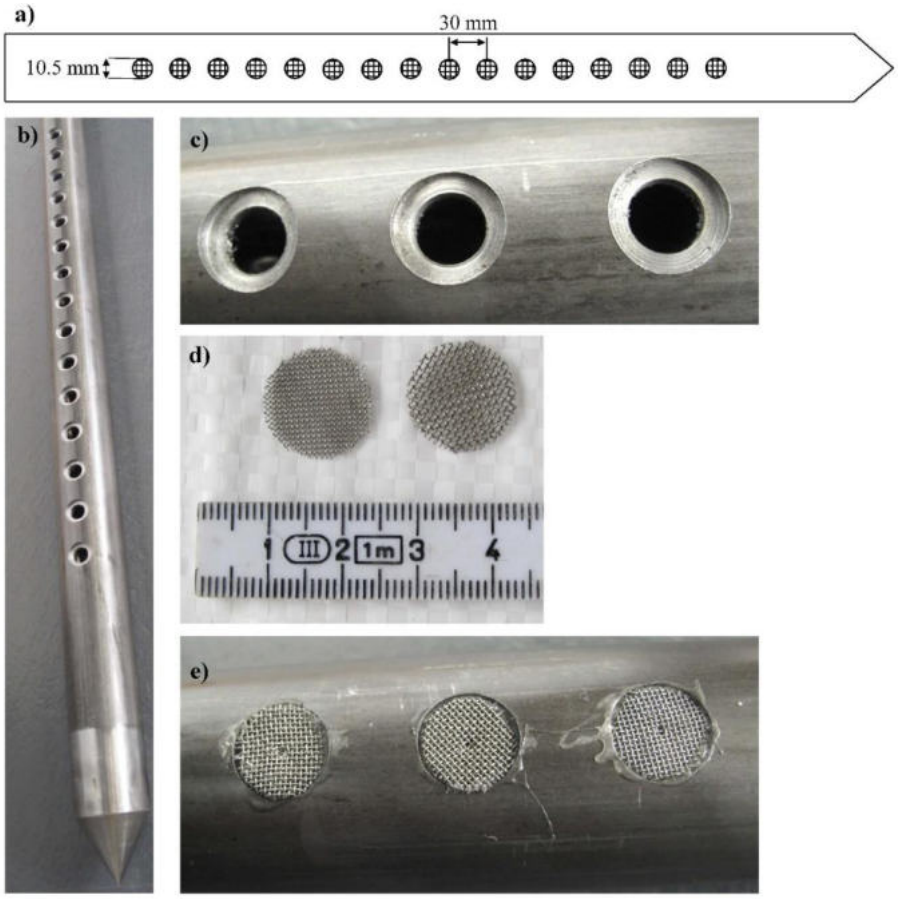

Figure 3.4: Set-up of the optimized standpipe a) schematic sketch of the standpipe b) standpipe without covering of the openings c) close up from the openings with the lowering for the mesh to be fixed d) fine mesh on the left side to prevent fine sediments to enter the standpipe and coarse mesh on the right side to protect the fine mesh from destruction e) example of glued mesh in the standpipe.

Double packer

The double packer consists out of two rubber segments (8.5 cm length each of it), which are placed on a metal stick (1.25 m total length) as displayed in Figure 3.5. On top of the upper rubber segment a second steel bar goes until the top of the packer. The double packer is placed inside the filter and by squeezing the second bar using a screw the two rubber parts of the packer expand and therefore seal the filter to the top and the bottom. The space between the two packer parts forms a chamber with a height of 2.5 cm as displayed in Figure 3.6. The chamber of the double packer is placed to cover an opening of the filter so that water can infiltrate into the chamber from the surrounding aquifer. The position of the double packer can be adjusted and placed at different depths within the filter. Four air ventilation hoists connecting the surrounding atmosphere with the chamber leading to atmospheric pressure in the chamber. Since the water level in the air ventilations will adjust according to the surrounding water level, check valves are installed at the end of the air ventilations to prevent water from flowing inside the hoists after the measurements.

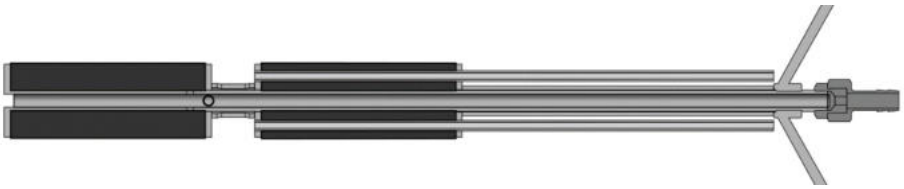

Figure 3.5: Schematic sketch of the deep double packer.

3.3.2 Experimental procedure

The filter is hammered into the riverbed until a depth of 45 cm and the double packer is placed inside the filter and fixed so that the chamber covers one of the openings of the filter (Figure 3.6). A five litre glass flask and a vacuum pump are connected to the double packer. The vacuum pump pumps the water which infiltrates into the chamber into the flask. Water is infiltrating into the chamber depending on the surrounding hydraulic pressure and the surrounding material. In case of coarse material in the surrounding of the standpipe more water infiltrates into the chamber compared to fine surrounding material. Since the chamber is connected to the surrounding atmosphere with the ventilation hoists, air can enter the chamber which leads to a mixed outflow including water and air which can be recognized by a typical slurping sound. Since remaining water is in the chamber and to some extend in the air ventilations it takes some time until slurping starts (slurping phase). The time before slurping starts the pump extracts water from the chamber only depending on the power of the vacuum pump due to negative pressure and sucks the water from the surrounding area (sucking phase). With initiating slurping phase water only infiltrates due to gravitational forces. As soon as slurping state is steady the time for a certain volume is measured. Since volume detection by eye is rather inaccurate the weight of the water is measured using a balance. Weight is then linearly transferred to volume and the slurping rate is determined. The change of weight is detected and recorded with a computer program enabling the observation of temporal trend from the slurping rate.

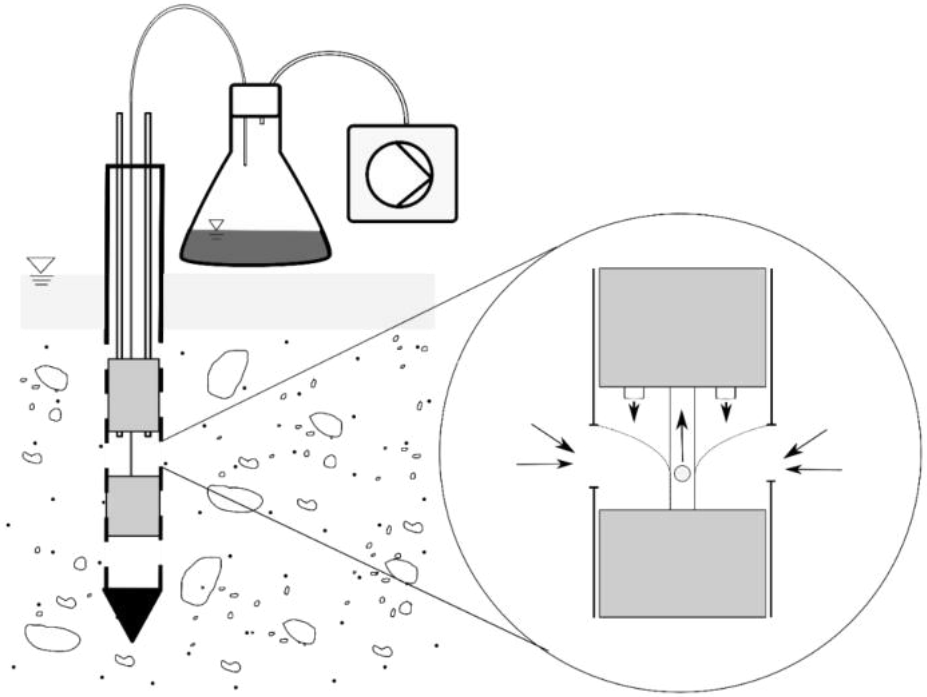

Figure 3.6: Set up of double packer with filter in riverbed and connection to flask and vacuum pump.

The position of the double packer can be varied within the standpipe in different depths enabling the measurement of a vertical profile with a vertical resolution of 3.0 cm. It is necessary to place the double packer correct in order not to block an opening and thus reducing the infiltrating area. Marks are placed on the steel bar to ensure correct positioning of the double packer in the standpipe.

3.3.3 Conversion of slurping rates into hydraulic conductivity using a groundwater model

This method results in different slurping rates for different material. Fine material shows low slurping rates compared to coarse material since only few water infiltrates into the chamber. For transferring slurping rates into hydraulic conductivities Terhune (1958) uses a correlation curve, where slurping rates are correlated with actual hydraulic conductivities (Figure 3.7). However, this method does not consider the influence of hydraulic head on the slurping rate for varying hydraulic conditions. The hydraulic head consists of two parts, the water level and the sediment depth into which the standpipe is driven. Both parameters have a significant influence on the slurping rate (see chapter 6.3).

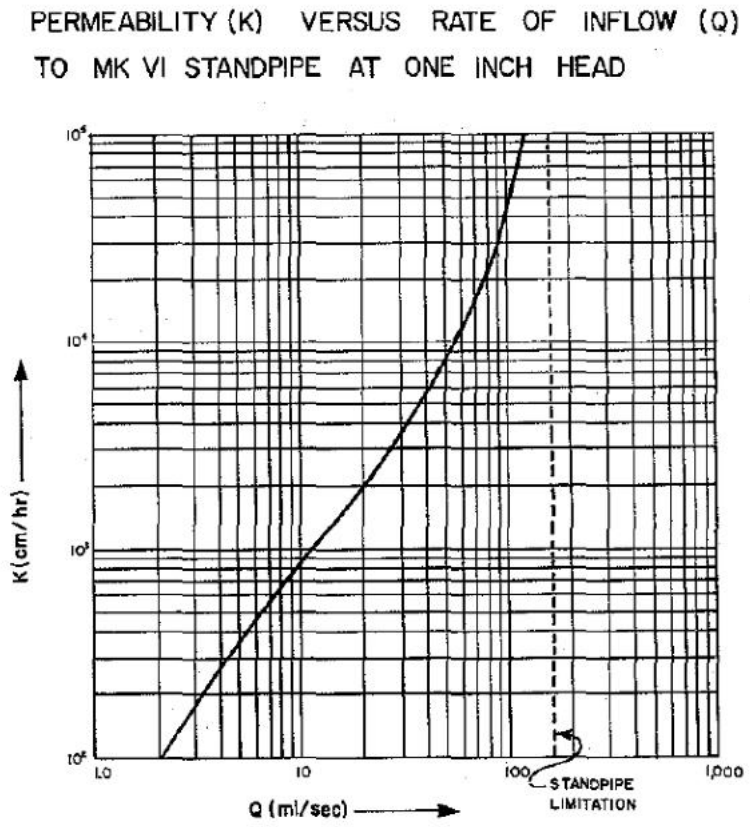

FIG. 6. Permeability (K) versus rate of inflow (Q) to Mark VI Groundwater Standpipe at one inch head.

Figure 3.7: Correlation curve for hydraulic conductivity and slurping rate according to Terhune (1958).

In this study a groundwater model is established to calculate k_f values based on measured slurping rates. In this way, the hydraulic conditions are considered leading to more reasonable results. The widely used MODFLOW-2005 (Harbaugh 2005) is used, which is a three-dimensional finite-difference groundwater model. The original groundwater model only solves the Darcy equation which is valid for low flow condition with Reynolds numbers below 10. However, especially in the hyporheic zone, where colmation takes place, turbulent conditions with Reynolds numbers above 10 occur and thus Darcy´s Law is not valid anymore. For Reynolds numbers above 10, inertial effects in the pores are not negligible and need to be considered using the Forchheimer equation:

$$\nabla h = -av - bv|v| \qquad (3.2)$$

Where h is the total hydraulic head [m], v is the Darcy velocity [m/s], a [s/m] and b [s²/m²] are Forchheimer coefficients. For low Reynolds numbers the quadratic term in the Forchheimer equation is negligible and turns the equation into Darcys Law.

In literature several approaches can be found to estimate the coefficients *a* and *b*. Some of the existing approaches are summarizes in Table 3.2. The Forchheimer coefficient *a* is the invers of the hydraulic conductivity k_f, thus it can also be estimated by an empirical approach to calculate hydraulic conductivity as introduced in Table 2.10 (chapter 0).

Table 3.2: Summary of approaches to estimate Forchheimers coefficients *a* and *b* from literature.

Equation	No. of equation	Reference
$a = \frac{\vartheta}{g\ k} = \frac{1}{k_f}$	3.3	Ward (1964)
$b = \frac{10.44}{g\ D}$	3.4	Ward (1964)
$a = \frac{150\ \vartheta\ (1-n)^2}{g\ n^3\ D^2}$	3.5	Ergun (1952)
$b = \frac{1.75\ (n-1)}{g\ n^3\ D}$	3.6	Ergun (1952)
$a = \frac{6570\ \vartheta\ (1-n)}{g\ D^2}$	3.7	Hill and Koch (2002) Valid for 10 < Re < 80
$b = \frac{98.1\ (n-1)}{g\ D}$	3.8	Hill and Koch (2002) Valid for 10 < Re < 80
$a = \frac{8316\ \vartheta\ (1-n)}{g\ D^2}$	3.9	Hill and Koch (2002) Valid for Re > 80
$b = \frac{88.65\ (n-1)}{g\ D}$	3.10	Hill and Koch (2002) Valid for Re > 80
$a = 0.003333\ D^{-1.500403} n^{0.06035}$	3.11	Sidiropoulou et al. (2007)
$b = 0.194325 D^{-1.265175} n^{-1.141417}$	3.12	Sidiropoulou et al. (2007)

Sidiropoulou et al. (2007) summarizes Forchheimer coefficients *a* and *b* from other studies with the corresponding grain size distribution and sorting index. The Forchheimer coefficients from this study are calculated with the different approaches according to Table 3.2 and compared to

the summary of Sidiropoulou et al. (2007). Based on this comparison the approach according to Ward (1964) is in best agreement with the data found in literature. Thus, the Forchheimer coefficient *b* in this study is estimated using equation 3.4. Forchheimer coefficient *a* is calculated using the inverse of the Kozeny-Carman equation (equation 2.28 in chapter 2.3.3).

In this study three different version of MODFLOW models are used hereinafter referred as V1, V2 and V3. V1 and V2 only solved the Darcy equation whereas V3 implies the Forchheimer equation. The input of V1 beside the hydraulic boundary conditions is the k_f value and it results in slurping rates. The input of V2 and V3 are slurping rates and the model output is an iterated k_f value valid for laminar flow (V2) and turbulent flow (V3). Table 3.3 summarizes the input and output data respectively for the MODFLOW models V1, V2 and V3. These values are only valid for the current geometry of the standpipe. In case of changes in the design of the standpipe (different size of openings or different mesh material) the values at "Geometry of standpipe" need to be adjusted accordingly.

Table 3.3: Input data of MODFLOW model V1, V1 and V3

Input	MODFLOW model
Geometry of standpipe openings [m]	V1, V2 and V3
General width and length of the system	V1, V2 and V3
Hydraulic conditions: Water level h [m] Sediment depth L [m]	V1, V2 and V3
Hydraulic conductivity kf [m/s]	V1
Slurping rate [m³/s]	V2 and V3
Forchheimer coefficient b/a	V3
Convergence criteria for iteration of Forchheimer´s approach	V3

Calibration and validation of the MODFLOW groundwater model

The MODFLOW model is based on cuboid elements. Since a radially symmetrical flow predominates during the VertiCo measurements around the standpipe, the groundwater model can be simplified by simulating only a certain angle from the circle. In this study a quarter of the circle is used, which means that only a quarter of the slurping rates is entered as input data in order to estimate the hydraulic conductivity. The openings of the standpipe are round and cannot be optimally represented by the cuboid elements of the model. Thus, a calibration is necessary to fit the opening in the model in order to reach the measuring slurping rates. The V1 model is used to fit the simulated slurping rates to measured slurping rates from laboratory experiments. The data from the P2 and the Water level experiment from fine sand are used for the calibration of the opening of the standpipe. The coarse sand from the P2 and Water level experiment is further used for the validation of the simulated slurping rates.

3.4 Intragravel dissolved oxygen saturation

The intragravel dissolved oxygen saturation is measured in-situ by applying a method adopted from Riss et al. (2008). Riss et al. (2008) presents a method where perforated steel tubes are driven into the riverbed, small amounts of interstitial water is withdrawn and the IDOS is measured using an optode. This method is adopted and transferred to the set-up of the double packer method. A measuring chamber including an optode (HACH HQ30d) is connected to the double packer instead of the vacuum pump (see Figure 3.8). The four air ventilation hoists are blocked so that no air from the surrounding can introduce into the chamber distorting the oxygen measurement. Small amount of water (approximately 50 ml - 150 ml) is sucked into the measuring chamber using a syringe. The syringe is used to only withdraw small amounts of interstitial water from the riverbed leaving the surrounding structure undisturbed. As for the slurping rate measurements the position of the double packer can be adjusted by moving the double packer leading to the measurement of a vertical profile of dissolved oxygen concentration. The same positions are used as for the VertiCo measurements allowing a direct comparison from the slurping rates to IDOS. In general, two repetitions are conducted for each measurement helping to identify measuring errors or non-plausible values. For the first measurement an amount of 150 ml is extracted from the interstitial pore space to enable that water which was already in the double packer and in the hoist, is completely replaced by the interstitial pore water. For the first and the second repetitions only 50 ml are extracted in order to avoid extracting water from other layers.

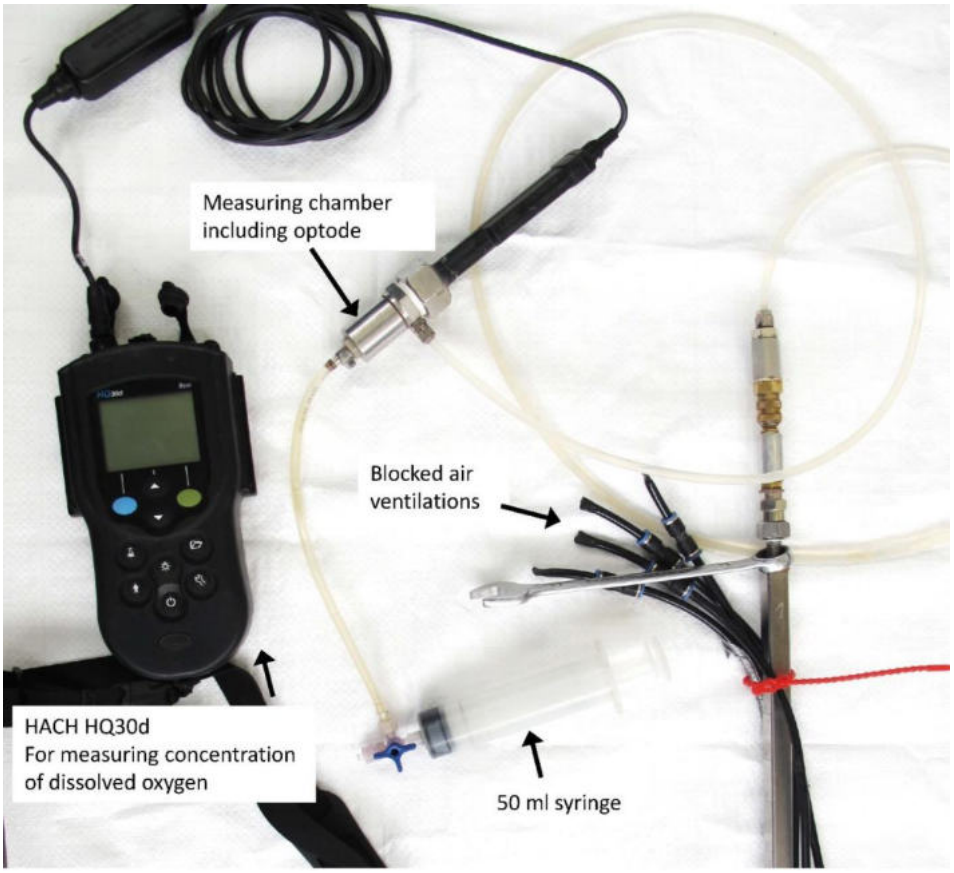

Figure 3.8: Set-up of dissolved oxygen measurement while connected to the double packer.

4. LABORATORY SET-UP AND FIELD APPLICATION

The following chapter presents the detailed laboratory set-up for both newly developed methods *porosity using SfM-MVS* and *hydraulic conductivity using the VertiCo method* as well as information about the study site and the experimental set-up for field applications. For both methods smaller preliminary experiments are conducted in order to evaluate the reproducibility applicability of the methods followed by the main laboratory experiments to prove the functionality and evaluated the accuracy of the method. Figure 4.1 gives an overview of the laboratory experiments in this study, the newly developed methods regarding the determination of porosity and hydraulic conductivity.

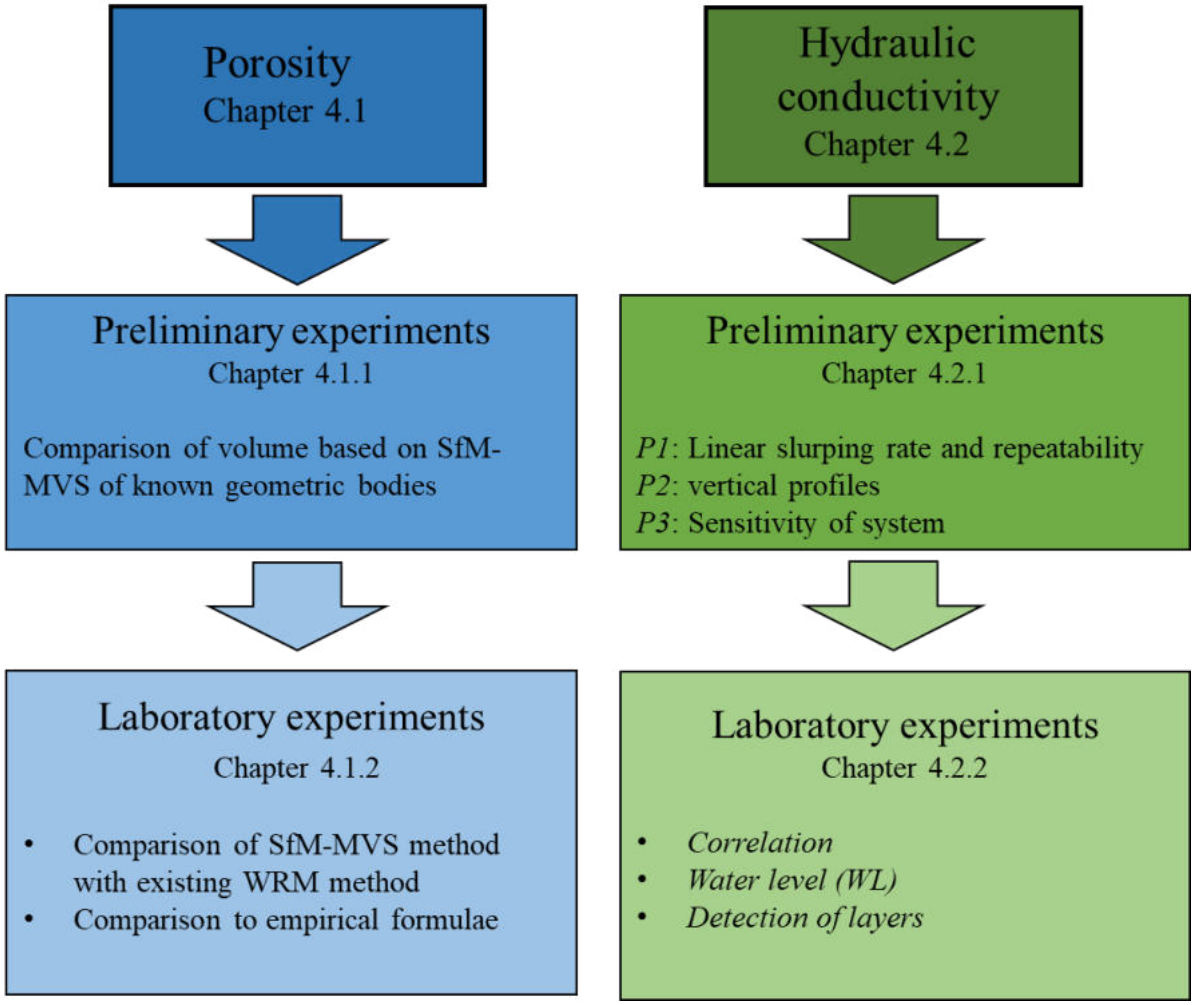

Figure 4.1: Overview of laboratory experiments in this study regarding the determination of porosity and hydraulic conductivity.

4.1 Preliminary tests and laboratory experiments to determine porosity based on SfM-MVS

Since SfM-MVS is an easy to apply method and rather cheap it has a broad range of applications (Westoby et al. 2012; Smith et al. 2015; Eltner et al. 2016). In this study a novel application is tested in order to derive porosity based on sediment samples where volume is estimated based on SfM-MVS. Since this has not been done before preliminary tests need to be conducted in the laboratory to test the procedure with respect to accuracy and applicability.

4.1.1 Preliminary experiments with geometric bodies

The first experiments aim to quantify the accuracy of SfM-MVS for volume detection of simple geometric bodies with known dimensions. Therefore, nine metal and wood bodies (K1-K9) with varying shapes (cylinder, cuboids, and spheres) are tested, ranging in volume from 160 ml to approx. 1700 ml (Table 4.1 and Figure 4.2). The simple geometry allows for the exact volume calculation of the sample. In addition, two artificially-glued sediment samples (SedSa1 and SedSa2), consisting of sand and gravel are investigated in this series of experiments to compare V_{SfM} to V_{WRM}. They are used in order to investigate bodies with complex structures similar to natural sediment samples without the risk of melting the frozen sediment sample. Therefore, bigger particles are glued on a core and a sand-gravel-glue mixture is pressed between the bigger stones in order to seal all pores. Due to this, the artificial sediment samples are not permeable to water and can be used for comparison reasons for determining total volume. The calculated volumes (V_{cal}) of the simple geometric bodies are directly compared to V_{SfM} and to the volumes determined with the WRM (V_{WRM}), while the volumes of the glued sediment samples are compared to WRM only (see results in chapter 5.2).

Table 4.1: Calculated volumes of the geometric bodies.

ID	Description	V_{cal} (ml)
K1	Cylinder	16968.4
K2	Cylinder	9359.1
K3	Cylinder	7787.3
K4	Cuboid	502.2
K5	Cuboid	312.0
K6	Cuboid	1428.3
K7	Cuboid	2858.3
K8	Cylinder	161.0
K9	Sphere	327.3
SedSa1	Sediment sample	-
SedSa2	Sediment sample	-

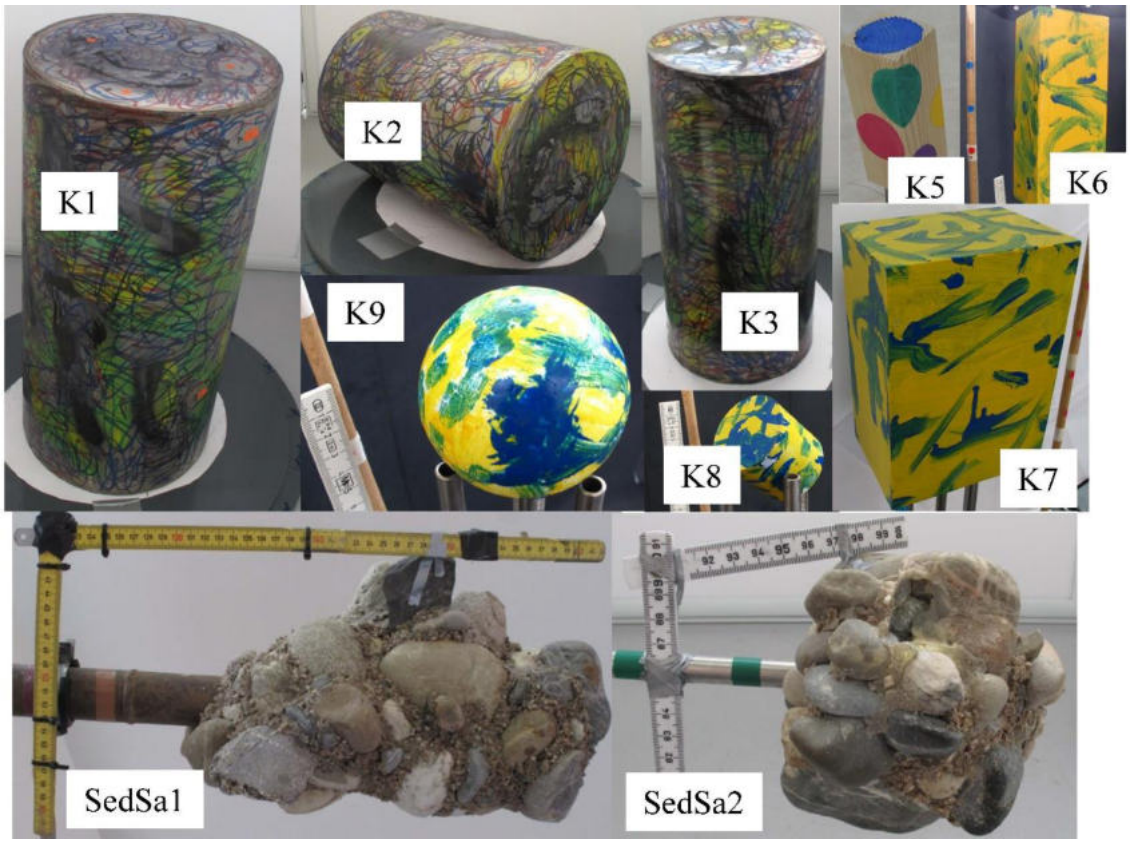

Figure 4.2: Picture of the different geometric bodies used for the preliminary study of SfM-MVS for volume determination.

4.1.2 Laboratory experiments for comparison SfM-MVS method with existing WRM method

Further laboratory experiments are used to test and optimize the developed method. An additional assessment of V_{tot} is conducted applying the commonly used WRM method for comparison and evaluation of the SfM-MVS method. Therefore, identical frozen sediment samples are taken for the assessment of total volume V_{tot} based on SfM (V_{SfM}) as well as for the Water Replacement Method (V_{WRM}), separately. The sediment sample is first used for taking images for SfM-MVS and afterwards it is used for WRM. The total volume V_{tot} of sediment samples and the subsequent specification of the porosity can therefore be used as comparison and evaluation criteria. The difference between both methods is in the evaluation of V_{tot}, as V_{Se} are analyzed for both cases with the WRM. The measurement of V_{tot} can be conducted in the field and in the laboratory whereas the determination of V_{Se} is carried out in the laboratory only after drying of the sediments and sieve analysis.

Applying the WRM a tank (0.4 m diameter and 0.7 m high) is filled with water to a defined level, which is recorded with an ultrasonic sensor (Pepperl+Fuchs, UB500-18GM75-U-V15, resolution of 0.1 mm). The frozen sediment sample is fully submerged in the water and the change in water level is measured with the ultrasonic sensor. Including additional information about the wetted area, the volume can be determined. For the determination of the final volume, the known volume of the core without sediment is excluded from the analysis. Due to the water

temperatures in the tank, the frozen water in the pores starts melting, which affects the total computed volume. Moreover, the melting process starts from the outside of the sediment core and leads to the spalling of grains. The dropped sediments are thus collected separately, dried and weighed, in order to estimate the error caused by the melting process. This aspect is later included in the analysis (see chapter 5.3).

Experimental determination of porosities based on different sediment mixtures

The next series of experiments included porosity measurements for homogeneous sediments and predefined sediment mixtures using SfM-MVS and WRM. Therefore, sediment samples with known grain-size distributions are filled in a cylindrical metal container (0.5 m diameter and 0.6 m height) and submerged with water until saturation is reached. A steel core, marked with a scale, is then driven into the sediments and the core is constantly filled with liquid nitrogen. After approximately 20 minutes, the sample is fully frozen and can be withdrawn from the tank. In total, 15 different sediment mixtures are analyzed in the laboratory, where three to five samples are taken from each mixture for reproducibility reasons. An initial test group (M1) is produced consisting of eight samples to cover a wide range of grain-size distribution. This mixture does not consist of duplicates such as the other mixtures. This results in a total of 65 laboratory samples and is supplemented by 10 freeze cores taken from the field (Naban River, Yunnan Province, Southwest China).

After applying SfM-MVS and WRM to determine V_{tot}, the sediment samples are dried in an oven at 105°C for 24 hours and sieved according the φ-scale (Krumbein 1955): 0.125 mm, 0.25 mm, 0.5 mm, 1 mm, 2 mm, 4 mm, 8 mm, 16 mm, 32 mm, 64 mm, 128 mm. Based on the grain-size distribution, several statistical sediment characteristics were derived such as D_{50} and the geometric standard deviation. Appendix 1.1 provides a table with information about the sediment characteristics of all sediment samples. The sediment samples vary highly in grain-size distribution and also in geometric standard deviation to ensure a broad spectrum of sediment variations. The geometric standard deviation varied from 0.2 – 3.3 and the median grain size varied from 0.29 mm to 80.1 mm.

The determination of V_{Se} is conducted after the sieve analysis with the WRM for both methods. Based on the data, porosity is then calculated using Equation (3.1. For further analysis, all samples are categorized into laboratory and field samples, whereby the laboratory samples are further distinguished between uniform and non-uniform samples based on the geometric standard deviation. Samples with $\sigma_G < 1$ are classified as uniform whereas samples with $\sigma_G > 1$ are classified as non-uniform, resulting in 22 uniform and 63 non-uniform samples (including field samples).

Comparison of measured porosity to empirical formulae

In a final step the mathematical predictors listed in Table 2.9 are applied to compare to the measured porosities with SfM-MVS. Only sediment samples, which are in the range of

application for each predictor (see Table 2.9), are used for this comparison. The results are analyzed for uniform and non-uniform samples as well as for laboratory and field samples separately and discussed in detail.

4.2 Experiment set-up – Hydraulic conductivity

The VertiCo method using a double packer is a newly developed method and thus no reference exists to compare the results. Therefore, some basic preliminary tests are necessary to assess the method and to establish general and reproducible regulations for measuring processes.

These preliminary tests are conducted mainly in the laboratory using two different kinds of experimental tanks. The first tank, further referred to as big tank is a 1 x 1 m steel tank with 1.5m height. It has an outlet in one of the corners. The second tank, further referred to as small tank, is a 0.7 x 1.0 m steel tank with a height of 0.6 m. The correlation experiments are conducted in the small tank; all other laboratory experiments are conducted in the big tank.

Sediments used in laboratory experiments

The laboratory experiments are conducted under controlled conditions in order to keep certain parameter constant and to reduce the complexity as found in natural conditions. An important parameter are the sediment characteristics used in the experiments. Since natural sediments show a high range of variation and heterogeneities, defined sediments are used in the tanks in order to investigate the response of the double packer method on different materials. Three different grain size distributions are available for the laboratory experiments. First, a uniform fine sand with a grain size of 0-1 mm (FS), second a non-uniform sand mixture (coarse sand, CS) with a grain size of 0-8 mm and uniform gravel with a grain size of 2-8 mm (G). For most of the experiments the sediment types are used as single material, except the calibration where mixtures based on the three materials are prepared. The preliminary and the main laboratory experiments are used with the materials described above. For the correlation experiment different mixtures with varying portions of fine sand, coarse sand and gravel are prepared (Table 4.3).

Table 4.2: Sediment characteristics including image and sieve curve from the sediment used in laboratory experiments (fine sand, coarse sand and gravel).

	Fine sand	Coarse sand	Gravel
			
D_m	0.3 mm	2.2	5.7
σ_G	1.0	1.7	0.6
SO	1.7	2.8	1.3

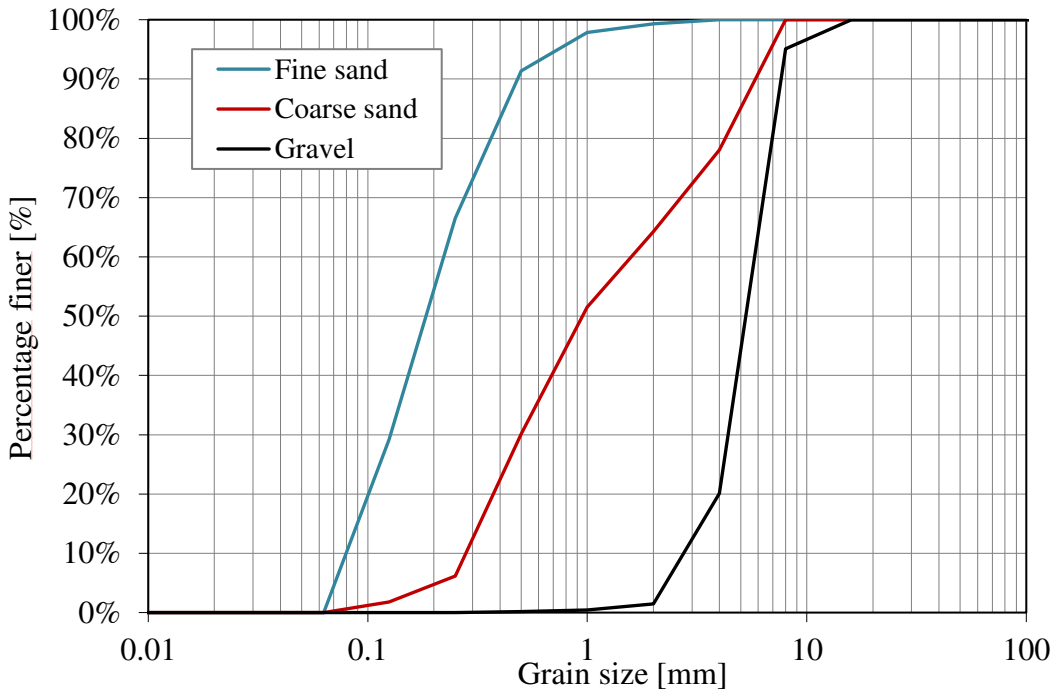

Figure 4.3: Sieve curve from the three different sediments used for laboratory experiments.

4.2.1 Preliminary tests for evaluating the VertiCo method

Before the preliminary test and the laboratory test are conducted a couple of Bachelor and Master Theses are done to test and optimize the new method. Information about these experiments can be found in Eurich (2016), Zaqout (2017) and Wokabi (2018).

Additional experiments are performed in the laboratory to further optimize the method and to provide a proof of concept. In addition to the laboratory study the preliminary experiment P3

and the repetition of P1 are also conducted in the field. These experiments are described in the following section.

P1 Development of slurping rate and repetition of experiments

The weight of the water which is slurped into the glass flask is recorded over time with a computer. The development of slurping rate is analyzed to investigate whether the slurping rate shows a constant value or if it changes over time. First experiments (Zaqout 2017) showed that the slurping rate measured at the same position changes with each repetition. Experiments are performed with a fixed position of the double packer to analyze the slurping rate over time. Up to 15 repetitions per position are conducted to assess the changes in slurping rate. This is conducted in the laboratory with the three different materials and in the field to assess the different behavior in natural systems.

P2 Comparison of vertical profiles under varying substrate conditions

The double packer method aims in detecting different substrate conditions and to differentiate between coarse and fine sediments. To assess the ability of detecting different substrate conditions vertical profiles are measured in different materials in the laboratory. The sediment tank is filled with the material and the water level is kept constant for all experiments. Three profiles are measured for each of the respective material. The experiments are conducted using the fine sand, coarse sand and gravel.

P3 Sensitivity of the systems regarding location of the standpipe

In order to develop a proper measuring process enabling high accuracy and a good reproducibility, tests to verify the measuring process are conducted. Therefore, different ways of repetition are conducted under laboratory conditions as well as in a natural river reach. First three vertical profiles are measured after each other keeping the standpipe at the same location (P3a). Second, three vertical profiles are measured at three different locations of the standpipe in the close vicinity of each other (P3b). Third, one vertical profile is measured with three repetitions at each position of the double packer in the standpipe before moving the double packer to the next position (P3c).

4.2.2 Laboratory experiments for evaluation the VertiCo method

On completion of the preliminary experiments main laboratory experiments are conducted in order to verify the new methods. A correlation curve is established as introduced by Terhune (1958) in order to check to what extend comparable behavior between slurping rate and hydraulic conductivity can be achieved. A further step to validate the method includes the assessment of hydraulic head dependency for different materials and the possibility to detect layers in a vertical profile with different hydraulic conductivities using the double packer.

Correlation

The correlation between slurping rates and hydraulic conductivities is conducted in the small tank in the laboratory. Different mixtures with varying grain size distribution and thus varying k_f values are used for the correlation. In a first step, the slurping rate is measured for the different materials under constant hydraulic conditions. The slurping rates are always measured at two different sediment depth with 19 cm and 22 cm depth a constant and steady water level of 5 cm. In a second step, the hydraulic conductivity is determined using the well-known constant head test in the laboratory as described in the following chapter.

Slurping rates for correlation

In total ten different mixtures are used for the correlation. The mixtures vary from pure gravel material to gravel – sand mixtures. Table 4.3 summarizes the ten different mixtures used for the correlation. Figure 4.4 shows seven different locations in the small tank where measurements are taken. At each location the first and the second position are chosen for the measurements with three measurements at each position leading to a total of 42 measurements for each correlation mixture. This ensures a sufficient amount of measurements and reduces the influence of outliers on the result.

Table 4.3: Gravel-sand mixtures used for correlation experiments

Correlation ID	Parts from coarse gravel (8-16 mm)	Parts from gravel (2-8 mm)	Coarse sand (0-8 mm)
Mixture 1	40 %	60 %	-
Mixture 2	33 %	66 %	-
Mixture 3	30 %	50 %	20 %
Mixture 4	20 %	45 %	35 %
Mixture 5	-	50 %	50 %
Mixture 6	-	40 %	60 %
Mixture 7	-	25 %	75 %
Mixture 8	-	100 %	-
Mixture 9	-	80 %	20 %
Mixture 10	-	75 %	25 %

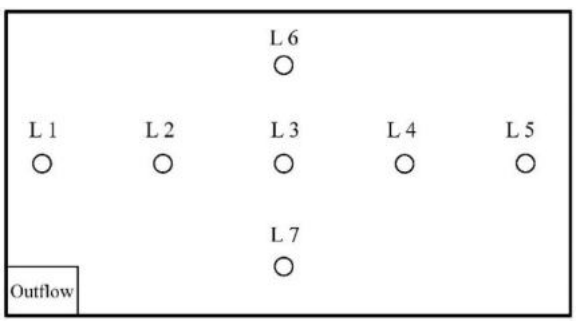

Figure 4.4: Plan view of measurement locations in the small tank for correlation experiments in the laboratory.

Constant head permeability test

The permeability test is based on Darcy´s Law where the hydraulic conductivity expressed as the k_f value is equal to the flow rate through a cross section under a hydraulic gradient (see chapter 0):

A 1.0 m column with a diameter of 0.1 m is used for the constant head tests. The material is added moist and manually compacted with a stamper into the column. The same degree of compaction is strived to be achieved as for the experiments with the slurping rate in the tank. This is later evaluated by determining the packing density of each mixture for the constant head test and for the slurping rate. After filling, the column is flooded with water and flushed with CO_2 in order to displace remaining air bubbles in the column. Three piezometer ports are connected along the column to detect and to read the head differences. Water flows through the column with a constant head. Constant pressure difference is guaranteed due to two reservoirs connected to the column; an adjustable constant head reservoir and an outlet reservoir to maintain the constant head. As soon as steady state conditions are reached the flow through the column is measured for a given time period (Head, 1982).

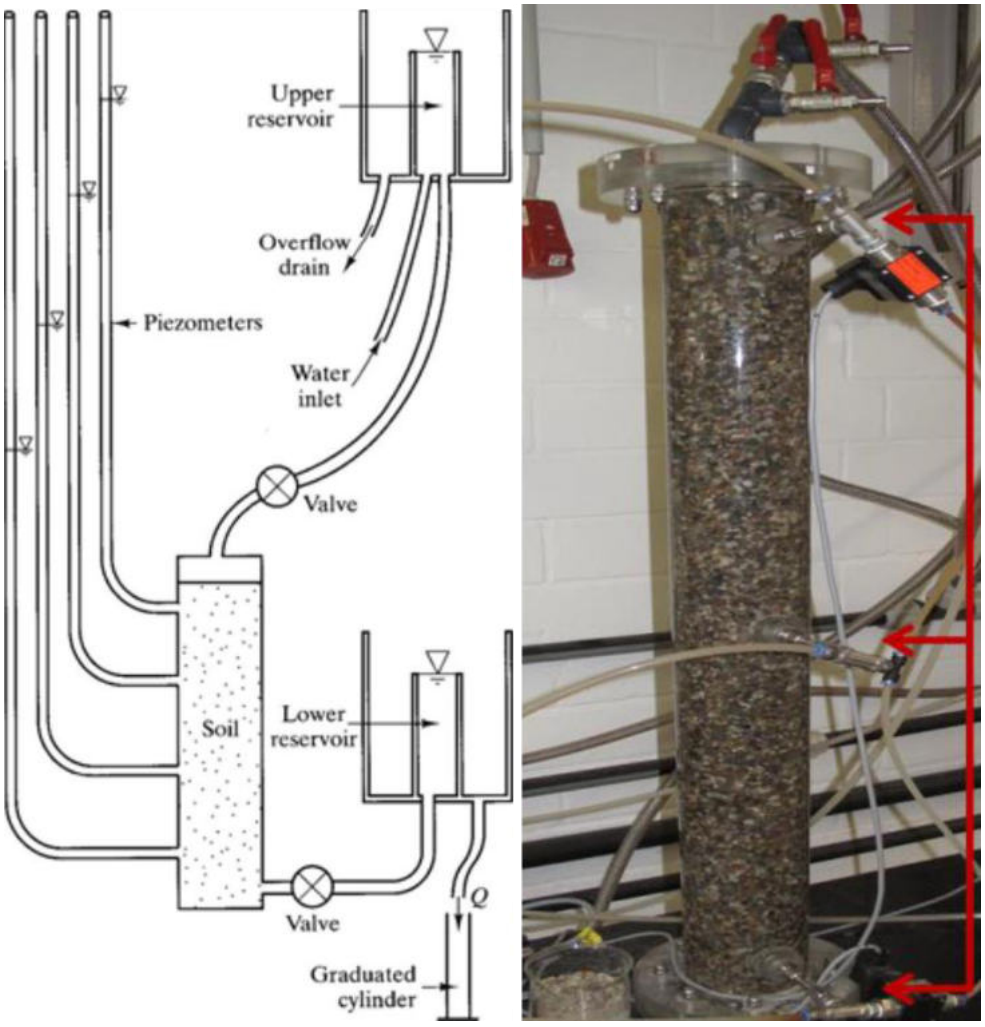

Figure 4.5: Schematic set-up of constant head permeability test (left, Head, (1982) and image from actual laboratory set-up of the laboratory filled with G (right).

Influence of hydraulic head on slurping rate

Previous experiments (Eurich 2016; Zaqout 2017; Wokabi 2018) showed that the hydraulic head strongly influences the slurping rate where an increase of hydraulic head increases the slurping rate. This water level (WL) experiment is repeated for all the three materials using the big tank. The slurping rates at the fixed position of the double packer is repetitiously measured with different water levels starting from an initial water level of 0.05 m and increasing the water level in 5 cm steps for each measurement. Each water level measurement is repeated three times and an average value is taken as final slurping rate.

Detection of layers with varying k_f values

To prove the method and to analyze to which extend layers with different material can be detected from the double packer method different experiments are conducted in the laboratory where layers with varying thickness and varying materials are implemented into the big tank. The basic material for all experiments is fine gravel from previous experiments. As layer with lower hydraulic conductivity the fine sand and coarse sand is used. In total five different experiments are conducted using the lower permeable layer. In a first experiment L1 the fine gravel is filled from the bottom until the middle of the standpipe is reached, a fine sediment layer (fine sand) of 5 cm thickness is added on the gravel and filled up again with gravel until all positions from the standpipe are covered. The fine material layer covers position 8 from the standpipe. In the next experiment L2 the thickness of the sand layer is 10 cm thick and covers three positions of the standpipe (positions 8, 9 and 10). L3 is comparable with L1, and L4 to L2 using the coarse sand material instead of fine sand.

In a fifth experiment L5 a non-permeable layer (pond liner) is added instead of a lower permeable layer which is sealed around the standpipe and sealed around the tank with tape to avoid a hydraulic circuit between the top and the bottom part of the tank. This experiment does not aim to simulate a confined aquifer, since the boundary conditions are not suitable for such an approach. The experiment aims in analyzing the behavior of the vertical profile and the disruption of a non-permeable layer.

4.3 Field applications of multi-parameter approach

After evaluation of new methods in the laboratory the multi-parameter approach is tested in the field. The chosen study sites as well as the general application of the measuring procedure with special regard on the slurping rate experiments is introduced in the following section.

4.3.1 Study site

The field experiments have been conducted in different rivers in South-West Germany (Baden-Württemberg). All investigated rivers and streams are located in the catchment of River Neckar. A total of eight rivers are investigated where all the rivers vary in size, flow regime and substrate composition. Between four to six sampling sites are selected at each river reach. The reaches

are divided into different morphological units such as pool, riffle or run and each unit is investigated. In homogeneous stretches, where no different morphological units are present different sampling sites along a longitudinal direction as well as in cross-sections are selected. This procedure results in a wide range of different conditions, which can also be used to identify relationships to morphological conditions. The following section presents a brief overview of the river reaches and sampling sites.

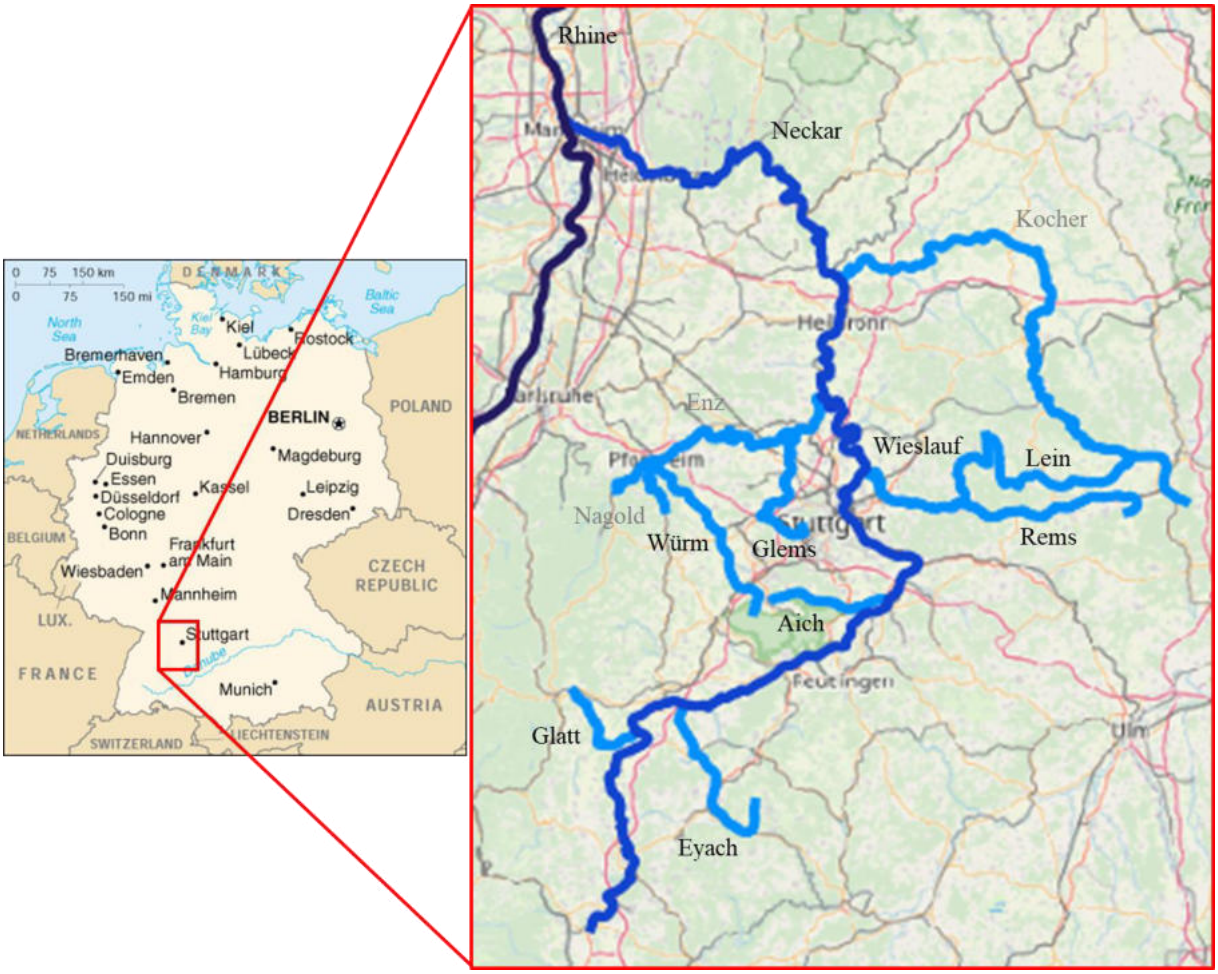

Figure 4.6: Map of Germany (left) and the investigated rivers (right).

Aich

The study site at River Aich is between Waldenbuch and Neuenhaus (48.634335; 9.168185) bordering a forest. The river has steep riverbanks which are mostly covered with vegetation. However, at some spots the bare soil is exposed to the current of the water leading to severe bank erosion and resulting in increased fine sediment intrusion into the river. Figure 4.7 shows an image of the study site to give an impression of the river. Table 4.4 summarizes hydrological information about River Aich and its catchment. The river width at the river reach is approximately 3-4 m wide and the water level varies between 5 cm on the riffle to 30 cm at the pool. High amount of fine sediments is visible on the riverbed which surrounds gravel substrate. The substrate is dense and removing stones from the surface reveals high amounts of fine sediments forming a large fine sediment plume. Four sampling sites have been chosen at River Aich which are presented in Figure 4.8. Two are located in the pool with low flow velocity and high water level (Aich 1 and 2). The other two are located on the riffle with higher slope, high flow velocity and low water level (Aich 3 and 4).

Table 4.4: Hydrological information for study site at River Aich.

River ID	River System	Length	Catchment area	Average slope	MQ at the closest gauging station	Category according to LAWA
DE: 23818	Neckar	30.4 km	179 km²	5.4 ‰	1.33 m³/s	Carbonate, fine material-rich streams in low mountain range (6)

Figure 4.7: Image of study site at River Aich.

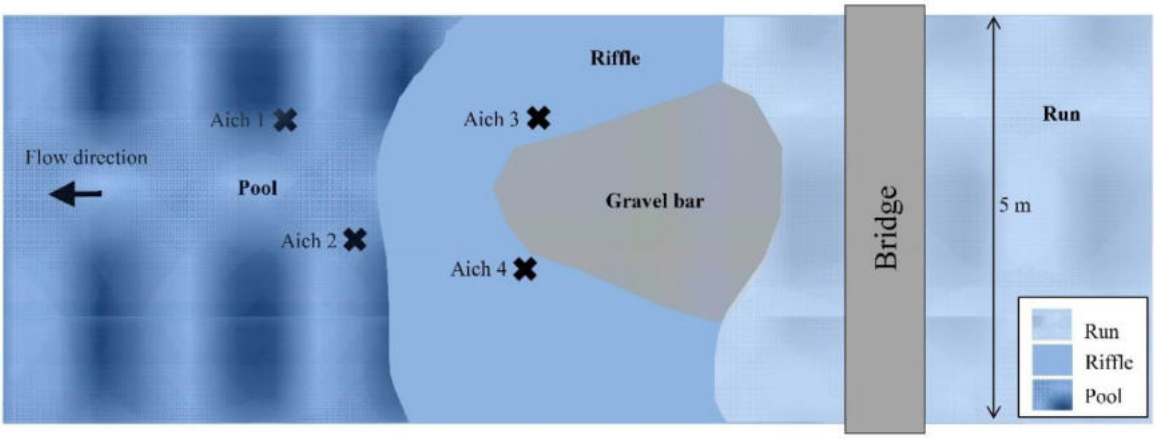

Figure 4.8: Schematic overview of sampling sites at River Aich

Eyach

The river reach of River Eyach is located between Bittelbronn and Trillfingen just upstream of the waste water treatment plant of Trillfingen (48.381194, 8.791721). Meadows dominate the surroundings. Vegetated river banks as well as embankments can be found at this reach. Table 4.5 summarizes the hydrological information about River Eyach. The river at this reach is approximately 5 m wide and the water level varies between 15 – 25 cm. This reach is characterized by clean and loose gravel. Only few fine sediments are mobilized when disturbing the surface layer of the river bed. However, deeper layer of the riverbed reveal higher amount of fine sediments. Four sampling sites have been chosen at this river reach. All of them are located on a riffle with rather high flow velocities and strong current. Figure 4.9 gives a schematic overview of the sampling sites. Site 1 and 4 as well as site 2 and 3 are located in the immediate vicinity, approximately one meter apart.

Table 4.5: Hydrological information for the study site at River Eyach.

River ID	River System	Length	Catchment area	Average slope	MQ at the closest gauging station	Category according to LAWA
DE: 23814	Neckar	50.4 km	349 km²	9.1 ‰	3.22 m³/s	Carbonate low mountain stream (9a)

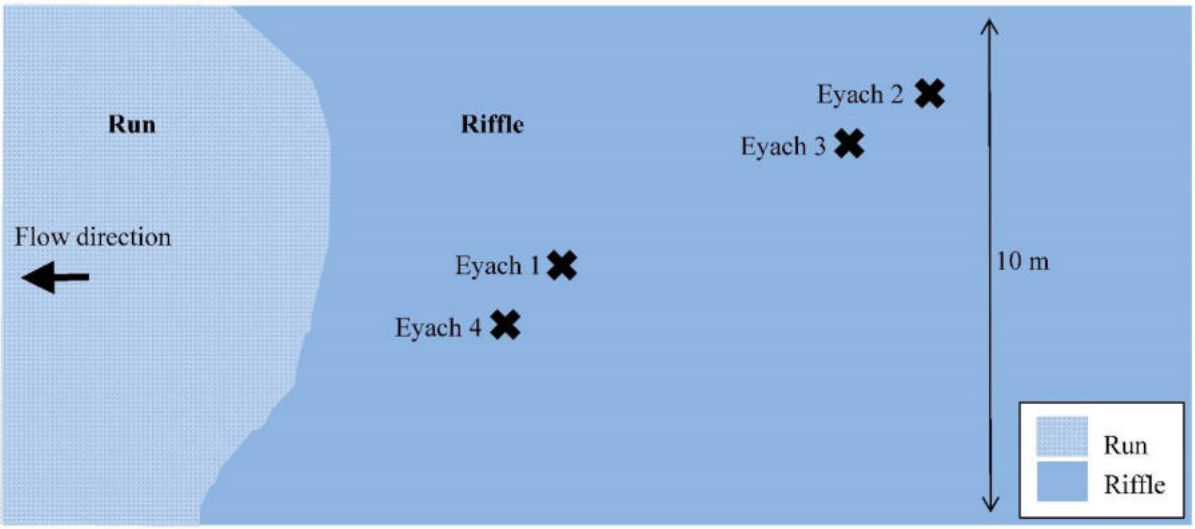

Figure 4.9: Schematic overview of sampling sites at River Eyach.

Glatt

The reach at the River Glatt is app. 200 m upstream of the junction to River Neckar (48.394786, 8.644655). The river width at this location is around 10 m. Embankments on both sites avoid

bank erosion. Dense vegetation covers both sites. The substrate of River Glatt is mainly gravel with some pebbles and boulders. The gravel riverbed is clean and only few fine materials is released when removing grains from the riverbed. In total six sampling sites are chosen in the selected reach, considering the different morphological units. First two sites are located on a riffle in the main stream (Glatt 1 and 2). Another two sites are located further downstream on a submerged gravel bar close to the left river bank (Glatt 5 and 6). Following the flow direction, the two sites furthest downstream are located downstream of a bridge in the middle of the river just behind each other (Glatt 3 and 4) (Figure 4.11).

Table 4.6: Hydrological information for the study site at River Glatt.

River ID	River System	Length	Catchment area	Average slope	MQ at the closest gauging station	Category according to LAWA
DE: 23812	Neckar	34.2 km	234.3 km²	9.2 ‰	4.09 m³/s	n.a.

Figure 4.10: Image of the study site at River Glatt. The image is taken under the bridge including sampling sites Glatt 3 and Glatt 4.

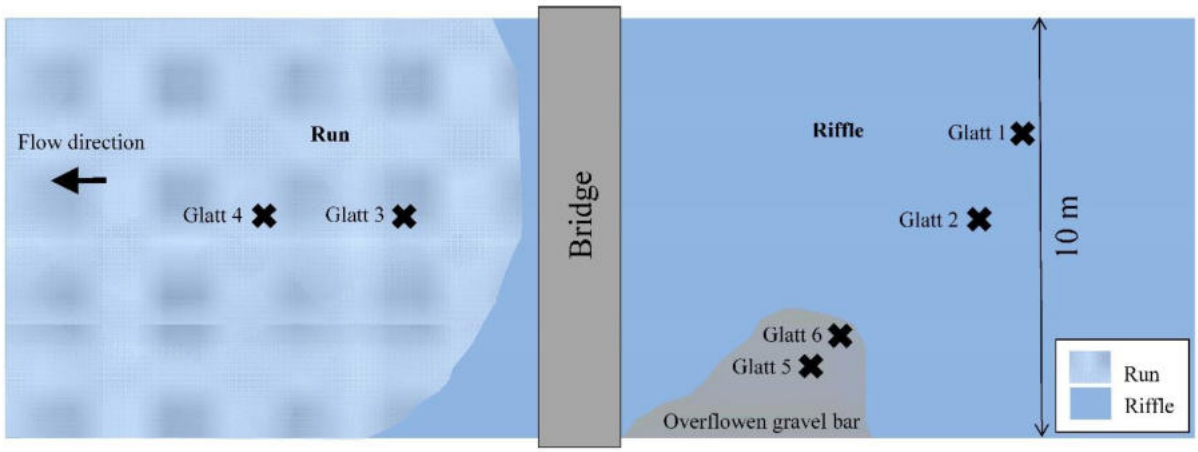

Figure 4.11: Schematic overview of sampling sites at River Glatt.

Glems

River Glems is a small stream flowing mainly through forest and agricultural areas. The study reach is located between Büsnau and Eltingen (48.756649, 9.069512). There are shallow river banks with sparse vegetation cover, thus fines sediments are washed out easily during rain events. Fine sediments from diffuse sources are not retained and get into the river due to missing vegetation cover at the river banks. The river width at the measuring location varies between 3 m to 4 m. The riverbed consists mainly out of fine material. Muddy parts especially close to the river bank are present and only a thin gravel layer can be found in the subsurface layer. However, also high amount of fine sediment is dominating this thin layer. Six sampling sites are chosen at this location. The first site is located at the tail of a pool (Glems 1) the others are located in a riffle (Glems 2 – 6). Glems 2, Glems 3 and Glems 4 are in a longitudinal profile and Glems 4, Glems 5 and Glems 6 represent a cross-sectional profile (Figure 4.13).

Table 4.7: Hydrological information about River Glems.

River ID	River System	Length	Catchment area	Average slope	MQ at the closest gauging station	Category according to LAWA
DE: 23846	Neckar	47 km	195.5 km²	5.4 ‰	1.09 m³/s	Carbonate, fine material-rich streams in low mountain range (6)

Figure 4.12: Image of River Glems including set up for the VertiCo measuring at Glems 1 at the tail of the pool (picture facing upstream direction).

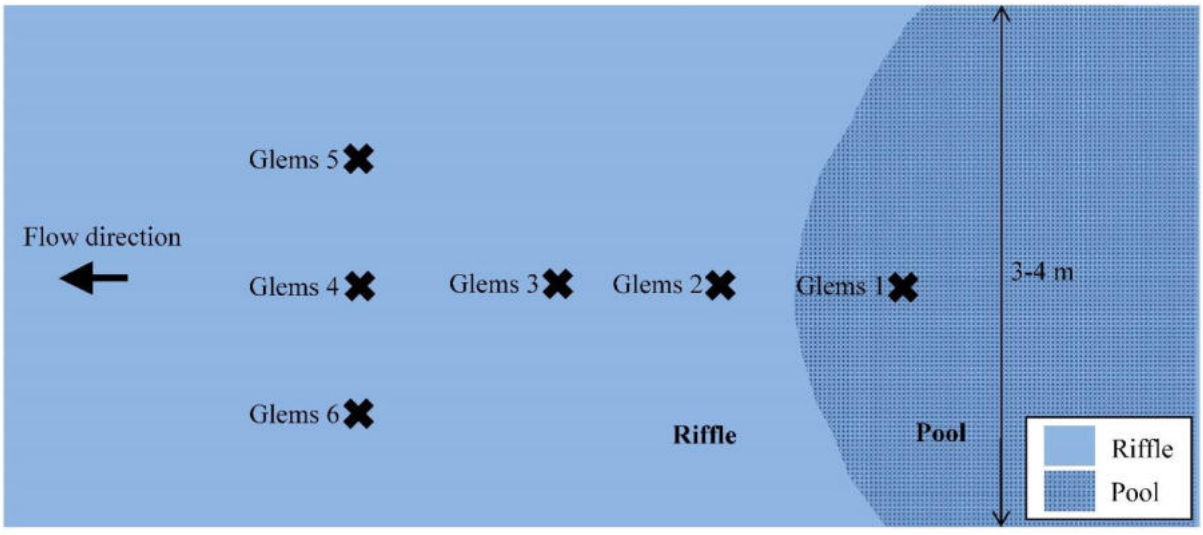

Figure 4.13: Schematic overview of the sampling sites at River Glems.

Lein

At River Lein, two reaches including two sampling sites each are chosen downstream of weirs. The two stretches are several kilometers apart. Downstream of the weirs the river is wider compared to the rest of the river with approximately 15 m width. Forrest and agricultural land surrounds River Lein. Although it has a gravelly riverbed with coarse gravel, an increased proportion of fine sediments can be observed blocking the pore space. This leads to a dense riverbed. At both locations the sampling sites are on a riffle. At the upstream Weir (Mulfingen) the two sites are approximately 5 m apart and at the second weir (Roßnagel) the two sites are approximately 12 m apart.

Table 4.8: Hydrological information about River Lein.

River ID	River System	Length	Catchment area	Average slope	MQ at the closest gauging station	Category according to LAWA
	Neckar	57 km	249.7 km²	3.1 ‰	3.6 m³/s	Carbonate, fine material-rich streams in low mountain range (6)

Figure 4.14: Image of the weirs at River Lein. Left image shows the upstream (Weir Mulfingen) and right downstream Weir Roßnagel.

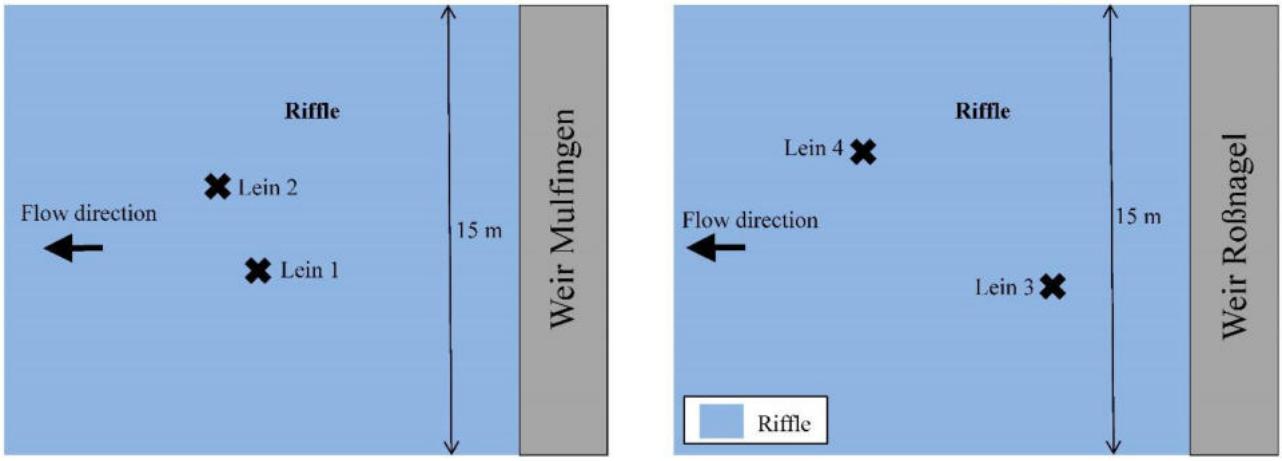

Figure 4.15: Schematic overview of the sampling sites at River Lein.

Rems

The study reach at River Rems is located in Plüderhausen (48.798250, 9.590109). The river in this area is channelized with embankment on both sides of the river. The dominating substrate in this reach is gravel. There is a fine sediment plume visible when disturbing the sediment structure; however, the gravel is loosely packed and easily moved. The reach is at a tail of a pool just at the transition to a riffle. Three sampling sites are in the pool (Rems 5, Rems 6 and Rems 7). Two sites are in the transition zone from pool to riffle (Rems 1 and Rems 2) and two sampling sites are in the riffle (Rems 3 and Rems 4).

Table 4.9: Hydrological information about River Rems.

River ID	River System	Length	Catchment area	Average slope	MQ at the closest gauging station	Category according to LAWA
DE: 23836	Neckar	78.4 km	586.4 km²	4.4 ‰	5.45 m³/s (Schorndorf, 2015)	n.a.

Figure 4.16: Image of River Rems facing downstream direction including measuring set up for Rems 1 and Rems 2.

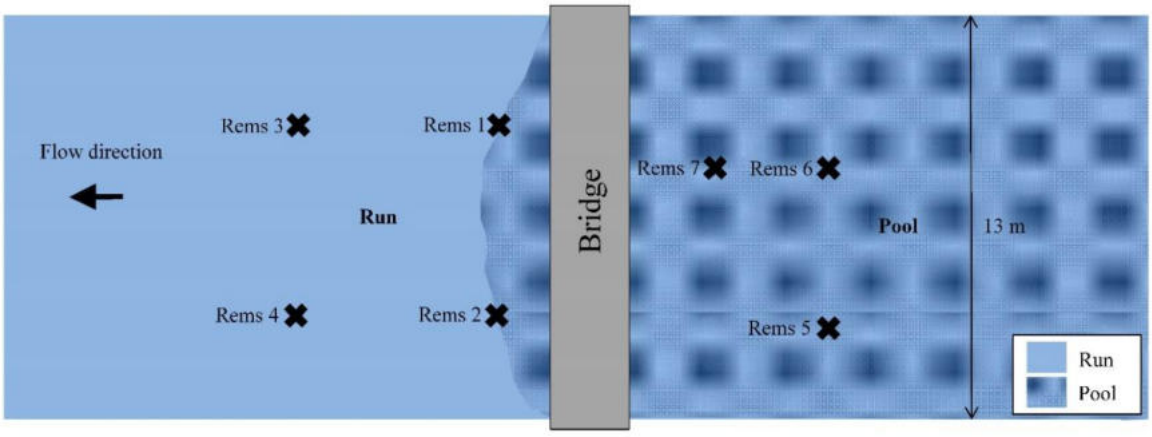

Figure 4.17: Schematic overview of sampling sites at River Rems.

Wieslauf

Wieslauf is a tributary to Rems. It is a small stream with a relatively high slope (12‰ on average). The study reach is located upstream of Oberndorf (48.893043, 9.556021). The riverbanks are not fixed and a dense vegetation cover protects the river banks from bank erosion. The reach holds coarse substrate consisting mainly out of gravel, pebbles and cobles.

There is also high amounts of fine sediments visible when removing grains from the riverbed. The riverbed is densely packed. Five sampling sites have been chosen in the River Wieslauf reach. The first three are located at a downstream section where Wieslauf 1 and Wieslauf 2 are in a riffle and Wieslauf 3 is measured in a pool. Two more sampling sites are located approx. 150 m upstream in a riffle (Wieslauf 4 and Wieslauf 5).

Table 4.10: Hydrological information about River Wieslauf.

River ID	River System	Length	Catchment area	Average slope	MQ at the closest gauging station	Category according to LAWA
DE: 238366	Neckar	23.7 km	77.2 km²	12 ‰	0.92 m³/s (Haubersbronn, 2015)	n.a.

Figure 4.18: Image of River Wieslauf facing downstream direction. Image is taken downstream of Wieslauf 1.

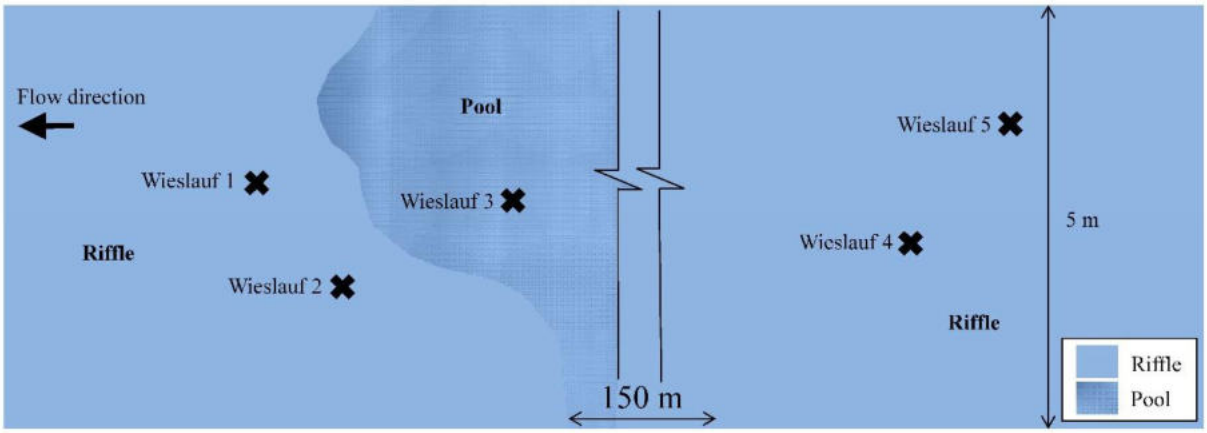

Figure 4.19: Schematic overview of sampling sites at River Wieslauf.

Würm

The study reach at River Würm is located in Merklingen, just outside the village (48.773044, 8.849048). The reach is a straight and channelized stretch, poor in structure, dominated by high and steep river banks, densely covered by vegetation.

The river with is around 13 m wide and the water level is between 20 and 30 cm. The dominating substrate is medium gravel; however, the gravel is packed dense and surrounded by fine sediments.

Since no varying morphological units are present at this river reach the sampling sites are allocated in a longitudinal direction and a cross section is measured as displayed in Figure 4.21.

Table 4.11: Hydrological information about River Würm

River ID	River System	Length	Catchment area	Average slope	MQ at the closest gauging station	Category according to LAWA
DE: 238448	Nagold-Enz-Neckar-Rhein	53.9 km	418.3 km²	4.7 ‰	4.7 m³/s	Carbonate low mountain stream (7)

Figure 4.20: Image of River Würm including set up for the VertiCo measurements at Würm 4 and freeze-core sampling at Würm 1. Image is facing downstream direction.

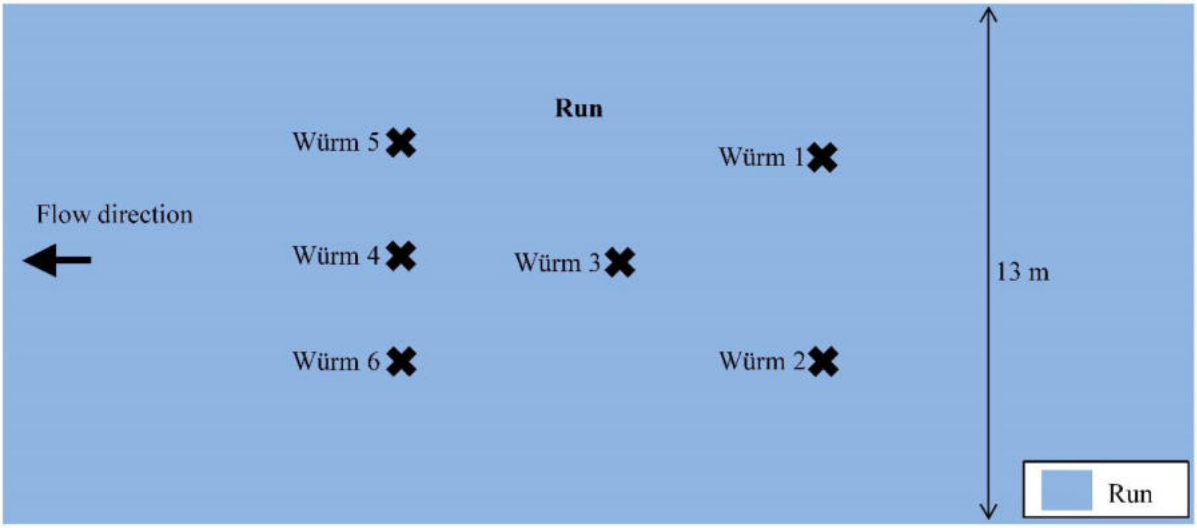

Figure 4.21: Schematic overview of the sampling sites at River Würm.

4.3.2 General Application

After laboratory tests confirmed the validation of the newly developed methods (determination of porosity using SfM-MVS and determination of hydraulic conductivity using the VertiCo method) it is tested in the field. An intensive field campaign is conducted to apply all of the four methods in the field with the overall aim to assess colmation effects. Different rivers are investigated allowing for a broad spectrum of data and thus a high significance of the results. In total eight rivers are investigated (see chapter 4.3.1) which differ in hydrology, slope, grain size distribution and colmation conditions.

Selecting location for measuring within the river

Colmation is a process with high spatial heterogeneity. Morphodynamic and also hydraulic conditions influence the infiltration process and impede the prediction at which specific location in a river reach colmation occurs. Thus, colmation not only varies over cross-section and longitudinal direction but also varies from different morphological units. For example, it tends to increase at pool tails since downwelling condition can enhance the infiltration of fine sediments into the hyporheic zone. In contrast, rivers with upwelling conditions are known to have less colmation effects since fine sediments do not infiltrate into the pore space. For the conducted field campaign four to six location are chosen at each river reach. These locations are distributed over different morphological units such as riffles, pools or runs to cover a broad spectrum of different variations. In case of homogeneous and channelized river reaches different longitudinal and cross-sectional profiles are chosen to investigate.

Order of measurement

As a first step the standpipe is introduced into the riverbed down to a depth of approximately 0.45 – 0.50 m using a sludge hammer. The first measurement is IDOS since it least disturbs the surrounding material and structure. The vertical profile of IDOS is commonly measured by moving the double packer from bottom to top of the standpipe. In some cases with low concentrations of dissolved oxygen the vertical profile was measured from top to bottom. By lifting up the double packer in the standpipe from bottom to top under muddy conditions a negative pressure is observed which sucks mud into the standpipe resulting in clogging of the filter mesh. This behavior is only observed in locations with muddy material. Two measurements of dissolved oxygen are conducted at each position of the double packer before moving to a new position and in case the two resulting value differ from each other a third measurement is conducted. The concentration of dissolved oxygen, the water temperature and the corresponding dissolved oxygen saturation (IDOS) is noted.

The double packer measurements are conducted after the measurements of IDOS. Similar to the measurement of IDOS the double packer measurement starts from bottom to top. Only in cases with high mud content are the measurements conducted from top to bottom. In total 15 positions with a vertical resolution of 3 cm are measured with 3 measurements at each position for each location of the standpipe. The change in weight from the slurped water is recorded for

two minutes after steady slurping conditions are reached. In case of high slurping rates the flask is filled before two minutes are reached reducing the measuring time to 30 - 60 seconds. After finishing the double packer measurement the standpipe is removed from the riverbed and the location is marked with a metal stick enabling to find the location on the following day for further measurements.

The sediment sample, as third method, is taken with the freeze-core technique as described in chapter 3.1 approximately 0.5 m upstream from the marked location of the standpipe. Subsequently to the sediment sampling the images for SfM-MVS are taken from the freeze-core sample (fourth method) before melting starts. The process of image acquisition and SfM-MVS is described in detail in chapter 3.2.

5. DETERMINATION OF POROSITY USING SfM-MVS

In this chapter the results from the preliminary experiments (chapter 5.1) as well as the main laboratory experiments (chapter 5.2) from the porosity determination is presented. In the following discussion (chapter 5.3), a systematic error, the application of SfM-MVS for porosity measurements and the applicability of mathematical predictors are discussed. The chapter ends with a concluding summary of the topic (chapter 5.4).

5.1 Results – Preliminary experiments for the determination of total volumes

The results from the study regarding the applicability of SfM-MVS for determining porosity of frozen sediment samples have been published and can be found in Seitz et al. (2018).

In advance to the experiments described in this study several preliminary experiments have been conducted in order to optimize the SfM-MVS procedure and thus guarantee a high reliability of the resulting SfM-MVS model. These experiments are conducted in a Bachelor Thesis and can be found in Klopfer (2016). The amount of pictures required for a good quality of the SfM-MVS model, the camera position and camera set up as well as the size and surface of the scalebar have been analysed in Klopfer (2016). Based on the results from Klopfer (2016) additional experiments are conducted in the laboratory which are described in this chapter.

For each geometric body between 70 and 80 images are taken and since the shape of the bodies is simple only three to four camera positions are chosen. More images (100 – 110) are taken for SedSa1 and SedSa2 because the structure is more complex and more heterogeneous. To measure the V_{tot} with the WRM the geometric bodies are submerged with water and the bodies stay in the water for several minutes until the water surface is completely calm. This guarantees high accuracy for the water level measurement and thus for the WRM; however, this procedure takes more time and cannot be applied for frozen sediment samples since melting process will start.

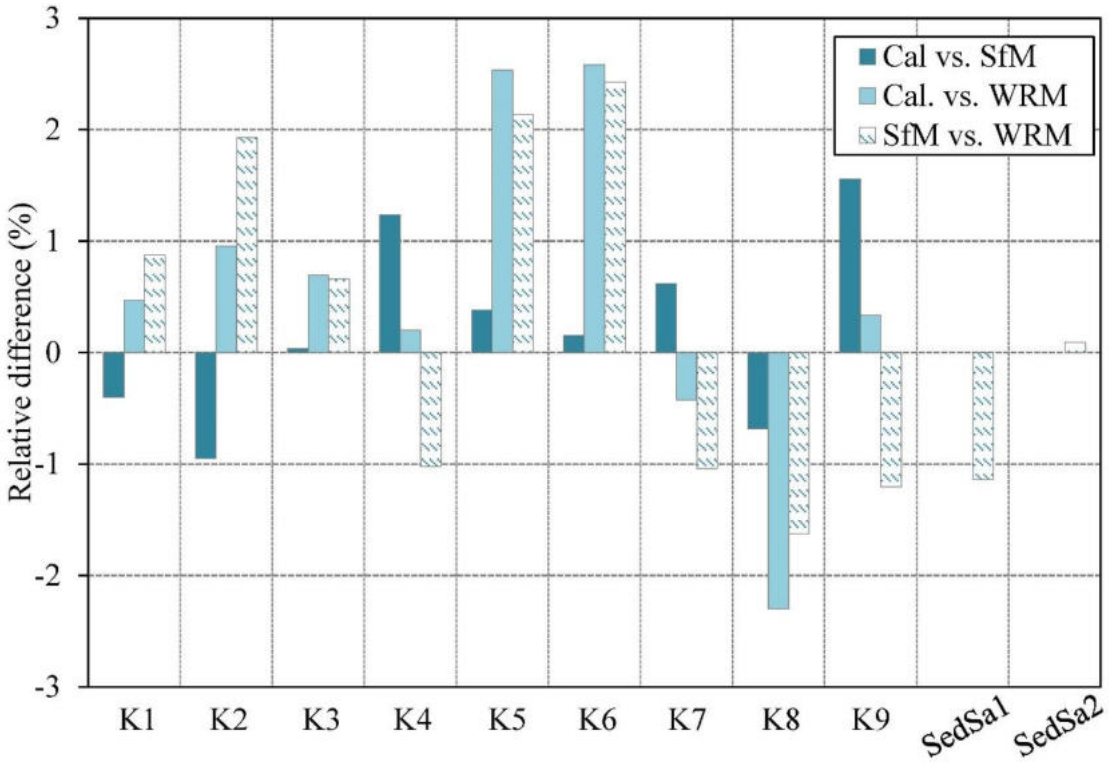

Figure 5.1: Relative difference (%) between V_{cal} and V_{WRM}; V_{cal} and V_{SfM} as well as V_{SfM} and V_{WRM} for K1-K9 and SedSa1 and SedSa2.

For both the simple geometries and the artificial sediment samples, SfM-MVS is more accurate than WRM in determining V_{tot}. In general, V_{SfM} shows a good agreement with both the calculated volumes of the simple geometric bodies as well as with WRM volumes (Table 5.1 and Figure 5.1). Comparing the calculated volumes of the simple geometric bodies (K1-K9) with V_{SfM} yields a maximum relative difference of 1.56 % (K9) and a mean absolute deviation of 0.55 %. SfM-MVS overestimates the total volume for six of the nine samples. Although volume differences using the WRM are slightly higher compared to SfM-MVS, they are in relatively good agreement with the calculated volumes of K1-K9. WRM deviations range from 0.2 - 2.58% and seven of nine samples overestimate the volume. The mean absolute deviation for the WRM is 0.95 %. The comparison between V_{SfM} and V_{WRM} shows the highest mean absolute deviation (1.29 %) ranging from 0.09 - 2.43 %. V_{SfM} from SedSa1 is higher than V_{WRM}, with a deviation of -1.14 %, while V_{SfM} from SedSa2 is lower than V_{WRM}, with a deviation of just 0.09 %. In the case of the geometric bodies and the artificial sediment samples, the measurement error appears to be randomly distributed (Table 5.1). For six of the geometric samples and one of the artificial sediment samples, the total volume from WRM is higher and for five of the samples and the other artificial sediment sample, the total volume from SfM-MVS is higher. Thus, no systematic error between SfM-MVS and WRM can be observed.

Table 5.1: Comparison of calculated volumes of simple geometries (K1-K9) and volumes derived from SfM-MVS and WRM. Bold indicates volume estimates that are closest to V_{cal}.

ID	Description	V_{cal} (ml)	V_{SfM} (ml)	V_{WRM} (ml)	$(V_{cal} - V_{SfM})/ V_{cal}$ (%)	$(V_{cal} - V_{WRM})/ V_{cal}$ (%)	$(V_{WRM} - V_{SfM})/V_{WRM}$ (%)
K1	Cylinder	16968.4	16900.0	17048.0	**-0.40**	0.47	0.88
K2	Cylinder	9359.1	9270.0	9448.7	**-0.95**	0.96	1.93
K3	Cylinder	7787.3	7790.0	7841.3	**0.03**	0.69	0.66
K4	Cuboid	502.2	508.4	503.2	1.23	**0.20**	-1.02
K5	Cuboid	312.0	313.2	319.9	**0.38**	2.53	2.14
K6	Cuboid	1428.3	1430.5	1465.2	**0.15**	2.58	2.43
K7	Cuboid	2858.3	2876.0	2846.1	0.62	**-0.43**	-1.04
K8	Cylinder	161.0	159.9	157.3	**-0.68**	-2.30	-1.63
K9	Sphere	327.3	332.4	328.4	1.56	**0.34**	-1.20
SedSa1	Sediment sample	-	3719.0	3676.7	-	-	-1.14
SedSa2	Sediment sample	-	552.0	552.5	-	-	0.09
Mean averaged deviation					0.55	0.95	1.29

5.2 Laboratory experiments for the determination of porosity using SfM-MVS

After the preliminary test have proven that the SfM-MVS method to determine V_{tot} works well for simplified bodies and artificial sediment samples it is tested on several frozen sediment samples based on laboratory samples as well as field samples. Therefore, the total volumes based on SfM-MVS are compared to the total volumes based on WRM. In a following step the applicability of mathematical predictors is analysed by comparing porosity based on SfM-MVS to calculated porosities based on mathematical predictors.

Reproducibility of SfM-MVS to determine the porosity

Reproducibility is essential for assessing any new method and ensures its functionality. Therefore, three to five sediment samples are taken from each laboratory mixture to assess the reproducibility of the proposed method. Figure 5.2 shows the standard error of the porosities of each mixture and the averaged geometric standard deviation of the grain size distribution of each mixture. The standard error considers the varying number of sediment samples for each mixture. Due to the large scatter, field samples are not considered in this assessment. In addition, M1 is excluded because no duplicate analysis is conducted for this mixture. The standard error of the determined porosities for each mixture varies between 0.0008 and 0.0076 and the average

standard error of the porosities is 0.004 (Figure 5.2). The heterogeneity of the mixtures clearly does not affect the accuracy of the results. Even mixtures with a high geometric standard deviation induce only small standard errors in porosity, and thus represent a good reproducibility of the results for laboratory mixtures.

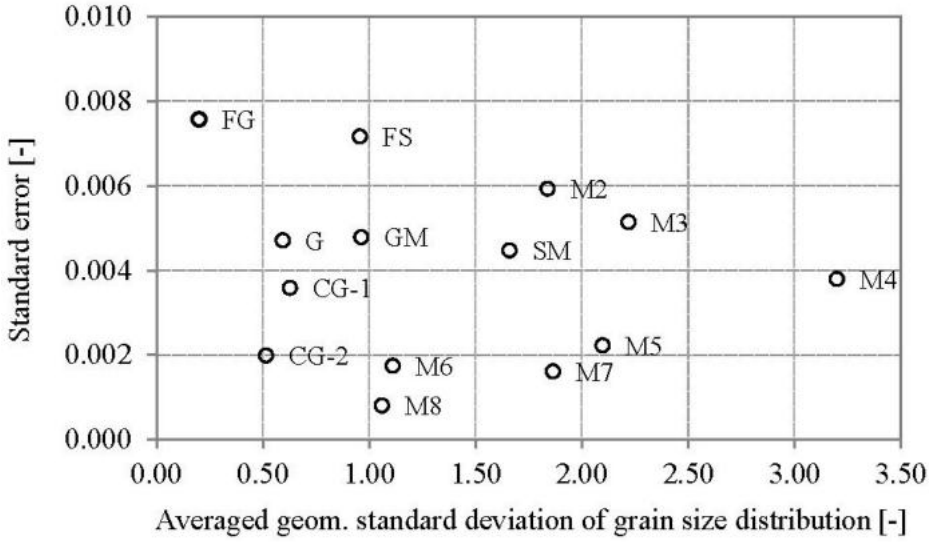

Figure 5.2: Relationship between the standard error of porosities of each sediment mixture group of laboratory samples and the average geometric standard deviation of the grain size distributions.

Comparison of porosity measurements between SfM-MVS and WRM

In order to compare porosities, three different categories (uniform, non-uniform and field samples) are assessed separately. For the measured volume the overall correlation coefficient is $r = 0.998$ ($p < 0.0001$) (Figure 5.3a), while the mean absolute error of the uniform laboratory samples is 2.84% (maximum 4.77%) and 2.77% (maximum 5.39%) for the non-uniform samples. Field samples have the highest mean absolute error of 3.81% between V_{SfM} and V_{WRM} (range from -6.01% to 5.58%). Although r is close to 1, V_{SfM} is systematically higher for all laboratory samples compared to V_{WRM}.

The correlation between n_{WRM} and n_{SfM} is shown in Figure 5.3b. As expected, non-uniform sediments have lower observed porosity than uniform sediments because the fine fractions occupy the available pore space among the coarser grains. The porosities of the uniform sediments vary from 0.28 to 0.44, whereas the range of the non-uniform sediment samples is between 0.16 and 0.30 and the field samples show a range from 0.17 to 0.32. Thus, the porosities assessed in the laboratory experiments represent a wide spectrum of possible porosities. Furthermore, the porosities determined from the field samples are found within this spectrum (Figure 5.3b). Therefore, the method described is deemed applicable for the analysis of all field samples in this study.

The highest porosity values (0.43-0.46) are found in the fine sand mixture (FS), with D_{50} of 0.26 mm and a geometric standard deviation of 0.94 (Figure 2.16). The lowest porosity value (0.16) is found in one of the M1 mixtures, which has a D_{50} of 6.96 mm and a rather high geometric standard deviation of 2.9. This mixture has a high amount of fine sediments < 2 mm (FSA < 2 mm) of 27.25 %, which results in a low porosity. With the exception of M1, the other mixtures have a maximum FSA < 2 mm of 1 % and do not occupy much available pore space.

The average deviation of porosities for the uniform mixtures, the non-uniform mixtures and the field samples are 5.5 %, 8.7 % and 10.5 %, respectively. Although n_{SfM} and n_{WRM} are highly correlated (r = 0.968, p < 0.0001), r for the porosities is found to be slightly lower and the mean absolute error is found to be higher compared to those of V_{SfM} and V_{WRM}. As V_{tot} occurs twice in Equation (2.13), this results in higher deviations of n compared to the deviations of V_{tot}.

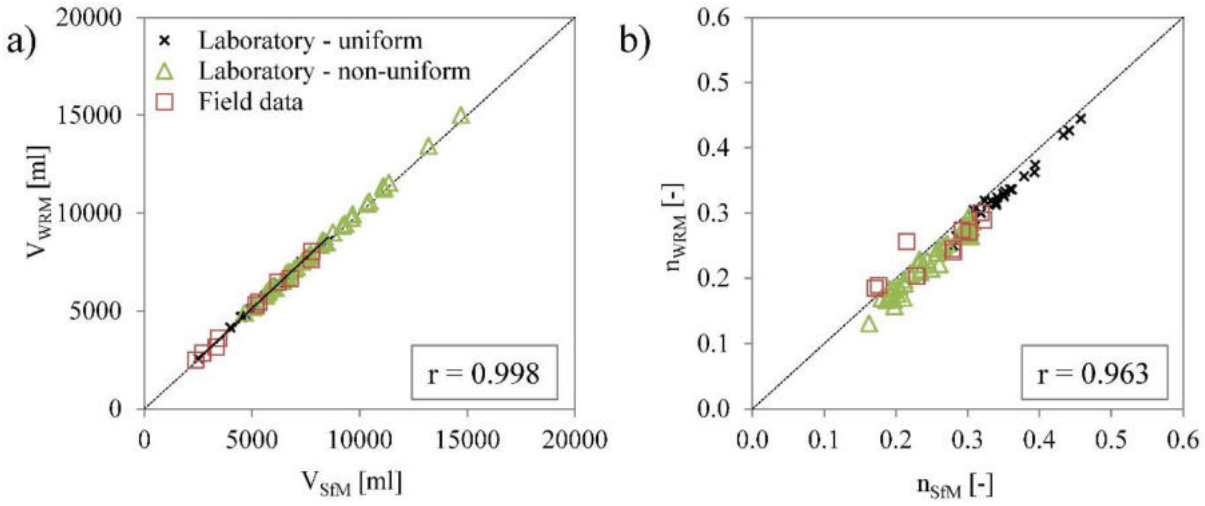

Figure 5.3: Correlation of SfM and WRM. (a) Correlation of VSfM to VWRM and (p < 0.0001, n = 75) (b) Correlation of n_{SfM} to n_{WRM} for all mixtures (p < 0.0001, n = 75). The dashed line represents a perfect correlation.

Comparison of SfM-MVS for porosity measurements with mathematical predictors

The mathematical predictors listed in Table 2.9 are applied to compare to the measured porosities with SfM-MVS. Only sediment samples, which are in the range of application for each predictor (see Table 2.9), are used for this comparison. Komura's (1961) approach gives the best results for the uniform samples (Figure 5.4a), but underestimates the porosities for the higher porosity values. The porosities from both the non-uniform and field samples are greatly overestimated, especially for low values of porosity. The field samples are predicted only slightly better than the non-uniform samples from the laboratory. The approaches of Carling and Reader (1981) (Figure 5.4b) and Wu and Wang (2006) (Figure 5.4c) both greatly underpredict porosity for the uniform samples. In addition, they also underpredict porosity in most of the uniform samples and overpredict porosity for the majority of non-uniform samples. Wooster et al. (2008) only used sediments with a $\sigma_G > 1$ in their study, thus all uniform sediments are excluded in Figure 5.4d. Their approach predicts porosity reasonably well for the

non-uniform sediments, but underpredicts the field samples. The approach of Frings et al. (2011) achieves good results for the non-uniform sediments, but underpredicts most of the uniform and field samples (Figure 5.4e).

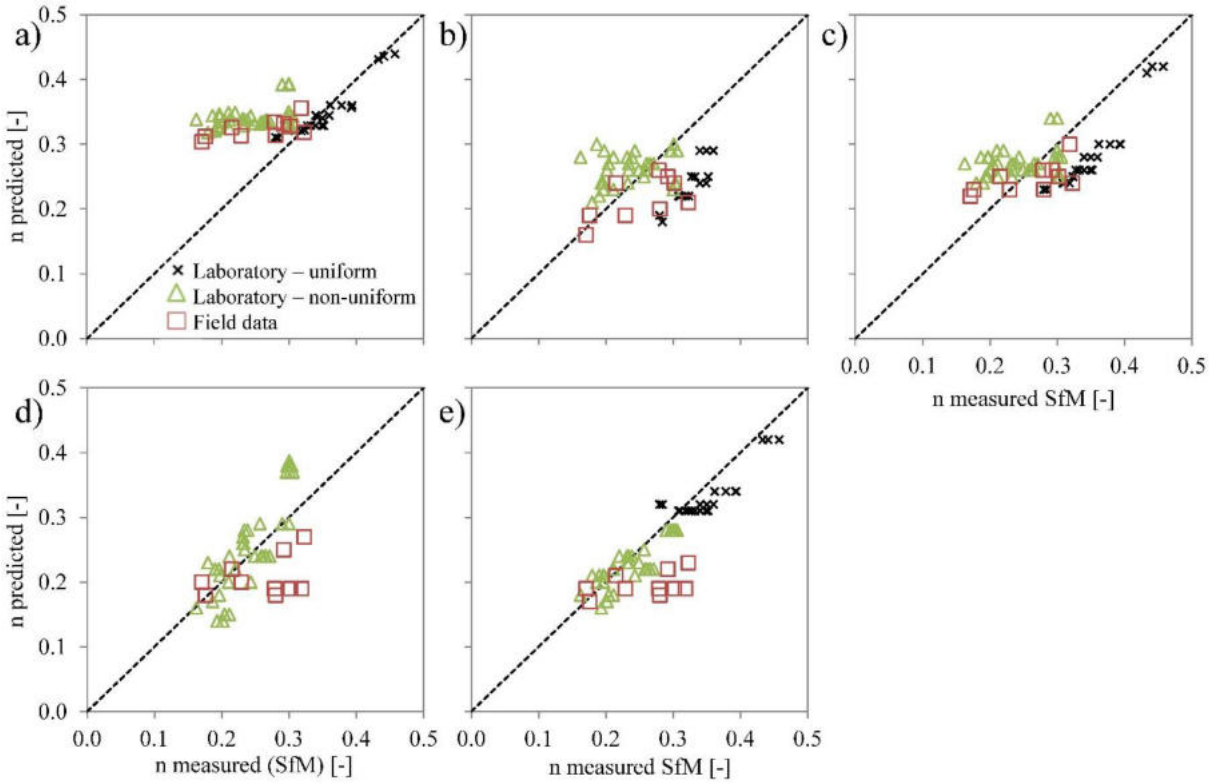

Figure 5.4: Comparison of measured porosities and porosities of mathematical predictors. The different symbols represent different categories: uniform, non-uniform laboratory samples and field samples. The dashed line represents a perfect correlation. Only samples within the respective range of application are considered. a) Komura (1961), b) Carling and Reader (1981), c) Wu and Wang (2006), d) Wooster et al. (2008) and e) Frings et al. (2011).

5.3 Discussion - Determination of porosity using SfM-MVS

5.3.1 Systematic error between SfM-MVS and WRM

The V_{WRM} is lower for all laboratory samples compared to $V_{SfM,}$ which leads to decreased n_{WRM} compared to n_{SfM} (Figure 5.3b). Since preliminary studies on solid objects with simple geometries (Table 5.1) do not show a systematic error between SfM and WRM, it can be assumed that this error is due to the melting processes of pore ice during WRM. For the WRM, the sediment sample needs to be fully submerged in the tank and it can take up to one minute until the water surface is smooth enough for accurate water-level measurements, which are made as soon as fluctuations are below 1 mm. Meanwhile, sediment particles begin to detach, especially when the water temperature is relatively high. Based on the determined porosity and the mass of the separated sediment particles in the laboratory sample, the amount of pore ice that melts during WRM can be estimated based on the total volume. Figure 5.5 expresses the

relationship between the volume of liquefied pore ice and the porosity based on SfM-MVS (Figure 5.5a) as well as the volume of liquefied pore ice and the geometric standard deviation (Figure 5.5b). However, no significant correlation is observed for either case, which suggests that the amount of molten pore ice is independent of the porosity and the geometric standard deviation. The grain size distribution characterized by the geometric standard deviation is a parameter that also describes the available pore size. Figure 5.5b shows that the different geometric standard deviation does not affect the melting progress of the pore ice. It is observed that grains immediately started detaching from the sample as soon as it is submerged in water. Based on these results it is evident that water temperature and the time that is needed to stabilize the water surface during the WRM measurements affects the number of particles that are detached.

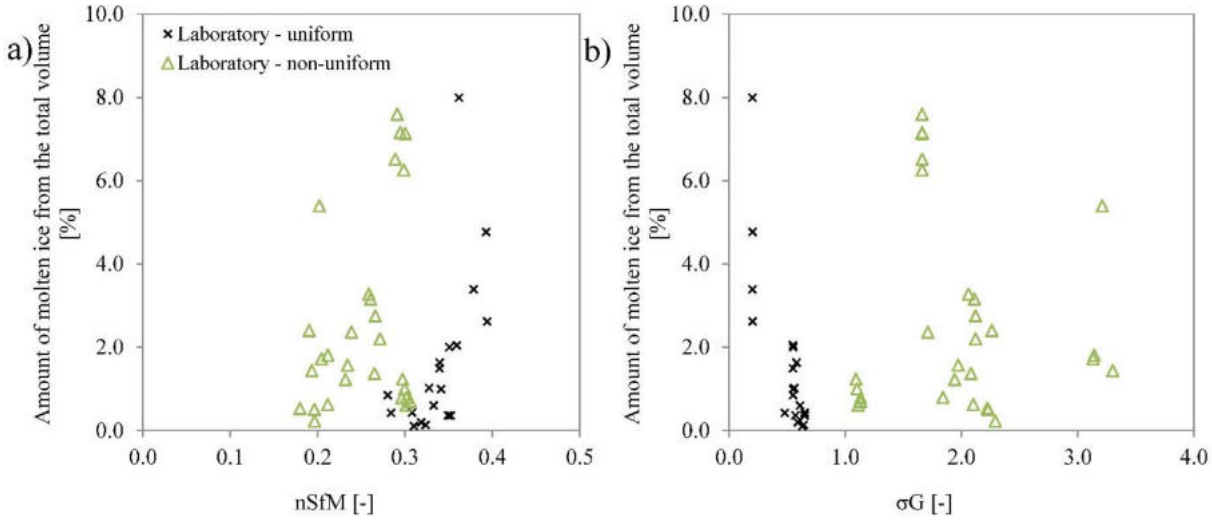

Figure 5.5: Relationship between (a) n_{SfM} and the amount of molten pore ice during WRM for determining V_{Se} and (b) the geometric standard deviation and the amount of molten pore ice during WRM for determining V_{Se}. The correlation was not significant for (a) ($p = 0.59$; $n = 47$).

5.3.2 Application of SfM-MVS for porosity measurements

Figure 5.6 shows that 89.3% of all samples are found within a range of $0.16 < n < 0.35$, which indicates the range of porosities that the results of this study are applicable. Differences between the laboratory and the field samples occur regarding the applicability of the SfM-MVS method. Field samples are more influenced by water and air temperature than laboratory samples, and the procedure in the field is more time-consuming than in the laboratory. This means that field samples are more likely to melt (especially during summer, when the river water temperature is higher) compared to laboratory samples where the temperature can be regulated. Therefore, it is recommended to optimize the sediment sampling procedure and the image acquisition for hot temperature.

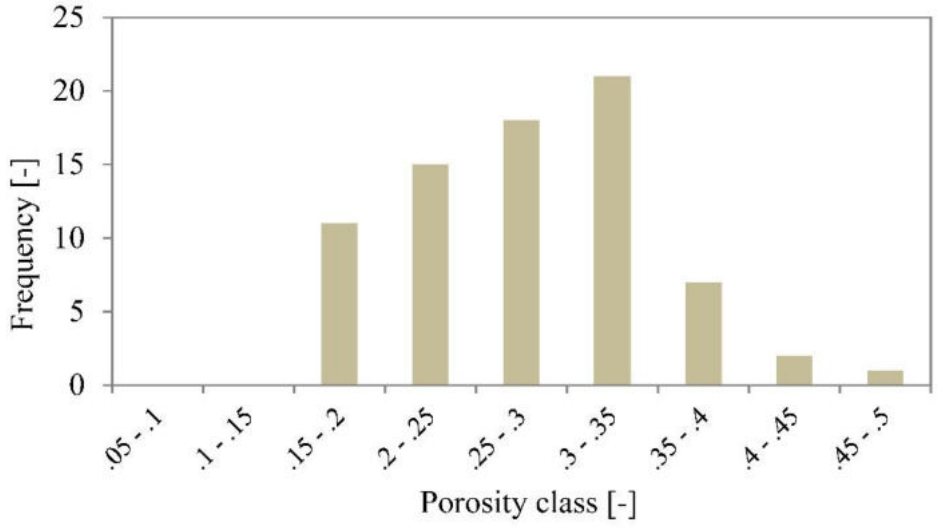

Figure 5.6: Frequency distribution of porosities assessed with SfM-MVS.

On average, all of the imagery necessary for SfM-MVS can be taken within 10-15 min. However, certain environmental parameters such as water and air temperatures are found to accelerate the melting of the sediment sample and in few cases the melting process already starts during the image acquisition. To avoid the problem with high-temperature gradients, it is recommended that field applications occur during winter.

Because only few field samples are included in this study, it is recommended to further analyze environmental factors influencing the melting process of the core sample in detail. In situations where sampling occurs in warmer conditions, the time required for image acquisition can be reduced by increasing the number of cameras used. A mount can be used to fix and align five cameras around the sediment sample into the positions needed for SfM-MVS. With this method, the sample would only need to be rotated once, which can provide a time savings of up to 80%. Further, a video camera (e.g., GoPro , Version 5) could be used to collect a short video sequence with high resolution (4K) and extract single frames for SfM-MVS during post-processing. However, this results in increasing post processing effort.

Light conditions are another factor that differs between laboratory and field application. While lighting can be assumed to be constant in the laboratory, it can change rapidly during field applications. Direct solar radiation may lead to reflection off the sample due to wet sediments, which can have a negative influence of model quality. This can be reduced by shading the experimental set-up with an umbrella or homogeneous background or positioning the set-up in a box with a homogeneous background.

Sample size is a crucial issue influencing the quality of the results. Contrasting the weight of the sediment samples with the criteria shown in Table 2.8, Figure 5.7 shows that most of the uniform sediment samples have a sufficient total weight. For non-uniform samples, the masses vary greatly and fulfill at least the criteria according to Church et al. (1987) for low precision. Six out of ten field samples do not fulfill the criteria for required sample mass. Haschenburger

et al. (2007) found a bias of around 10% for most of the percentiles with sample masses ranging between 12% and 50% of the required samples size. Applying this outcome to this study fulfills the Church criteria for high precision of all laboratory samples. However, this does not account for field samples where the actual mass from three of the samples is still slightly below the Church criteria for low precision. Another way to fulfill the mass criteria would be to analyze two samples in close proximity together as suggested by Rood and Church (1994).

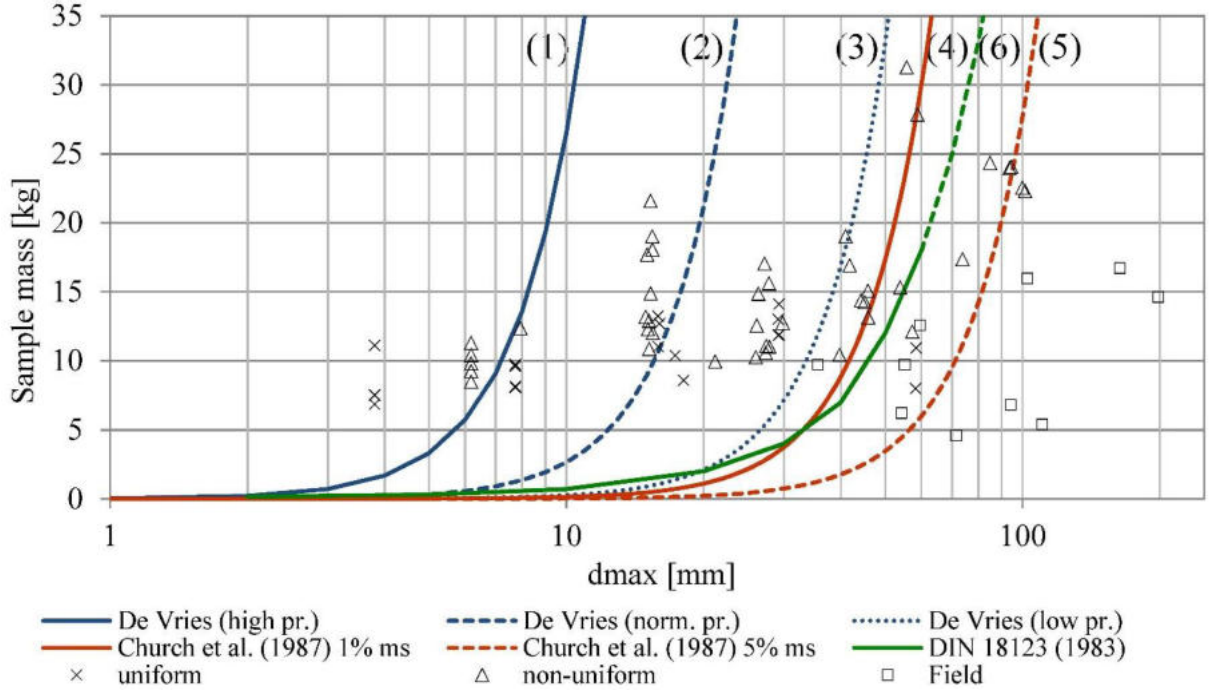

Figure 5.7: Relationship between maximum grain size and recommended sample size for different levels of precision (De Vries, 1970): (1) high, (2) normal and(3) low precision; Church et al. (1987) (4) normal and(5) low precision; and (6) the German Standard DIN (1983).

As described earlier, Frings et al. (2011) used the WRM by removing sediment from the riverbed and filling the excavation with water to determine V_{tot}. This procedure can also be applied using the SfM-MVS method when overlapping images are taken from the excavation and a 3D model of the excavation is created, resulting in a larger sample mass. However, this requires a non-wetted area such as a gravel bar or the application of a diving bell, which highly increases the effort required for field application.

5.3.3 Applicability of mathematical predictors to determine porosities

The results from the comparison of the measured porosities and the porosities from mathematical predictors (Figure 5.4) show that the porosities of the uniform samples can be reproduced if the uniform sediments are within the valid range of the mathematical approach. All approaches (Komura, 1961; Carling and Reader, 1982; Wu and Wang, 2006) that are based on the D_{50} are not necessarily suitable to predicting the porosity of non-uniform sediments. This

can be expected since the D_{50} cannot represent the heterogeneity of grain size distributions. This result is also supported by Frings et al. (2011), who reported a weak correlation between the D_{50} and porosity. Furthermore, Frings et al. (2011) observed that σ_G was more highly correlated to porosity than the D_{50}. Our results suggest that the performance for non-uniform samples (in the lab, not for field samples) is much better for predictors using σ_G as opposed to the D_{50}.

5.4 Summary - Determination of porosity using SfM-MVS

Structure-from-Motion with Multi View Stereo (SfM-MVS) is used to determine the total volume of a frozen sediment sample based on the generation of 3D models using 2D images. The results are compared to volumes based on the commonly applied water replacement method (WRM). Both methods demonstrated high accuracy in determining the total volume of simple geometries. SfM-MVS proves to perform well in determining the total volume of frozen sediment samples that are further used to analyze porosity. Comparing the results from SfM-MVS to WRM produced a systematic error as porosity determined from WRM is generally lower than porosity determined using SfM. This can be explained by the melting of pore ice during WRM. The experiments show that SfM-MVS is a reproducible and accurate method that is easy to apply and requires less equipment in the field (i.e., camera, tripod, sample support) compared to WRM. Another advantage is that the sample remains intact after image collection, whereas the immersion of samples into water (WRM) results in the loss of sediment due to thawing. The experiment show that SfM-MVS is able to determine porosities for a broad spectrum of sediment grain sizes. Mathematical predictors performed best for uniform samples in the laboratory. Predictors based on the standard deviation performed better in predicting the porosities of non-uniform samples compared to predictors based on D_{50}, whereas none of the predictors effectively estimated the porosities of the field samples.

6. DETERMINATION OF HYDRAULIC CONDUCTCITVITY USING THE VERTICO METHOD

This chapter presents the results of the laboratory experiment from the VertiCo method. In a first step the preliminary experiments P1 – P3 are presented in chapter 6.1. Based on the results and the following discussion, a final measurement set-up for the laboratory experiments is established (chapter 6.2). Chapter 6.3 presents the results from the laboratory experiments of the investigation regarding the influence of water level and sediment depth on the slurping rate as well as the detection of layers with varying hydraulic conductivities. Additionally, the calibration of the MODFLOW groundwater model is shown where the slurping rates are transferred into actual hydraulic conductivities. These results are further discussed in chapter 6.4 followed by a concluding summary regarding the newly developed method in chapter 6.5.

6.1 Results - Preliminary experiments

Before the VertiCo method can be applied in laboratory experiments and in the field, numerous optimization steps are required. During this study one Bachelor thesis (Eurich 2016) and two Master thesis (Zaqout 2017 and Wokabi 2018) have been supervised, which optimized the method and investigated its applicability. Following the optimization of the VertiCo method, preliminary experiments are carried out in the laboratory. The results from these experiments (P1- P3) are shown in the following chapter.

6.1.1 P1 Development of slurping rate and repetitions of experiments

By recording the weight in the glass flask the evolution of slurping rate can be observed. Figure 6.1 displays the temporal development of measured weight in the glass flask during the slurping phase. The rise of weight is linear for different slurping rates over detection time and thus leads to a constant slurping rate. The measurement can be recorded as soon as slurping phase initiates. In cases where the two minutes cannot be recorded due to high slurping rates a shorted measuring period is also enough since linear values can be expected.

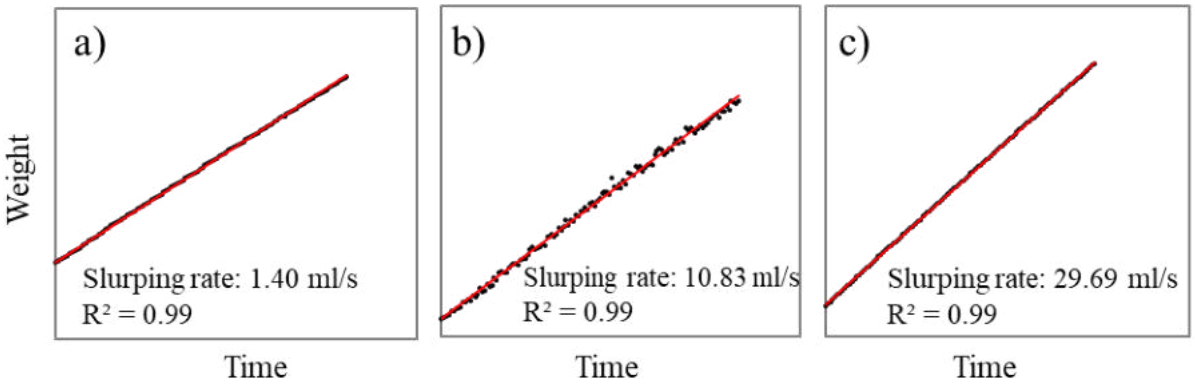

Figure 6.1: Temporal development of weight during slurping phase for low slurping rate a), moderate slurping rate b) and high slurping rate c).

Figure 6.2 shows the changing slurping rates with several repetitions in laboratory studies. The behavior for the repetitions depends on the material and mostly on the amount of fine sediments. Slurping does not influence the surrounding system and thus should not lead to a change in slurping rate over time. However, during the short sucking phase (approx. 5 – 15 sec) at the beginning of each measurement fine sediments are sucked into the standpipe from the close vicinity influencing the surrounding system. In most of the cases where the mixture contains a high amount of fine sediments (Figure 6.2 a) the slurping rate increases over time until a constant value is reached after the 7th repetition. In this case the slurping rate increased up to 10 % from the initial value to the last repetition. Increasing slurping rates could also be observed in mixtures with less fine sediment concentration (Figure 6.2 b); however, it only increased up to 3 % from the initial to the final value. It could also be observed that the slurping rate does not change over time even with high content of fine sediments (Figure 6.2 c). In this case the slurping rate is considerably low which means only very little water infiltrates into the standpipe and also little fine sediment is transported with the water. The general grain size distribution and the packing density might influence whether fine particles can be sucked into the standpipe or not.

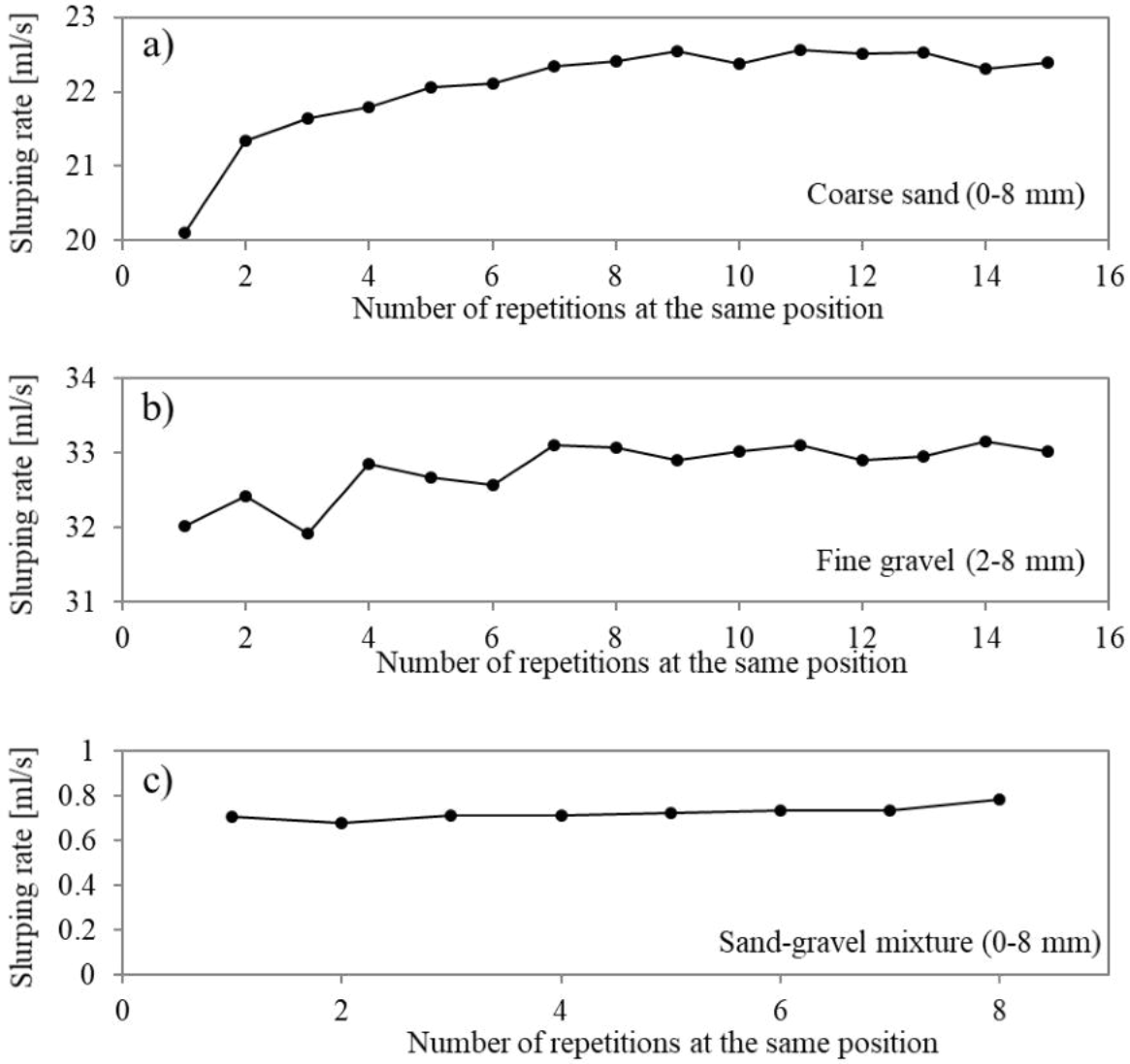

Figure 6.2: Variation of slurping rates over several repetitions at the same position for different materials in laboratory study. Coarse sand a), fine gravel b) and sand-gravel mixture c).

Figure 6.3 shows the variation of slurping rate over several repetitions in field experiments. The first profile of slurping rates (Figure 6.3 a) shows an increase of slurping rate over the 15 repetitions about 23.7 %. The slurping rates rise from 34.13 ml/s for the first repetition to 42.22 ml/s for the last measurement. In this case, the highest increase is between the first and the second measurement where slurping rate increases about 7.7 %. During the other measurements, the slurping rate increases only on average about 1.6 %. Contradicting to the monotonous increase of slurping rates over several repetitions Figure 6.3 b shows highly variable slurping rates. Increases as well as decreases can be observed in this experiment showing no clear trend. The behavior of slurping rates might also depend on the environment such as packing density and grain size characteristics and cannot be assumed to always increase monotonously. Both experiments are measured at the River Rems where loosely bedded gravel conditions with low amounts of fine sediments can be found.

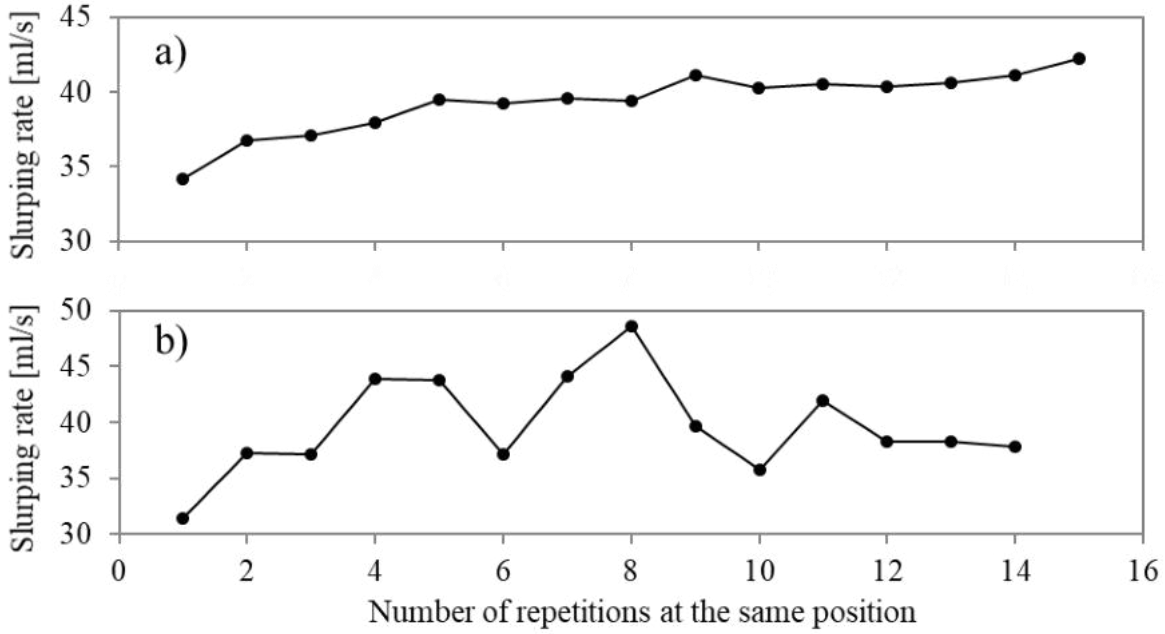

Figure 6.3: Variation of slurping rates over several repetitions at the same position of the double packer in field experiments at river Rems.

6.1.2 P2 Comparison of vertical profiles under varying sediment conditions

For evaluation whether the new double packer method is suitable for detecting different kinds of material, slurping rates are measured for three different pre-defined materials. The big tank is filled with one material at the time and a vertical profile is measured with steady water level. The results are displayed in Figure 6.4 and it is clearly obvious that different material (different grain size characteristics) result in different slurping rates. The red line displays the vertical profile for fine sand and shows the lowest slurping rates around 3.6 ml/s. The measured coarse sand (blue line in Figure 6.4) results in higher slurping rates on average around 9.1 ml/s for the vertical profile. Beside the higher slurping rates coarse sand also shows higher variabilities of slurping rates over the vertical profile. However, a clear trend over the vertical profile cannot be observed. The measurements of gravel material results in highest slurping rates ranging from 20 ml/s to 67 ml/s. The highest slurping rates also show the highest variability of slurping rates. The fine sand material is rather uniform and does not show high variations in packing density. The coarse sand shows higher non-uniformities resulting in different packing densities. However, the variations in slurping rates are rather low compared to the gravel material. The gravel material is also uniform and cannot be compacted thus local variations in packing densities can be neglected. The high variations of slurping rates for gravel can be explained from different locations of single grains in front of the standpipe openings. If the standpipe moves some single grains during installation in the close vicinity of the standpipe, it might open a gap, which leads to increased slurping rates. In case that a single grain is directly located in front of one of the openings it reduces the inflow area resulting in reduced slurping rates. Thus, single outliers can be explained by this behavior and does not necessarily mean that the material changes at this position. In contrast to fine sand and coarse sand, gravel shows a decrease of

slurping rate with increasing sediment depth. This might be explained by the fact that gravel has less friction compared to fine sand, and coarse sand and water can flow through gravel more easily the less gravel is on top of the double packer position. Thus, the closer the double packer reaches the sediment surface more water flows into the measuring chamber. This is only observed for gravel and not for fine sand and coarse sand.

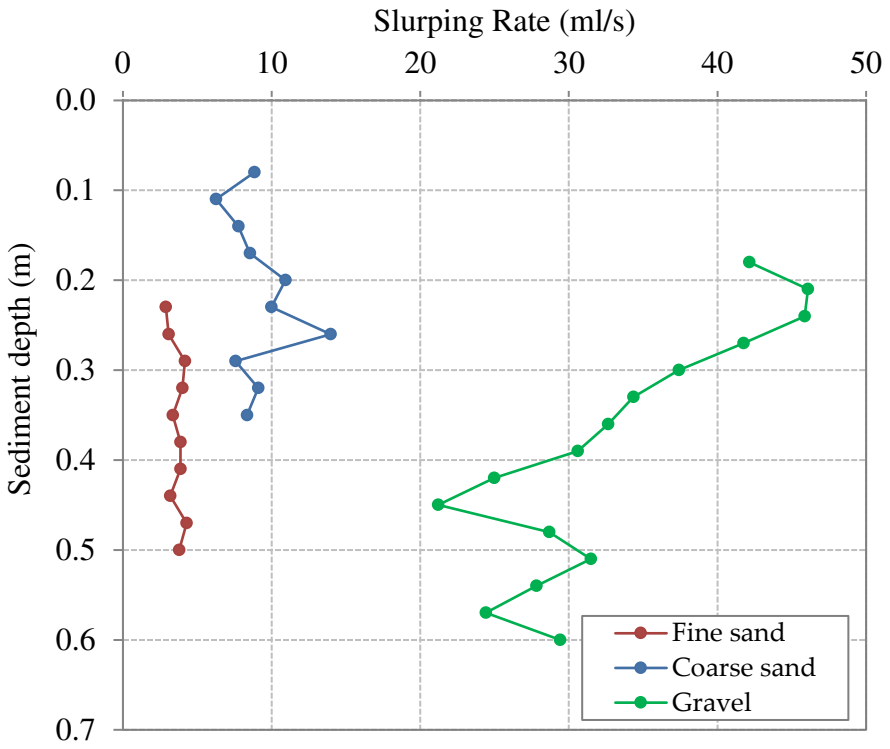

Figure 6.4: Vertical profiles of different materials (laboratory experiments).

6.1.3 P3 Sensitivity of the system regarding location of the standpipe

Laboratory experiments P3

The experiment P3 aims on analysing a procedure to repeat single measurements, which ensures the most accurate way for reproducible data. Fine sand and coarse sand only have very low fluctuations in slurping rate compared to gravel, which is much more sensitive regarding repeatability. Therefore, the experiments are conducted with the gravel material. The left graphic of Figure 6.5 (P3a-L) shows the results from three different vertical profiles measured one after the other at the same location of the double packer. The slurping rate increase for each profile for the lower positions of the double packer (sediment depth 0.6 m – 0.36 m) and are closer together for the higher positions (sediment depth 0.36 – 0.18 m). The variation of slurping rates for each position varies highly and can increase for more than the factor of two. This high variation might result from movement of the double packer in the standpipe. The double packer

fits quite tight in the standpipe and moving it up or downwards, sucks water inside the standpipe or pushes it outside the openings, respectively.

The middle graphic of Figure 6.5 (3Pb-L) shows the results from three vertical profiles measured at three different locations of the standpipe very close together. The locations are chosen in a triangle where the distance from one location to the other is approximately 15-20 cm. The vertical profile from location 1 and location 3 show a good agreement of the measured slurping rates except one area where higher slurping rates are measured at location 3. In contrast to this location 2 shows considerably higher slurping rates and also more heterogeneities of the vertical profile compared to location 1 and 3.

The third experiment (Figure 6.5 right site, P3c-L) shows three repetitions from one vertical profile. At each position of the double packer measurements are repeated for two times and then the double packer is moved to the next position. The graph shows the three profiles are close together and show only low variability in slurping rates over the repetitions compared to the previous two experiments. The variations of slurping rate are on average between 15 - 18 % with a few exceptions where the slurping rate from the third measurement is two times the slurping rate from the first measurement.

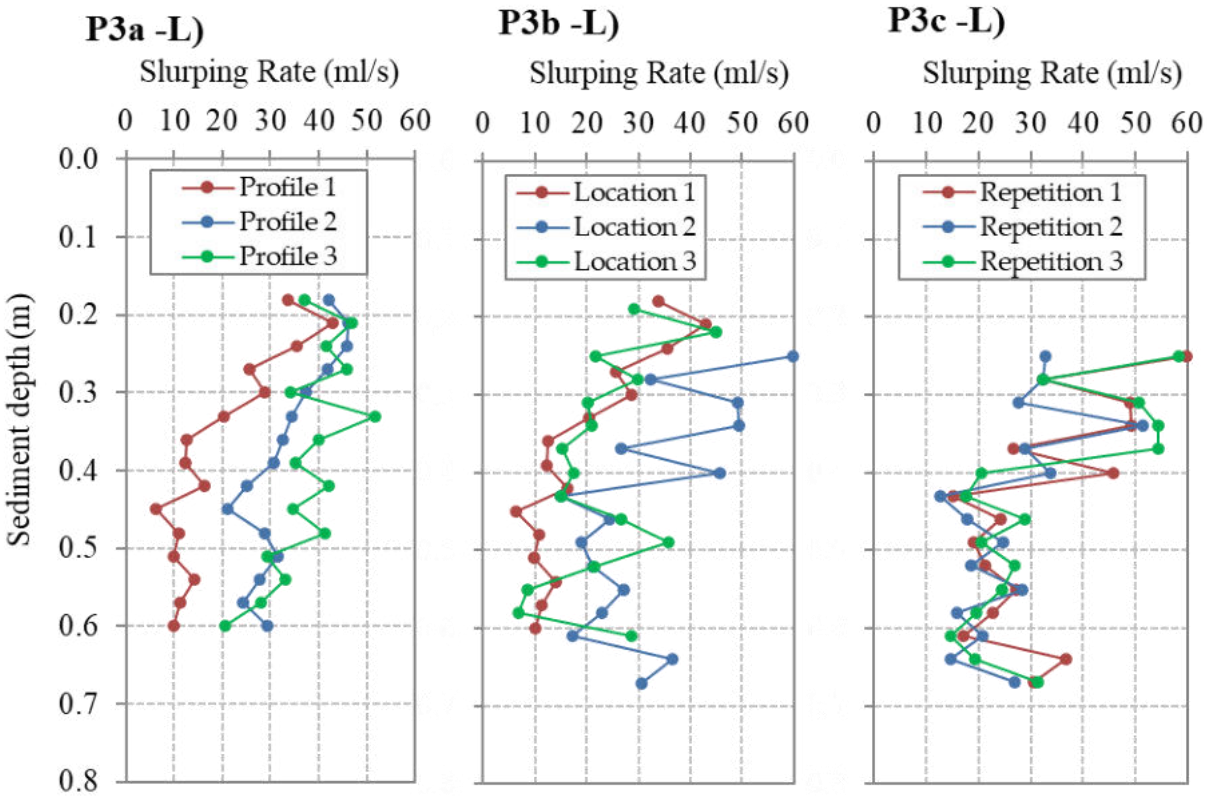

Figure 6.5: P3a – P3c - Variation of repetition of three vertical profiles at the same location of the standpipe (P3a-L). Three vertical profiles at different locations close to each other (P3b-L). One vertical profile with three repetitions at each double packer position (P3c-L).

Field experiments P3

The experiments P3a-L – P3c-L are repeated in the field to investigate possible differences between simplified laboratory conditions and natural conditions in a river. The experiments are conducted at the River Rems (Figure 6.6 a-c).

Measuring three vertical profiles at the same location of the standpipe after each other (P3a) leads to high variations of slurping rates for each profile (Figure 6.6 left site). The field data show even higher variations of the vertical profiles than the laboratory results from this experiment. Although the slurping rates from the laboratory experiment varied highly from each other the same trend of the vertical profile could be observed. This cannot be observed for the field experiment where the single slurping rates vary less from each other but show a totally different trend of the vertical profile.

The vertical profiles from three different locations (P3b) close to each other also show high variations of slurping rates for each position. For field application this can represent the influence of moving the double packer on the vertical profile or it represents local heterogeneities of the sediments.

Figure 6.6 (right) shows the results from P3c where one profile is measured with two repetitions at each double packer position. The three resulting profiles show the same curse of vertical profile. However, the slurping rate increase for each repetition. This phenomenon can also be observed in P1 where several repetitions are measured after each other. In the course of the field experiments it could be observed that during the sucking phase of the first measurement rather dirty and turbid water was sucked into the glass flask. This means that a lot of fine sediments are transported during the measurement and transported out of the surrounding system. Following measurements showed less fine sediment in the glass flask and thereby less disruption of the surrounding and therefore less increase of slurping rates.

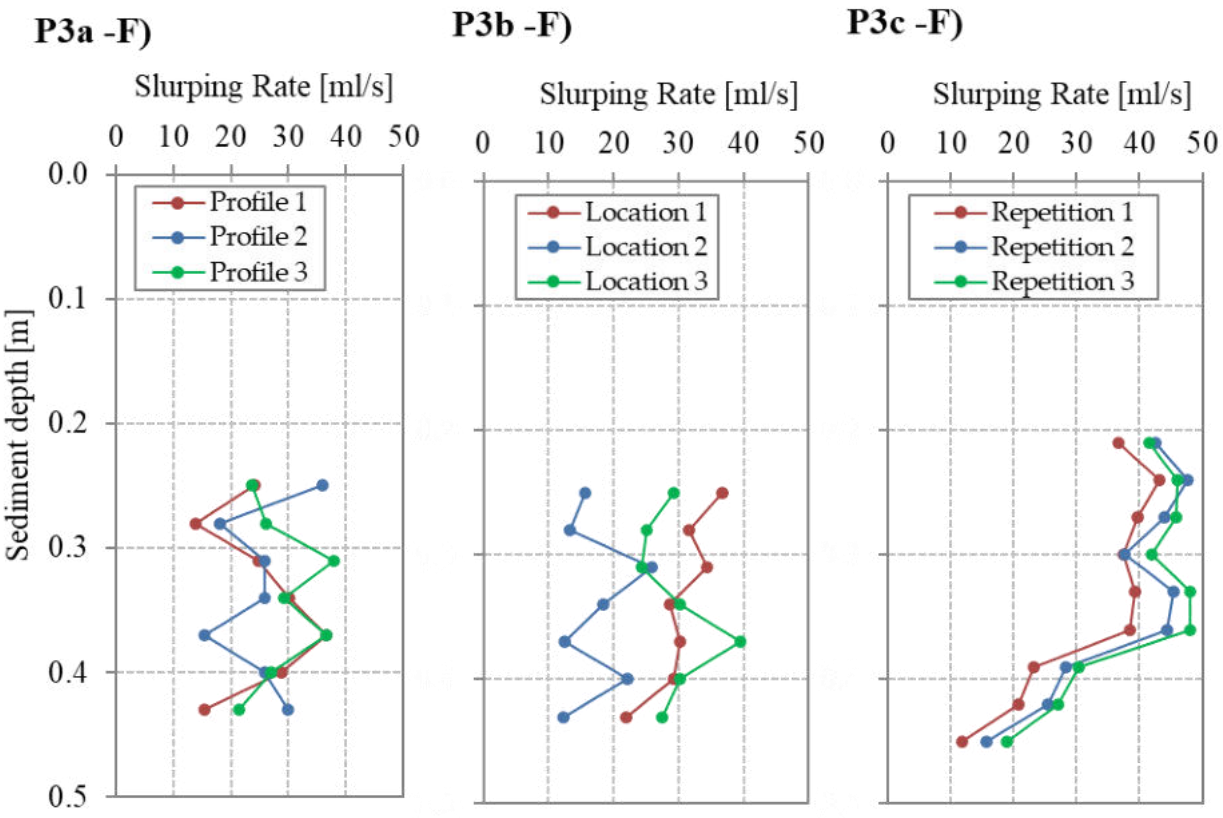

Figure 6.6: P3a – P3c - Variation of repetition of three vertical profiles at the same location of the standpipe (P3a, left). Three vertical profiles at different locations close to each other (P3b, middle). One vertical profile with three repetitions at each double packer position (P3c, right). All experiments are measured at River Rems.

6.2 Discussion and Conclusion - Preliminary experiments

The preliminary tests show that the method delivers reproducible results (P1) and it is possible to differentiate between different sediment conditions by the resulting slurping rates (P2). The slurping rate achieves a constant value during each measurement, which suggests steady state conditions. The results from P1 show that the slurping rate changes for different conditions, which means that the measurements somehow influence the surrounding system. It can be assumed that the slurping rates change more in case where higher fine sediment amounts are available since the initial sucking phase transports fine sediments out of the surrounding substrate and thus alters the slurping rate of the following measurement. Results from the laboratory experiments supports this assumption since the gravel material does not contain a lot of fine sediments and the laboratory experiment did not show the increasing slurping rate but rather a general variation of slurping rates for the three repetitions.

The double packer can be used to detect different material properties as the results from P2 showed. Fine sediments lead to much smaller slurping rates than coarse material. Thus, the method is suitable to detect the effect of different grain size characteristics.

Based on the results from P3a-c, a measurement procedure could be developed to ensure good reproducibility and low fluctuations of the measured slurping rates. It is recommended to measure one vertical profile including three repetitions at the same position of the double packer rather than repeating the vertical profile since the results show that moving the double packer in the standpipe leads to a change in the surrounding substrate and alters the slurping rate. The first and the second repetition are measured as backup to evaluate possible measuring error and to ensure reproducibility. In case the slurping rates increase markedly within the three measurements only the first slurping rate is used for analysis since the systems seem to be disturbed for the next two measurements. If slurping rates stay within a certain range an average slurping rate based on the three measurements is used for further analysis.

The single measurement is recorded as soon as steady slurping conditions are reached. Even though this can be visually observed it should also be crosschecked with the recordings of the balance where a linear increase of weight can be observed, and a different slope occurs between sucking phase and slurping phase.

6.3 Results - Laboratory experiments for determining hydraulic conductivity using VertiCo

In this chapter the results from the laboratory experiments are presented. The correlation between slurping rate and hydraulic conductivity (chapter 6.3.1) is investigated in a first step followed by the analysis regarding the influence of varying hydraulic conditions on the slurping rate (chapter 6.3.2). Further, the capability of detecting layers with lower hydraulic conductivity is presented in chapter 6.3.3 as well as the calibration of the numerical groundwater model MODFLOW (chapter 6.3.4).

6.3.1 Correlation

The slurping rates from the correlation mixtures (see chapter 3.3.1) respond well to the varying amount of fine sediments (Figure 6.7). Slurping rates are highest for the gravel mixture and the pure gravel (Mixture 2, 3, 9 and 11) and are lowest for the mixtures with high fine sediment contents (Mixture 4 – 8). It can be noted that the variation of slurping rates is higher for the coarse gravel material compared to mixtures with higher fine sediment. The higher variation of slurping rates in coarse material has also been observed in the preliminary experiments and might result from the higher pore space and thus higher heterogeneities in front of the standpipe openings. The slurping rate of the coarsest material (Mixture 2) ranges from 26.3 ml/s to a maximum of 57.3 ml/s with a median value of 48.5 ml/s. This results in a variation of slurping rate of almost 120 %. The high bias of the data reduces with adding fine sediments to the mixture. Calibration 8 is the mixture with the highest fine sediment amount and the slurping rates vary between 1.0 ml/s and 2.0 ml/s and a median slurping rate of 1.5 ml/s. The error for this mixture is also 100 %; however, the total values are much closer together. The median value (middle line in the beige box shown in Figure 6.7) is taken for the correlation between slurping rate and k_f values.

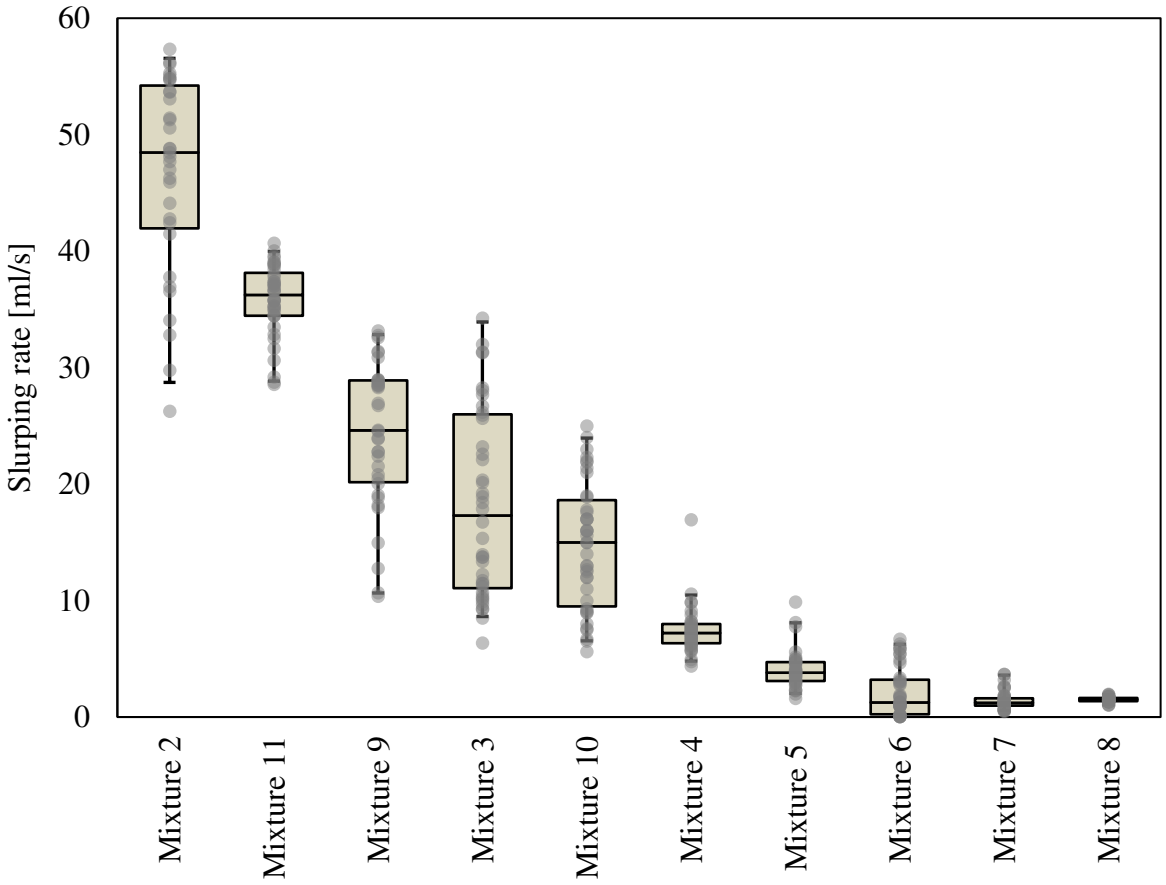

Figure 6.7: Slurping rate for the ten calibration mixtures showing each measurement (dots), the first and third quartile (P25%, P75%) as well as P95% and P5% as Whiskers.

Determining the k_f value using constant head tests the measurement of the head difference of the piezometer and the discharge through the column is required. Both values are measured three times to exclude possible measurement errors. Figure 6.8 displays the corresponding k_f values from the calibration mixtures using the constant head test and a good response to the different grain size characteristics can be observed. The k_f values are highest for the gravel mixtures and reduce significantly with increasing amount of fine sediments. The variation of the three single measurement is relatively low compared to the variations of the slurping rates, resulting in almost overlying dots in Figure 6.8. For the final correlation the average values based on the three measurements are taken. The correlation mixture 2 has the coarsest material and the highest hydraulic conductivity with a k_f value of 8.1E-2 m/s. This value can be classified between high and medium permeable and stands for gravel or coarse sand (Klute and Dirksen 1986). The lowest k_f value is measured for the correlation mixture 8 (highest amount of fine sediments) with an average hydraulic conductivity of 2.2E-5 m/s, which represents the transition of low to very low hydraulic conductivity and can generally be found in fine sand and sandy clay mixtures (Klute and Dirksen 1986). The values measured in the laboratory experiments cover a wide spectrum of hydraulic conductivities as they occur in nature.

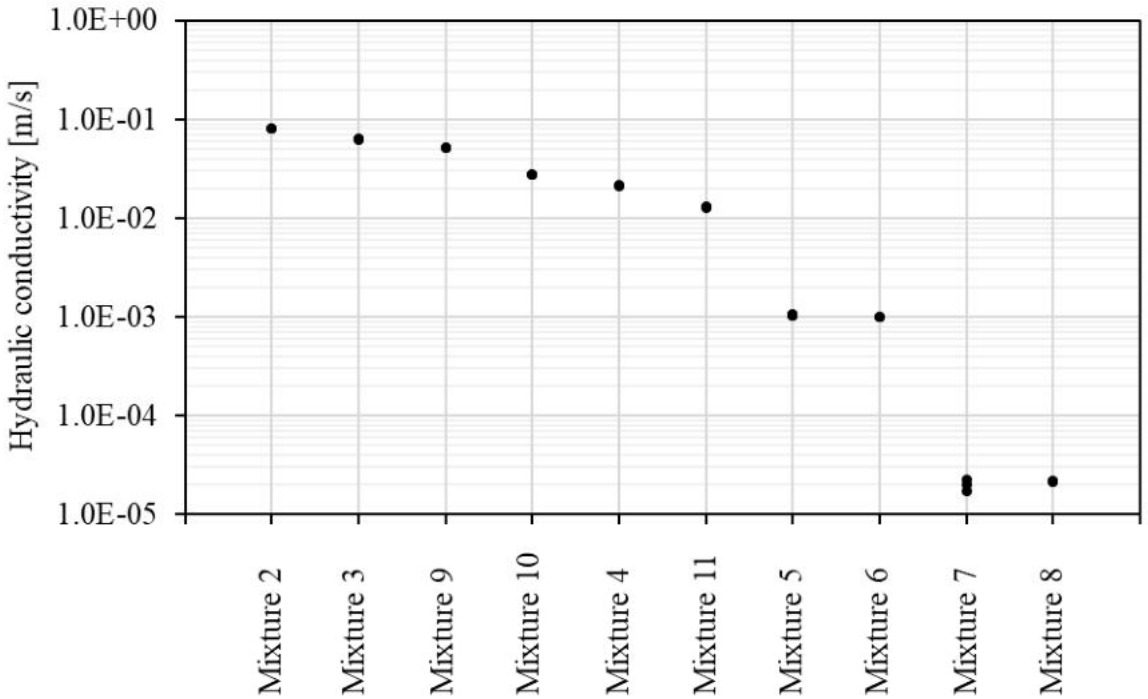

Figure 6.8: k_f values for the ten mixtures based on the constant head experiments.

A linear relation between slurping rate and hydraulic conductivity can be observed based on the results (Figure 6.9). This is also supported by the observation from Terhune (1958). A very good agreement between the k_f values and the median value of the slurping rates is achieved showing a coefficient of determination $R^2 = 0.9$.

This relation leads to a function to estimate the k_f values of measured slurping rates. The equation to transfer slurping rates can be written as follow:

$$k_f = \frac{SR}{X} = \frac{SR}{463.3} \qquad (6.1)$$

k_f is the hydraulic conductivity [m/s], SR is the slurping rate [ml/s] and the constant factor X has the unit m/ml. It is important to note that the factor X takes the value 463.3 only for this type of geometry. It changes with changing area from the openings, changing mesh covering the openings and changing standpipe geometries. In addition, this correlation coefficient does not consider the influence of hydraulic head caused by different water levels or varying sediment depths and can therefore not be applied to transform the measured slurping rates into hydraulic conductivities. See chapter 6.3.2 for detailed information about the influence of varying hydraulic heads on slurping rates.

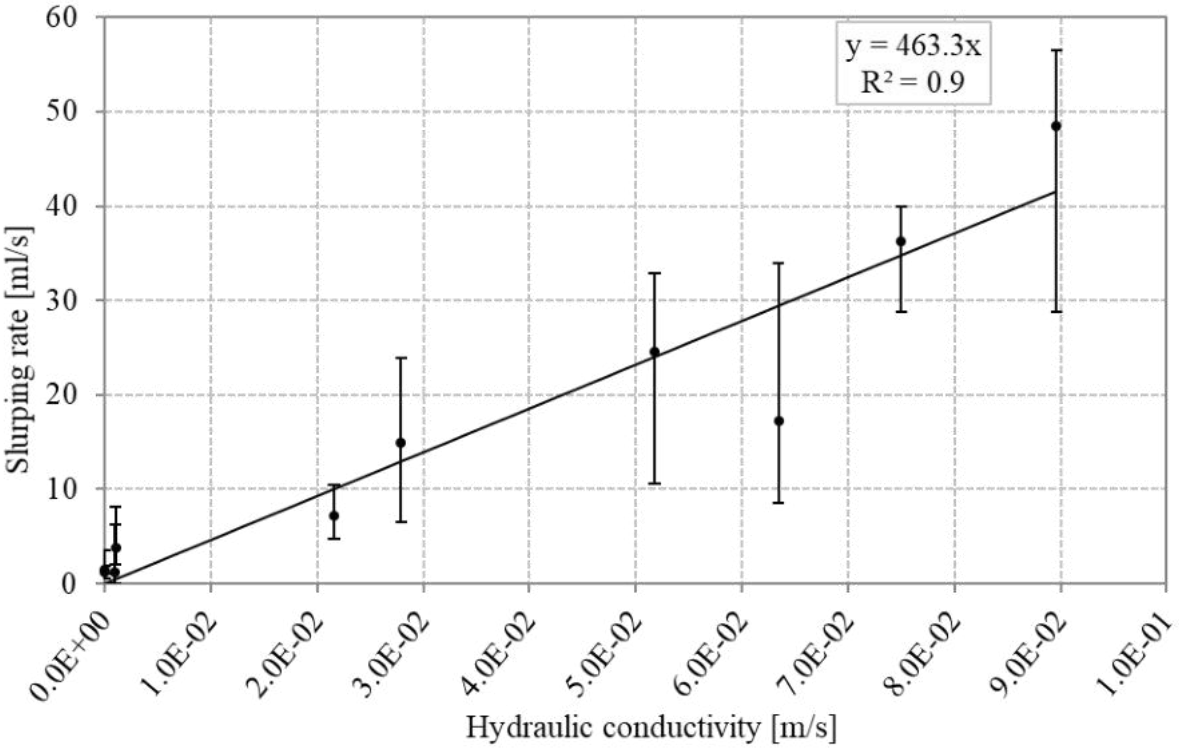

Figure 6.9: Correlation between hydraulic conductivity (k_f value) based on constant head test and the slurping rate from laboratory mixtures.

6.3.2 Dependency of water level and sediment depth on slurping rate

Preliminary experiments conducted by Eurich (2016) have shown a clear dependency of water level on the slurping rate. In addition, the preliminary experiment P2 in this study not only shows the dependency of the slurping rates from different materials but also demonstrates the dependency of varying sediment depth on the slurping rate. The P2 experiment will be investigated in this section with focus on the influence of varying sediment depth. In addition, the results from the water level experiment (WL) is shown in this chapter, where the double packer stays at a fixed position (fixed sediment depth) and the water levels are increased in 5 cm steps.

Varying water level and fixed sediment depth

Increasing the water level and keeping the double packer at a fixed position leads to a linear increase in slurping rate. Figure 6.10 summarizes the results from water level dependency on the slurping rate for three different materials analyzed in the laboratory. The two red lines in Figure 6.10 (fine sand 1-2) represents fine sand material and show the lowest slurping rates ranging from 0.43 ml/s to 0.73 ml/s. Further, a very low increase is detected in slurping rate with increasing hydraulic head and thus the least influence of hydraulic head compared to other materials. Here, the slurping rate increases on average about 0.1 ml/s (4.1 %) for a n incremental rise in water level of 5 cm. The slurping rates measured in coarse sand (coarse sand 1-2, blue lines in Figure 6.10) range between 12.8 ml/s and 24.7 ml/s and show an average increase about

1.3 ml/s (8.3 %) with each 5 cm rise of water level. The gravel material (gravel 1-2) shows the highest slurping rates and the highest influence of slurping rate with increasing water level. The slurping rates range between 25.8 ml/s and 46.0 ml/s and increase on average about 3.8 ml/s (11.1 %) with an incremental increase of the water level by about 5 cm.

The influence of rising water levels on slurping rates shows a clear material dependency (different slopes) and increases as the material becomes coarser. Fine sand only shows a slight influence of water level increase on the slurping rate and the influence increases further from coarse sand to gravel. The slopes from fine sand 1 and 2 are 2.2 and 1.2, respectively. For coarse sand 1 and 2 the slope increases to 27.7 and 27.1, respectively. Gravel has the highest slope (64.7 and 78.1) and is thus affected most by a rise in water level. Fine sand has a D_m of 0.3 mm and σ_G of 1.0 and shows the least influence of water level, whereas the coarse sand and the gravel have a D_m of 2.2 mm and 5.7 mm, respectively and a σ_G of 1.7 and 0.6, respectively (see also chapter 4.2.2).

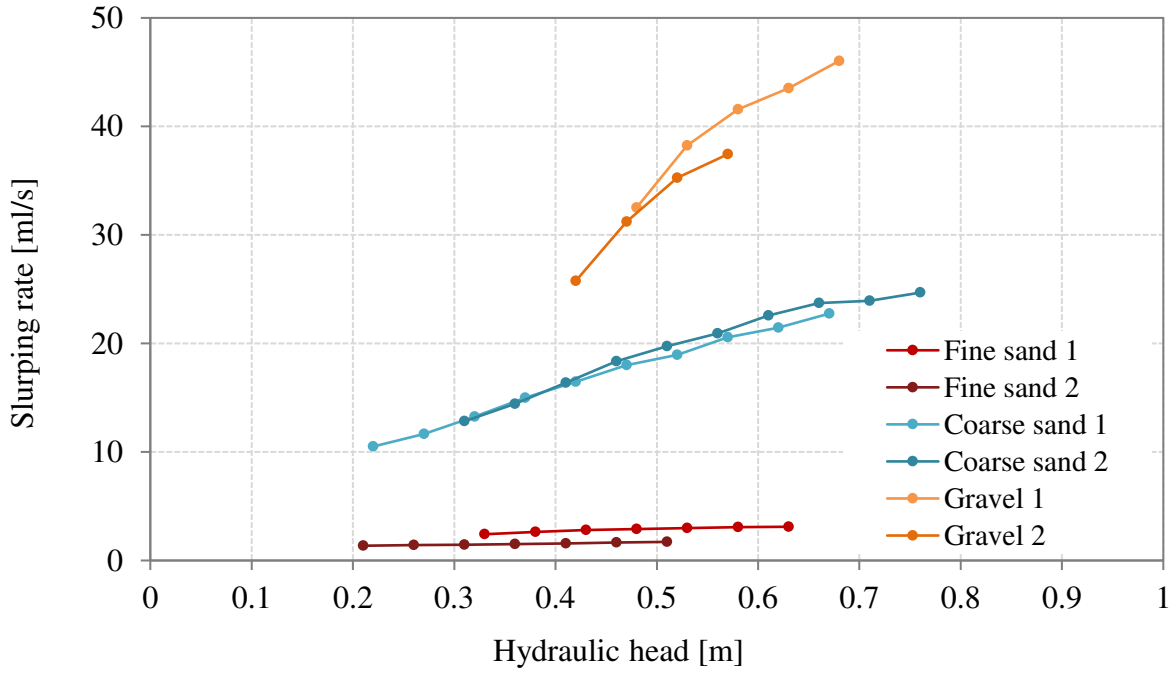

Figure 6.10: Dependency of slurping rate under changing hydraulic head for different material including fine sand (FS1-2), coarse sand (CS1-2) and gravel (G1-2).

Varying sediment depth and fixed water level

In contrast to the WL experiment, P2 examined vertical profiles of slurping rates with constant water level and varying sediment depth. Both experiments are conducted with the same material. In this case the water level is kept constant and the double packer is moved from bottom to top of the standpipe to measure a vertical profile. Figure 6.11 shows the P2 experiments in a rearranged version.

Neither the fine sand nor the coarse sand shows a clear trend of slurping rates with increasing hydraulic head. Gravel shows a much more heterogeneous behavior compared to the sandy materials. The results from P2 do not show a clear dependency of sediment depth on the slurping rate except for gravel material. The slurping rates from gravel decrease with increasing sediment depth and behave contrary to the water level experiment, where the slurping rates increase with increasing water level.

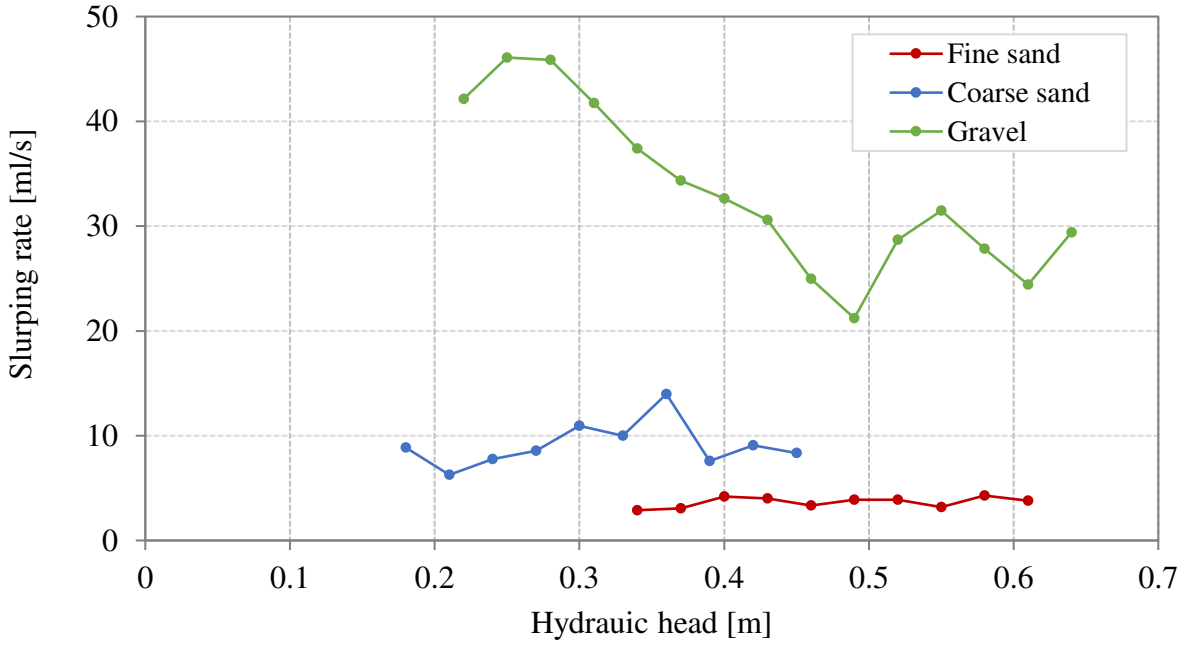

Figure 6.11: P2 experiment with varying sediment depth and fixed water level for the three different materials.

6.3.3 Detection of layers with varying k_f values

Figure 6.12 shows the results from the implemented layer experiment L1 and L2 using fine sand as layer and gravel as basic surrounding material below and above the layer. For the experiment L1 a 5 cm thick layer is implemented, and two profiles are measured at the same location in the tank. The colored bar in Figure 6.12 represents the fine sand layer, located at position 8 of the standpipe (sediment depth: 0.50 m). The slurping rate ranges from 21 ml/s to 52 ml/s in the gravel material and shows a significant decrease in the sand layer where slurping rate reduces to 8.5 ml/s in the first profile and 7.3 ml/s in the second profile. Both profiles have a high variation in the gravel part as already observed in previous experiments but show a very good agreement in the fine layer. In the next experiment L2 the thickness of the fine sand layer is 10 cm covering position 8 - 10 of the standpipe (sediment depth: 0.30 m-0.40 m). Moving the double packer towards the fine sand layer the slurping rates are almost constant around 40 ml/s. Then a sudden decrease ranging from 2 ml/s to 5.2 ml/s is measured within the fine sand layer followed by an increase of the slurping rate above the fine sediment layer to values ranging between 20 ml/s and 40 ml/s.

The slurping rate from the fine sand in this experiment agree well with the results from P2 where an average slurping rate of the fine sand on average of 3.6 ml/s is measured.

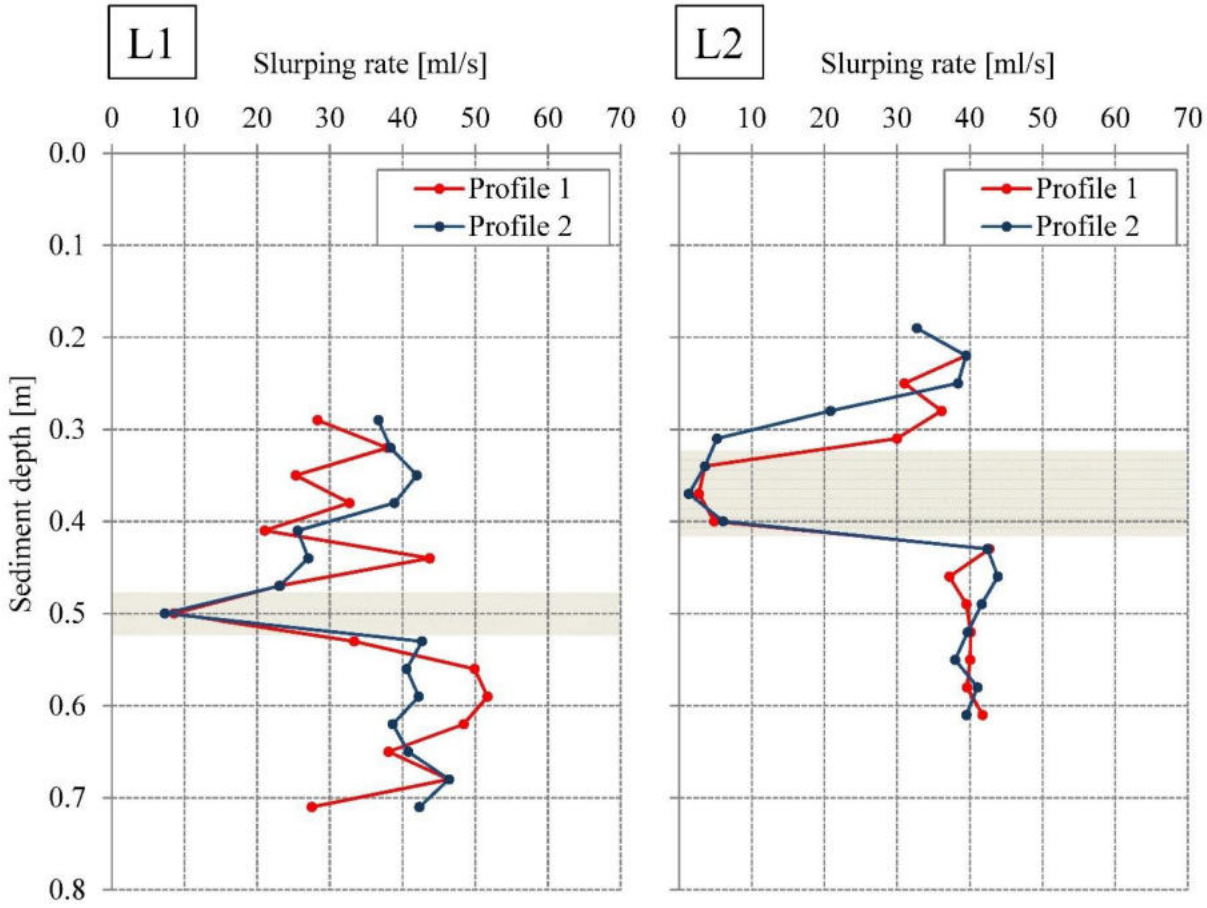

Figure 6.12: Implementation of layers into gravel material with varying thickness. L1: 5 cm fine sediment layer; L2: 10 cm fine sand layer.

In the next experimental set-up (L3 and L4) the layer from L1 and L2 are replaced with coarse sand material. The results from these experiments are displayed in Figure 6.13. The first profile for L3 shows lower variations in slurping rate compared to the second profile moving the double packer from the bottom towards the coarse sand layer. The second profile shows the same course but with higher variations of slurping rates. The slurping rate at the positions just below (position 7) and above (position 9) the coarse sand layer reduces to 26 ml/s for both profiles. The slurping rate at position 8 which is covered with the coarse sand layer reduces to 13.1 ml/s and 16.2 ml/s for the first and the second profile, respectively. L4 in general shows less variations and a rather constant slurping rate below the coarse sand layer compared to L1 and L3. Within the coarse sand layer, the lowest slurping rate decreases to 14.8 ml/s and 15.4 ml/s for the two profiles. The following two standpipe positions are still covered by the fine material layer; however, increasing slurping rate within the layer are observed. Position 10 in the first profile already reaches the same slurping rate in the coarse sand layer as measured above the layer. Above the layer the slurping rates further increase ranging between 30 ml/s and 40 ml/s.

The resulting slurping rates from L3 and L4 are also in good agreement with the results from P2 where an average slurping rate for the coarse sand of 9.1 ml/s is measured.

In all the four experiments the layer could be well detected using the VertiCo method. Comparing the fine sand layer L1 and L2 with the coarse sand layer L3 and L4, fine sand leads to higher reductions in slurping rate. Thus, the method proved not only to detect layers with different hydraulic conductivities, it is also possible to differentiate between different materials.

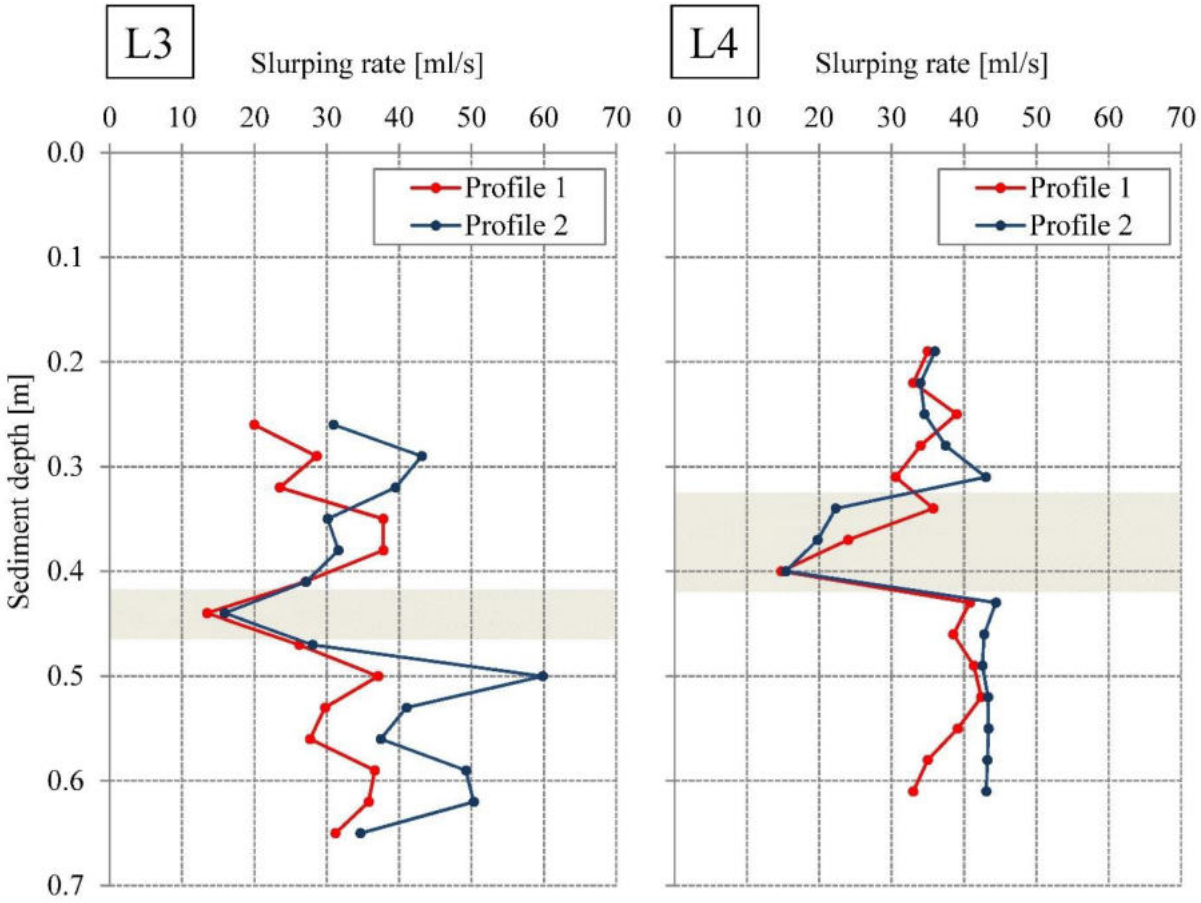

Figure 6.13: Implementation of layers into gravel material with varying thickness. Left: 5 cm coarse sand layer; right: 10 cm coarse sand layer.

A fived experiment is conducted (L5) where the low permeable layer is replaced by a non-permeable plastic layer. The plastic layer is placed at a sediment depth of 0.35 m (position 8 of the double packer). The results from this experiment are displayed in Figure 6.14 where the blue and the red line present the two measured profiles of this experiment. Even though the two profiles differ from each other, they show the same general systematic and the same behavior at the plastic layer. The blue line shows a stronger characteristic and higher fluctuations of slurping rates compared to the red line. The slurping rates are lower just below the plastic layer since less water from the top is available at the location. The slurping rates increases just above the plastic layer with increasing availability of water from the surrounding environment.

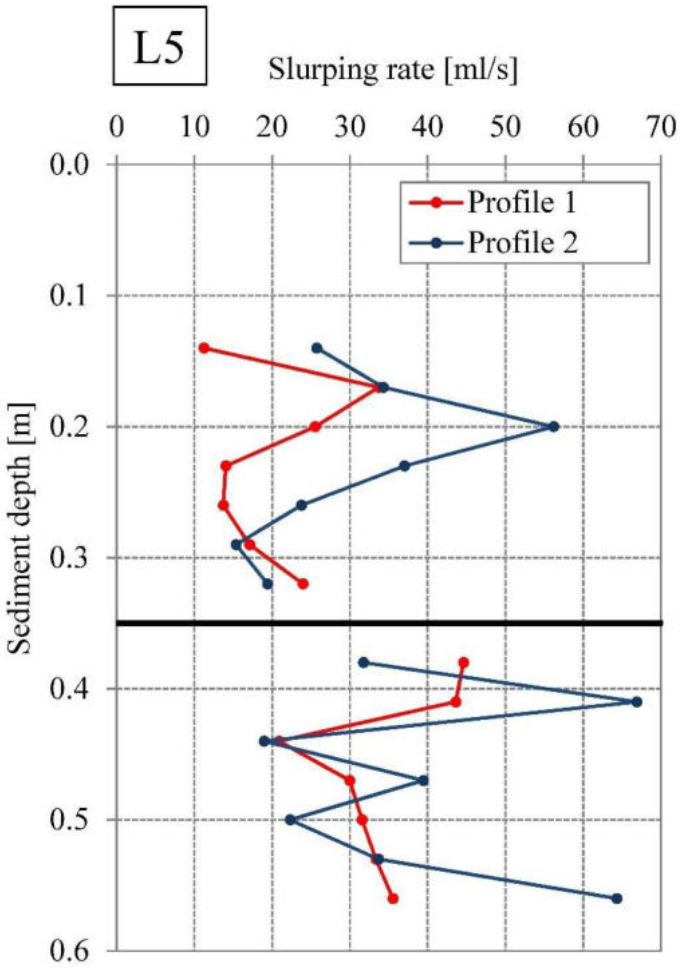

Figure 6.14: Implementation of non-permeable plastic layer.

6.3.4 Calibration and validation of the MODFLOW groundwater model

The V1 model is used to calibrate the openings from the standpipe in the groundwater model. The simulated slurping rates are compared to the measured slurping rates from the P2 and WL experiment. Since V1 is only valid for Darcy flow (Re < 10) gravel material is excluded from this analysis and only fine sand and coarse sand is used for the calibration and validation, respectively. Figure 6.15 (fine sand) shows the results from the calibration, where the blue line represents the measured slurping rates and the red line are the simulated slurping rates for the P2 experiment and both WL experiments. In general, the systematics can be well represented by the model, although the slope differs between the measured slurping rates and the simulated slurping rates by an average factor of 3.2. The comparison of the measured slurping rates and the simulated ones from the validation is summarized in Figure 6.16 a – c. The simulated slurping rates match the measured ones very well with only an averaged factor of 1.3. For the calibration and the validation, the slope from simulation is higher compared to the measurement. No different systematic can be observed for the experiments P2 and WL. Since P2 experiments have higher variations of each slurping rate, the slope cannot be detected as simple as for WL experiments. However, a trend line gives a very reliable indication. Although the slope from the simulated and the measured slurping rates differ from each other, the model

results already provide very good agreement between measured and simulated slurping rates. The determination of hydraulic conductivity is highly biased by several factors and difference in slope by an average factor of 3.2 (fine sand) and 1.3 (coarse sand) is already a very satisfyingly result.

For further analysis the calibrated and validated values for the openings of the standpipe are transferred into the V2 and V3 model. In case of modification of the geometry of the standpipe, especially the size of the openings or the mesh material, the area for the slurping rate is modified and needs to be re-calibrated.

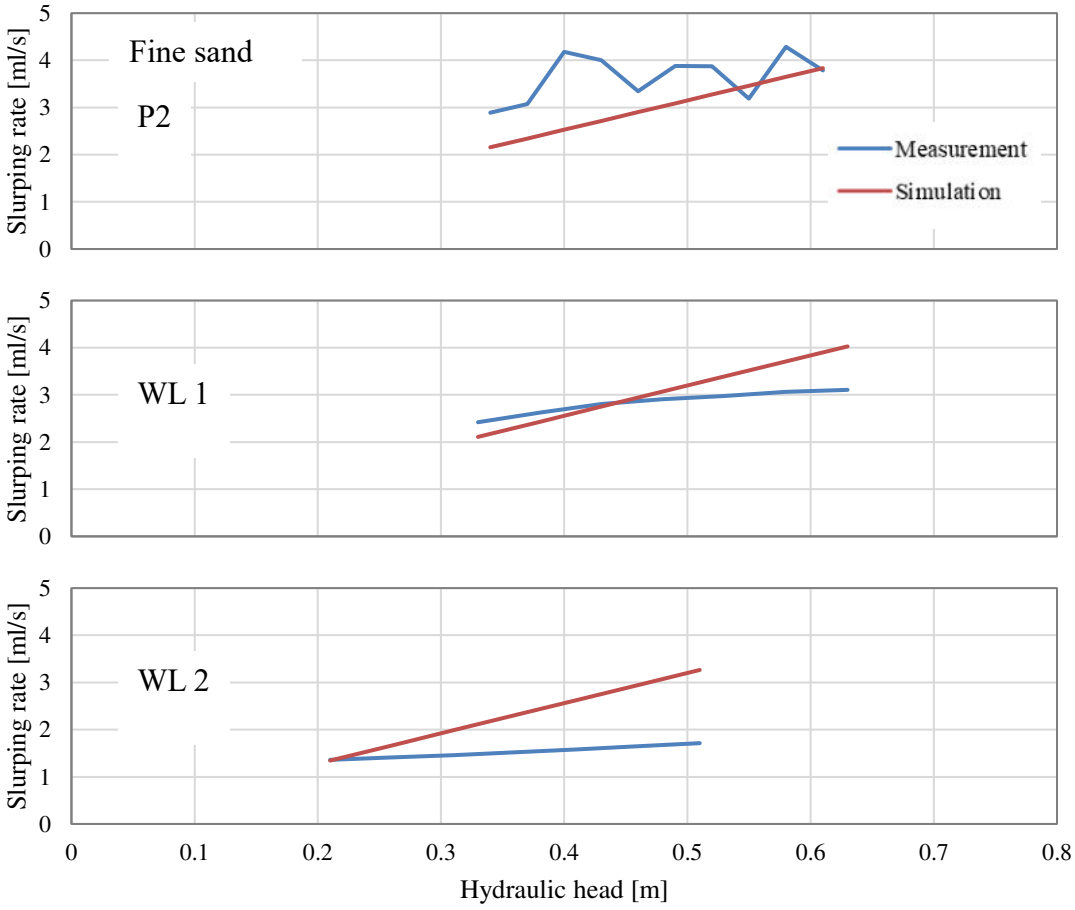

Figure 6.15: Comparison between measurement and simulation of slurping rates for P2 experiment and water level experiments (WL1 and WL 2) for fine sand.

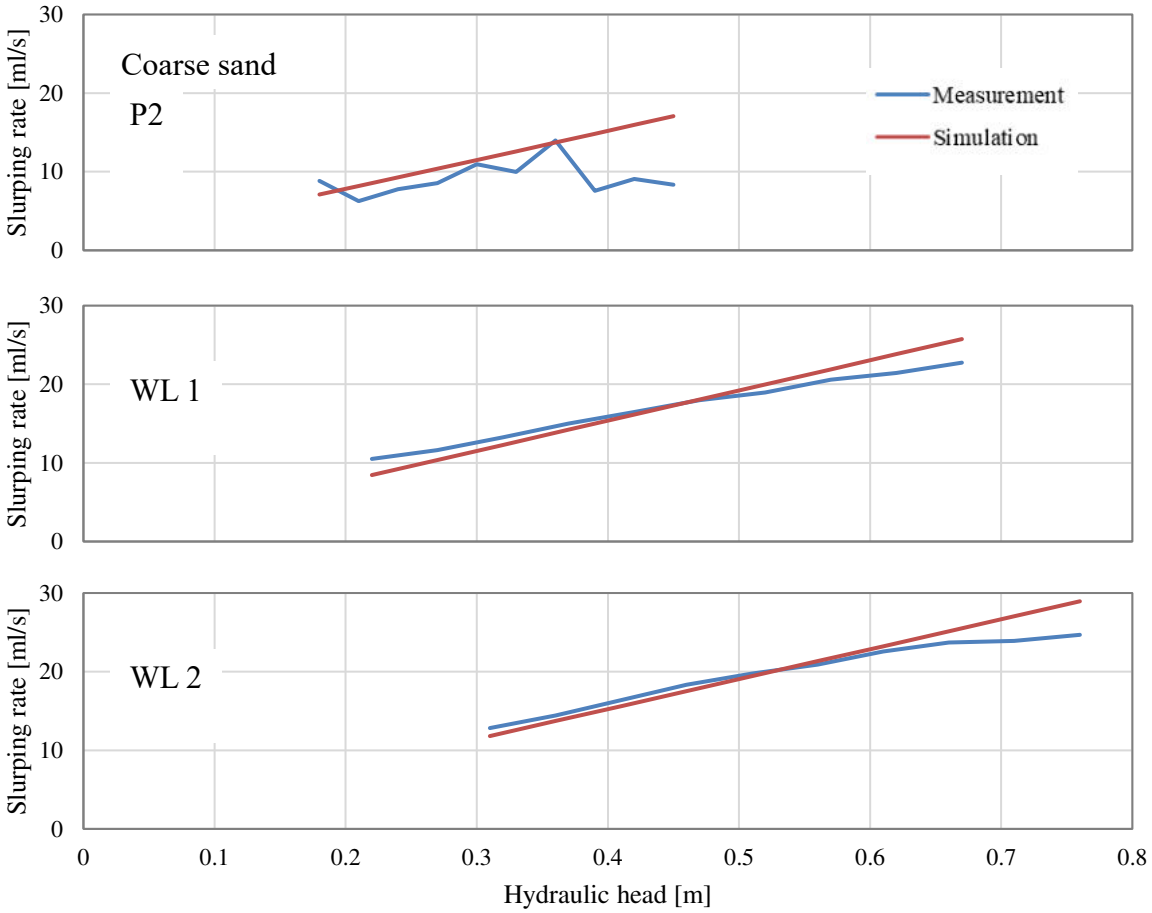

Figure 6.16: Comparison between measurement and simulation of slurping rates for P2 experiment and water level experiments (WL1 and WL 2) for coarse sand.

6.4 Discussion - Laboratory experiments for determining hydraulic conductivity using VertiCo

In the following chapter the results from the laboratory experiments are discussed. In addition, the newly developed method for hydraulic conductivity determination using the VertiCo method is analyzed and verified in detail using a groundwater model. Since the slurping method is a novel method no evaluation data set exists to compare the results of the method. Existing methods to determine the hydraulic conductivity are not applicable to compare the values from the experiments since no vertical profiles can be measured with these experiments.

In order to convert the slurping rates into hydraulic conductivity a numerical groundwater model (MODFLOW, see also chapter 3.3.3) is developed, which calculates the slurping rate based on a given k_f value (V1) or iteratively estimates a k_f values based on a measured slurping rate (V2 valid for Re < 10 and V3 valid for Re < 10 and Re > 10). This model is further used in this section to evaluate and verify the new method by comparing measured and simulated results.

6.4.1 Comparison to Mark IV standpipe according to Terhune (1958)

The VertiCo method is an advancement of the Mark IV standpipe introduced by Terhune (1958) by adding a double packer to measure a vertical profile. In the study of Terhune (1958) a correlation curve is developed to convert the measured slurping rates into hydraulic conductivities also shown in the correlation experiment in chapter 6.3.1. However, this correlation curve does not consider the influence of hydraulic head on the slurping rate and is only valid for one water level and one sediment depth. The method introduced by Terhune (1958) only measures a single value instead of a vertical profile, thus there is no varying sediment depth to consider. However, different water levels need to be considered. Moreover, the results from chapter 6.3.1 show a clear material dependency regarding the influence of changing water level on the slurping rates, where fine sand shows less influence of changing water level on the slurping rate compared to coarse sand or gravel. In order to consider this material dependency, different correlation curves based on different materials need to be established. In addition to the material dependency, different correlation curves for different hydraulic conditions are required resulting in a matrix of correlation curves. For practical use in field experiments this means that especially the grain size distribution is required for each position of the double packer since the water level and the sediment depth are easy to measure. In case where the grain size distribution is not available in such high resolutions, slurping rates cannot be transferred sufficiently into hydraulic conductivity. This is especially an issue when detecting colmation layers with lower hydraulic conductivity. Such a layer can be quite thin and difficult to detect in a sediment sample. This means, layers with different hydraulic conductivities might be a high bias due to the application of an insufficient correlation curve.

6.4.2 Numerical verification of laboratory tank using a groundwater model

Laboratory experiments are conducted in a tank as described in chapter 3.3. In order to evaluate whether the size of the tank is appropriate or whether boundary effects influence the result, slurping rates are simulated using the MODFLOW groundwater model in the tank with reducing the distance towards the wall. The MODFLOW V1 model is used for this evaluation presenting slurping rates based on known k_f values as output data. Wokabi (2018) showed in the laboratory experiments, using the same tank, that boundary effects only occur with a distance to the wall with less than 0.20 m. Measurements close to the centre did not lead to significant variations of the resulting slurping rates. In this study, measurements in the tank are conducted in the centre of the tank where the distance to the wall is 0.50 m. Thus, boundary effects in the laboratory experiments can be ignored. Figure 6.17 shows the results from the different slurping rates for the three materials used, where the simulated slurping rates are constant for all three materials with reducing distance to the wall until a certain distance is reached where the slurping rate starts to drop. Gravel material shows the highest influence of boundary effects where the slurping rate drops at 0.20 m from the wall. The slurping rate from coarse sand starts to drop at 0.15 m and the slurping rates from fine sand only start to drop at 0.10 m from the wall. The results from this simulation support the outcomes from Wokabi (2018). Thus, it can be assumed that the laboratory tank has a sufficient size and boundary effects can be neglected.

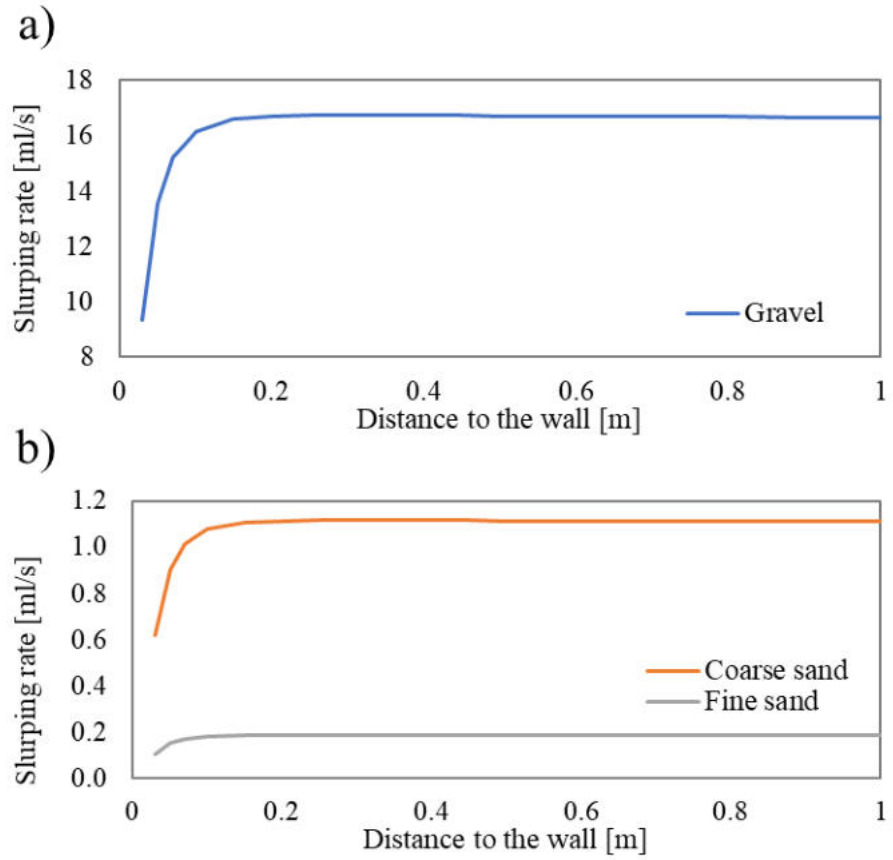

Figure 6.17: Influence of boundary effects in the numerical groundwater model (V1) for varying distances to the wall for a) gravel and for b) coarse sand and fine sand.

6.4.3 Discussion of P2 and WL experiments

Fine sand and coarse sand do not show a clear dependency of varying sediment depth on slurping rates, but a clear influence of changing water level can be observed in these materials. However, the results from the P2 and the WL experiments shows contradicting results for gravel material. In contrast to the water level experiment the results from P2 shows a decrease of slurping rate with increasing hydraulic head and thus behaves contrary to the water level experiments where the slurping rates increase with increasing hydraulic head. Both experiments demonstrate a dependency of the hydraulic head on the slurping rate. However, an increase in water level leads to different results compared to an increase in sediment depth. This might be explained by the fact that the friction and friction losses in the sediment layer caused by the sediment increases with increasing sediment depth leading to reduced slurping rates at deeper positions. In contrast to this, when increasing the water level, the friction caused by the sediment stays constant, but the hydraulic pressure increases which “pushes” more water into the measuring chamber of the double packer for deeper positions leading to higher slurping rates.

6.4.4 Numerical verification of laboratory experiments using the MODFLOW groundwater model

The V3 model is used to calculate the k_f values based on measured slurping rates from the P2 and the WL experiment and compare it to the k_f values obtained from the constant head experiments. The V3 model is further used to calculate the k_f values from the correlation and the layering experiment. In case of the correlation experiment, the simulated k_f values are compared to the measured k_f values from the constant head tests. Since no measurement of hydraulic conductivity exist from the layering experiment the resulting k_f values are displayed and the general systematic of the results is discussed and compared to the results from the slurping rates.

P2 and Water level experiments using MODFLOW V3

Figure 6.18 shows the simulated k_f values (scatter) and the k_f value measured with the constant head experiment (blue line). The simulated k_f values from fine sand and coarse sand agree well with the measured k_f values. Only the simulated k_f values from gravel material differ more from the measured value; however, it is still in the same order of magnitude. It should be noted that gravel results in higher uncertainties during measurement for the slurping rates and also in the constant head experiment.

The results from the P2 experiments show an increase of hydraulic conductivity with increasing Re for all materials. In contrast to this the simulated k_f values from the WL experiment from fine sand decrease with increasing Re and the simulated k_f values from coarse sand do not show a clear trend with increasing Re. Only the results from gravel show an increase of k_f values with increasing Re for both experiments.

Note that the calculation of hydraulic conductivity in the constant head test is based on Darcy´s Law. This is also applied for gravel material in this study where Darcy´s Law is not valid anymore. This might also be one fact which explains the difference between the simulated and measured k_f values for gravel. In this case the simulated k_f values might be more accurate compared to the measured one.

Since for low Reynold numbers the Forchheimer equation becomes the Darcy equation the results from simulation from V2 and V3 should be identical. With increasing Reynold numbers the influence of the inertial effects increase and the results differ more and more. For fine sand where rather low Reynold numbers exist ($0.15 < Re < 0.32$) the results from V2 and V3 match well with each other. Only four exceptions exist, where V3 results in higher k_f values compared to V2. For coarse sand the difference between V2 and V3 becomes higher with increasing Re. This also shows the transition zone between Darcy regime and Forchheimer regime. Until $Re = 6$ V2 and V3 agree well to each other and with $Re > 6$ the difference between the approach according to Darcy and Forchheimer becomes visible.

The standard deviation for all three materials for the simulated k_f values are very low with 0.0001 (V2 and V3) for fine sand, 0.0004 (V2) and 0.0005 (V3) for coarse sand and the highest standard deviation of 0.0065 for gravel (V3 only). These results are also a verification for the MODFLOW V3 model which shows a good performance with regard to reliable k_f values (good

agreement to measured k_f values from laboratory experiments) and with regard to reproducible results (matching k_f values for different hydraulic conditions; P2 and WL).

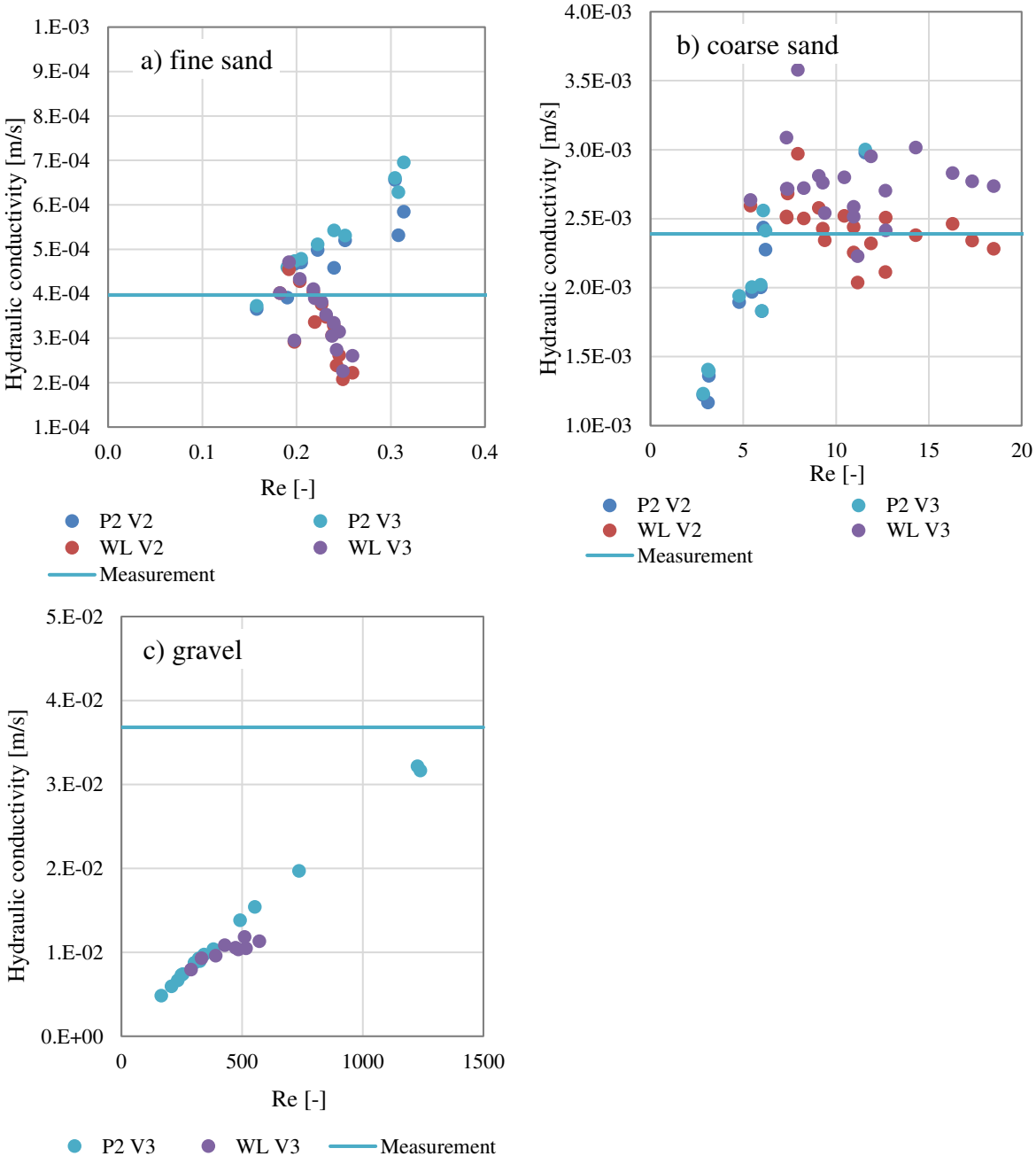

Figure 6.18: Comparing V2 and V3 to measured k_f values for fine sand and coarse sand and comparison between V3 and measurement for gravel.

Discussion and numerical verification of the correlation experiments using V3

Determination of k_f values is based on Darcy`s Law as explained in the previous section. The laboratory experiments show that Reynolds numbers for gravel are between 150 and 1500 and thus out of range for Darcy´s Law (Re < 10). However, Darcy´s Law is applied for gravel

material for the calculation of the k_f values from the constant head tests. The minimum diameter from the column for conducting the constant head test is 10 • D_{max}. The gravel in this study has a D_{max} of 8 mm and the diameter of the column is 0.1 m und thus fulfill the minimum requirement for the column experiment. However, Darcy´s Law is not valid due to turbulent conditions. This might lead to an error in the determination of hydraulic conductivity for coarse material such as gravel and mixtures with high gravel amount. The comparison of simulated and measured k_f values from gravel in Figure 6.18c showed that the measurement overestimates the k_f value compared to the simulation. This happens when Darcy´s Law is applied outside the valid range since the inertial effects from turbulent conditions are not considered resulting in higher k_f values. The resulting error in the k_f value influences the correlation curve (Figure 6.9 in chapter 6.3.1), which might result in a different slope. An attempt to deal with this issue would be to conduct more measurements with material, which is valid for Darcy´s Law and then linearly extrapolate to the coarse material.

The V3 model is used to simulated k_f values from the correlation experiment (chapter 4.2.2 and chapter 6.3.1) and compare them to the measured values. Figure 6.19 shows the k_f values from the simulation and the measurement and the dashed line gives the 1:1 line. Some of the simulated k_f values underestimate the measured ones and vice versa. For lower k_f values the simulated ones underestimate the measured ones and for higher k_f values the simulated ones overestimate the measured ones. Several facts need to be considered before interpreting these results. Firstly, the uncertainties for the constant head experiments are quite high, especially for coarse material such as the gravel used in this study. Secondly, the Modflow V3 models requires information about the *a* and *b* Forchheimer coefficient (chapter 3.3.3). The *a* coefficient is the inverse of the k_f value and the *b* values can be estimated using different approaches from literature (summarized in Sidiropoulou et al. 2007). All these approaches require information about D_m and/or porosity. The estimation from k_f value for the *a* factor can be derived from the empirical approach form Kozeny-Carman. This approach also requires detail information about grain size distribution. However, the information is not known, since the different mixtures are not analyzed in detail. Thus, the Forchheimer coefficients *a* and *b* where roughly estimated and kept constant for the simulation of all mixtures. Considering the high uncertainties, the simulated and measured k_f values agree well to each other.

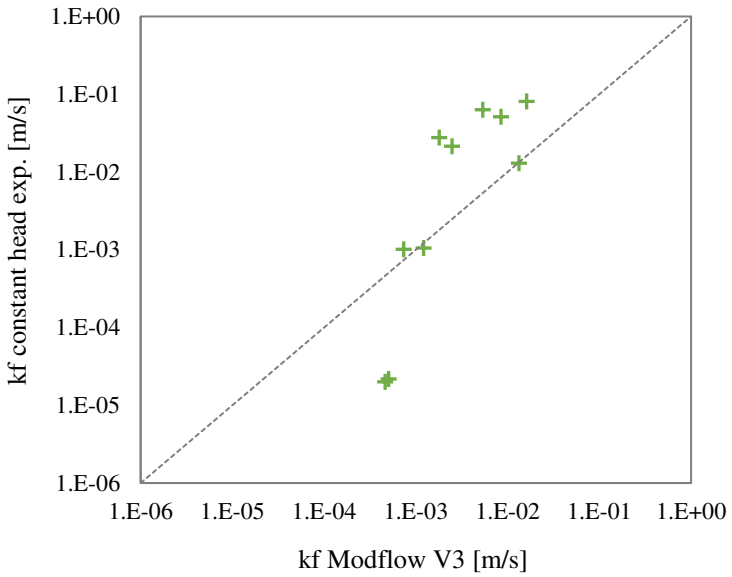

Figure 6.19: Correlation between simulated k_f values based on MODFLOW V3 and k_f values based on laboratory constant head experiments.

Layering experiments using MODFLOW model V3

The slurping rates from the layering experiments (chapter 4.2.2 and chapter 6.3.1) are transferred into k_f values using the V3 model. A comparison of the k_f values and the slurping rates is not appropriate since the influence of the hydraulic head is still included in the slurping rates. Since there are no measured data to compare the results from the experiment the resulting vertical profile will be presented in this section and interpreted based on the general systematic. The vertical profiles from the layering experiments in Figure 6.20 top and bottom are displayed on a logarithmic scale. The beige bar represents the layer with finer material and thus lower hydraulic conductivity. The hydraulic conductivity reduces strongly within the lower permeable layer and increases afterwards again for all experiments. For the experiments with a 10 cm layer (L2 and L4) the k_f values below the layer is lower than the ones above the layer. A denser packing can be precluded since gravel material is quite homogeneous and cannot be compacted. Less water can infiltrate through the lower permeable layer leading to a reduced slurping rate and thus to lower k_f values below the layer. This behavior cannot be observed for the experiments with 5 cm thick layer (L1 and L3) where the k_f values are constant below and above the layer. The influence of the 5 cm layer on the deeper positions is less compared to the 10 cm layer.

The results from this simulation confirm the possibility of the V3 model to produce reliable results by detecting the layers.

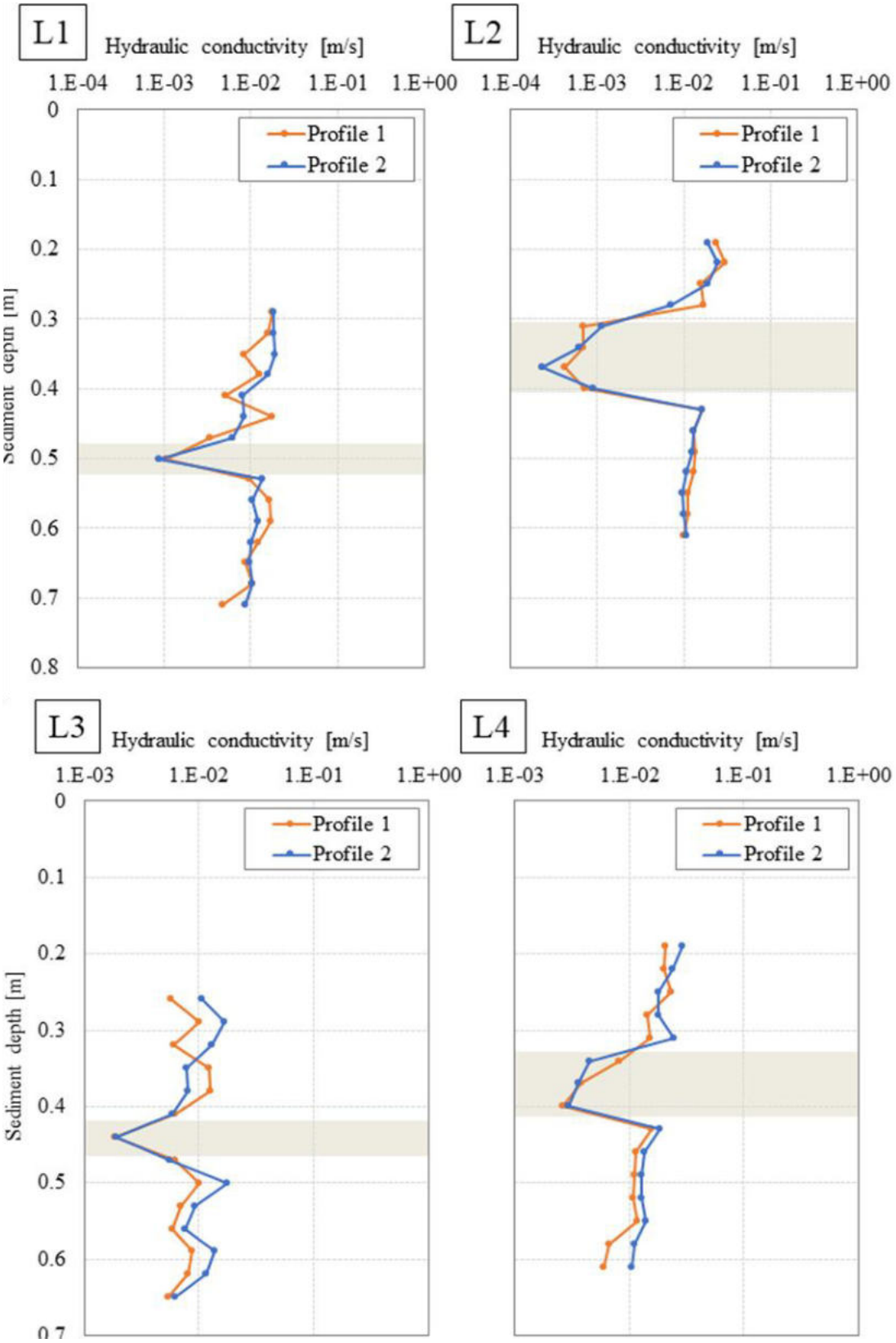

Figure 6.20: Layering experiment with k_f values for fine sand: top left 5 cm layer (L1), top right 10 cm layer (L2) as well as for coarse sand: bottom left 5 cm layer (L3) and bottom right 10 cm layer (L4).

6.5 Summary - Laboratory experiments for determining hydraulic conductivity using VertiCo

Laboratory experiments to determine hydraulic conductivity by using the new developed VertiCo method are conducted in order to test the method under fixed and simplified conditions. The experiments show that the influence of water level and varying sediment depth have a strong influence on the slurping rates. Thus, slurping rates need to be transferred into hydraulic conductivities in consideration of the influence of the hydraulic head. A simple correlation curve as introduced in the study from Terhune (1958) is not appropriate since the influence of varying water level and sediment depth is highly material dependent. Thus, another method is required to transfer slurping rates into hydraulic conductivities. In this study three different MODFLOW groundwater models are developed, which calculate the slurping rate based on a given k_f value (V1), or iteratively estimates the k_f values based on given slurping rates for Re < 10 (V2) and for Re > 10 (V3). The models are further used to evaluate the laboratory experiments by comparing the measured k_f values to the simulated ones.

In a first step the size of the tank used for the laboratory experiments is analyzed regarding boundary effects. The results from the simulation show that the size of tank is sufficient and boundary effects can be neglected. This also supports the studies from Wokabi (2018) and Zaqout (2017), which have shown that the influence of boundary effect can be neglected when measuring in the center of the tank. However, the closer the standpipe is set to the wall the higher fluctuations of slurping rates occur.

The influence of hydraulic head on the slurping rate is an important issue in this study which is analyzed in detailed. Experiments with varying water level (WL experiments) or with varying sediment depth (P2) show a significant influence of hydraulic head on the slurping rate. WL experiments show an increase of slurping rate with an incremental rise in water level for all materials. In contrast to this, the gravel material shows a decrease of slurping rates with increasing sediment depth. Fine sand and coarse sand do not show any influence of increasing sediment depth on the slurping rates. The comparison of the measured and the simulated slurping rates (V1) show that the measured values match well to the simulated ones from the P2 and WL experiment. Also, the comparison of simulated k_f values from the P2 and WL experiment results in a very good agreement to the measured k_f values from the constant head experiment.

A correlation experiment is conducted to correlate slurping rates based on different grain size distributions to the corresponding hydraulic conductivities. The hydraulic conductivity is measured in the laboratory by applying constant head tests. The results confirm the assumption of a linear relation between slurping rate and hydraulic conductivity. Based on the linear relation, an equation (6.1) can be set up to calculate k_f values based on slurping rates. However, this equation is only valid for the current geometry of the standpipe and the hydraulic conditions (water level and sediment) depth used in the experiments. A modification of the standpipe, for example changing the size of openings or changing the mesh on top of the openings will result in a different correlation. Also varying water levels or different sediment depth will modify the

correlation. When measuring a vertical profile, a clear influence of varying sediment depth on the slurping rate can be observed (see P2 experiment) and thus the correlation cannot be applied for measuring vertical profiles. A comparison between the simulated (V3) and the measured k_f values from the correlation experiment showed a good agreement where the simulated values match the measured values

An experiment with different layers of finer material is conducted in order to analyze whether the VertiCo method is suitable to detect colmation layers with lower hydraulic conductivities. The resulting slurping rates show that layers with finer material can be detected very well and the transferred k_f values from the V3 support these outcomes. The vertical profile with k_f values shows a clear decrease of hydraulic conductivity at the positions with finer material.

The laboratory experiments and the comparison of the experimental results to the simulated k_f values from the MODFLOW groundwater model confirm the accuracy, repeatability and the general applicability of the new developed method to determine hydraulic conductivity with the VertiCo method. The MODFLOW model perform well in estimating the k_f values based on measured slurping rates and thus it can be applied to transfer the measured slurping rates into k_f values under consideration of the respected hydraulic conditions. Layers with lower hydraulic conductivity as present in colmation layers can be detected with the new method.

7. MULTI-PARAMETER APPROACH – FIELD APPLICATION

For testing the multi-parameter approach in the field in total 41 data sets are gathered from eight different rivers. In a first step, the results are analyzed regarding the required sample mass to check representability (chapter 7.1). According to different criteria found in literature the sediment samples and the porosity analysis is modified. Therefore, large grains are excluded from further analysis. In a next step, all gathered data are presented in an overview for each river showing all parameters from the multi-parameter approach (chapter 7.2). Therefore, the slurping rates are transferred into hydraulic conductivities using the V3 model. The gathered data as well as their relation between each other are analyzed, interpreted, and discussed in detail in chapter 7.3. Therefore, the analysis regarding the relations between the parameters from the multi-parameter approach is carried out under a river specific point of view and by applying a 3-parameter analysis where the data sets are sorted into different classes of porosity or sediment characteristics. Chapter 7.4 finally summarizes and concludes the outcomes of the multi-parameter approach.

7.1 Sediment samples and its required sample mass

As already discussed, (chapter 2.3.1) samples sizes is a crucial factor when evaluating the quality of sediment samples. A representative sample requires a certain sample mass in order to neither overestimate large fraction nor underestimate smaller fraction. For the field samples the samples mass is analysed with respect to the criteria summarized in Table 2.8. The grain size distribution is further modified and cut to fulfil the criteria in cases where sample mass is not sufficient. Since large grains also influence porosity, large grains are also excluded from the porosity analysis if required. Therefore, the volume of a size fraction is estimated using the calculated density from the total sample mass. According to (Church et al. 1987) the 5% criterion (dotted blue line in Figure 7.1) is sufficient for samples with fractions larger than 128 mm. All other samples need to fulfil at least the 1% criterion (solid blue line in Figure 7.1) according to Church et al. (1987) or the German Standard (DIN; green line in Figure 7.1). The criterion according to De Vries (1970) (red lines in Figure 7.1) can only be partly fulfilled for field data based on gravel material. It is more common for soil samples with small size fractions.

15 out of 41 samples fulfil the 1% criterion of Church et al. (1987) and do not need to be modified at all (solid grey triangles in Figure 7.1). Eleven samples fulfil the Church 1% criterion when excluding all grains larger than 128 mm (solid filled black triangles in Figure 7.1). Only three samples need to be cut at 64 mm to fulfil the Church 1% criterion (black empty triangles in Figure 7.1) and 12 samples need to be cut at 128 mm to fulfil the 5% Church criterion (orange rhombus in Figure 7.1). Table 7.1 summarizes the samples IDs from adapted sediment samples.

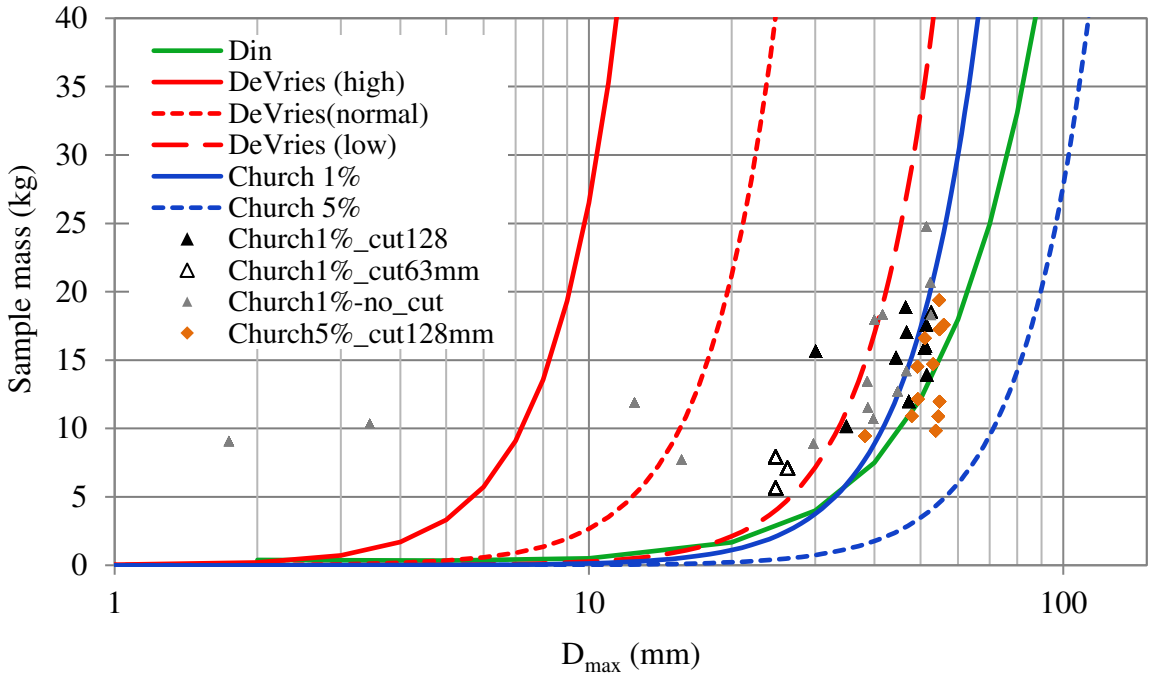

Figure 7.1: Required sample mass to fulfil criteria for representative samples.

Table 7.1: Summarized samples ID with modification according to Figure 7.1

No modification needed	Cut at 128 mm according to 5% criterion Church et al. (1987)	Cut at 128 mm according to 1% criterion Church et al. (1987)	Cut at 64 mm according to 1% criterion Church et al. (1987)
Aich 2	Eyach 1 – 4	Aich 3	Aich 1
Glems 1	Eyach 2	Glatt 5	Aich 4
Glems 2	Eyach 3	Glatt 6	Glatt 1
Glems 3	Eyach 4	Lein 1	
Glems 4	Glatt 2	Lein 2	
Glems 5	Glatt 3	Lein 3	
Glems 6	Glatt 4	Wieslauf 2	
Rems 2	Lein 4	Würm 1	
Rems 3	Wieslauf 1		
Rems 5	Wieslauf 3		
Würm 2	Wieslauf 4		
Würm 3	Wieslauf 5		
Würm 4			
Würm 5			
Würm 6			

7.2 Results - Multi-parameter approach

A summary of the four parameters gathered from field experiments is presented in the following chapter. One representative example of a vertical profile of hydraulic conductivity and interstitial oxygen saturation is shown in detail for each river. Additionally, the range of all vertical profiles of hydraulic conductivity and interstitial oxygen saturation are summarized by an enveloping curve. Finally, boxplot diagrams of the grain size analysis of the sediment sample are shown for every sample including additional information about the sediment characteristics as well as the porosity of the sediment sample based on the SfM-MVS method. A more detailed summary of each vertical profile of slurping rate, hydraulic conductivity and interstitial oxygen saturation as well as the cumulative sieve curve of each sediment sample including an image of the sediment sample can be found in Appendix 2.

The multi-parameter approach performed well in the field and it proved to be robust enough for measurements in coarse gravel rivers. After setting up the equipment (approx. 30 – 45 min) the first measurement is the vertical profile of IDOS which takes approx. one hour to conduct. The following VertiCo method takes around three hours for one vertical profile with 15 vertical measuring positions and a resolution of 3 cm including three measurements per position. The sediment sample is taken in the close vicinity of the location from the VertiCo method approx. 0.5 m – 1.0 m upstream and lasts about 30 min. The following image acquisition with the frozen sediment sample for the SfM-MVS method takes approx. 10 – 15 min.

7.2.1 Aich

The results of River Aich are shown in Figure 7.2 a - c. Aich 4 is shown in detail in Figure 7.2a where relatively low hydraulic conductivities and high IDOS can be observed. The vertical profile of k_f does not show a strong variation over depth (Figure 7.2 a) ranging from 5.2E10^{-4} m/s to a maximum of 3.7E-3 m/s. IDOS has a strong increase from the lowest to the second lowest position from 56.9 % saturation to 83.4 % saturation and a further slight increase until 102.2 % saturation for the highest position.

The vertical profiles of k_f of the other locations at River Aich are also characterized by relatively low values (Figure 7.2 b) and a low decrease of hydraulic conductivities over depth. Only single points show low hydraulic conductivities such as Aich 2 with the lowest hydraulic conductivity of 1.6E-6 m/s at a sediment depth of 0.35 m. In contrast to IDOS at Aich 4, the other measurements show a stronger decrease of IDOS with increasing sediment depth. Especially IDOS of Aich 4 reaches the lowest value of 6.3 %.

The porosity from Aich 1 and Aich 2 (Figure 7.2 c) is 46.4 % and 47.7 %, respectively. The two locations are measured in pools and this high porosity value might be due to muddy material in this location. This is supported by the high amount of fine sediments. Location Aich 3 and Aich 4 are measured on a small riffle with higher flow velocity. This can directly be seen by the lower porosities of 29.9 % and 32.9 % which indicates fewer fine sediments. However, the grain size distribution of all locations is rather homogeneous and do not show high differences between

pool and riffle location. The D_m and σ_g of all samples is in a close range between 8.4 mm and 11.5 mm and between 2.3 and 2.9, respectively.

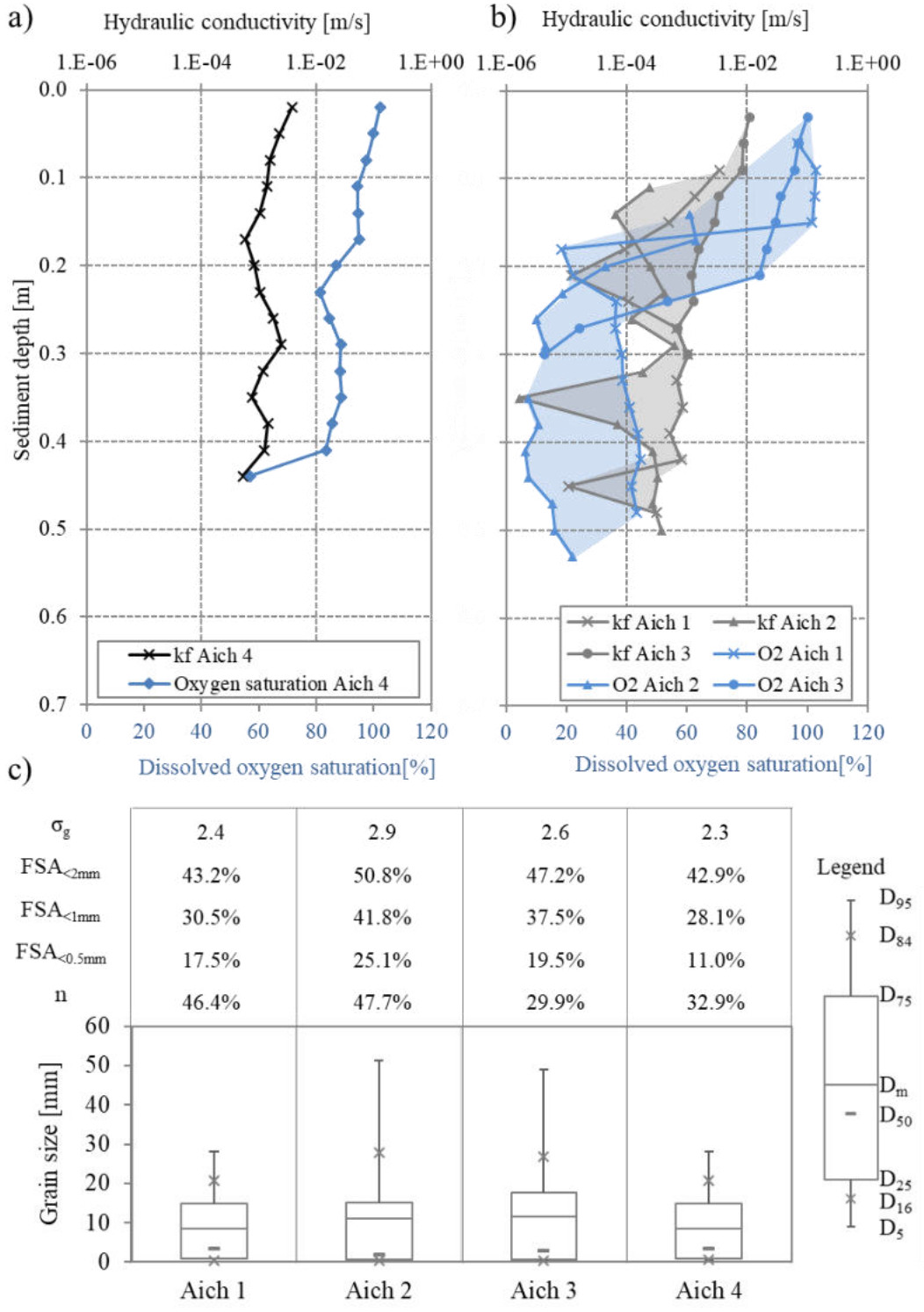

Figure 7.2: Results from field experiment at River Aich showing a) a representative example of a vertical profile from hydraulic conductivity and intragravel dissolved oxygen saturation, b) the remaining data sets of hydraulic conductivity and intragravel dissolved oxygen saturation c) boxplot diagrams for each sediment sample including grain size characteristics as well as porosity.

7.2.2 Eyach

Figure 7.3 a - c summarizes the results from River Eyach. Eyach 4 is displayed in Figure 7.3a, it has rather moderate to low hydraulic conductivities for the lowest 20 cm ranging between 3.9E-4 m/s and 2.2E-3 m/s and it even decreases slightly with increasing height. Hydraulic conductivity increases steadily and ranges around 1.5E-2 m/s for the upper 15 cm. The vertical profile from IDOS starts with low values around 50 % and shows a slight decrease between the sediment depths of 0.4 m to 0.3 m. At a sediment depth of 0.26 m IDOS strongly increases reaching saturation values of more than 100 % close to the surface. The combination of high IDOS and high k_f values close to the surface enables high exchange processes into the hyporheic zone.

The three remaining vertical profiles of hydraulic conductivity at River Eyach show a wide range of values (Figure 7.3 b). Eyach 1 shows rather low k_f values and high heterogeneities until the top most 0.1 m where the values increase to around 1.0E-2 m/s. IDOS reaches stable values above 100 % saturation starting from a sediment depth of 0.2 m. Eyach 2 and 3 do have higher k_f values compared to Eyach 1 and 4 starting already with values around 5.0E-3 m/s for the lowest positions. Both locations do not show high increase in hydraulic conductivities since the values are already quite high. Except a few jumps to smaller k_f values the hydraulic conductivity seems to have a constant course over depth. This behaviour is also observed for IDOS where no increase over depth is observed except for Eyach 1 which shows lower IDOS until a sediment depth of 0.25 m.

The porosity and the grain size characteristics are rather homogeneous for the four locations and do not show high variations in the values (Figure 7.3 c). The porosity ranges between 26.2 % and 29.8 %. Compared to River Aich the sediments are coarser, the D_m ranges between 21.7 mm and 25.9 mm. In agreement with high slurping rates and oxygen saturation less fine sediments are detected at River Eyach compared to River Aich. The FSA below 2 mm ranges between 11.8 % and 14.0 % and the FSA below 0.5 mm ranges between 2.8 % and 5.7 %.

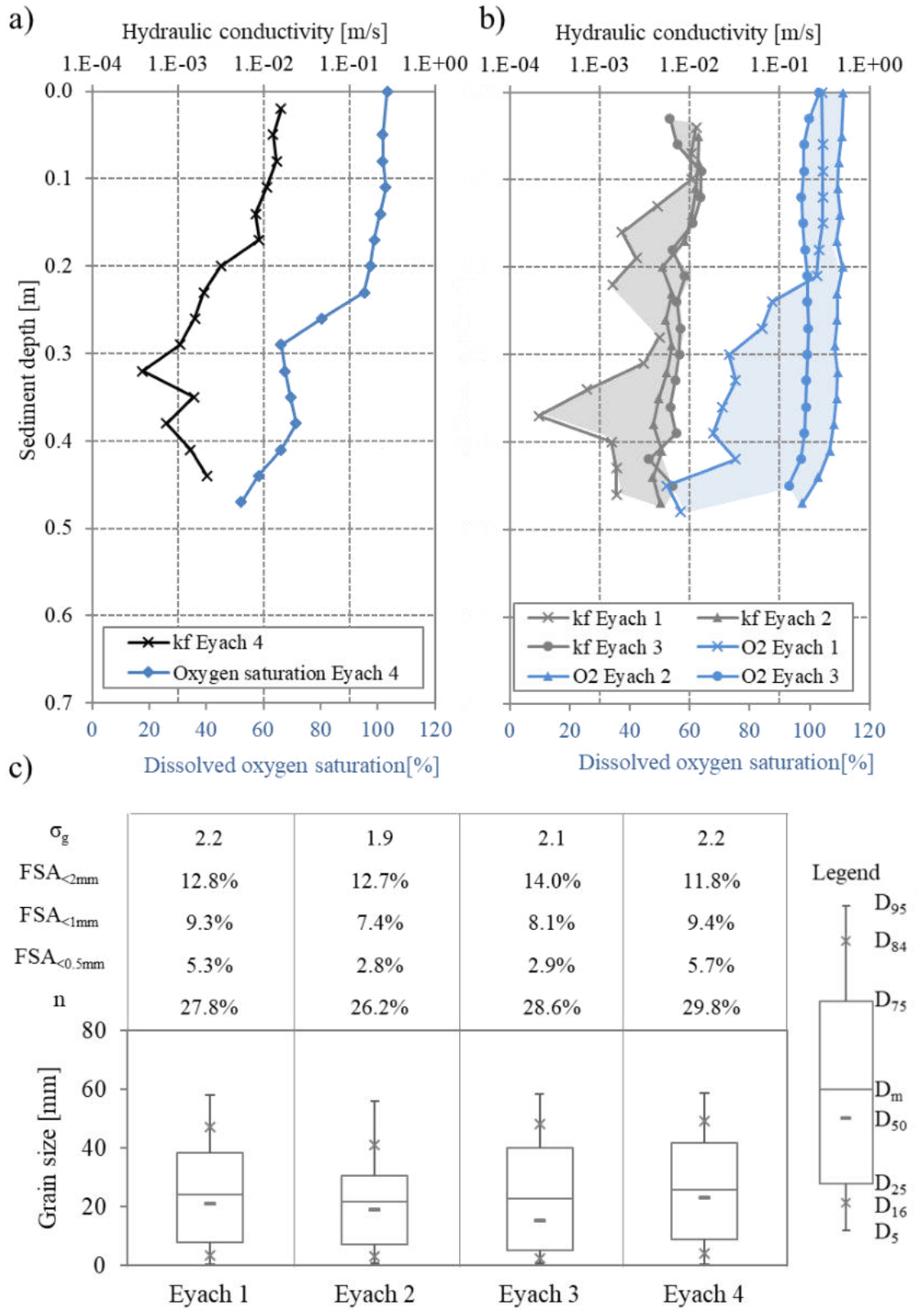

Figure 7.3: Results from field experiment at River Eyach showing a) a representative example of a vertical profile from hydraulic conductivity and intragravel dissolved oxygen saturation, b) the remaining data sets of hydraulic conductivity and intragravel dissolved oxygen saturation c) boxplot diagrams for each sediment sample including grain size characteristics as well as porosity.

7.2.3 Glatt

The results from monitoring campaign at River Glatt are summarized in Figure 7.4 a - c. The vertical profile of the hydraulic conductivity and IDOS from location Glatt 2 is displayed in Figure 7.4 a. The hydraulic conductivity linearly increases with increasing height starting from low values at the lowest position of 2.2E-4 m/s and rising to 9.6E-3 m/s for the highest position representing good exchange conditions for the upper layer of the riverbed. Values for IDOS at Glatt 2 show an increase for the lowest 0.25 m from 69 % to 100 % saturation and then stable values around 110 % saturation for the upper 0.25 m also supporting the good exchange conditions at this location.

Most of the vertical profiles of hydraulic conductivity at River Glatt have low values for the deepest positions (Figure 7.4 b) and steady increase with increasing height. Glatt 6 is an exception showing already good exchange conditions based on high k_f values for the lowest positions and homogenous values over depth. The vertical profiles from IDOS measurements show a wide range of values for the deepest positions, which means that different conditions can be found here. However, the values becoming more homogenous for the top layer in the upper 0.1 m of the riverbed where all values exceed 100 % saturation and some values even reach 120 % saturation.

The porosity and the grain size characteristics show higher variations for the different locations compared to River Eyach and River Aich (Figure 7.4 c). The porosity ranges from 17.8 % at Glatt 6 to the highest value of 30.5 % at location Glatt 4. Contradicting to the highest porosity values location Glatt 1 and 4 have the lowest D_m of 10.6 mm and 17.1 mm, respectively. The other D_m values range between 19.0 mm and 25.4 mm. The grain size distribution also show high variations between the single locations where for example Glatt 1 only has a narrow grain size distribution but a high amount of fine sediments compared to Glatt 2 and 3 which have a wider range of the grain size distribution and significantly lower amount of fine sediments.

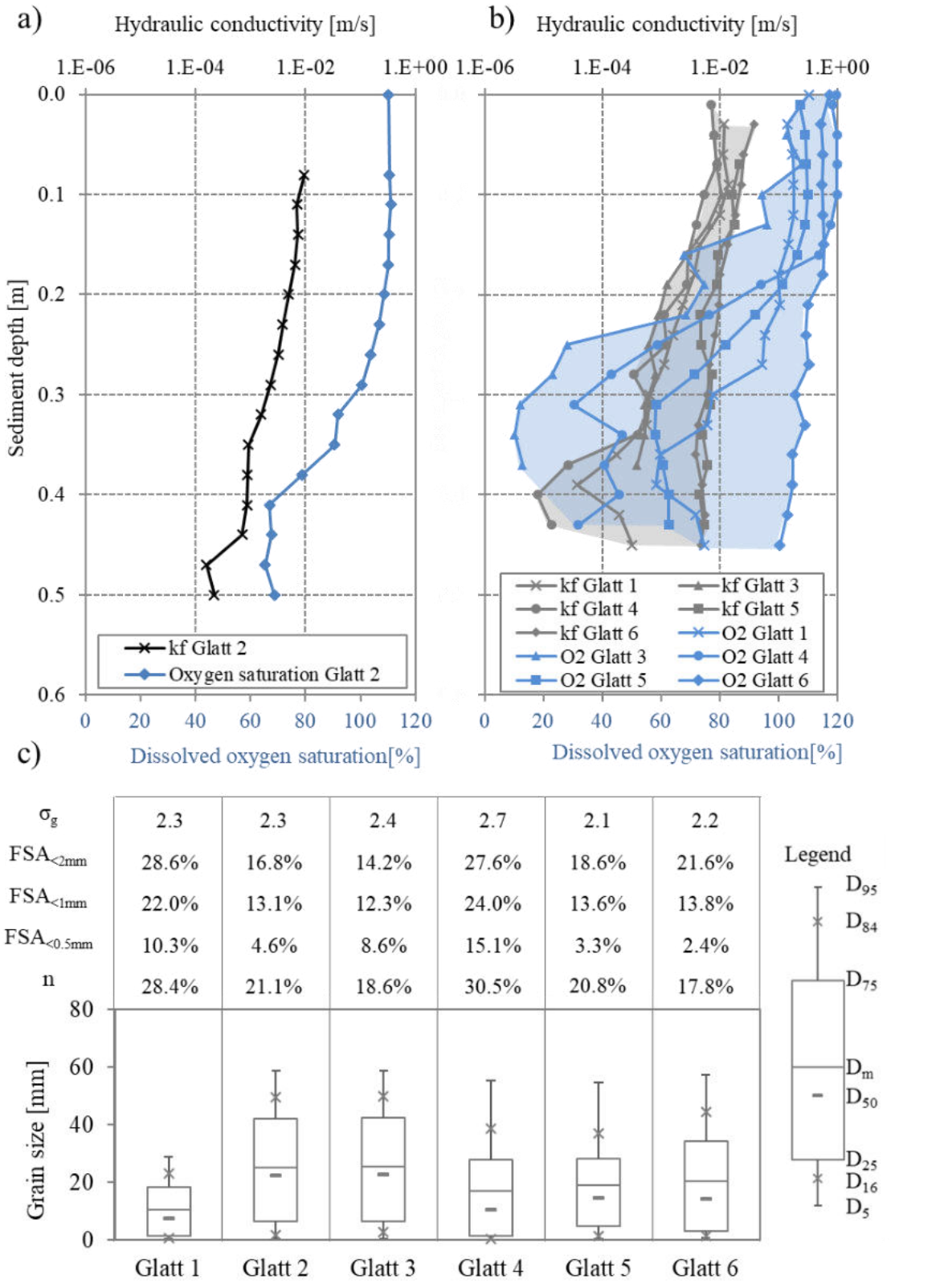

Figure 7.4: Results from field experiment at River Glatt showing a) a representative example of a vertical profile from hydraulic conductivity and intragravel dissolved oxygen saturation, b) the remaining data sets of hydraulic conductivity and intragravel dissolved oxygen saturation c) boxplot diagrams for each sediment sample including grain size characteristics as well as porosity.

7.2.4 Glems

The results from River Glems are summarized in Figure 7.5 a - c. Figure 7.5a presents the vertical profile of hydraulic conductivity and IDOS from location Glems 1. The k_f values are extremely low ranging from 1.7E-5 m/s to 9.0E-5 m/s for lowest 0.35 m. The values then slightly increase for the upper 0.1 m reaching a maximum value of 2.5E-3 m/s for the position closest to the surface. This low hydraulic conductivity means poor exchange conditions for the riverbed. IDOS is also relatively low at the deepest locations showing a linear increase from 17.9 % saturation to 37 % saturation at a sediment depth of 0.13 m. For the upper four measuring points the slope of the vertical profile changes and IDOS increases further to values of 88.8 % saturation for the position closest to the surface.

The results from the remaining five locations of River Glems are summarized in Figure 7.5 b showing similar low hydraulic conductivities as Glems 1. There is almost no increase observed for the k_f values resulting in poor exchange conditions in the whole reach. This can be supported by the relatively low IDOS values for the different locations. The saturations are low, ranging between 0 % and 20 % saturation for the vertical profiles until a sediment depth of 0.2 m. Then the values increase reaching maximum values of 89.8 % saturation for the upper position. Glems 4 is an exception having higher IDOS at lower positions. In general, the k_f values show low variation for the different sample sites meaning that there are not many variations in the riverbed composition.

River Glems has the finest riverbed material of all sampled rivers in this study. The riverbed consists most of fine material what can be seen from the high FSA summarized in Figure 7.5 c. The sediment samples from Glems 1 only consist of fine sediments with a FSA<2 mm of 91.7 %. The FSA<0.5 mm including the cohesive particles is 55.9 % and thus contributes for more than half of the sample. Glems 2 has the lowest FSA<2 mm with 45.9 % which means that almost half of the sample consists out of these fine particles explaining the low slurping rates and oxygen saturation. The D_m ranges from 1.0 mm (Glems 1) to 15.4 mm (Glems 2). Glems 2 and Glems 6 are the coarsest samples at this location. In this case a small gravel layer at the top layer was observed leading to lower FSA in general and a wider range in grain size distribution. It is noticeable that the porosities at River Glems are unexpectedly high, reaching values up to 43.1 %. This can be explained with the high amount of cohesive material in the riverbed which leads to such high porosities. Liu et al. (2018) for instance reports porosities from clay material in impounded river section and lakes around 80 %.

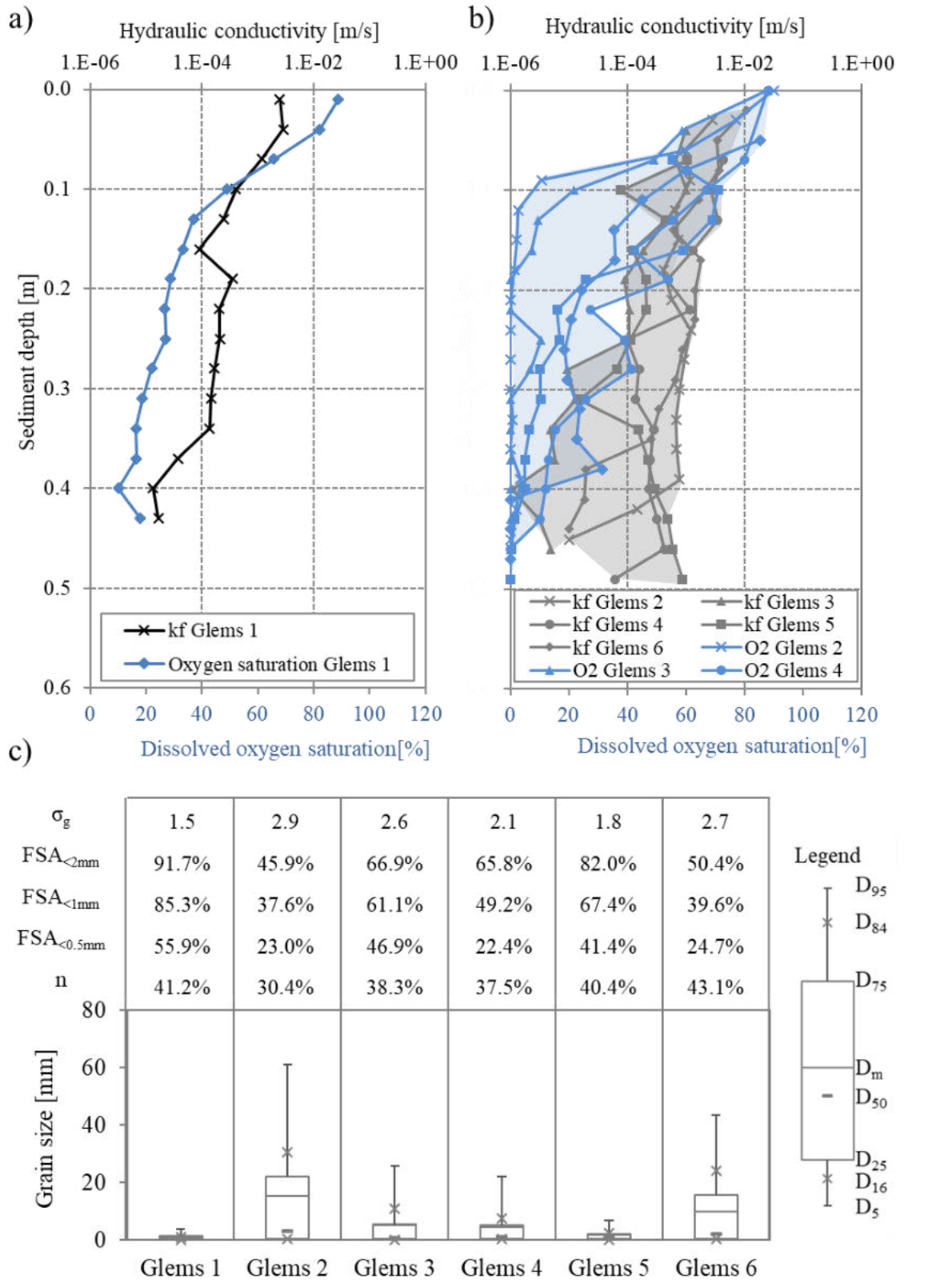

Figure 7.5: Results from field experiment at River Glems showing a) a representative example of a vertical profile from hydraulic conductivity and intragravel dissolved oxygen saturation, b) the remaining data sets of hydraulic conductivity and intragravel dissolved oxygen saturation c) boxplot diagrams for each sediment sample including grain size characteristics as well as porosity.

7.2.5 Lein

Two sampling sites are chosen downstream of each of the two weirs at River Lein. The results are shown in Figure 7.6 a - c. The results from Lein 1 are displayed in Figure 7.6 a where low and almost constant k_f values around 5.0E-4 m/s are measured at the deeper positions until 0.2 m sediment depth. Then the k_f values increase steadily until a maximum value of 1.2E-2 m/s is reached. No IDOS can be detected (values close to zero) for the deepest six positions until a sediment depth of 0.26 m. Then IDOS starts to rise constantly to a maximum value of 76.7 % for the highest position within the sediment and 90 % for the surface water. Since the measuring location is just downstream of a weir where good aeration is expected the relatively low IDOS values might be explained by the fact that the measuring campaign was shortly after a rain event which could explain the low oxygen values from the surface water.

The results from Lein 2 - 4 are displayed in Figure 7.6 b. Lein 2 is measured downstream of the same weir as Lein 1. Lein 3 and 4 are measured downstream of a second weir several km downstream of the first weir. Lein 2 and 4 show a relatively similar pattern as Lein 1. Only Lein 3 detects a decrease of hydraulic conductivity with increasing height for the lowest 10 cm and then constant values around 7.0E-4 m/s for the following 0.2 m. Lein 1 and Lein 3 generally show low decrease of k_f values with increasing sediment depth. However, the hydraulic conductivity at Lein 4 decreases by more than three orders of magnitude and at Lein 2 for more than four orders of magnitude. These low hydraulic conductivities also explain the very low IDOS at deep sediment locations. The saturation of dissolved oxygen behaves similar for all four locations where no dissolved oxygen can be detected for the deepest positions except Lein 2 where oxygen saturation up to 20 % is measured for the deepest positions. Then all the vertical profiles show an increase of dissolved oxygen reaching values close to 100 % saturation for the positions close to the surface.

The riverbed material at location Lein 1 and 2 is coarser compared to the riverbed material at location Lein 3 and 4 (Figure 7.6 c). The coarse material from Lein 1 and 2 is reflected in the larger D_m of 15.3 mm and 18.1 mm, respectively, compared to the D_m from Lein 3 and 4 of 10.1 mm and 10.7 mm, respectively. Lein 1 and 2 also show a wider range of grain size distribution compared to Lein 3 and 4 (Figure 7.6 c). The porosity and the grain size characteristics correlate poorly. The coarser location Lein 1 and 2 have the lowest porosities of 26.2 % and 26.3 % whereas the location Lein 3 and 4 with finer riverbed material have higher porosities. This might be explained by the fact that bigger stones have no porosity and artificially decrease the porosity of a sample. An interesting difference is the FSA between Lein 3 and 4. Whereas both samples have almost the same FSA< 2 mm of 49.0 % and 49.6 % the FSA<0.5 mm differs widely from 6.0 % (Lein 3) and 36.4 % (Lein 4). This means that Lein 3 contains a large sand fraction without high amounts of cohesive sediments whereas most of the fine sediments from Lein contain cohesive particles.

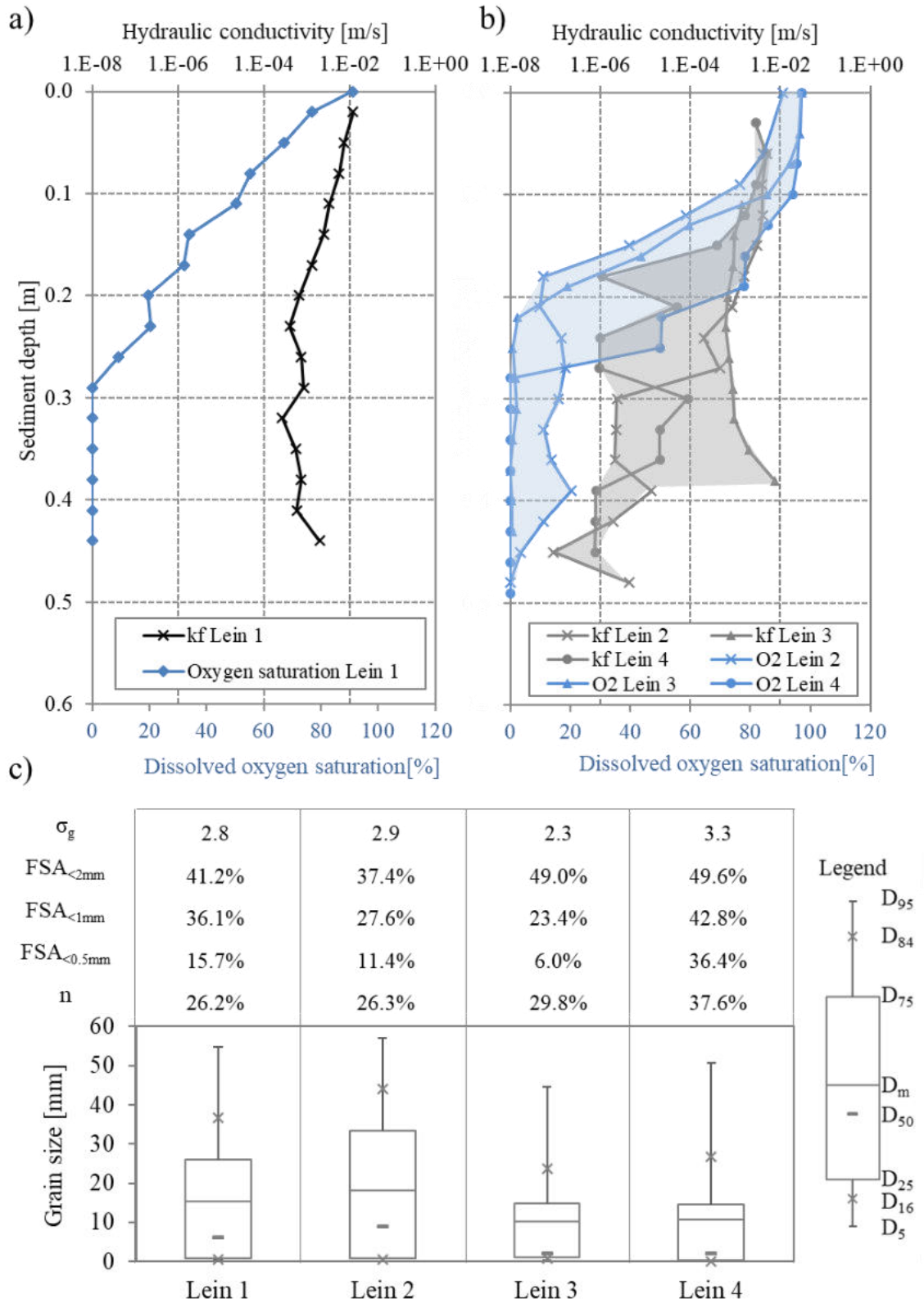

Figure 7.6: Results from field experiment at River Lein showing a) a representative example of a vertical profile from hydraulic conductivity and intragravel dissolved oxygen saturation, b) the remaining data sets of hydraulic conductivity and intragravel dissolved oxygen saturation c) boxplot diagrams for each sediment sample including grain size characteristics as well as porosity.

7.2.6 Rems

In total six locations are measured at River Rems. The results are displayed in Figure 7.7 a - c. The results from Rems 6 are shown in Figure 7.7 a. Rems 6 was located in a pool with low flow velocities which are also reflected by the moderate to low hydraulic conductivities. The vertical profile is not steep which means that the values do not change greatly over depth. The values vary little and vary around a value of 1.0E-3 m/s. The hydraulic conductivity reduces for the two topmost points close to the surface which might be due to the low flow conditions at this sampling site supporting outer colmation on top of the riverbed. In contrast to the vertical profile of the k_f values the vertical profile of IDOS shows a steady increase with increasing height. A value of 18.8 % saturation is measured for the deepest position and the values increase until 121.4 % saturation is reached for the highest values.

The results from the vertical profiles of the hydraulic conductivity and IDOS from the five locations at River Rems are summarized in Figure 7.7 b. The locations Rems 1 - 3 are located in a riffle with higher flow velocities compared to Rems 5 and 7 which are located in a pool. Reflecting the vertical profiles of the hydraulic conductivities, which are lower for the pool data compared to the riffle data. This means the riverbed in the riffle location has a higher hydraulic conductivity compared to the riverbed in the pool. Especially Rems 5 and Rems 7 have low IDOS compared to the location measured in the riffle. However, towards the surface all oxygen values become more similar and show values between 100 % and 140 % saturation. These are remarkably high oxygen values and represent very good exchange conditions in the upper top layer.

In contrast to the hydraulic conductivities and IDOS neither the porosity nor the grain size characteristics show a significant difference between data gathered in the pool and in the riffle. The determined porosities are in a close range between 23.9 % and 26.7 % except Rems 7 which has the highest porosity of 31.5 %. Also the D_m of all samples is in a really close range between 21.9 mm and 24.8 mm and as shown in the boxplot diagrams in Figure 7.7 c there is no large variation in the different grain size distributions. The FSA<2 mm are in a moderate range between 9.9 % and 19.7 %. The averaged FSA<0.5 mm is 4.8 %, which means that only low cohesive particles are included in the riverbed material.

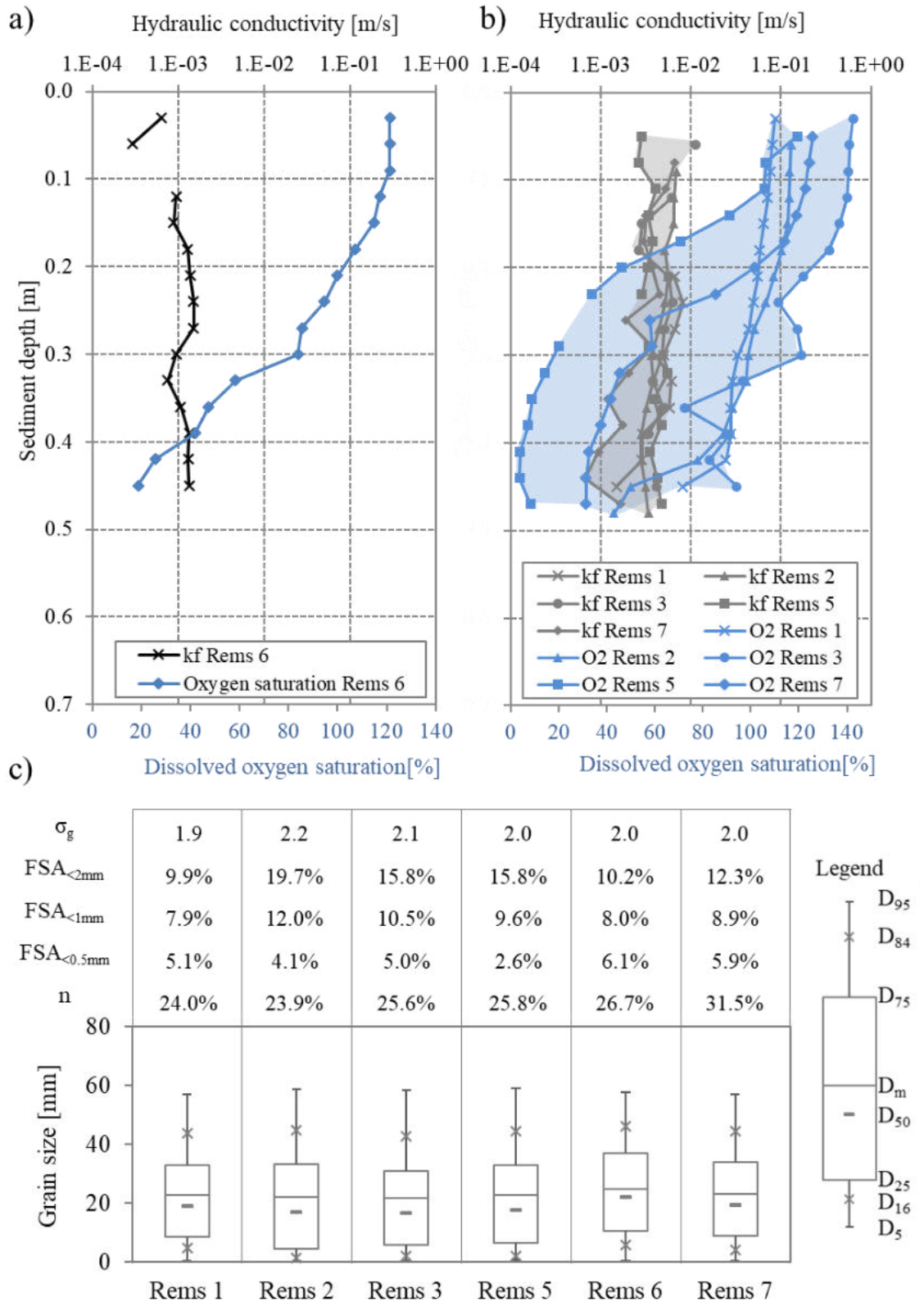

Figure 7.7: Results from field experiment at River Rems showing a) a representative example of a vertical profile from hydraulic conductivity and intragravel dissolved oxygen saturation, b) the remaining data sets of hydraulic conductivity and intragravel dissolved oxygen saturation c) boxplot diagrams for each sediment sample including grain size characteristics as well as porosity.

7.2.7 Wieslauf

Five locations are investigated at River Wieslauf and the results are displayed in Figure 7.8 a - c. The vertical profiles of k_f and IDOS from location Wieslauf 2 (riffle) are shown in Figure 7.8a. The hydraulic conductivities are low and do not show variations over depth, only a slight increase with decreasing sediment depth. In contrast to the relatively low hydraulic conductivities, high IDOS is measured for this location. The lowest position already has an oxygen saturation of 90.6 % and it rises over depth up to 105.6 % for the topmost location. This low variation over depth means the lower part of the riverbed is well supplied with oxygen-rich surface water enabling good conditions for exchange processes.

A quite narrow spectrum of hydraulic conductivities is observed for the top 0.25 m where all sampling sites lie in a similar range. Only Wieslauf 3 and Wieslauf 4 show a strong decrease of hydraulic conductivity with increasing sediment depth whereas Wieslauf 1, Wieslauf 2 and Wieslauf 5 show almost no variation of hydraulic conductivity over depth. IDOS of Wieslauf 3 is in good agreement with the measurement of hydraulic conductivity since both values are exceptionally low for high sediment depth. Since the sampling site of Wieslauf 3 is located at a tail of a pool, thus this behavior is expected. Both IDOS measurements of Wieslauf 1 and Wieslauf 2 show remarkably high saturations and no marginal reduction with increasing sediment depth.

In contrast to the hydraulic conductivity and IDOS, no difference can be observed between riffle (Wieslauf 1,2,4 and 5) and pool (Wieslauf 3) data regarding the grain size distribution and porosity. The porosity values are in a narrow range varying from 22.1 % to 27.0 %. Although River Wieslauf has a high amount of large grains such as cobbles and boulders in the river the FSA is quite high varying around 21.6 % to 35.8 % for FSA<2 mm and 7.0 % to 12.9 % for FSA<0.5 mm. Large grains are excluded from the analysis and thus leading to relatively high amount of fine sediments. However, the low hydraulic conductivity and the low oxygen saturation also support the high fine sediment amount.

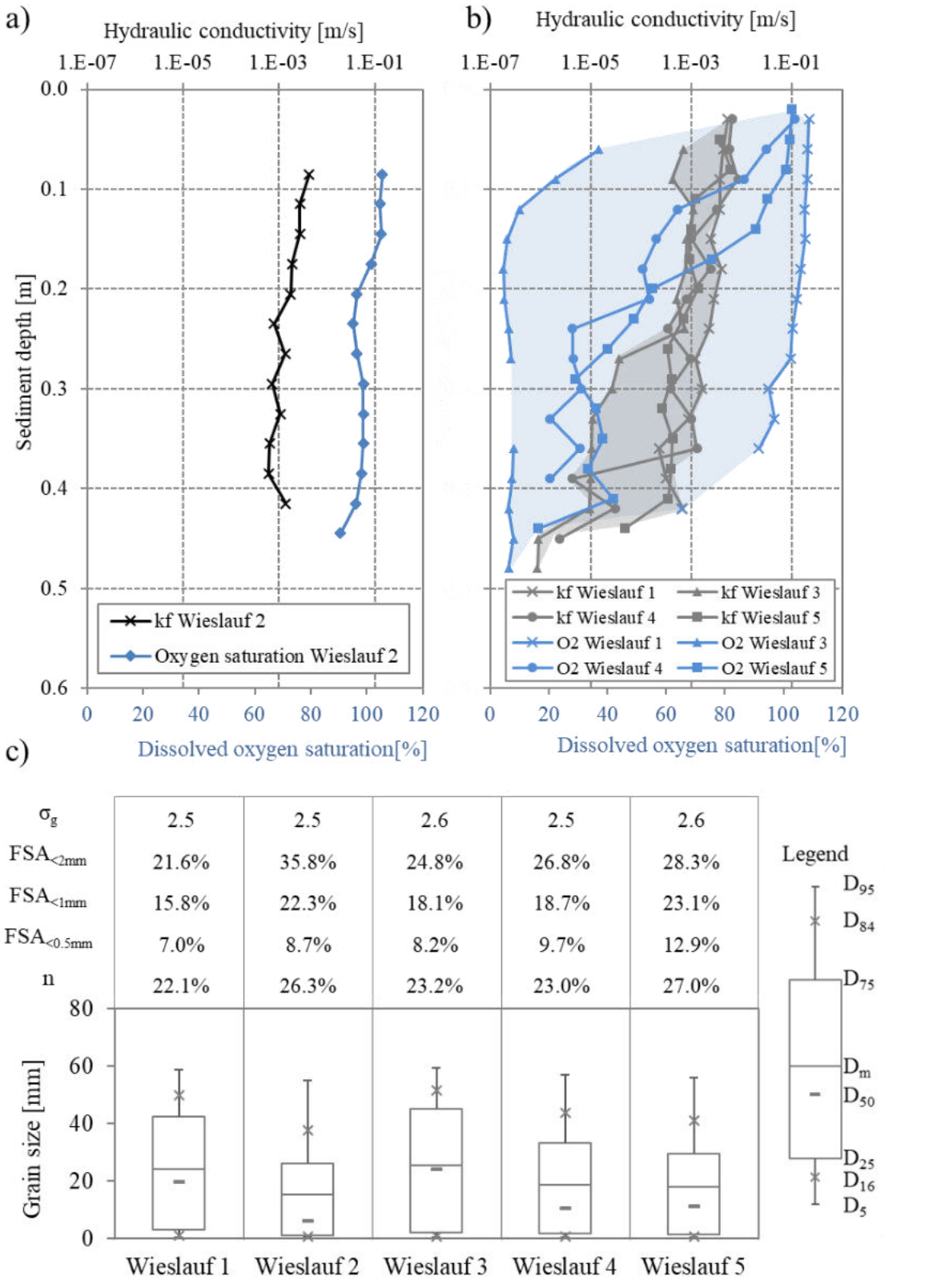

Figure 7.8: Results from field experiment at River Wieslauf showing a) a representative example of a vertical profile from hydraulic conductivity and intragravel dissolved oxygen saturation, b) the remaining data sets of hydraulic conductivity and intragravel dissolved oxygen saturation c) boxplot diagrams for each sediment sample including grain size characteristics as well as porosity.

7.2.8 Würm

Six locations are measured and sampled at River Würm (Figure 7.9 a - c). The vertical profiles from the hydraulic conductivities and k_f values of sampling site Würm 3 are summarized in Figure 7.9 a. In the deepest 0.25 m the hydraulic conductivities stay constant with increasing height reaching only low values around 3.7E-4 m/s. At the sediment depth of 0.2 m the values start to rise steadily until a maximum value of 7.0E-3 m/s is reached for the topmost position. The oxygen values at this location show a similar trend. The deepest positions only show a slight increase of IDOS rising from 47.0 % to 59.6 % until a sediment depth of 0.26 m. Then IDOS increase faster with increasing height reaching 104.0 % saturation for the topmost 0.1 m.

The general course of the vertical profiles from the hydraulic conductivitiess at River Würm (Figure 7.9 b) is characterized by lower k_f values in the deeper positions and only a slight increase of the values with increasing height. All values start to increase faster at a sediment depth of 0.1 m leading to better hydraulic conductivities in the top layer of the riverbed reaching values around 5.0E-3 m/s. Some of the vertical profiles even show a slight decrease with increasing height before the top layer starts. The IDOS profiles show a steadier increase with increasing height. Except location Würm 1 and 2 IDOS is quite low for the deepest position ranging below 20 % saturation for the deepest 0.15 m. IDOS increases and reaching values between 92 % and 110 % saturation.

The grain size distribution and the porosity values from all locations at River Würm are displayed in Figure 7.9 c. The grain size distribution and the porosity lie all in a close range. The porosity ranges from 23.3 % to a maximum of 26.8 %. Regarding the grain size distribution Würm 5 differs from the other locations with low FSA values and a lower geometric standard deviation σ_g compared to the other locations. However, the D_m from all samples are in a close range varying from 14.9 mm to 18.5 mm.

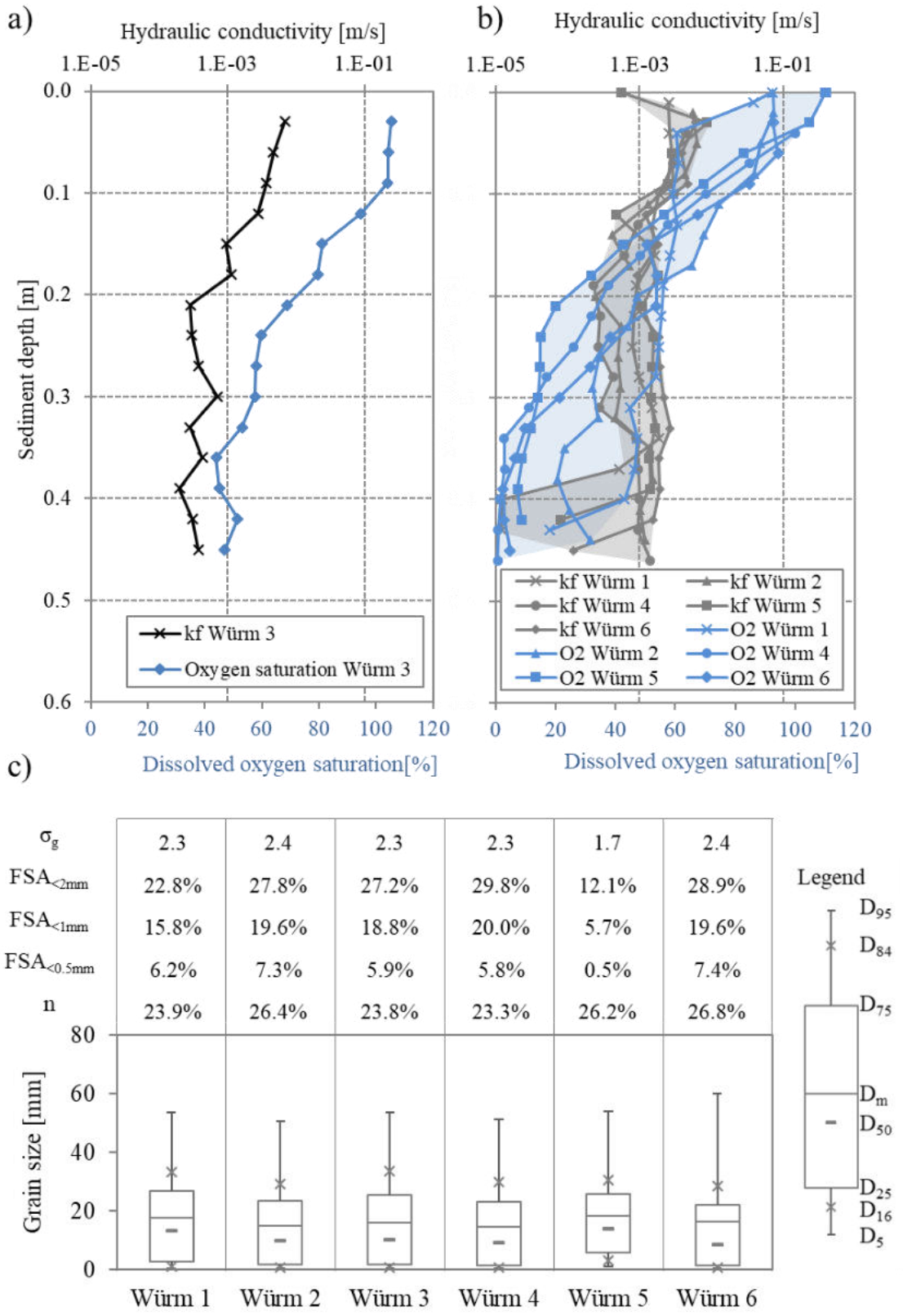

Figure 7.9: Results from field experiment at River Würm showing a) a representative examples of a vertical profile from hydraulic conductivity and intragravel dissolved oxygen saturation, b) the range from the rest of the data sets and c) boxplot diagrams for each sediment sample including grain size characteristics as well as porosity.

Figure 7.10: Layer with fine material at the bottom of the two sediment samples Würm 1 (left) and Würm 6 (right).

Figure 7.10 shows the beginning of fine material layers from the bottom of two sediment samples (Würm 1 and 6). This is in good agreement with the vertical profile from Würm 1 and 6 where the bottom most k_f values are extremely low compared to the rest of the vertical profile. Würm 5 also has a reduced k_f value for the bottom most value. However, the sediment samples from Würm 5 does not contain a fine sediment layer. This might be because sediment samples are taken close to the slurping spot and not at the same location. Since these layers can have a high spatial variety it has not been detected at sampling site 5.

7.3 Discussion - Multi-parameter approach

In this chapter the multi-parameter approach is discussed in detail. Initially the relation between the single parameters used in the multi-parameter approach is analyzed and possible correlations are investigated. Secondly, the challenge in determining colmation is discussed and compared to existing assessment methods.

7.3.1 How do all these parameters relate to each other?

In this section the relations between the different parameter are analyzed in detail. Investigations about possible correlations between the single parameters is conducted and discussed with regard to existing literature where possible. In a first step, k_f is compared to IDOS, n, FSA<0.5 mm and σ_g. FSA<0.5 mm is chosen over FSA<1 mm and FSA<2 mm. FSA<1 mm and <2 mm also contribute to colmation since this sediment size mainly reduces the pore space (see chapter 2.2.1). However, FSA<0.5 mm is the main driver for the reduction of the hydraulic conductivity due to the cohesive character of this grain size classes. σ_g is chosen as sediment characteristic since it serves as measure for the sorting and the spectrum of the sediment sample and is more informative compared to D_m, D_{50} or any other single sediment percentile. In a next step the relation between IDOS and n, FSA<0.5 mm and σ_g is investigated followed by the analysis about the relation between n and FSA0.5 mm and σ_g.

Relation between hydraulic conductivity and intragravel oxygen saturation

The hydraulic conductivity is first compared to IDOS since both parameters are measured in a vertical profile and thus result in more data points to compare with. Figure 7.11a summarizes all rivers in one figure. There is no clear trend to observe for the two parameters. However, the high fluctuation of hydraulic conductivity decreases with increasing IDOS indicated by the two gray bars. For IDOS between 0 % and 25 % the k_f values vary in a range for more than four orders of magnitudes. This reduces for higher IDOS between 100 % and 120 %, where k_f values only vary less than two orders of magnitudes. High IDOS (100 % to 120 %) can only be reached for high k_f values around 1.0E-03 m/s to 1.0E-02 m/s. Being in line with expectations, as exchange processes of oxygen-rich water require good hydraulic conductivity. However, low IDOS (0 % to 50 %) occur for low and high k_f values, meaning low IDOS can occur even with good exchange conditions. There are several effects that can overlap. Exfiltrating groundwater conditions where groundwater with low oxygen saturation infiltrates into the river leads to reduced IDOS in the hyporheic zone. Further, biological oxygen consumption reduces the oxygen concentration in the hyporheic zone. Especially in the topmost 10 – 20 cm of the riverbed, where microbial activity is high, high oxygen consumption can occur. Chemical oxidation also consumes oxygen in the riverbed. Both, chemical oxidation and biological oxygen consumption are dependent on the availability of organic matter.

In order to prevent overlapping effects of different rivers, the relation between k_f and IDOS is also analyzed for each river separately. Some rivers show a strong positive correlation between k_f and IDOS whereas some do not show any relation between the two parameters. For most of the sampling sites a positive relation is observed, where k_f increases with increasing IDOS. Table 7.2 summarizes the correlation coefficient (R^2) for the linear relation between k_f and IDOS where the bold numbers show the data sets with a good correlation ($R^2 > 0.65$). River Aich is the only river where no correlation is observed for any of the sampling sites. River Glatt and River Rems have the best correlation between k_f and IDOS where three sampling sites have a strong correlation with a correlation coefficient above 0.7 for both rivers. At River Glatt the remaining three sampling sites have a moderate to good correlation with a correlation coefficient ranging between 0.49 to 0.56 and River Glems has two remaining sampling sites with a moderate to good correlation with 0.57 and 0.60 and only Glems 5 does not show any correlation ($R^2 = 0.00$). At River Lein there are also two sampling sites with a strong correlation ($R^2 = 0.77$ and 0.88), one sampling site with a good correlation ($R^2 = 0.62$) and only one sampling site with a weak correlation ($R^2 = 0.10$). Both River Eyach and River Würm only have one sampling site showing a strong correlation with a correlation coefficient of $R^2 = 0.72$ for Eyach 4 and $R^2 = 0.75$ for Würm 3. The remaining sampling sites show only moderate correlations (ranging around 0.50) or weak correlations (between 0.0 – 0.40). Both River Rems and River Wieslauf have two sampling sites with a strong correlation ($R^2 \geq 0.70$).

It is interesting to note, that some of the relations found between k_f and IDOS are linear whereas other relations seem to follow an exponential growth. Figure 7.11 b - e gives some example of sampling sites from different rivers with a strong correlation ($R^2 > 0.65$) with linear and exponential behavior. The correlation of the remaining rivers is displayed in Appendix 3. River

Rems (Figure 7.11 b) and River Lein (Figure 7.11 c) show a strong linear relation between the two parameters. In contrast to this, some sampling sites from River Glatt (Figure 7.11 d) and River Eyach (Figure 7.11 e) show an exponential increase of k_f over IDOS.

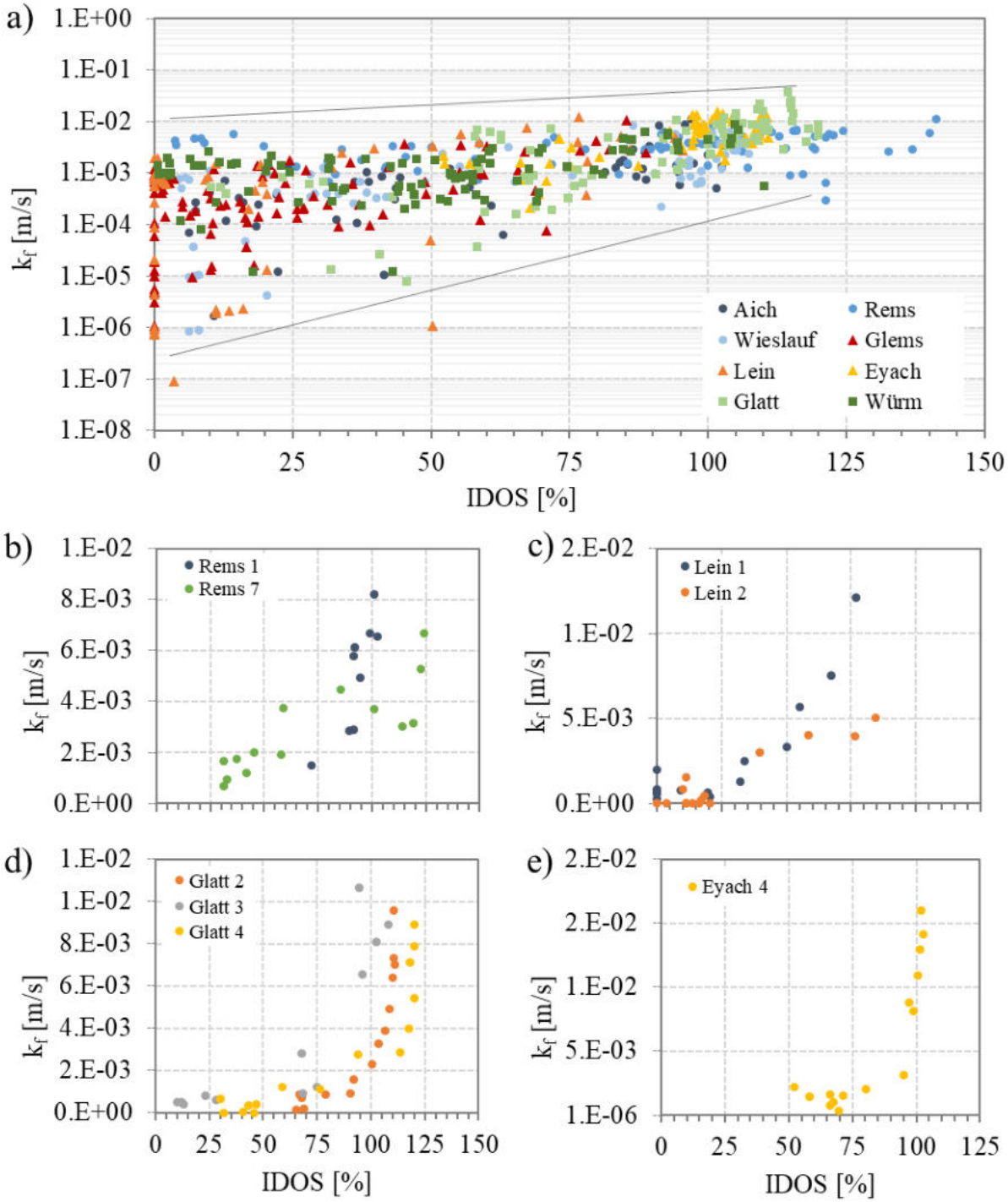

Figure 7.11: Relation between hydraulic conductivity and intragravel dissolved oxygen saturation for a) all rivers, b) River Rems, c) River Lein, d) River Glatt and e) River Eyach.

Table 7.2: Correlation coefficients for the linear relation between k_f and IDOS for each sampling site.

River	R^2	p	River	R^2	p
Aich 1	0.44	0.0131	Rems 3	0.10	0.3544
Aich 2	0.03	0.5900	Rems 5	0.27	0.0695
Aich 3	0.47	0.0402	Rems 6	0.16	0.1804
Aich 4	0.25	0.0703	**Rems 7**	**0.69**	**0.0005**
Lein 1	**0.80**	**<0.0001**	Eyach 1	0.37	0.0210
Lein 2	**0.88**	**<0.0001**	Eyach 2	0.26	0.0656
Lein 3	0.10	0.4029	Eyach 3	0.08	0.3168
Lein 4	0.61	0.0010	**Eyach 4**	**0.77**	**<0.0001**
Wieslauf 1	0.47	0.0094	**Glems 1**	**0.86**	**<0.0001**
Wieslauf 2	**0.67**	**0.0012**	Glems 2	0.58	0.0015
Wieslauf 3	0.03	0.5957	**Glems 3**	**0.71**	**0.0002**
Wieslauf 4	**0.79**	**<0.0001**	Glems 4	0.60	0.0012
Wieslauf 5	0.53	0.0046	Glems 5	0.03	0.5571
Glatt 1	0.51	0.0040	**Glems 6**	**0.75**	**<0.0001**
Glatt 2	**0.68**	**0.0003**	Würm 1	0.39	0.0162
Glatt 3	**0.69**	**0.0016**	Würm 2	0.49	0.0053
Glatt 4	**0.76**	**<0.0001**	**Würm 3**	**0.75**	**<0.0001**
Glatt 5	0.54	0.0061	Würm 4	0.60	0.0012
Glatt 6	0.50	0.0046	Würm 5	0.23	0.0807
Rems 1	**0.70**	**0.0259**	Würm 6	0.33	0.0322
Rems 2	0.63	0.0011			

The exponential relation might result from the overlapping effects such as exfiltration conditions or biological oxygen consumption which can lead to low IDOS for high k_f values. However, in this study no biological data or information about groundwater conditions are recorded to prove the assumption. In order to analyze the behavior in more detail and to gather a better understanding of the complex relation, a third parameter is taken into consideration. In contrast to a river specific classification, in the following section the data sets are sorted into different classes of porosity, FSA<0.5 mm and σ_g. The classes for porosity and FSA<0.5 mm are set to 5% steps and for σ_g the classes are sorted into steps of 0.5 except the class from 2.0 to 2.5, which is split into classes of 0.1 since a large number of data points are included in this class.

The classification according to different parameter does not lead to new findings. Some of the classes show strong correlation between k_f and IDOS with a correlation coefficient > 0.65, whereas most of the different classes do not show any relation. All relations according to different classification are displayed in Appendix 3. Figure 7.12 a – c summarizes some examples with good correlations. For the classification of porosity only the lowest class (0.16

> n > 0.20) show a strong exponential correlation with a correlation coefficient $R^2 = 0.83$ (Figure 7.12 a). The other classes range between $0.0 < R^2 < 0.5$. (see Appendix 3). For FSA<0.5 mm three different classes show a good correlation with correlation coefficients > 0.65. Figure 7.12 b shows the relation between k_f and IDOS for the highest class of FSA<0.5 mm ranging between 51 % - 55 %. Two classes with the highest FSA show the best relation between the two parameter k_f and IDOS ($R^2 > 0.8$). A third class with FSA<0.5 mm ranging between 36 % - 40 % still have a good correlation with a correlation coefficient of $R^2 = 0.6$. The classes with low FSA<0.5 mm do not show any relation between the two parameters. When sorting the data into classes of σ_g, only one class with the highest σ_g (3.0 – 3.5) shows a strong correlation ($R^2 = 0.7$) whereas the remaining classes do not show any relation ($R^2 < 0.4$).

The result from this "3-parameter analysis" indicates the best correlation between k_f and IDOS exists for conditions with low porosity but high FSA and high σ_g. Low porosity means the pore space is filled with fine materials and thus leading to high FSA. This is also in agreement with high σ_g since this parameter is a measure for the heterogeneity of a sediment sample indicating a wide spectrum of sediments with a high σ_g value. However, River Glatt, Rems and Eyach also do show high correlation between k_f and IDOS and these rivers are characterized by coarse material, few fine sediment amount and good exchange conditions.

Since no biological data is measured during the field campaign the influence of biological oxygen consumption cannot be estimated. It is recommended for further studies to also collect biological data such as the content of organic matter or the biochemical oxygen demand (BOD).

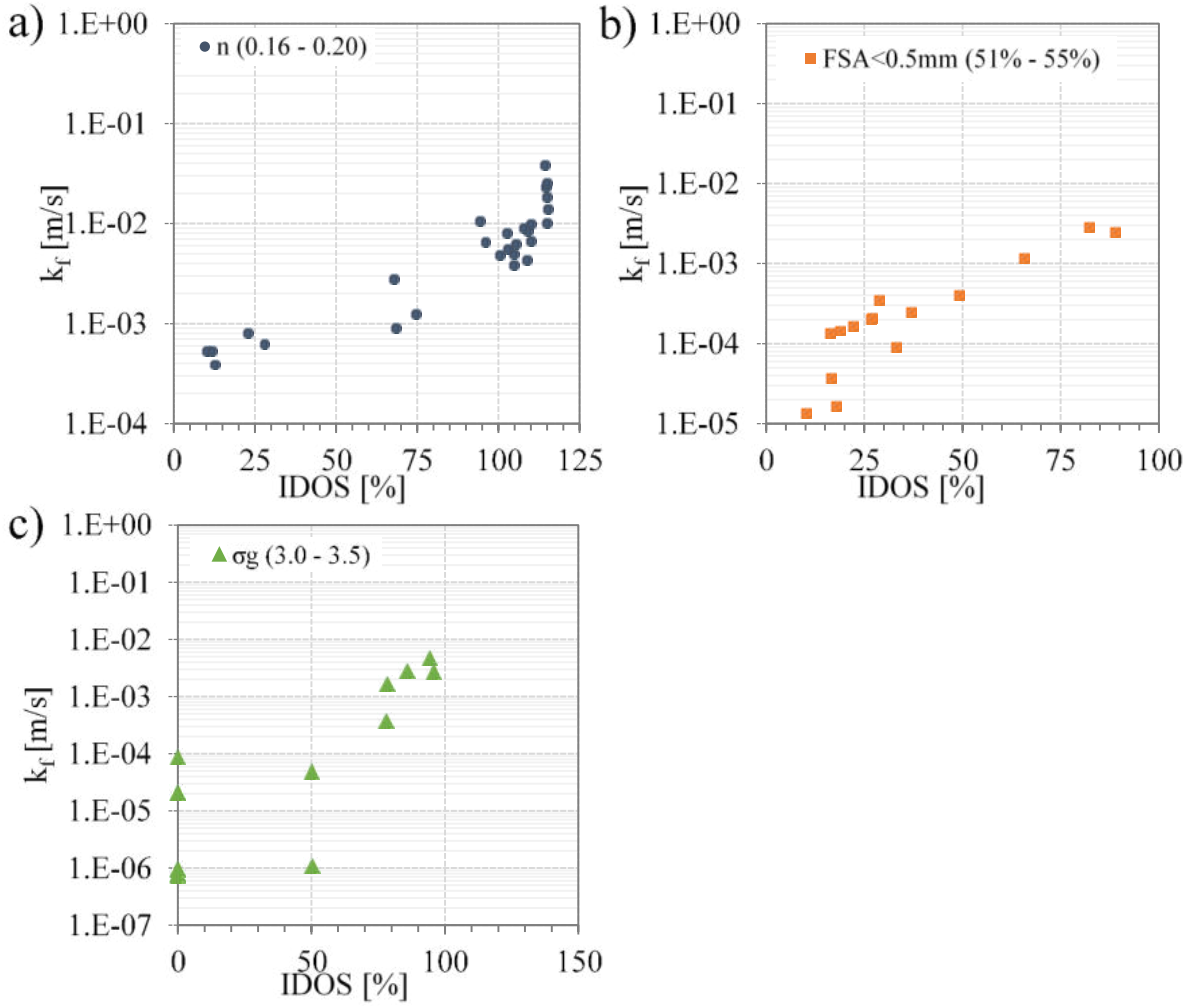

Figure 7.12: Relation between hydraulic conductivity and intragravel dissolved oxygen saturation sorted according to a) porosity, b) FSA<0.5 mm and c) geometric standard deviation of the grain size distribution.

Relation between hydraulic conductivity and porosity

In contrast to the comparison between k_f and IDOS, where two vertical profiles are compared to each other, the comparison between the vertical profile of k_f and the bulk porosity of the sediment samples leads to less informative results. In a first step the river specific relation between k_f and n is analyzed followed by the classification into FSA<0.5 mm and σ_g.

The relation between k_f and n is displayed in Figure 7.13. No clear trend can be detected when comparing k_f and n for all rivers in one figure. However, a slight decrease of k_f with increasing n can be observed (Figure 7.13a). In order to prevent overlapping effects of the different rivers, results from the analysis is displayed separately for all rivers. A slight correlation can only be observed for River Aich and River Glatt which is indicated by the grey bars in Figure 7.13 a and b. The relation between k_f and n of the remaining rivers is displayed in Appendix 3.

A slight decrease of k_f can be observed for increasing n for both rivers. There is no common ground between the two rivers, as they are vastly different. River Aich is characterized by fine material with a FSA<0.5mm ranging from 11.0 % to 25.1 %, porosities ranging around 30.0 % at the riffle sampling sites (Aich 3 and Aich 4) and around 47 % for the pool sampling sites (see Figure 7.2 in chapter 7.2.1). In contrast to this, River Glatt shows coarse riverbed material with a FSA<0.5mm between 2.4 % and 15.1 % and porosities between 17.8 % and 30.5 % (see Figure 7.4 in chapter 7.2.3). This negative relation between k_f and n is also supported by Morin (2006), who finds a negative relation between k_f values and n for granular material and a natural sand-gravel aquifer. However, the other rivers do not indicate any relation between the two parameters. It should be considered that n is only a depth-integrated measurement and thus difficult to compare to the vertical profile of k_f. In contrast to the study from Morin (2006), other studies have shown a positive relation between k_f and n, where the relation can be described by a power law (Kozeny-Carman 1939, Zamarin 1928, Zunker 1932). In Figure 7.14 the relation between k_f and n is displayed according to the Kozeny-Carman equation (equation 2.27 in chapter 2.3.1) as well as to the empirical equation from Zunker (1932) and Zamarin (1928) (found in Morin 2006). Here, the relation is described as a power function where k_f increases steadily with increasing n. However, this positive relation is not observed in any of the rivers in this study.

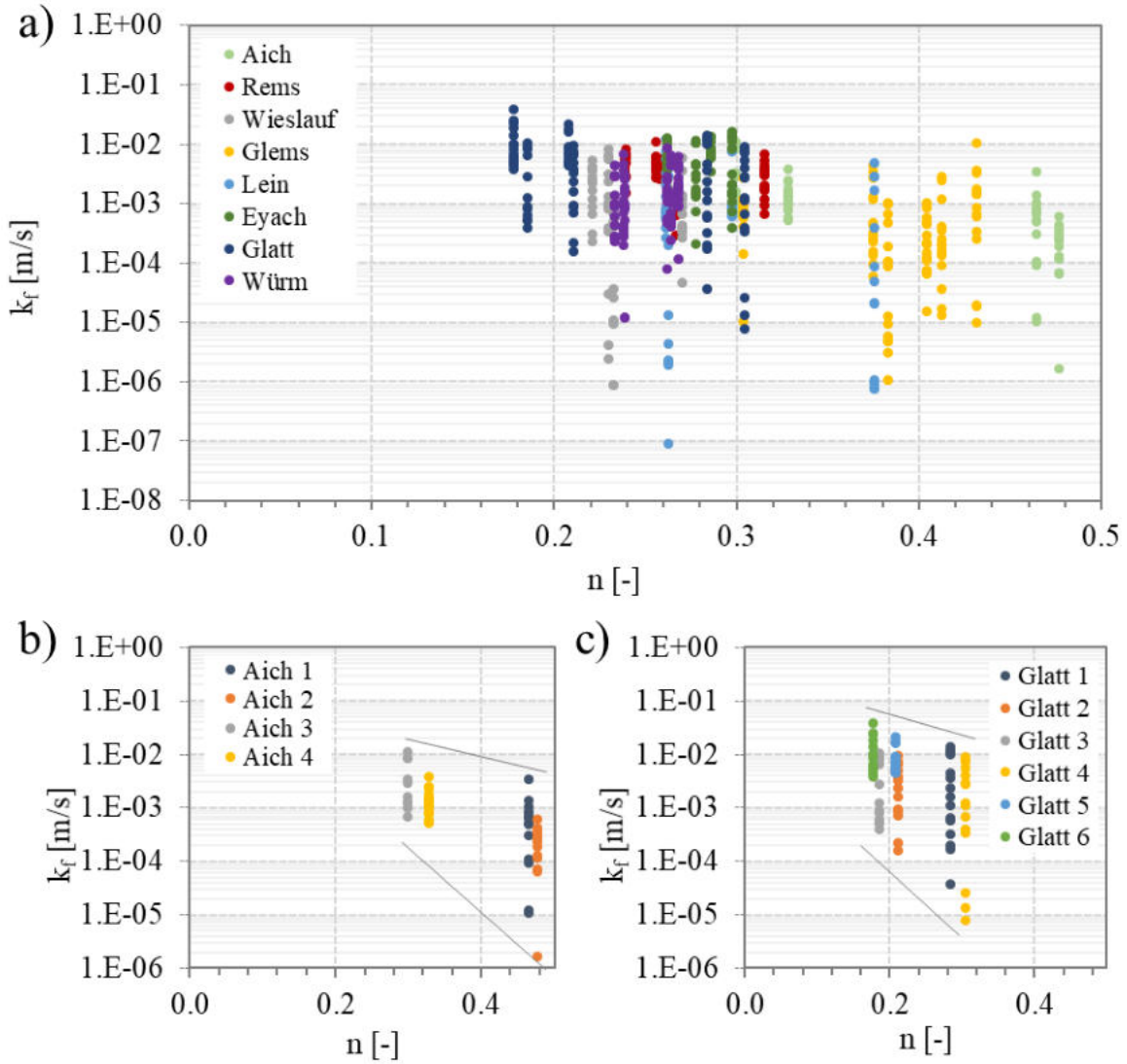

Figure 7.13: Relation between hydraulic conductivity and porosity for a) River Aich and b) River Glatt.

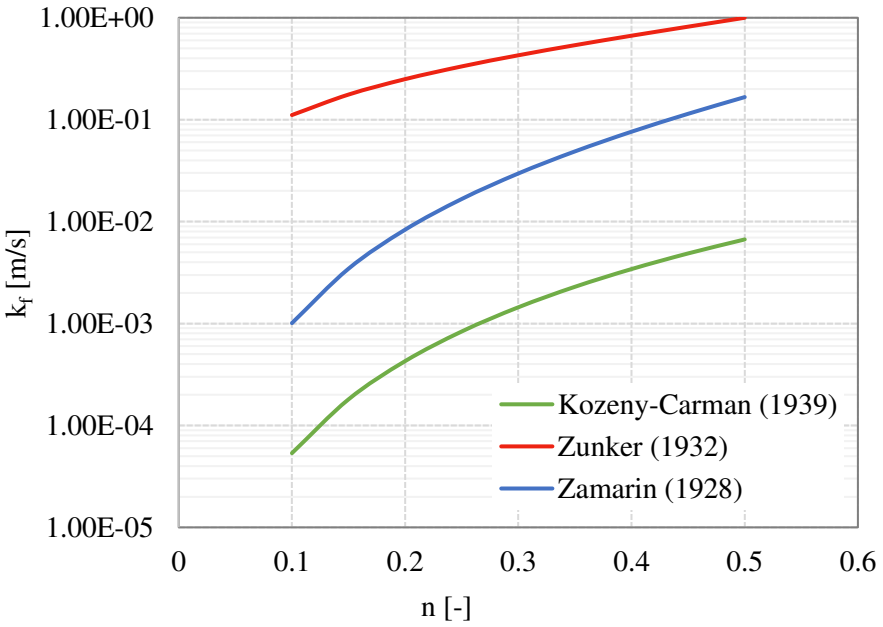

Figure 7.14: Relation between hydraulic conductivity k_f and porosity n according to empirical formulae.

The classification into different classes of FSA<0.5 mm results in two classes with clear decreasing k_f values with increasing porosity (see example in Figure 7.15 a). The other class with decreasing k_f values over n is 16 % < FSA<0.5 mm < 20 % (see Appendix 3). In contrast to the classification into classes of porosity, the classification into classes of σ_g results in a total of four classes where a clear decrease of k_f over n can be observed. Figure 7.15 b) gives an example of one of the σ_g classes where the negative relation between k_f and n can be observed. Meaning that σ_g might be more meaningful in the relation between k_f and n compared to the FSA<0.5 mm.

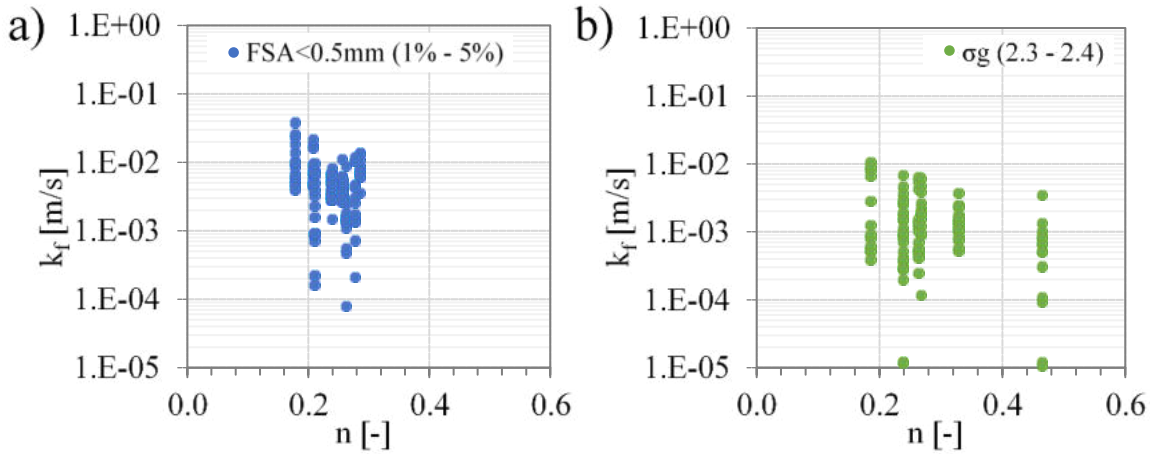

Figure 7.15: Example for relation between hydraulic conductivity and porosity sorting into classes of a) FSA<0.5mm and b) geometric standard deviation of the grain size distribution.

Relation between hydraulic conductivity and sediment characteristics

In literature several empirical equations can be found where grain size distribution is linked to hydraulic conductivity (see Table 2.10 in chapter 2.3.3, Hazen 1893; Kozeny Carman 1939; Alyamani and Şen 1993). The equation according to Hazen (1893) uses the D_{10} to estimate k_f. Alyamani and Sen (1993) includes D_{10}, D_{50} and the intercept of the grain size distribution to estimate k_f. In the equation according to Kozeny-Carman (1939) a specific surface per unit volume is taken into consideration which is simplified to a shape factor and the weighted portion of each sieve fraction according to Carrier (2003). In this section the relation between k_f and different grain size characteristics is analyzed. The percentiles D_{10} and D_{50} are used as well as the FSA<0.5 mm and σ_g. Note that the hydraulic conductivity is measured in a vertical profile and the sediment characteristics are depth-integrated results. The D_{10} and the FSA<0.5 mm are both a measure for the amount of fine sediment in a sediment sample which is assumed to influence the hydraulic conductivity significantly. Therefore, a relation is expected. However, D_{10} does not give information about the amount of fine sediments but rather about the size of the smallest fractions. Thus, for homogeneous and coarse gravel river, the D_{10} might already be quite high. The D_{50} is a widely used statistic parameter since it is easy to determine, but this parameter is rather meaningless and does not give information about the general grain size distribution. In contrast to this σ_g considers the whole grain size distribution and gives more information about the general distribution. However, it does not give information about the grain size.

Figure 7.16 a - d summarizes the river-specific relation between k_f and different grain size characteristics. The figures with single presentation of each river as well as the classification according to porosity can be found in Appendix 3. The best trend, even though only a slight trend, can be observed for the relation between k_f and FSA>0.5 mm where k_f slightly decreases over the broad range of FSA<0.5 mm. No trend can be observed for σ_g (Figure 7.16 b). This supports the idea that the whole grain size distribution does not influence the hydraulic conductivity but only the fine fractions. This is also supported by Figure 7.16 c which shows the relation between k_f and D_{10}. There is no clear relation to be observed but low k_f values only occur for low D_{10} values and no low k_f values are measured for high D_{10} values. There are also other effects that overlap and ensure that high k_f values are achieved even at low D_{10} values. There is a higher number of low k_f values at low D_{50} than at large values of D_{50}. This is also no clear correlation, but a certain relation can be observed. The coarser the material the more likely it is that good exchange conditions occur due to high k_f values.

It is important to note that higher correlation between k_f and the different grain size characteristics is expected. Especially the FSA<0.5 mm is expected to show significant relation to k_f. However, the grain size characteristics in this study are based on a bulk sample and do not have the same resolution as the hydraulic conductivity. Serving the sediment characteristics in a vertical distribution more significant relation are expected. Thin layers with a high content of fine sediments influence the hydraulic conductivity significantly. However, these layers are not considered according to their impact. Furthermore, other sediment characteristics such as the shape factor and the structure (armour layer) are not considered in this study. Other parameters

might help to understand the complex processes and thus are recommended to be collected in further studies.

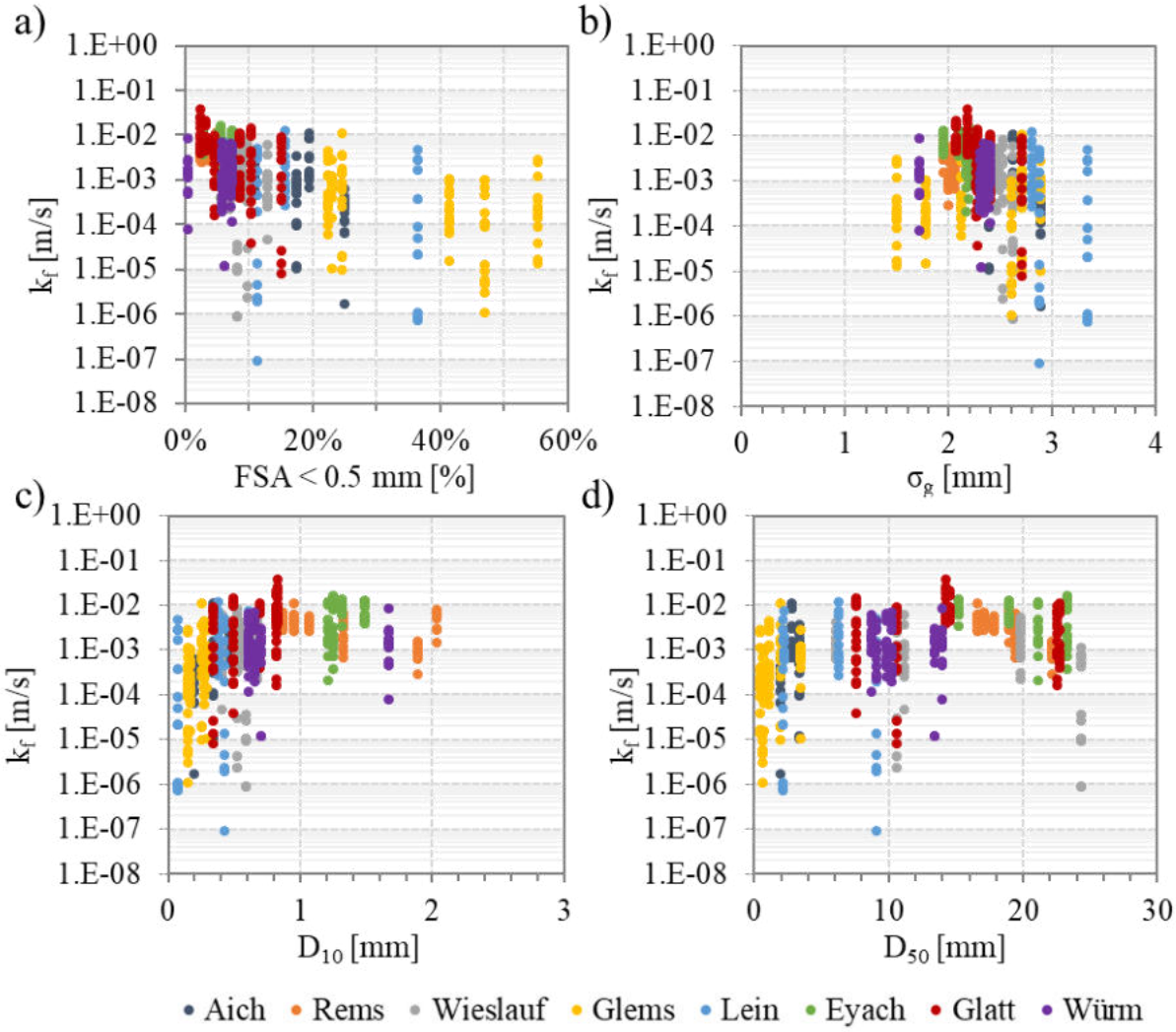

Figure 7.16: River-specific relation between hydraulic conductivity and a) FSA<0.5 mm, b) geometric standard deviation of the grain size distribution, c) D10 and d) D50.

Relation between intragravel dissolved oxygen saturation and porosity as well as sediment characteristics

Figure 7.17 shows the relation between IDOS and porosity (Figure 7.17 a) as well as the sediment characteristics FSA<0.5 mm (Figure 7.17 b) and σ_g (Figure 7.17 c). Note that IDOS is measured in a vertical profile and the porosity as well as the sediment characteristics are based on bulk samples. Higher relations are expected when measuring the porosity and the sediment characteristics in a vertical profile. Slight trends can be observed in all three figures where IDOS shows a negative relation to the parameters. IDOS reduces with increasing n and increasing FSA<0.5 mm. σ_g does not show such a clear trend. For low σ_g IDOS is increasing until a certain point (approximately σ_g = 2) and decreasing afterwards. This is the same

"threshold" as already observed for the relation between k_f and σ_g (Figure 7.16 b). Increasing porosity is no evidence for the pore size or the grain size distribution; however, in this study, high porosity values occurred at river with high amount of fine sediments (Glems and Aich). Increasing FSA<0.5 mm values reduce hydraulic conductivity as it is shown in Figure 7.16 a and thus reduces the exchange capacity of oxygen-rich water resulting in reduced IDOS values.

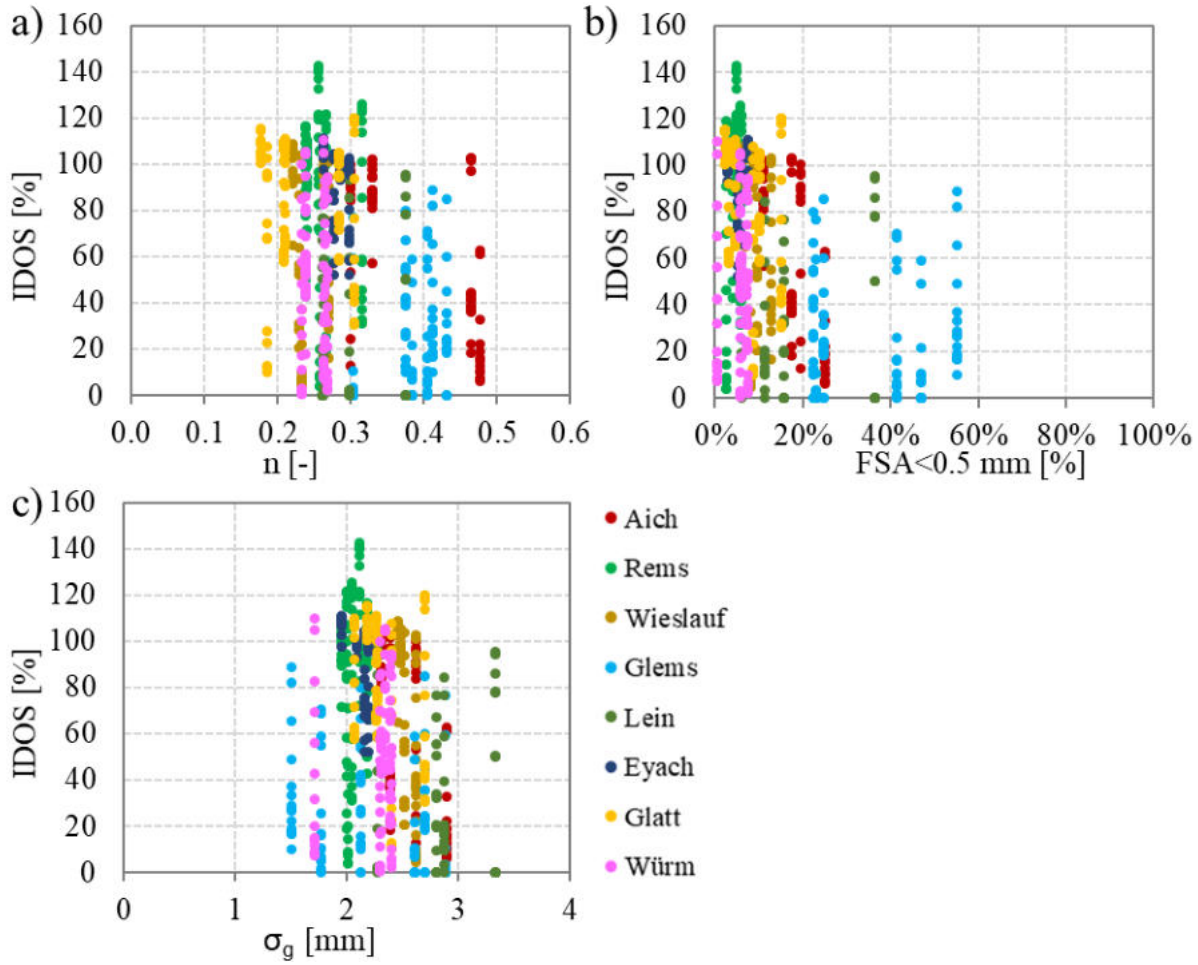

Figure 7.17: Relation between intragravel dissolved oxygen saturation and a) porosity, b) and c) grain size characteristics.

Relation between porosity and sediment characteristics

Several empirical equations exist to calculate n based on grain size parameter (see Table 2.9 in chapter 2.3.2). The most common approaches are based on the D50 (Carling and Reader 1982; Wu and Wang 2006). However, more recent studies are based on σ_g Wooster et al. (2008) and Frings et al. (2011) made a multivariate regression function with σ_g, FSA<0.5 mm and n. In this section the relation between n and different sediment characteristics are analyzed. The sediment characteristics are chosen according to the parameter used in literature. Figure 7.18 a - d summarizes the relation between n and different grain size characteristics. There is a medium linear relation between n and FSA<0.5 mm with a correlation coefficient of $R^2 = 0.54$. This agrees with the outcome of Frings et al. (2011) who also observe a linear relation. In contrast

to the FSA<0.5 mm there is no relation between n and σ_g in this study. Wooster et al. (2008) found a strong correlation between n and σ_g with a correlation coefficient of $R^2 = 0.85$. However, it cannot be supported by the outcome of this study. For low D_{10} values (D_{10} < 1mm), n is decreasing with increasing D_{10} and with further increasing D_{10}, n shows a rather constant course. The same can be observed for D_{50}. For low D_{50}, n is decreasing and later showing an asymptotic course.

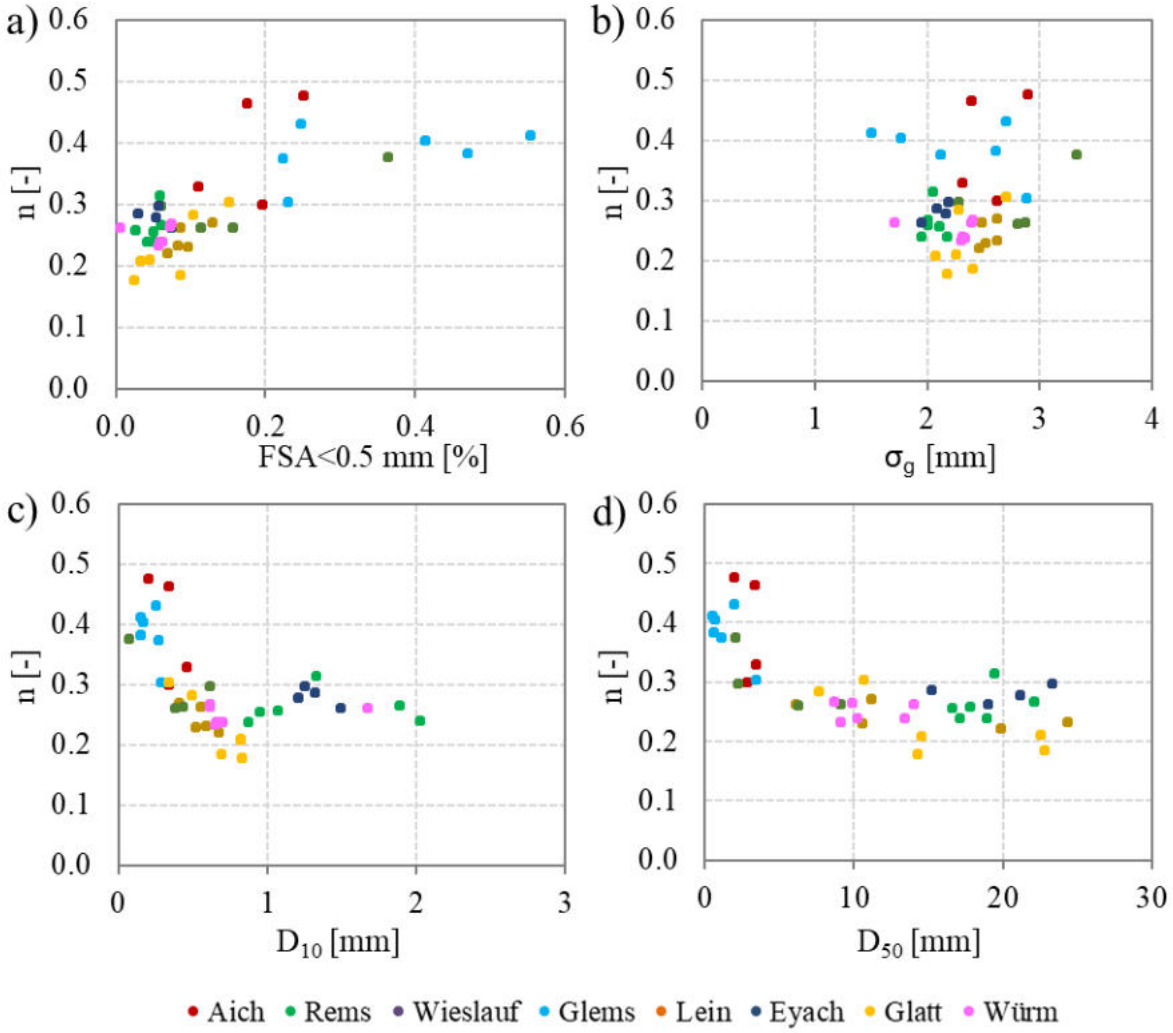

Figure 7.18: Relation between n and a) FSA<0.5 mm, b) sigmaG, c) D10 and D) D50.

7.3.2 Challenge in the determination of colmation

There is still a lack of knowledge regarding the determination and evaluation of colmation. Although there is no parameter defined to describe colmation yet and no valid definition about any thresholds of colmation, a few values quantifying colmation can be found in literature. These values are derived from empirical experiments and have so far only been carried out from a sedimentological point of view, whereby the thresholds are set arbitrarily (e.g. Blaschke et al. 2003). Blaschke et al. (2003) and Datry et al. (2015) for instance classified colmation according to the hydraulic conductivity whereas Maridet und Philippe (1995) used porosity for

classification. Ulrich et al. (2015) observed a reduction of hydraulic conductivity by a factor of four in association with a 10 % increase of fine sediments. Table 7.3 summarizes these different thresholds according to literature. The thresholds set in the different studies do not consider the natural state of the river and classify colmation arbitrarily. The use of FSA for instance is only suitable when comparing sampling spots to reference reaches. In Seitz et al. (2016) for instance the amount of fine sediments as well as the dissolved oxygen saturation of a residual flow reach are compared to unaffected reaches up- and downstream of the residual flow reach. In this case, the use of FSA is appropriate to evaluate the conditions of the riverbed. However, these results are only river-specific and cannot be transferred to other rivers. And in most cases unaffected reaches or reference reaches are hard to find. A further possibility is to compare the investigated river to the respective type of river according to LAWA as it is applied in the European Water Framework Directive (Commission 2000).

Table 7.3: Quantitative values for colmation based on values found in existing literature.

Classification	Hydraulic conductivity [m/s]	Efficient porosity [%]	Reference
No colmation	$1 \cdot 10^{-3} - 1 \cdot 10^{-4}$		Blaschke et al. (2003)
Incipient colmation	$1 \cdot 10^{-5} - 5 \cdot 10^{-6}$		Blaschke et al. (2003)
Colmation	$1 \cdot 10^{-7} - 5 \cdot 10^{-7}$		Blaschke et al. (2003)
Incipient outer colmation	$5 \cdot 10^{-8} - 1 \cdot 10^{-7}$		Blaschke et al. (2003)
Outer colmation	$< 1 \cdot 10^{-8}$		Blaschke et al. (2003)
No colmation	$1 \cdot 10^{-4} - 1.60 \cdot 10^{-4}$		Datry et al. (2015)
Colmation	$0.2 \cdot 10^{-4} - 0.55 \cdot 10^{-4}$		Datry et al. (2015)
Colmation		5 – 6	Maridet und Philippe (1995)

Colmation affects ecological aspects mostly and it is recommended to shift the point of view from a sedimentological perspective to an ecological perspective. In order to link colmation to ecological aspects, ecological data is required. Colmation can be linked to the reproduction success of gravel spawning fish. For example Gustafson-Greenwood and Moring (1991) applied the Mark IV standpipe in their study investigating the hydraulic conductivity of redd sites during redd construction and after fry emergence. Gibson (1993) reports high survival rates of salmonid eggs with hydraulic conductivity around 2000 cm/h with some outliers around 1.39E-02 m/s. He further observed no emergence of fry when hydraulic conductivity is around 1.7E-03 m/s. In literature several studies can be found, in which intragravel dissolved oxygen concentration (IDOC) is linked to egg-to-fry survival (see Table 2.1 in chapter 2.1.2). IDOS is an important parameter regarding the determination of colmation since it has a huge influence of the reproduction success of gravel spawning fish. However, the results in this study show that IDOS is not suitable as solely parameter to determine colmation since it can be overlapped by other factors. Thus, low IDOS values do not necessarily indicate colmation but can also indicate high biological oxygen consumption.

Another possibility is to link colmation to the abundance of macroinvertebrates since they serve as indicator species and thus enable to evaluate the respective river reach to a good or bad ecological state. Therefore, it is recommended to collect macroinvertebrates in a vertical structure to link it to the vertical profiles of hydraulic conductivity and intragravel dissolved oxygen saturation.

7.4 Summary - Multi-parameter approach

The multi-parameter approach including the two newly developed methods to determine porosity and hydraulic conductivity is tested in a field campaign. In total eight different rivers are investigated whereas at each river four to six sampling sites are measured and sampled leading to a total of 41 data sets. Each of these data sets contain a vertical profile of hydraulic conductivity and intragravel dissolved oxygen saturation as well as the depth-integrated porosity of the sample and the detailed sediment characteristics of the sediment sample including the fine sediment amount (FSA) and the geometric standard deviation as measure for the heterogeneity of the sample. The results from the application of the multi-parameter approach in the field show that detailed information about the sediment characteristic including colmation effects due to reduced hydraulic conductivity can be detected. Nevertheless, each method has its advantages and disadvantages.

The measurement of vertical profiles results in high resolution data of the riverbed condition. With the resolution of 3 cm steps detailed information about colmation processes and its location can be detected. The measurement of IDOS is conducted by using the standpipe and the double packer. For this measurement only a small amount of water is extracted with a syringe. The VertiCo method can easily be extended to further water quality parameters. Thus, the gathered data do not only rely on one single parameter, but the results can be secured by the other parameters.

However, the application of the multi-parameter is time-consuming; especially the measurement of vertical profiles from the VertiCo method takes approx. 3 hrs. Since two people are generally needed for measurements in rivers for safety reasons, it is recommended to use two sets of equipment of the VertiCo method simultaneously to save time. A main disadvantage of the developed multi-parameter approach is that only two out of four parameters are determined in a vertical profile. The sediment characteristics and the porosity are based on one depth-integrated sediment sample without a vertical resolution. Thus, small-scale information is lost and colmation layers cannot be detected by these two parameters.

The analysis of the relation between the four parameters show that hydraulic conductivity and intragravel dissolved oxygen saturation correlate well with each other. The relation between the remaining parameters are not that strong. However, some correlations between porosity and sediment characteristics can be observed. It can be assumed that the relation between the parameters would be stronger when measuring all parameters in a vertical profile. IDOS is influenced by further aspects such as biological oxygen consumption of exfiltrating groundwater and is thus only a supporting parameter. However, the additional measurement of

organic matter or the determination of loss of ignition might be helpful in distinguishing between the respective effects.

8. CONCLUSION

8.1 Summary and conclusion

Colmation is defined as the infiltration and accumulation of fine sediments in the riverbed. It has severe negative effects on aquatic ecosystems. It negatively influences the reproduction of gravel spawning fish and the living conditions for aquatic animals such as macroinvertebrates due to the clogging of pore space and the relating reduction of exchange processes into the hyporheic zone. Existing methods to determine colmation are based on single parameters and fail to gather these complex processes of colmation. There are four promising parameter which can be used to describe colmation: namely the grain size distribution, the intragravel dissolved oxygen saturation, the porosity and the hydraulic conductivity. This study aims in developing a multi-parameter approach based on the mentioned parameter to determine colmation. Existing methods to determine grain size distribution and intragravel dissolved oxygen saturation are well established and can be applied for this study. However, new methods for determining porosity and hydraulic conductivity need to be developed. A requirement for the hydraulic conductivity is the applicability of the method in coarse riverbed and the measurement of a vertical profile. The vertical profile gives more information compared to a point measurement since colmation is also a heterogeneous process which takes place in the riverbed.

For the determination of porosity, a photogrammetric approach using structure from motion with multi-view stereo (SfM-MVS) is applied in this study to determine the total volume of a frozen sediment sample. Therefore, a 3D model based on different images of the sediment samples is created for which the total volume can be calculated. For the evaluation of the method and its accuracy several laboratory experiments are conducted where the SfM-MVS method is compared to simple geometric bodies and to the commonly used water replacement method (WRM). The results show both methods perform well in determining the volume of simple geometry bodies. The experiments and comparison to the WRM show SfM-MVS is a reproducible and accurate method to determine the total volume of a broad range of uniform and nonuniform sediment samples. It is easy to apply, requires only few additional equipment in the field and is not time consuming. However, compared to the WRM method the postprocessing in the office where images are masked to cover the background is more time consuming compared to WRM. Another advantage is the sample remains intact after image collection, whereas the immersion of samples into water (WRM) results in the loss of sediment due to thawing. The melting also produces a systematic error where porosity based on WRM is generally lower compared to porosity based on SfM-MVS due to immersion of the sample into water during WRM.

The newly developed VertiCo method is applied and tested to measure a vertical profile of hydraulic conductivity. In a first step the slurping rate is measured in a vertical profile using a perforated standpipe and a double packer. In a second step a MODFLOW groundwater model is applied to simulate k_f values based on the measured slurping rates and the respective hydraulic conditions. The model uses the Forchheimer equation which is valid for higher interstitial flow

velocities where Darcy´s Law is not valid anymore (Re > 1). Laboratory tests are conducted in order to test and to prove the new method. The experiments show that the method is able to detect layers with lower k_f values. A linear correlation between slurping rate and hydraulic conductivity is established. However, the experiments further show a high influence of hydraulic head exists which influences the correlation between k_f and slurping rates. Thus, a simple calculation of k_f based on slurping rate is not possible. The influence of hydraulic head is material dependent and cannot be considered by a simple correction function. The MODFLOW model considers this effect and estimates the k_f values iteratively based on the respective hydraulic head. The simulated k_f values agree well with the measured k_f values from column experiment applying the constant head test.

The developed multi-parameter approach is tested in a field campaign where eight different rivers are investigated. At each river four to six sampling sites are chosen resulting in a total of 41 data sets. The results from the field campaign show that the newly developed methods for determining porosity and hydraulic conductivity can be applied in the field, especially in gravel rivers. The vertical profiles of hydraulic conductivity and IDOS show the reduction of these values over depth. Different systematics can be distinguished where either a linear reduction occurs or a certain reduction. The certain reduction indicates the presence of a colmation layer due to a sharp jump. The multi-parameter approach is time consuming in the field, but it results in high resolution data about the riverbed structure and its clogging status.

The analysis of the parameters shows different relations between the parameters. The strongest relation is between k_f and IDOS. Linear and exponential correlation is observed for some of the sampling points. However, there are other parameters such as exfiltrating groundwater effects or biological oxygen consumption that can overlap and influence the IDOS values greatly. A negative relation between k_f and n is found in the results. This is in agreement with outcomes of other published studies. However, most of the relation found in literature report a positive relation between k_f and n. Only slight trends can be detected between k_f and grain size characteristics such as FSA<0.5 mm and σ_g. However, these parameters are only available in bulk data and are thus less informative compared to vertical profiles. Thin layers with fine sediment, indicating colmation, cannot be detected by the bulk samples of porosity or grain size analysis.

To conclude this research, the multi-parameter approach proved to be an extremely useful method towards the determination of colmation. However, additionally parameters are required to analyze colmation sufficiently. To gain more understanding in the complex processes of colmation, porosity and sediment characteristics are also required to determine in a vertical resolution. Further, ecological data is required simultaneously to the multi-parameter approach.

8.2 Future research

The analysis of the multi-parameter approach shows a strong relation between k_f and IDOS. However, other parameters from the multi-parameter approach do not have a strong relation as the relation between k_f and IDOS. Hydraulic conductivity and IDOS are the two parameter

which are measured in a vertical profile. Porosity and the grain size distribution is only a depth-integrated bulk sample and is not split in vertical direction. It is recommended for future research to develop a method to also measure *n* and grain size characteristics in a vertical resolution. Thus, layers with fine sediments and clogged pore space can be detected. A possibility is to cut the frozen sediment sample directly after retrieving into layer of 5 - 10 cm. For cutting the sample, the frozen sediment sample can be removed from the core by heating the core from the inside (hot water or heat gun) and keep the sample intact. To prevent melting of the sediment sample, liquid nitrogen can be used to sprinkle the subsamples during cutting and keep it frozen. SfM-MVS can then also be applied in order to determine the total volume of the subsamples. The fine resolution as the VertiCo method might not be achieved; however, a division into smaller fraction already enables the detection of different sediment characteristics. This might result in subsamples that are not representative anymore. This aspect needs to be considered. However, this effect might be reduced by applying different criterion of a representative sampling mass as presented in chapter 2.3.1. The criterions can be fulfilled by reducing the sampling mass by removing the coarse sediments from the sample. Another possibility is to take several samples in a close range to each other and add the data from the subsamples to one sample. This gives a hint on the heterogeneity of the surrounding material and reduces the uncertainty of just one sample. By measuring all data in a vertical profile, further knowledge gaps regarding the complex processes of colmation can be closed.

The determination of colmation can be conducted under different perspectives. A sedimentological perspective can be established when all parameters are measured in a vertical profile. A threshold is set where k_f values are classified as low permeable and this threshold can be transferred to other parameters. However, since colmation effects ecology significantly, ecological aspects should be considered in the determination of colmation. Therefore, measurements with the multi-parameter approach should be conducted simultaneously to measurements of ecological significant indicator species such as macroinvertebrates. In this way, different categories can be established to classify colmation according to biota.

Another possibility towards determination of colmation is the systematic investigation of river types according to LAWA. This classification can be conducted according to the EU Water Framework Directive (WFD) where different river types are regarded as reference type. Enabling the derivation of comparative hydromorphological values of which an assessment, according to the WFD is possible for other water bodies.

Further, additionally it is recommended to collect data to estimate the content of organic matter. This can be done by measuring the biochemical oxygen consumption which is quite complex or to determine the loss of ignition of the sediment sample. This can estimate the content of organic matter and thus help to distinguish between overlapping effects for IDOS.

Bibliography

Alyamani, Mahmoud S., and Z. Şen. 1993. Determination of Hydraulic Conductivity from Complete Grain-Size Distribution Curves. *Ground Water* 31 (4).

Amoozegar, A., and A. W. Warrick. 1986. "Hydraulic Conductivity of Saturated Soils: Field Methods." In *Methods of Soil Analysis: Part 1—Physical and Mineralogical Methods*, 735–770.

Angradi, T. R. 1999. Fine Sediment and Macroinvertebrate Assemblages in Appalachian Streams: A Field Experiment with Biomonitoring Applications. *Journal of the North American Benthological Society* 18 (1): 49–66. https://doi.org/10.2307/1468008.

Argent, D. G., and P. A. Flebbe. 1999. Fine Sediment Effects on Brook Trout Eggs in Laboratory Streams. *Fisheries Research* 39 (3): 253–262.

Armstrong, J. D., P. S. Kemp, G. J. A. Kennedy, M. Ladle, and N. J. Milner. 2003. Habitat Requirements of Atlantic Salmon and Brown Trout in Rivers and Streams. *Fisheries Research* 62 (2): 143–170.

Banscher, E. 1976. Gesetzmäßigkeiten Der Kolmationsentwicklung. *Wasserwirtschaft-Wassertechnik*, *9*, 320-323

Barnard, K., and S. McBain. 1994. Standpipe to Determine Permeability, Dissolved Oxygen and Vertical Partical Size Distribution in Salmonid Spawning Gravels. *Fish Habitat Relationships - Technical Bulletin* 15.

Barzilai, R., J. B. Laronne, and Ian Reid. 2013. Effect of Changes in Fine-Grained Matrix on Bedload Sediment Transport in a Gravel-Bed River: Fine-Grained Matrix Effect on Bedload Transport in a Gravel-Bed River. *Earth Surface Processes and Landforms* 38 (5): 441–48. https://doi.org/10.1002/esp.3288.

Bernier-Bourgault, I., and P. Magnan. 2002. Factors Affecting Redd Site Selection, Hatching, and Emergence of Brook Charr, Salvelinus Fontinalis, in an Artificially Enhanced Site. *Environmental Biology of Fishes* 64 (1–3): 333–341.

Beschta, R. L., and W.L. Jackson. 1979. The Intrusion of Fine Sediments into a Stable Gravel Bed. *Journal of the Fisheries Research Board of Canada* 36: 204–10.

Beschta, R. L., and W. L. Jackson. 1978. The Intrusion of Fine Sediments into a Stable Gravel Bed. *J.Fish.Res.Board Can.* 36: 204–10.

Beyer, W., and E. Banscher. 1975. Zur Kolmation Der Gewässerbetten Bei Der Uferfiltratgewinnung. *Zeitschrift Fuer Angewandte Geologie* 21 (12).

Blaschke, A. P., R. Braunshofer, H. Feregyhazy, D. Gutknecht, H. Habersack, C. Karner, P. Mayr, et al. 2002. Kolmationsprozesse Am Beispiel Des Stauraumes Freudenau - Projektphase 2. Schriftenreihe der Forschung im Verbund 75.

Blaschke, A. P., K.-H. Steiner, R. Schmalfuss, D. Gutknecht, and D. Sengschmitt. 2003. Clogging Processes in Hyperheic Interstices of an Impounded River, the Danube at Vienne, Austria. *International Review of Hydrobiology* 88.

Blott, S. J., and K. Pye. 2001. GRADISTAT: A Grain Size Distribution and Statistics Package for the Analysis of Unconsolidated Sediments. *Earth Surface Processes and Landforms* 26 (11): 1237–48. https://doi.org/10.1002/esp.261.

Bo, T., S. Fenoglio, G. Malacarne, M. Pessino, and F. Sgariboldi. 2007. Effects of Clogging on Stream Macroinvertebrates: An Experimental Approach. *Limnologica - Ecology and Management of Inland Waters* 37 (2): 186–92. https://doi.org/10.1016/j.limno.2007.01.002.

Boano, F., J. W. Harvey, A. Marion, A. I. Packman, R. Revelli, L. Ridolfi, and A. Woerman. 2014. Hyporheic Flow and Transport Processes: Mechanisms, Models, and Biogeochemical Implications. *Reviews of Geophysics* 52 (4): 603–79. https://doi.org/10.1002/2012RG000417.

Boulton, A. J., S. Findlay, P. Marmonier, E. H. Stanley, and H. Maurice Valett. 1998. The Functional Significance of the Hyproheic Zone in Streams and Rivers. *Annual Review of Ecology and Systematics* 29: 59–81.

Bouwer, H., and R. C. Rice. 1976. A Slug Test for Determining Hydraulic Conductivity of Unconfined Aquifers with Completely or Partially Penetrating Wells. *Water Resources Research* 12 (3): 423–428.

Brunke, M. 1999. Colmation and Depth Filtration within Streambeds: Retention of Particles in Hyporheic Interstices. *International Review of Hydrobiology* 84 (2): 99–117.

Brunke, M., and T. Gonser. 1997. The Ecological Significance of Exchange Processees between Rivers and Groundwater. *Freshwater Biology* 37: 1–33.

Buendia, C., C. N. Gibbins, D. V., Ramon J. Batalla, and A. Douglas. 2013. Detecting the Structural and Functional Impacts of Fine Sediment on Stream Invertebrates. *Ecological Indicators* 25: 184–96. https://doi.org/10.1016/j.ecolind.2012.09.027.

Bunte, K., and S. R. Abt. 2001. Sampling Surface and Subsurface Particles-Size Distribution in Wadable Gravel- and Cobble-Bed Streams for Analyses in Sediment Transport, Hydraulics, and Streambed Monitoring. General Technical Report RMRS-GTR-74.

Capece, M., Z. Huang, D. To, M. Aloia, C. Muchira, R.N. Davé, and A.B. Yu. 2014. Prediction of Porosity from Particle Scale Interactions: Surface Modification of Fine Cohesive Powders. *Powder Technology* 254 (March): 103–13. https://doi.org/10.1016/j.powtec.2014.01.006.

Cardenas, M. B., A. E. Ford, M. H. Kaufman, A. J. Kessler, and P. L. M. Cook. 2016. Hyporheic Flow and Dissolved Oxygen Distribution in Fish Nests: The Effects of Open Channel Velocity, Permeability Patterns, and Groundwater Upwelling: Hyporheic Flow and DO

Inside Fish Nests. *Journal of Geophysical Research: Biogeosciences* 121 (12): 3113–30. https://doi.org/10.1002/2016JG003381.

Cardenas, M. B., and V. A. Zlotnik. 2003. A Simple Constant-Head Injection Test for Streambed Hydraulic Conductivity Estimations. *Ground Water* 41 (6): 867–71.

Carling, P. A., and N. A. Reader. 1981. A Freeze-Sampling Technique Suitable for Coarser River Bed-Material. *Sedimentary Geology* 29: 233–39.

Carling, P. A., and N. A. Reader. 1982. Structure, Composition and Bulk Properties of Upland Stream Gravel. *Earth Surface Processes and Landforms*, no. 7: 349–65.

Carman, P. C. 1939. Permeability of Saturated Sands, Soils and Clays. *The Journal of Agricultural Science* 29 (2): 262–273.

Carrier, D. W. 2003. Goodbye, Hazen; Hello, Kozeny-Carman. *Journal of Geotechnical and Geoenvironmental Engineering* 129 (11): 1054–56. https://doi.org/10.1061/~ASCE!1090-0241~2003!129:11~1054!

Chapman, D. W. 1988. Critical Review of Variables Used to Define Effects of Fines in Redds of Large Salmonids. *Transactions of the American Fisheries Society* 117 (1): 1–21.

Chen, X. 2004. Streambed Hydraulic Conductivity for Rivers in South-Central Nebraska. *Journal of the American Water Resources Association* 40 (3): 561–73.

Church, M. 1987. River Bed Gravels - Sampling and Analysis. In *Sediment Transport in Gravel-Bed Rivers*, edited by C.R. Thorne, J.C. Bathurst, and R.D. Hey, 43–88. Chichester, West Sussex, England; Hoboken, N.J: John Wiley & Sons.

Clark, L. C., and C. Lyons. 1962. Electrode Systems for Continuous Monitoring in Cardiovascular Surgery. *Annals of the New York Academy of Sciences* 102 (1): 29–45.

Commission. 2000. Establishing a Framework for Community Action in the Field of Water Policy. Luxembourg: European Commission. PE-CONS 3639/1/100 Rev 1.

Crisp, D. T. 1996. Environemtal Requirements of Commen Riverine European Salmonid Fish Species in Fresh Waer with Particular Reference to Physical and Chemical Aspects. *Hydrobiologia* 323: 201–21.

Crisp, D. T., and P. A. Carling. 1989. Observations on Siting, Dimensions and Structure of Salmonid Redds. *Journal of Fish Biology* 34 (1): 119–134.

Crisp, D. T. 1981. A Desk Study of the Relationship between Temperature and Hatching Time for the Eggs of Five Species of Salmonid Fishes. *Freshwater Biology* 11 (4): 361–368.

Crisp, D. T. 1993. The Environmental Requirements of Salmon and Trout in Fresh Water. In *Freshwater Forum*, 3:176–202.

Cui, B., Q. Yang, Z. Yang, and K. Zhang. 2009. Evaluating the Ecological Performance of Wetland Restoration in the Yellow River Delta, China. *Ecological Engineering* 35 (7): 1090–1103. https://doi.org/10.1016/j.ecoleng.2009.03.022.

Cunningham, A. B., C. J. Anderson, and H. Bouwer. 1987. Effects of Sediment-Laden Flow on Channel Bed Clogging. *Journal of Irrigation and Drainage Engineering* 113 (1): 106–118.

Datry, T., N. Lamouroux, G. Thivin, S. Descloux, and J. M. Baudoin. 2015. Estimation of Sediment Hydraulic Conductivity in River Reaches and Its Potential Use to Evaluate Streambed Clogging: Spatial Variability in Streambed Hydraulic Conductivity. *River Research and Applications* 31 (7): 880–91. https://doi.org/10.1002/rra.2784.

De Vries, M. 1970. On the Accuracy Of Bed-Material Sampling. *Journal of Hydraulic Research* 8 (4): 523–33. https://doi.org/10.1080/00221687009500329.

Descloux, S., T. Datry, and P. Marmonier. 2013. Benthic and Hyporheic Invertebrate Assemblages along a Gradient of Increasing Streambed Colmation by Fine Sediment. *Aquatic Sciences* 75 (4): 493–507. https://doi.org/10.1007/s00027-013-0295-6.

Descloux, S., T. Datry, M. Philippe, and P. Marmonier. 2010a. Comparison of Different Techniques to Assess Surface and Subsurface Streambed Colmation with Fine Sediments. *International Review of Hydrobiology* 95 (6): 520–40. https://doi.org/10.1002/iroh.201011250.

Descloux, S., T. Datry, M. Philippe, and P. Marmonier. 2010b. Comparison of Different Techniques to Assess Surface and Subsurface Streambed Colmation with Fine Sediments. *International Review of Hydrobiology* 95 (6): 520–40. https://doi.org/10.1002/iroh.201011250.

DIN. 1996. DIN 18123 - Bestimmung Der Korngrößenverteilung.

Diplas, P. 1986. Bed Load Transport in Gravel-Bed Streams: Some Properties. *Proc. of III-ISRS* River Sedimentation 3: 925–34.

Diplas, P., and G. Parker. 1992. Deposition and Removal of Fines in Gravel-Bed Streams. *Dynamics of Gravel-Bed Rivers*, 313–29.

Duan, X., Z. Wang, M. Xu, and K. Zhang. 2009. Effect of Streambed Sediment on Benthic Ecology. *International Journal of Sediment Research* 24: 325–38.

Dumas, J., and S. Marty. 2006. A New Method to Evaluate Egg-to-Fry Survival in Salmonids, Trials with Atlantic Salmon. *Journal of Fish Biology* 68 (1): 284–304.

Einstein, H. A. 1968. Deposition of Suspended Particles in a Gravel Bed. *Journal of the Hydraulic Division* 94 (HY5).

Eltner, A., A. Kaiser, C. Castillo, G. Rock, F. Neugirg, and A. Abellán. 2016. Image-Based Surface Reconstruction in Geomorphometry; Merits, Limits and Developments. *Earth Surface Dynamics* 4 (2): 359–89. https://doi.org/10.5194/esurf-4-359-2016.

Ergun, S. 1952. Fluid Flow through Packed Columns. *Chemical Engineering Progress* 48: 89–94.

Eurich, T. 2016. Bestimmung der hydraulischen Durchlässigkeit mittels Doppelpacker – Systemoptimierung. Bachelor Thesis, Stuttgart, Germany: University of Stuttgart.

Finstad, A. G., S. Einum, T. Forseth, and O. Ugedal. 2007. Shelter Availability Affects Behaviour, Size-Dependent and Mean Growth of Juvenile Atlantic Salmon. *Freshwater Biology* 52 (9): 1710–18. https://doi.org/10.1111/j.1365-2427.2007.01799.x.

Fox, J. F. 2016. Prediction of the Clogging Profile Using the Apparent Porosity and Momentum Impulse. *Journal of Hydraulic Engineering* 142 (11): 06016016. https://doi.org/10.1061/(ASCE)HY.1943-7900.0001187.

Franssen, J., M. Lapointe, and P. Magnan. 2014. Geomorphic Controls on Fine Sediment Reinfiltration into Salmonid Spawning Gravels and the Implications for Spawning Habitat Rehabilitation. *Geomorphology* 211: 11–21. https://doi.org/10.1016/j.geomorph.2013.12.019.

Fraser, H. J. 1935. Experimental Study of the Porosity and Permeability of Clastic Sediments. *The Journal of Geology* 43 (8, Part 1): 910–1010.

Fries, J. S., and G. L. Taghon. 2010. Particle Fluxes into Permeable Sediments: Comparison of Mechanisms Mediating Deposition. *Journal of Hydraulic Engineering* 136 (4).

Frings, R. M., H. Schüttrumpf, and S. Vollmer. 2011. Verification of Porosity Predictors for Fluvial Sand-Gravel Deposits: Porosity Prediction. *Water Resources Research* 47 (7): n/a-n/a. https://doi.org/10.1029/2010WR009690.

Frostick, L. E., P. M. Lucas, and I. Reid. 1984. The Infiltration of Fine Matrices into Coarse-Grained Alluvial Sediments and Its Implications for Stratigraphical Interpretation. *Journal of the Geological Society* 141 (6): 955–65. https://doi.org/10.1144/gsjgs.141.6.0955.

Gayraud, S., and M. Philippe. 2003. Influence of Bed-Sediment Features on the Interstitial Habitat Available for Macroinvertebrates in 15 French Streams. *International Review of Hydrobiology* 88 (1): 77–93.

Genereux, D. P., S. Leahy, H. Mitasova, Casey D. Kennedy, and D. Reide Corbett. 2008. Spatial and Temporal Variability of Streambed Hydraulic Conductivity in West Bear Creek, North Carolina, USA. *Journal of Hydrology* 358 (3–4): 332–53. https://doi.org/10.1016/j.jhydrol.2008.06.017.

Gibson, R.J. 1993. The Atlantic Salmon in Fresh Water: Spawning, Rearing and Production. *Reviews in Fish Biology and Fisheries* 3: 39–73.

Gibson, S. D. Abraham, R. Heath, and D. Schoellhamer. 2009. Vertical Gradational Variability of Fines Deposited in a Gravel Framework. *Sedimentology* 56 (3): 661–76. https://doi.org/10.1111/j.1365-3091.2008.00991.x.

Gibson, S. D. Abraham, R. Heath, and D. Schoellhamer. 2010. Bridging Process Threshold for Sediment Infiltrating into a Coarce Substrate. *Journal of Geotechnical and Geoenvironmental Engineering* 136 (2): 402–6.

Goldschneider, A. A., K. A. Haralampides, and K.T.B. MacQuarrie. 2007. River Sediment and Flow Characteristics near a Bank Filtration Water Supply: Implications for Riverbed

Clogging. *Journal of Hydrology* 344 (1–2): 55–69. https://doi.org/10.1016/j.jhydrol.2007.06.031.

Gordon, N.D., T. A. McMahon, B. L. Finlayson, C.J. Gippel, and R.J. Nathan, eds. 2004. Stream Hydrology: An Introduction for Ecologists. 2nd ed. Chichester, West Sussex, England ; Hoboken, N.J: Wiley.

Graton, L.C., and H. J. Fraser. 1935. Systematic Packing of Spheres - with Particular Relation to Porosity and Permeability. *The Journal of Geology* 43 (8): 785–909.

Greig, S. M., D. A. Sear, and P. A. Carling. 2007. A Review of Factors Influencing the Availability of Dissolved Oxygen to Incubating Salmonid Embryos. *Hydrological Processes* 21 (3): 323–34. https://doi.org/10.1002/hyp.6188.

Greig, S.M., D.A. Sear, and P.A. Carling. 2005. The Impact of Fine Sediment Accumulation on the Survival of Incubating Salmon Progeny: Implications for Sediment Management. *Science of The Total Environment* 344 (1–3): 241–58. https://doi.org/10.1016/j.scitotenv.2005.02.010.

Gustafson-Greenwood, K. I., and J. R. Moring. 1991. Gravel Compaction and Permeabilities in Redds of Atlantic Salmon, Salmo Salar L. *Aquaculture and Fisheries Management* 22: 537–40.

Harbaugh, A. 2005. MODFLOW-2005*,* The U.S. Geologiccal Survey Modular Ground-Water Model - the Ground-Water Flow Process. U.S. Geological Survey Techniques and Methods 6-A16, Variously p.

Hausle, D. A. 1973. Factors Influencing Embryonic Survival and Emergence of Brook Trout (Salvelinus Fentinalis). Dissertation, University of Wisconsin.

Hayes, F. R. 1949. The Growth, General Chemistry, and Temperature Relations of Salmonid Eggs. *The Quarterly Review of Biology* 24 (4): 281–308.

Hazen, A. 1893. Some Physical Properties of Sands and Gravels, with Special Reference to Their Use in Filtration. 24th Annual Report of the State Board of Heath of Massachusetts For.

Head, K.H. 1982. Manual of Soil Laboratory Testing. Pentech Press.

Heywood, M. J. T., and D. E. Walling. 2007. The Sedimentation of Salmonid Spawning Gravels in the Hampshire Avon Catchment, UK: Implications for the Dissolved Oxygen Content of Intragravel Water and Embryo Survival. *Hydrological Processes* 21 (6): 770–88. https://doi.org/10.1002/hyp.6266.

Hill, R. J., and D. L. Koch. 2002. The Transition from Steady to Weakly Turbulent Flow in a Close-Packed Ordered Array of Spheres. *Journal of Fluid Mechanics* 465: 59–97.

Hiscock, K.M., and T. Grischek. 2002. Attenuation of Groundwater Pollution by Bank Filtration. *Journal of Hydrology* 266 (3–4): 139–44. https://doi.org/10.1016/S0022-1694(02)00158-0.

Hitchman, M.L. 1978. Measurement of Dissolved Oxygen. Chemical Analysis 49. John Wiley & Sons.

Hvorslev, J. M. 1951. Time Lag and Soil Permeability in Ground-Water Observations. Waterways Experiment Station Bulletin No. 36. Corps of Engineers, U.S. Army. Vicksburg, Mississippi. http://www.paducaheic.com/media/39984/LB09905-0404-GRC01.PDF.

Ingendahl, D. 2001. Dissolved Oxygen Concentration and Emergence of Sea Trout Fry from Natural Redds in Tributaries of the River Rhine. *Journal of Fish Biology* 58 (2): 325–41. https://doi.org/10.1006/jfbi.2000.1447.

Jones, J. I., J. F. Murphy, A. L. Collins, D. A. Sear, P. S. Naden, and P. D. Armitage. 2012. The Impact of Fine Sediment on Macro-Invertebrates. *River Research and Applications* 28 (8): 1055–71. https://doi.org/10.1002/rra.1516.

Jonsson, B., and N. Jonsson. 2009. A Review of the Likely Effects of Climate Change on Anadromous Atlantic Salmon *Salmo Salar* and Brown Trout *Salmo Trutta*, with Particular Reference to Water Temperature and Flow. *Journal of Fish Biology* 75 (10): 2381–2447. https://doi.org/10.1111/j.1095-8649.2009.02380.x.

Jonsson, B., and N. Jonsson. 2011. Ecology of Atlantic Salmon and Brown Trout. Dordrecht: Springer Netherlands. http://link.springer.com/10.1007/978-94-007-1189-1.

Kell, G. S. 1975. Density, Thermal Expansivity, and Compressibility of Liquid Water from 0 to 150 C: Correlations and Tables for Atmospheric Pressure and Saturation Reviewed and Expressed on 1968 Temperature Scale. *J. Chem. Eng. Data* 20 (1): 97–105.

Klopfer, C. 2016. Konzeption und Durchführung von Versuchen zur Bestimmung der Porosität von Sedimentproben mittels Structure-from-Motion und Wasserverdrängungsmethode. Bachelor Thesis, Stuttgart, Germany: University of Stuttgart.

Klute, A. 1986. Methods of Soil Analysis - Part 1 - Physical and Mineralogical Methods. Second Edition. Madison, Wisconsin, USA: American Society of Agronomy, Inc.

Klute, A., and Ch Dirksen. 1986. Hydraulic Conductivity and Diffusivity: Laboratory Methods. In *Methods of Soil Analysis: Part 1—Physical and Mineralogical Methods*, 687–734.

Kondolf, G. M., and M.G. Wolman. 1993. The Size of Salmonid Spawning Gravels. *Water Resources Research* 29 (7): 2275–85.

Kondolf, G. M. 2000. Assessing Salmonid Spawning Gravel Quality. *American Fisheries Society* 129: 262–81.

Kondolf, G. M., Y. Gao, G. W. Annandale, G. L. Morris, E. Jiang, J. Zhang, Y. Cao, et al. 2014. Sustainable Sediment Management in Reservoirs and Regulated Rivers: Experiences from Five Continents: Kondolf. *Earth's Future* 2 (5): 256–80. https://doi.org/10.1002/2013EF000184.

Kondolf, G. M., J. G. Williams, T. C. Horner, and D. Milan. 2008. Assessing Physical Quality of Spawning Habitat. *American Fisheries Society Symposium* 65.

Krumbein, W. C. 1938. Graphic Presentation and Statistical Analysis of Sedimentary Data. University of Chicago, Chicago, Illinois

Krumbein, W. C., G. D. Monk, and others. 1943. Permeability as a Function of the Size Parameters of Unconsolidated Sand. *Transactions of the AIME* 151 (01): 153–163.

Lachance, S., and M. Dubé. 2004. A New Tool for Measuring Sediment Accumulation with Minimal Loss of Fines. *North Americal Journal of Fisheries Management* 24: 303–10.

Landon, M. K., D. L. Rus, and F. E. Harvey. 2001. Comparison of Instream Methods for Measuring Hydraulic Conductivity in Sandy Streambeds. *Ground Water* 39 (6): 870–85.

Lenz, I. 2018. Expertenbefragung Zum Thema Kolmation. Bachelor Thesis, Stuttgart, Germany: University of Stuttgart.

Liang, R., T. Schruff, X. Jia, H. Schüttrumpf, and R. M. Frings. 2015. Validation of a Stochastic Digital Packing Algorithm for Porosity Prediction in Fluvial Gravel Deposits. *Sedimentary Geology* 329: 18–27. https://doi.org/10.1016/j.sedgeo.2015.09.002.

Lindroth, A. 1942. Sauestoffverbrauch der Fische. II Verschiedene Engwicklungs- und Altersstadien vom Lachs und Hecht. *Zeitung für Vergleichende Physiologie* 29: 583–94.

Lisle, T. E. 1989. Sediment Transport and Resulting Deposition in Spawning Gravels, North Coastal California. *Water Resources Research* 25 (6): 1303–19.

Liu, L., T. De Kock, J. Wilkinson, V. Cnudde, S. Xiao, C. Buchmann, D. Uteau, S. Peth, and A. Lorke. 2018. Methane Bubble Growth and Migration in Aquatic Sediments Observed by X-Ray MCT. *Environmental Science & Technology* 52 (4): 2007–15. https://doi.org/10.1021/acs.est.7b06061.

Lotspeich, F. B., and F. H. Everest. 1981. A New Method for Reporting and Interpreting Textural Composition of Spawning Gravel. Vol. 369. US Dept. of Agriculture, Forest Service, Pacific Northwest Forest and Range Experiment Station.

Lunt, I. A., and J. S. Bridge. 2007. Formation and Preservation of Open-Framework Gravel Strata in Unidirectional Flows. *Sedimentology* 54 (1): 71–87. https://doi.org/10.1111/j.1365-3091.2006.00829.x.

Mahoney, D., and D. C. Erman. 1984. An Index of Stored Fine Sediment in Gravel Bedded Streams. *Water Resources Bulletin* 20 (3).

Maridet, L., and M. Philippe. 1995. Influence of Substrate Characteristics on the Vertical Distribution of Stream Macroinvertebrates in the Hyporheic Zone. *Folia Fac. Sci. Nat. Univ. Masaryk. Brun.*, 1995.

Maridet, L., J.-G. Wasson, and M. Philippe. 1992. Vertical Distribution of Fauna in the Bed Sediment of Three Running Water Sites: Influence of Physical and Trophic Factors. *River Research and Applications* 7 (1): 45–55.

Marmonier, P., Y. Delettre, S. Lefevre, J. Guyon, and A. J. Boulton. 2004. A Simple Technique Using Wooden Stakes to Estimate Vertical Patterns of Interstitial Oxygenation in the Beds of Rivers. *Archiv Für Hydrobiologie* 160 (1): 133–43. https://doi.org/10.1127/0003-9136/2004/0160-0133.

Milan, D. J., G. E. Petts, and H. Sambrook. 2000. Regional Variations in the Sediment Structure of Trout Streams in Southern England: Benchmark Data for Siltation Assessment and Restoration. *Aquatic Conservation: Marine and Freshwater Ecosystems* 10: 407–20.

Mitchell, Thomas O. 2006. Luminescence Based Measurement of Dissolved Oxygen in Natural Waters. *Hach Company, Loveland, CO*.

Morin, Roger H. 2006. Negative Correlation between Porosity and Hydraulic Conductivity in Sand-and-Gravel Aquifers at Cape Cod, Massachusetts, USA. *Journal of Hydrology* 316 (1–4): 43–52. https://doi.org/10.1016/j.jhydrol.2005.04.013.

NASCO. 2018. The Atlantic Salmon. North Atlantic Salmon Conservation Organization. 2018. http://www.nasco.int/atlanticsalmon.html.

Nogaro, G., T. Datry, F. Mermillod-Blondin, S. Descloux, and B. Montuelle. 2010. Influence of Streambed Sediment Clogging on Microbial Processes in the Hyporheic Zone: Influence of Clogging on Microbial Processes. *Freshwater Biology* 55 (6): 1288–1302. https://doi.org/10.1111/j.1365-2427.2009.02352.x.

Ottaway, E. M., P. A. Carling, A. Clarke, and N. A. Reader. 1981. Observations on the Structure of Brown Trout, Salmo Trutta Linnaeus, Redds. *Journal of Fish Biology* 19 (5): 593–607. https://doi.org/10.1111/j.1095-8649.1981.tb03825.x.

Owens, P. N., R. J. Batalla, A. J. Collins, B. Gomez, D. M. Hicks, A. J. Horowitz, G. M. Kondolf, et al. 2005. Fine-Grained Sediment in River Systems: Environmental Significance and Management Issues. *River Research and Applications* 21 (7): 693–717. https://doi.org/10.1002/rra.878.

Packman, A. I., and J. S. MacKay. 2003. Interplay of Stream-Subsurface Exchange, Clay Particle Deposition, and Streambed Evolution. *Water Resources Research* 39 (4): n/a-n/a. https://doi.org/10.1029/2002WR001432.

Packman, A. I., M. Salehin, and M. Zaramella. 2004. Hyporheic Exchange with Gravel Beds: Basic Hydrodynamic Interactions and Bedform-Induced Advective Flows. *Journal of Hydraulic Engineering* 130 (7).

Petts, G. E. 1988. Accumulation of Fine Sediment within Substrate Gravels along Two Regulated Rivers, UK. *Regulated Rivers: Research & Management* 2: 141–53.

Pholkern, K., K. Srisuk, T. Grischek, M. Soares, S. Schäfer, L. Archwichai, P. Saraphirom, P. Pavelic, and W. Wirojanagud. 2015. Riverbed Clogging Experiments at Potential River Bank Filtration Sites along the Ping River, Chiang Mai, Thailand. *Environmental Earth Sciences* 73 (12): 7699–7709. https://doi.org/10.1007/s12665-015-4160-x.

Pires, L. F., and A. B. Pereira. 2014. Gamma-Ray Attenuation to Evaluate Soil Porosity: An Analysis of Methods. *The Scientific World Journal* 2014: 1–10. https://doi.org/10.1155/2014/723041.

Platts, W. S., W. S. Megahan, and G. W. Minshall. 1983. Methods for Evaluating Stream, Riparian, and Biotic Conditions. General Technical Report INT-138. Ogden: U.S. Department of Agriculture, Forest Service, Intermountain Forest and Range Experiment Station.

Rabeni, C. 1997. Sediment in Streams: Sources, Biological Effects, and Control." *Transactions of the American Fisheries Society* 126 (6): 1048–51. https://doi.org/10.1577/1548-8659-126.6.1048.

Rehg, K. J., A. I. Packman, and J. Ren. 2005. Effects of Suspended Sediment Characteristics and Bed Sediment Transport on Streambed Clogging. *Hydrological Processes* 19 (2): 413–27. https://doi.org/10.1002/hyp.5540.

Reiser, D. W., and R. G. White. 1988. Effects of Two Sediment Size-Classes on Survival of Steelhead and Chinook Salmon Eggs. *North American Journal of Fisheries Management* 8 (4): 432–37. https://doi.org/10.1577/1548-8675(1988)008<0432:EOTSSC>2.3.CO;2.

Ren, J., and A. I. Packman. 2004. Modeling of Simultaneous Exchange of Colloids and Sorbing Contaminants between Streams and Streambeds. *Environmental Science & Technology* 38 (10): 2901–11. https://doi.org/10.1021/es0348521.

Richards, C., and K. L. Bacon. 1994. Influence of Fine Sediment on Macroinvertebrate Colonization of Surface and Hyporheic Stream Substrates. *The Great Basin Naturalist*, 106–113.

Riss, W. H., E. I. Meyer, and O. Niepagenkemper. 2008. A Novel and Robust Device for Repeated Small-Scale Oxygen Measurement in Riverine Sediments - Implications for Advanced Environmental Surveys. *Limnol. Oceanogr.* 6: 200–207.

Rombough, P. J. 1988. Growth, Aerobic Metabolism, and Dissolved Oxygen Requirements of Embryos and Alevins of Steelhead, Salmo Gairdneri. *Canadian Journal of Zoology* 66 (3): 651–660.

Rood, K., and M. Church. 1994. Modified Freeze-Core Technique for Sampling the Permanently Wetted Streambed. *North American Journal of Fisheries Management* 14 (4): 852–61. https://doi.org/10.1577/1548-8675(1994)014

Rubin, J.-F., and C. Glimsater. 1996. Egg-to-Fry Survival of the Sea Trout in Some Streams of Gotland. *Journal of Fish Biology* 48 (4): 585–606. https://doi.org/10.1111/j.1095-8649.1996.tb01454.x.

Ryan, R. J., and M. C. Boufadel. 2006. Influence of Streambed Hydraulic Conductivity on Solute Exchange with the Hyporheic Zone. *Environmental Geology* 51 (2): 203–10. https://doi.org/10.1007/s00254-006-0319-9.

Schaelchli, U.. 1992. The Clogging of Coarse Gravel River Beds by Fine Sediment. *Hydrobiologia* 235/236: 189–97.

Schälchli, Ueli. 1993. Die Kolmation von Fließgewässersohlen: Prozesse Und Berechnungsgrundlagen. Dissertation: ETH Nr. 10293, Zürich: ETH Zürich.

Schaelchli, U. 2002. Kolmation - Methoden Zur Erkennung Und Bewertung.

Schiemer, F., H. Keckeis, and E. Kamler. 2003. The Early Life History Stage of Riverine Fish: Ecophysiological and Environmental Bottlenecks. *Comparative Biochemistry and Physiology Part A* 133: 439–49.

Schmidt, C. K, F. T. Lange, H.-J. Brauch, and W. Kühn. 2003. Experiences with Riverbank Filtration and Infiltration in Germany.

Schubert, J. 2002. Hydraulic Aspects of Riverbank Filtration-Field Studies. *Journal of Hydrology* 266: 145–61.

Scrivener, J. C. 1988. Two Devices to Assess Incubation Survival and Emergence of Salmonid Fry in an Estuary Streambed. *North American Journal of Fisheries Management* 8 (2): 248–58. https://doi.org/10.1577/1548-8675(1988)008

Sear, D. A. 1993. Fine Sediment Infiltration into Gravel Spawning Beds within a Regulated River Experiencing Floods: Ecological Implications for Salmonids. *Regulated Rivers: Research & Management* 8: 373–90.

Sear, D.A., J.I. Jones, A.L. Collins, A. Hulin, N. Burke, S. Bateman, I. Pattison, and P.S. Naden. 2016. Does Fine Sediment Source as Well as Quantity Affect Salmonid Embryo Mortality and Development? *Science of The Total Environment* 541: 957–68. https://doi.org/10.1016/j.scitotenv.2015.09.155.

Sear, D. S., L. B. Frostick, G. Rollingson, and T. E. Lisle. 2008. The Significance and Mechanics of Fine-Sediment Infiltration and Accumulation in Gravel Spawning Beds. *American Fisheries Society Symposium* 65.

Seitz, L., C. Haas, M. Noack, and S. Wieprecht. 2018. From Picture to Porosity of River Bed Material Using Structure-from-Motion with Multi-View-Stereo. *Geomorphology* 306: 80–89. https://doi.org/10.1016/j.geomorph.2018.01.014.

Seitz, L., I. Lenz, M. Noack, S. Wieprecht, and C. Haas. 2019. Kolmation - Eine unterschätzte Größe in der Gewässerbewertung? *Wasserwirtschaft* 109 (2–3): 41–46. https://doi.org/10.1007/s35147-019-0005-y.

Seitz, L., M. Noack, S. Haun, R. Reindl, G. Senn, and M. Schletterer. 2016. Analysing Sediment Characteristics of the Alpine River Brixentaler Ache (Austria) Including in-Situ Measurements of Dissolved Oxygen. In *River Sedimentation*.

Sennatt, K. M., N. L. Salant, C. E. Renshaw, and F. J. Magilligan. 2006. Assessment of Methods for Measuring Embeddedness: Application to Sedimentation in Flow Regulated Streams. *Journal of the American Water Resources Association* 42 (6): 1671–82.

Sidiropoulou, M. G., K. N. Moutsopoulos, and V. A. Tsihrintzis. 2007. Determination of Forchheimer Equation Coefficients. *Hydrological Processes* 21 (4): 534–54. https://doi.org/10.1002/hyp.6264.

Smith, M.W., J.L. Carrivick, and D.J. Quincey. 2015. Structure from Motion Photogrammetry in Physical Geography. *Progress in Physical Geography* 40 (2): 247–75. https://doi.org/10.1177/0309133315615805.

Soulsby, C., A. F. Youngson, H. J. Moir, and I. A. Malcolm. 2001. Fine Sediment Influence on Salmonid Spawning Habitat in a Lowland Agricultural Stream: A Preliminary Assessment. *The Science of the Total Environment* 265 (1–3): 295–307.

Sperry, J. M., and J. J. Peirce. 1995. A Model for Estimating the Hydraulic Conductivity of Granular Material Based on Grain Shape, Grain Size, and Porosity. *Ground Water* 33 (6).

Sylte, T. L., and C. Fischenich. 2002. Techniques for Measuring Substrate Embeddedness.

Tappel, P.D., and T.C. Bjornn. 1983. A New Method of Relating Size of Spawning Gravel to Salmonid Embryo Survival. Idaho Cooperative Fishery Research Unit. Moscow, Idaho: University of Idaho.

Terhune, L.D.B. 1958. The Mark VI Groundwater Standpipe for Measuring Seepage through Salmon Spawning Gravel. *J.Fish.Res.Board Can.* 15 (5): 1027–63.

Thoms, M. C. 1992. A Comparison of Grab-and Freeze-Sampling Techniques in the Collection of Gravel-Bed River Sediment. *Sedimentary Geology* 78 (3–4): 191–200.

Thurmann, C., and T. Zumbroich. 2013. Resilientvermögen von Interstitialräumen Verschiedener Gewässertypen Bezüglich Kolmation.

Tonina, D. 2005. Interaction between River Morphology and Intra-Gravel Flow Paths within the Hyporheic Zone. University of Idaho.

Tonina, D., and J. M. Buffington. 2009. A Three-Dimensional Model for Analyzing the Effects of Salmon Redds on Hyporheic Exchange and Egg Pocket Habitat. Edited by Michael Bradford. *Canadian Journal of Fisheries and Aquatic Sciences* 66 (12): 2157–73. https://doi.org/10.1139/F09-146.

Ulrich, C., S. S. Hubbard, J. Florsheim, D. Rosenberry, S. Borglin, M. Trotta, and D. Seymour. 2015. Riverbed Clogging Associated with a California Riverbank Filtration System: An Assessment of Mechanisms and Monitoring Approaches. *Journal of Hydrology* 529: 1740–53. https://doi.org/10.1016/j.jhydrol.2015.08.012.

Ward, J. C. 1964. Turbulent Flow in Porous Media. *Journal of Hydraulic Division* 90 (5): 1–12.

Weigelhofer, G., and J. Waringer. 2003. Vertical Distribution of Benthic Macroinvertebrates in Riffles versus Deep Runs with Differing Contents of Fine Sediments (Weidlingbach, Austria). *International Review of Hydrobiology* 88 (34): 304–13. https://doi.org/10.1002/iroh.200390027.

Wentworth, C. K. 1922. Scale of Grade and Class Terms for Clastic Sediments. *The Journal of Geology* 30 (5): 377–392.

Westoby, M.J., J. Brasington, N.F. Glasser, M.J. Hambrey, and J.M. Reynolds. 2012. 'Structure-from-Motion' Photogrammetry: A Low-Cost, Effective Tool for Geoscience Applications. *Geomorphology* 179 (December): 300–314. https://doi.org/10.1016/j.geomorph.2012.08.021.

Wharton, G., S. H. Mohajeri, and M. Righetti. 2017. The Pernicious Problem of Streambed Colmation: A Multi-Disciplinary Reflection on the Mechanisms, Causes, Impacts, and Management Challenges. *Wiley Interdisciplinary Reviews: Water 4*, 19. https://doi.org/10.1002/wat2.1231.

Wilcock, P. R. 1988. Methods for Estimating the Critical Shear Stress of Individual Fractions in Mixed-Size Sediment. *Water Resources Research* 24 (7): 1127–35.

Wilcock, Peter R., and Stephen T. Kenworthy. 2002. A Two-Fraction Model for the Transport of Sand/Gravel Mixtures. *Water Resources Research* 38 (10): 12-1-12–12. https://doi.org/10.1029/2001WR000684.

Wokabi, J.W. 2018. Laboratory Experiments to Detect Hydraulic Conductivities in Gravel Beds Using a Deep Double Packer. Master Thesis, Stuttgart, Germany: University of Stuttgart.

Wondzell, S. M., and F. J. Swanson. 1996. Seasonal and Storm Dynamics of the Hyporheic Zone of a 4th-Order Mountain Stream. I: Hydrologic Processes. *Journal of the North American Benthological Society* 15 (1): 3–19. https://doi.org/10.2307/1467429.

Wooster, J. K., S. R. Dusterhoff, Y. Cui, L. S. Sklar, W. E. Dietrich, and M. Malko. 2008. Sediment Supply and Relative Size Distribution Effects on Fine Sediment Infiltration into Immobile Gravels. *Water Resources Research* 44 (3): n/a-n/a. https://doi.org/10.1029/2006WR005815.

Wu, W., and S. S. Wang. 2006. Formulas for Sediment Porosity and Settling Velocity. *Journal of Hydraulic Engineering* 132 (8): 858–862.

Yu, A. B., and N. Standish. 1991. Estimation of the Porosity of Particle Mixtures by a Linear-Mixture Packing Model. *Ind. Eng. Chem. Res.* 30: 1372–85.

Zaqout, T.A.M. 2017. Laboratory Experiments to Calibrate a Novel Method to Determine the Hydraulic Conductivity from Gravel and Sand Mixtures. Master Thesis, Stuttgart, Germany: University of Stuttgart.

Zimmermann, A. E., and M. Lapointe. 2005. Intergranular Flow Velocity through Salmonid Redds: Sensitivity to Fines Infiltration from Low Intensity Sediment Transport Events. *River Research and Applications* 21 (8): 865–81. https://doi.org/10.1002/rra.856.

Zou, R.P., M.L. Gan, and A.B. Yu. 2011. Prediction of the Porosity of Multi-Component Mixtures of Cohesive and Non-Cohesive Particles. *Chemical Engineering Science* 66 (20): 4711–21. https://doi.org/10.1016/j.ces.2011.06.037.

Zumbroich, T., and H.-J. Hahn. 2018. Feinsedimenteinträge in Gewässer Und Deren Messung - Kolmation Als Bedeutsamer Störfaktor Bei Der Umsetzung Der EG-WRRL. In *M^3 - Messen, Modellieren, Managen in Hydrologie Und Wasserressourcenbewirtschaftung*. Vol. 39.18. Dresden. https://doi.org/10.14617/for.hydrol.wasbew.39.18.

Appendix

Appendix 1 – Results from porosity experiments

Appendix 1.1: Averaged sediment characteristics from laboratory mixtures and field samples including determination of VSfM, VWRM, nSfM, nWRM, as well as MAEV and MAEn***.

Sample ID									
No of repetitions	M1	SM	GM	G	CG2	CG1	FS	FG	-
Sample mass	8	5	4	5	3	4	3	4	
D_{10}	13004.6	9498.8	8885.0	11191.3	8011.7	12723.8	6291.2	8506.7	g
D_{50}	0.24	0.21	1.67	6.37	19.56	9.31	0.10	2.18	mm
D_{60}	5.33	0.78	5.18	11.68	36.53	18.13	0.23	2.99	mm
D_{90}	7.52	1.02	5.97	12.76	41.96	20.89	0.28	3.19	mm
FSA < 2mm*	37.27	3.07	10.48	16.63	58.25	29.20	0.51	3.80	mm
FSA < 0.5 mm**	35.45	0.79	0.14	0.10	0.00	0.18	1.00	0.01	%
σ_G	19.44	0.38	0.00	0.06	0.00	0.00	0.90	0.00	%
$V_{tot\ (WRM)}$	2.57	1.66	0.55	0.59	0.48	0.63	0.96	0.20	-
$V_{tot\ (SfM)}$	6325.8	7272.7	5389.9	6355.9	3987.3	7524.5	4237.0	4925.5	ml
MAE_V***: $V_{SfM} - V_{tot\,(WRM)}/ V_{tot\,(SfM)}$	6509.8	7519.0	5582.3	6535.4	4155.5	7644.2	4342.8	5118.7	ml
n (SfM)	3.14	3.29	3.44	2.78	2.61	1.62	2.43	3.81	%
n (WRM)	0.23	0.29	0.35	0.34	0.28	0.31	0.44	0.38	-
MAE_n***: $(n_{SfM} - n_{WRM})/n_{SfM}$	0.20	0.27	0.33	0.32	0.25	0.30	0.43	0.36	-
	12.21	7.47	5.72	5.54	6.76	3.61	3.12	6.43	%

F	M8	M7	M6	M5	M4	M3	M2
10	4	5	5	4	5	4	4
10243.5	12075.0	15367.1	13393.0	17117.3	23060.0	22110.3	13686.8
1.07	2.36	1.31	2.37	0.55	0.18	1.71	0.89
22.62	13.57	6.92	5.25	8.08	9.43	16.83	10.34
33.94	16.14	8.51	8.93	9.98	16.35	26.87	13.28
94.42	27.61	42.05	15.08	15.38	73.33	90.69	26.42
0.22	0.03	0.13	0.01	0.42	0.31	0.11	0.15
0.05	0.00	0.06	0.00	0.06	0.24	0.04	0.07
2.42	1.06	1.87	1.11	2.10	3.20	2.22	1.84
5086.3	6376.9	7436.8	7197.1	8699.9	10996.4	10289.8	6780.6
5167.3	6663.9	7599.8	7358.4	8935.0	11261.4	10443.5	6945.9
1.87	4.36	2.20	2.32	2.78	2.48	1.51	2.58
0.26	0.30	0.23	0.30	0.26	0.22	0.19	0.24
0.25	0.27	0.22	0.28	0.24	0.20	0.18	0.22
10.49	10.53	6.31	5.57	8.04	9.06	6.27	8.21

* Fine sediment amount < 2.0 mm
** Fine sediment amount < 0.5 mm
*** Mean absolute error based on the total volume (MEA_V) and porosity (MEA_n)

Appendix 2 – Results from field campaign and the application of the multi-parameter approach

Appendix 2. 1: Results from Aich 1 including image of sediment sample, cumulative sieve curve and vertical profiles from slurping rate, IDOS and kf.

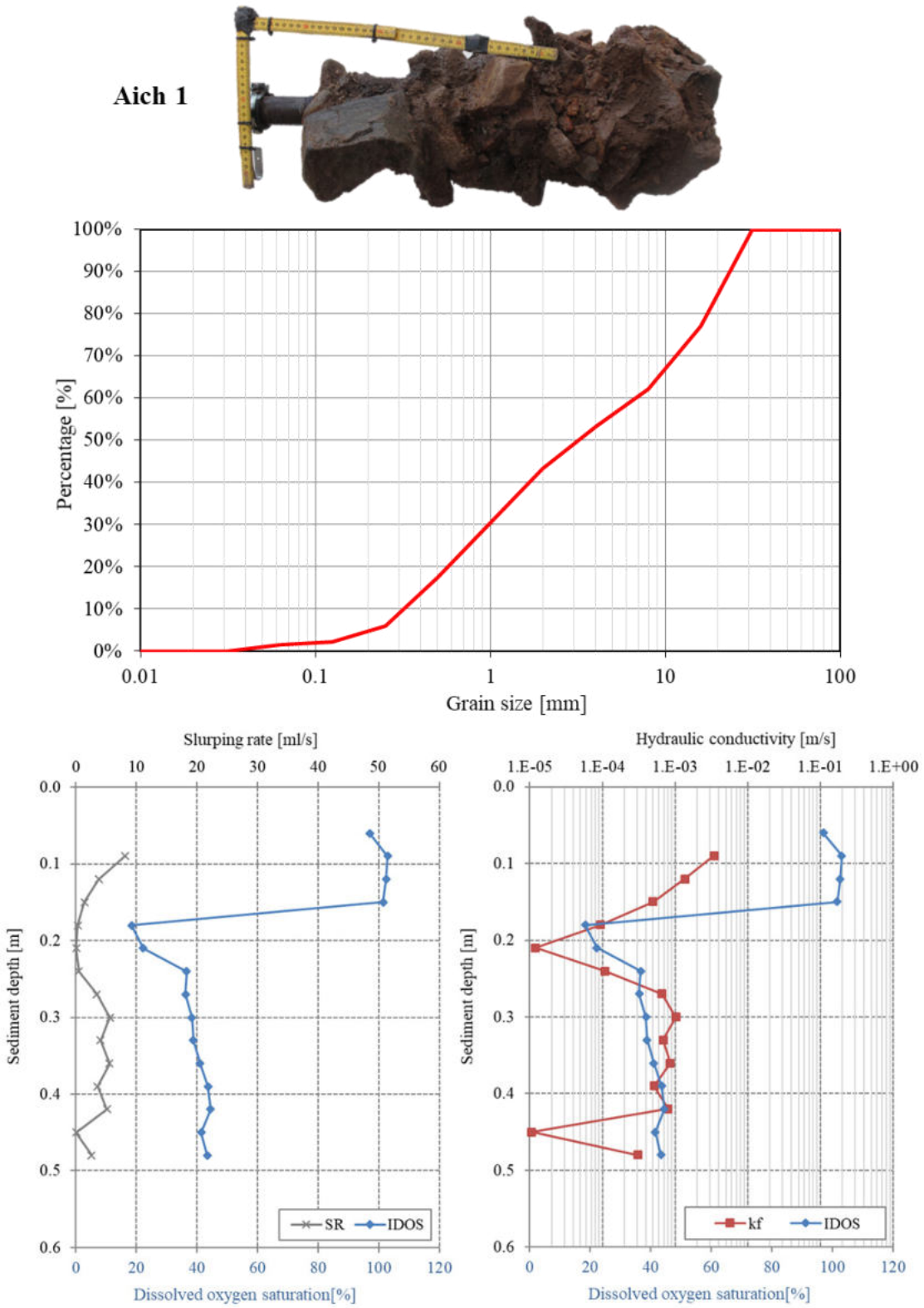

Appendix 2. 2: Results from Aich 2 including image of sediment sample, cumulative sieve curve and vertical profiles from slurping rate, IDOS and kf.

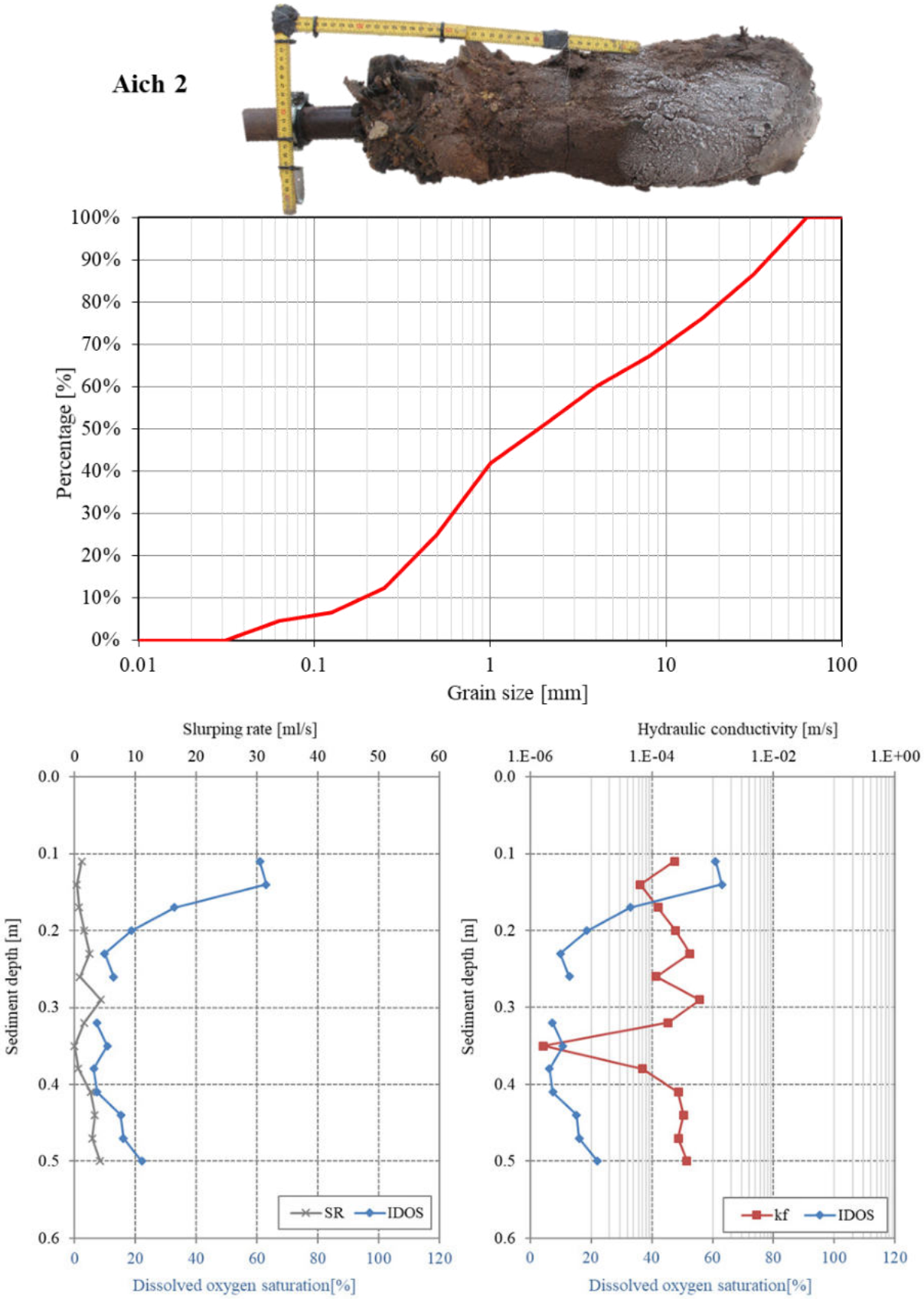

Appendix 2. 3: Results from Aich 3 including image of sediment sample, cumulative sieve curve and vertical profiles from slurping rate, IDOS and kf.

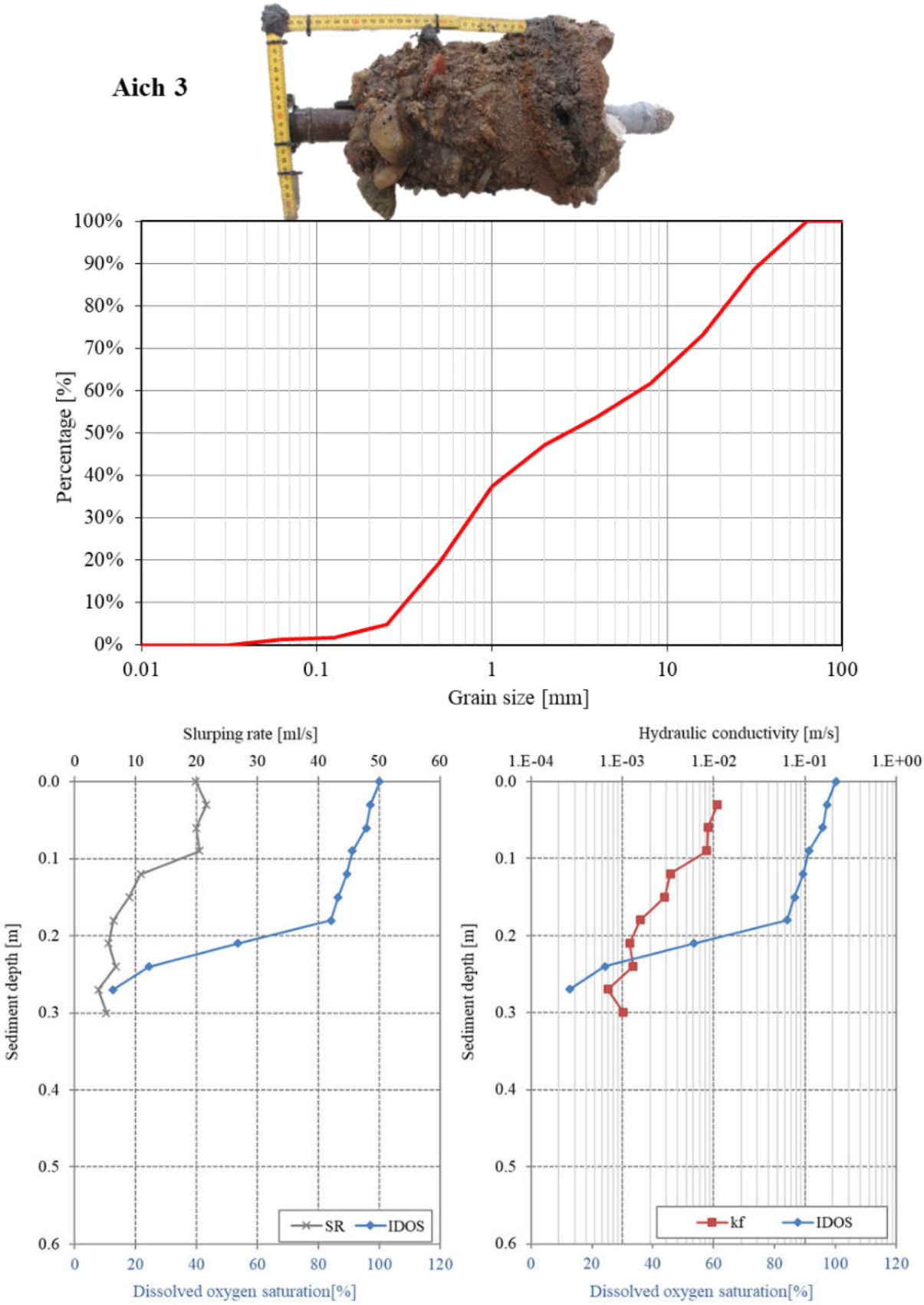

Appendix 2. 4: Results from Aich 4 including image of sediment sample, cumulative sieve curve and vertical profiles from slurping rate, IDOS and kf.

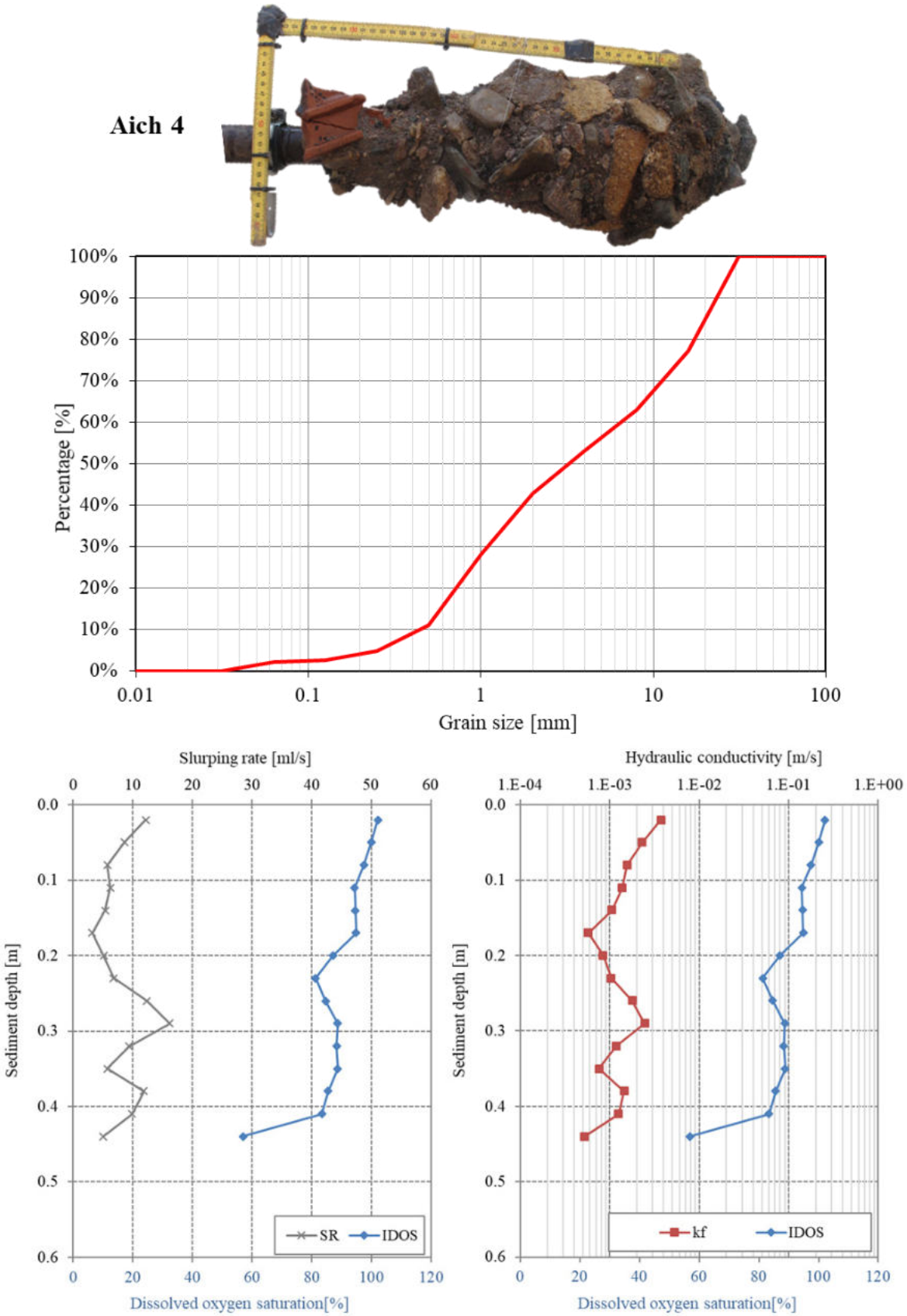

Appendix 2. 5: Results from Rems 1 including image of sediment sample, cumulative sieve curve and vertical profiles from slurping rate, IDOS and kf.

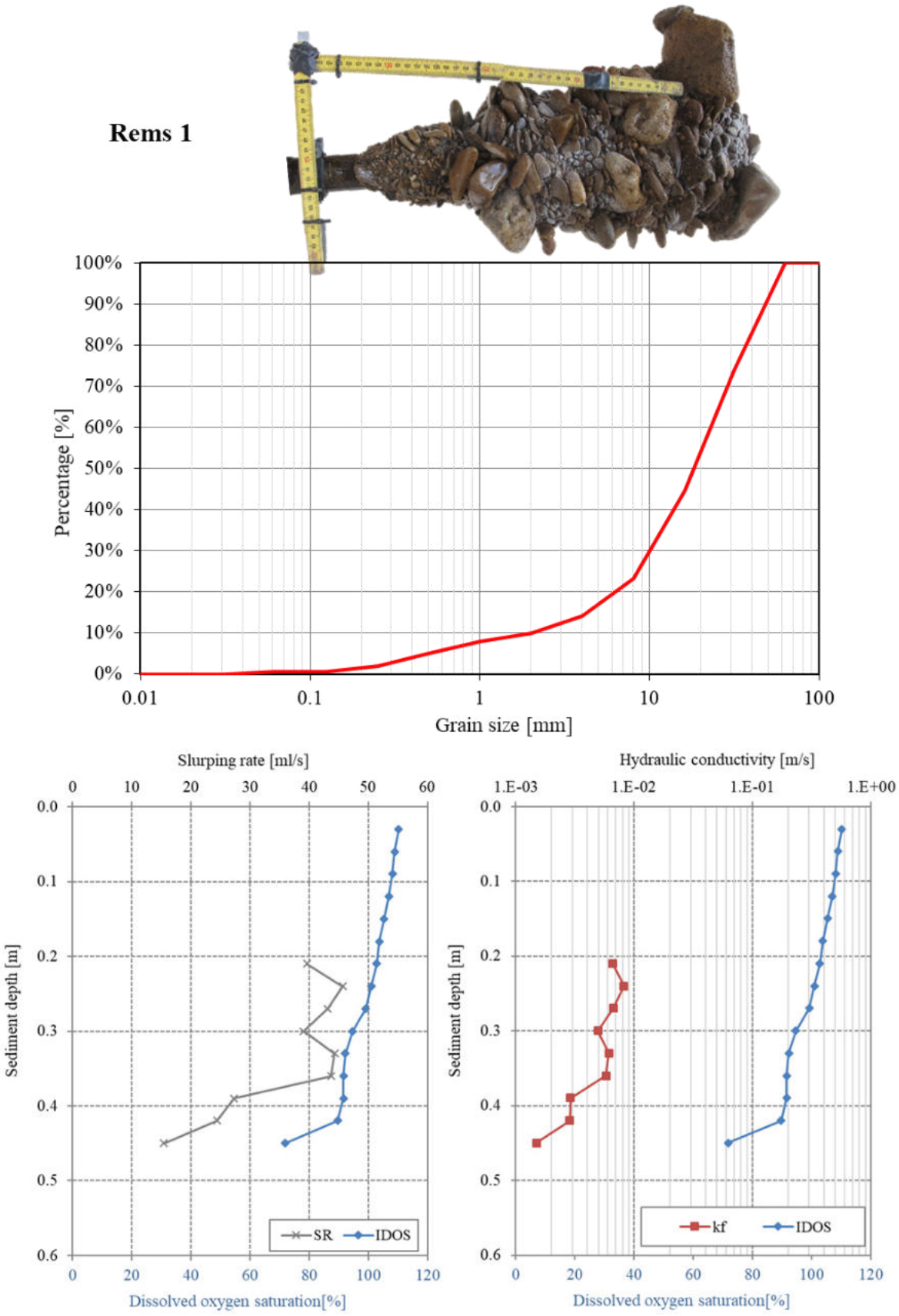

Appendix 2. 6: Results from Rems 2 including image of sediment sample, cumulative sieve curve and vertical profiles from slurping rate, IDOS and kf.

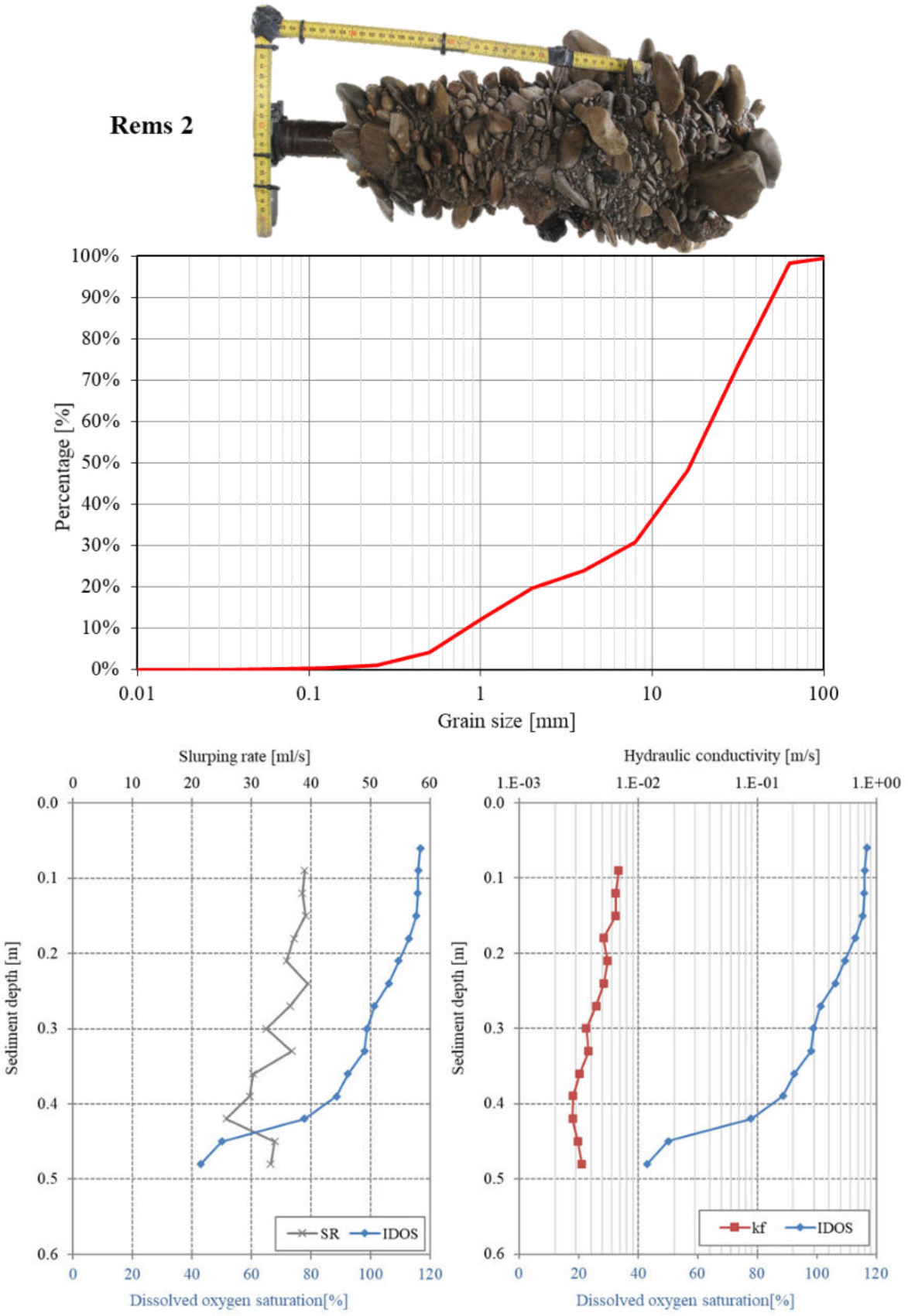

Appendix 2. 7: Results from Rems 3 including image of sediment sample, cumulative sieve curve and vertical profiles from slurping rate, IDOS and kf.

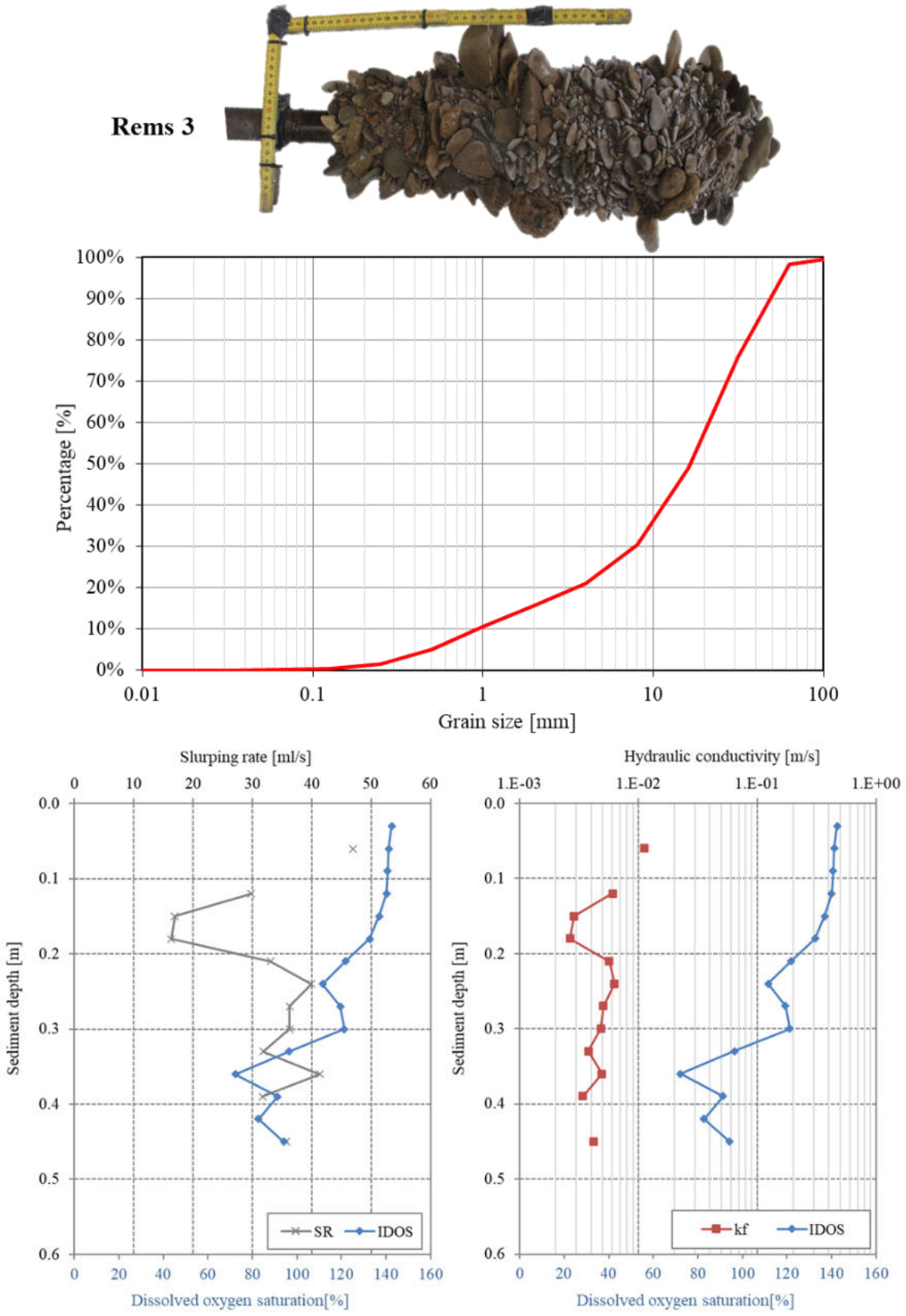

Appendix 2. 8: Results from Rems 5 including image of sediment sample, cumulative sieve curve and vertical profiles from slurping rate, IDOS and kf.

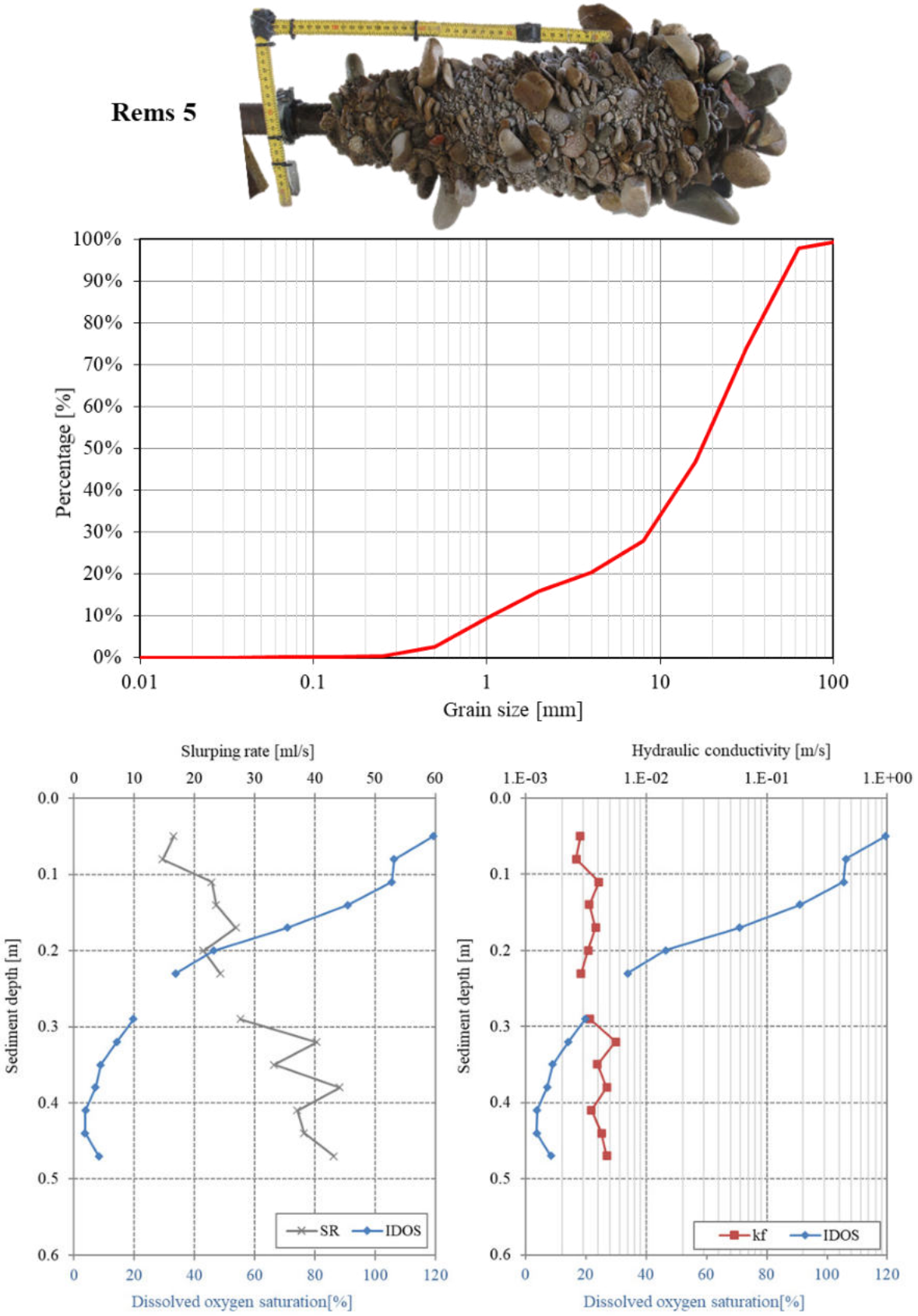

Appendix 2. 9: Results from Rems 6 including image of sediment sample, cumulative sieve curve and vertical profiles from slurping rate, IDOS and kf.

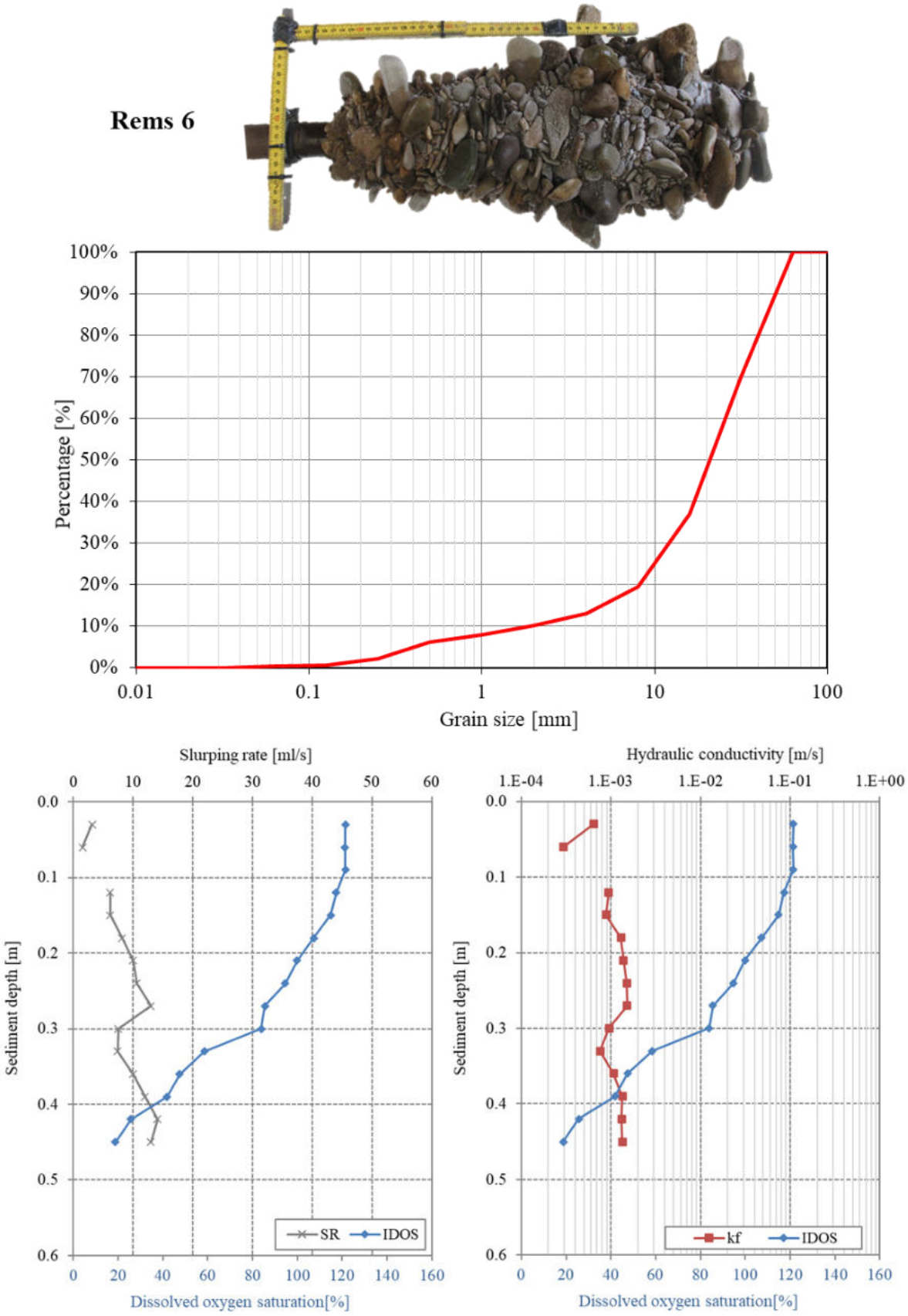

Appendix 2. 10: Results from Rems 7 including image of sediment sample, cumulative sieve curve and vertical profiles from slurping rate, IDOS and kf.

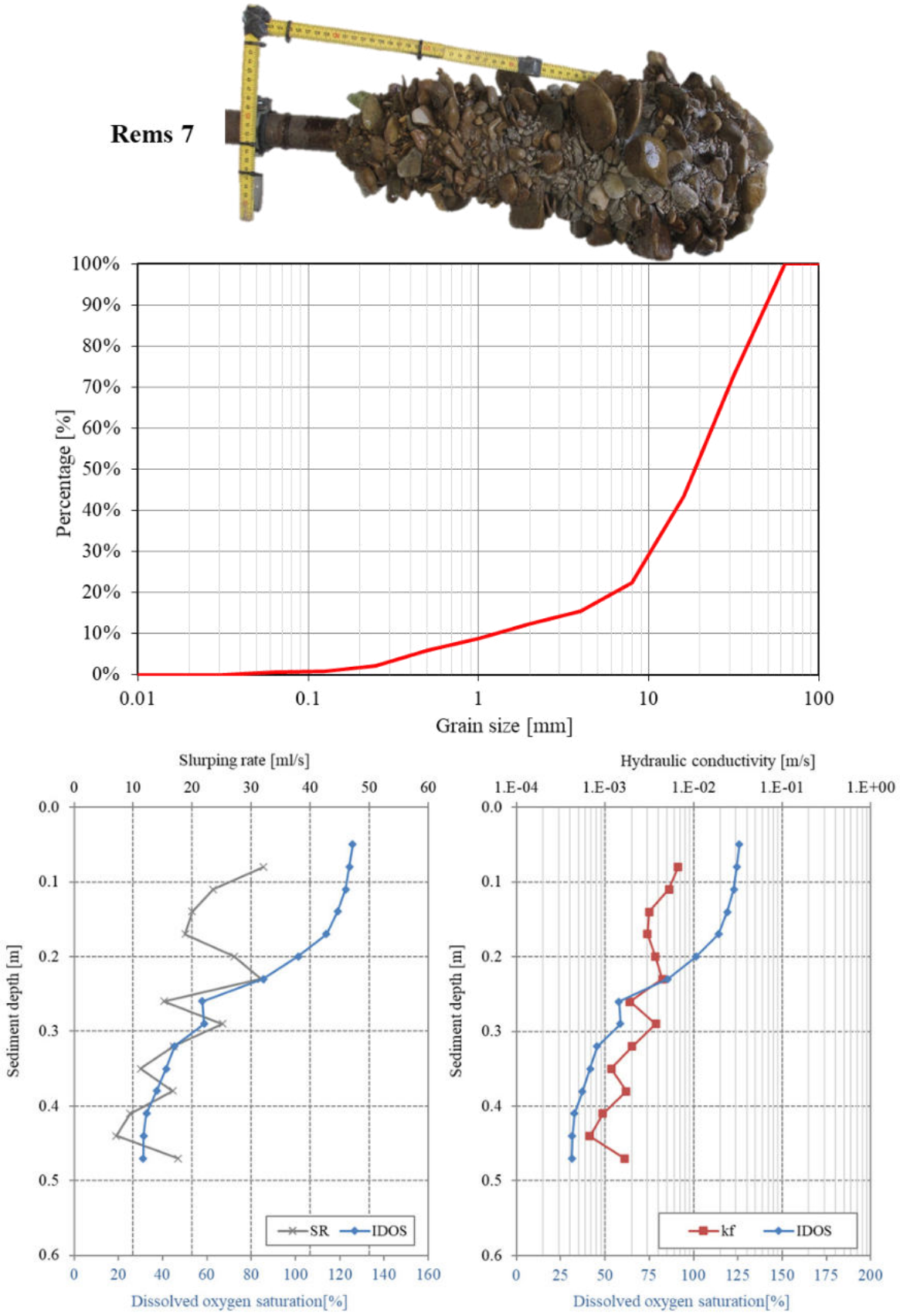

Appendix 2. 11: Results from Wieslauf 1 including image of sediment sample, cumulative sieve curve and vertical profiles from slurping rate, IDOS and kf.

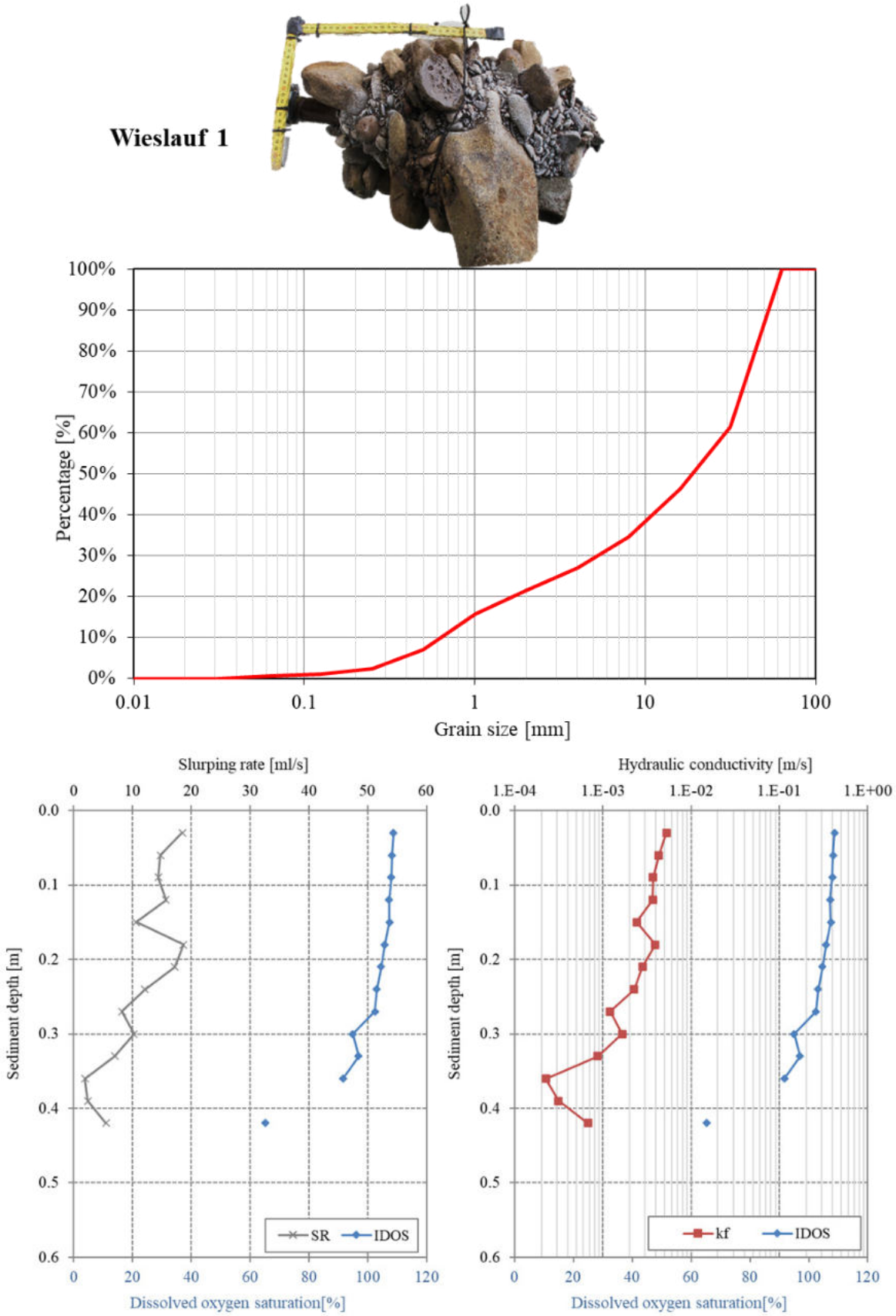

Appendix 2. 12: Results from Wieslauf 2 including image of sediment sample, cumulative sieve curve and vertical profiles from slurping rate, IDOS and kf.

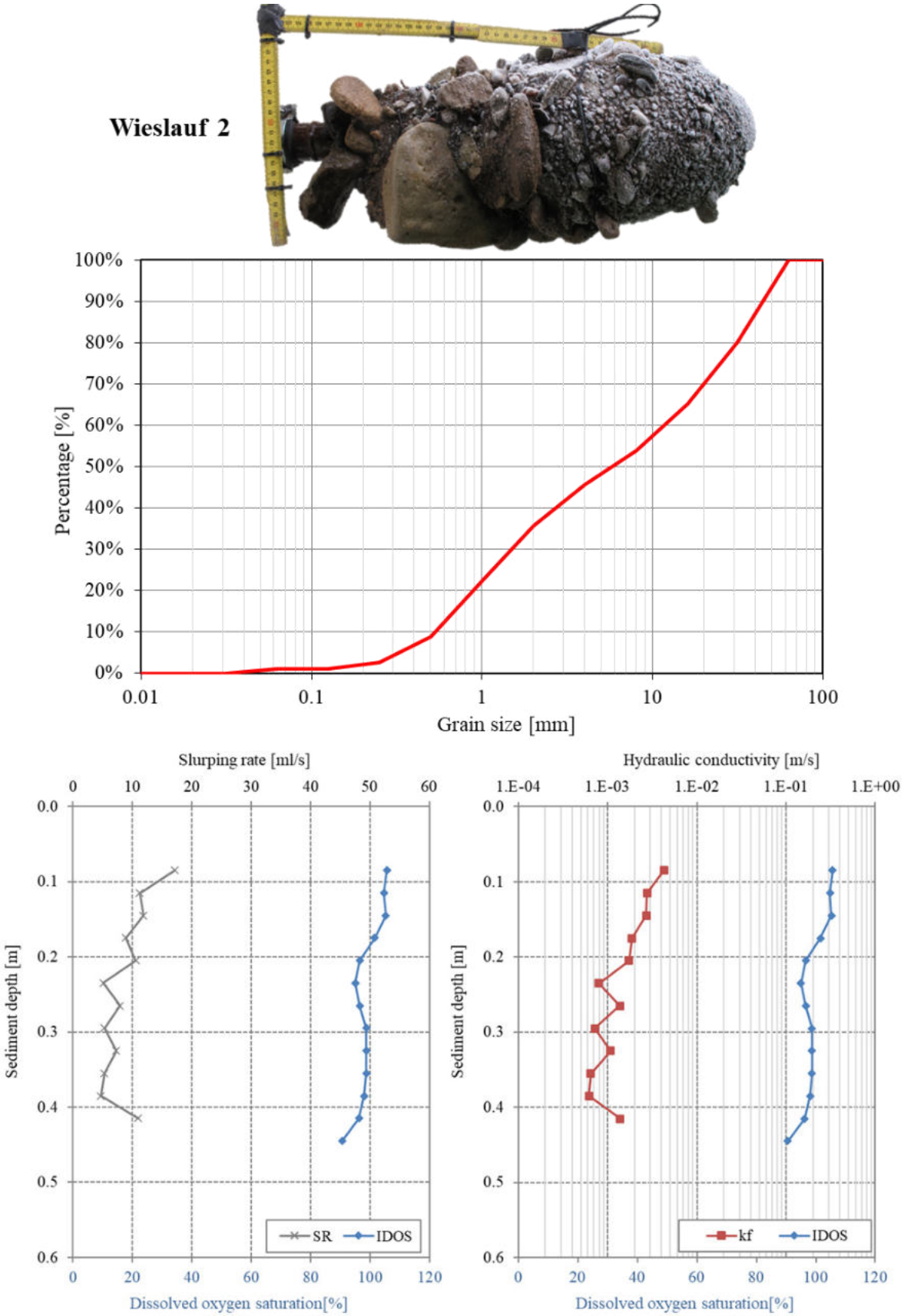

Appendix 2. 13: Results from Wieslauf 3 including image of sediment sample, cumulative sieve curve and vertical profiles from slurping rate, IDOS and kf.

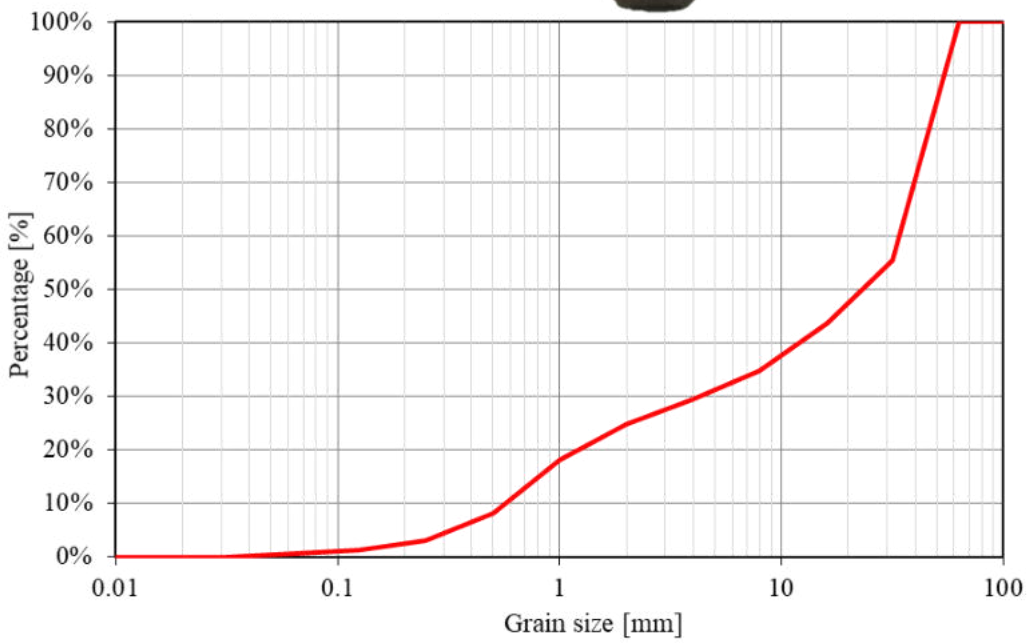

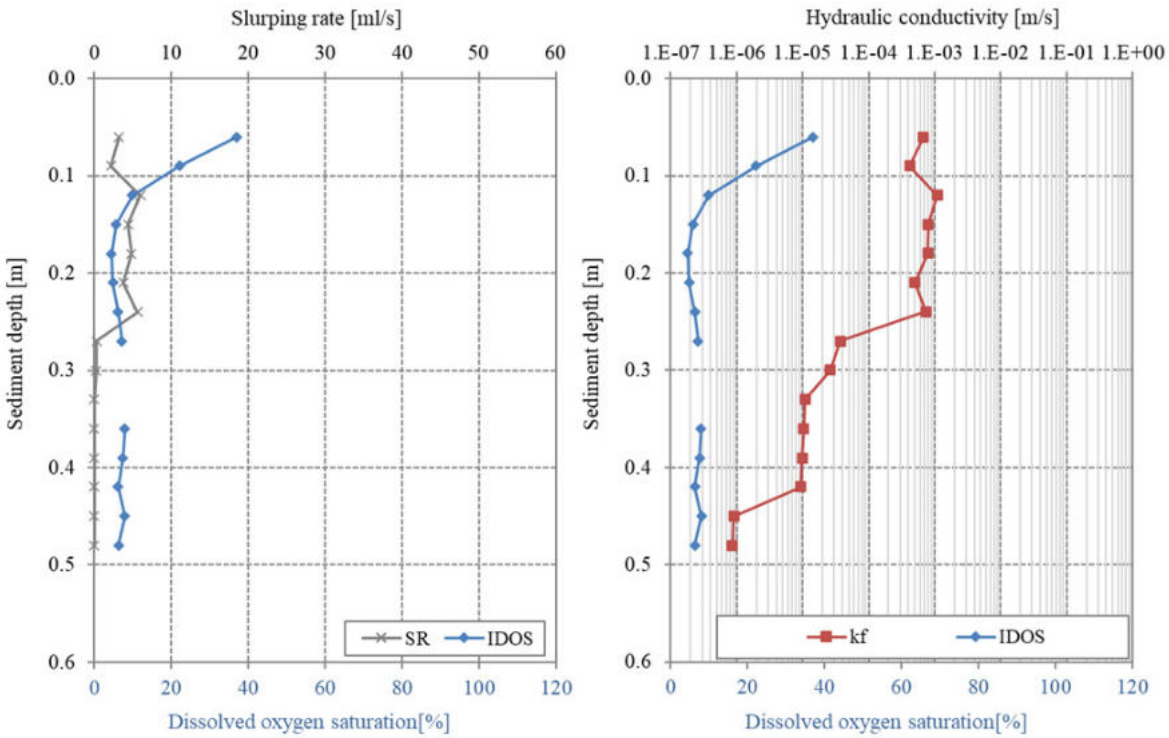

Appendix 2. 14: Results from Wieslauf 4 including image of sediment sample, cumulative sieve curve and vertical profiles from slurping rate, IDOS and kf.

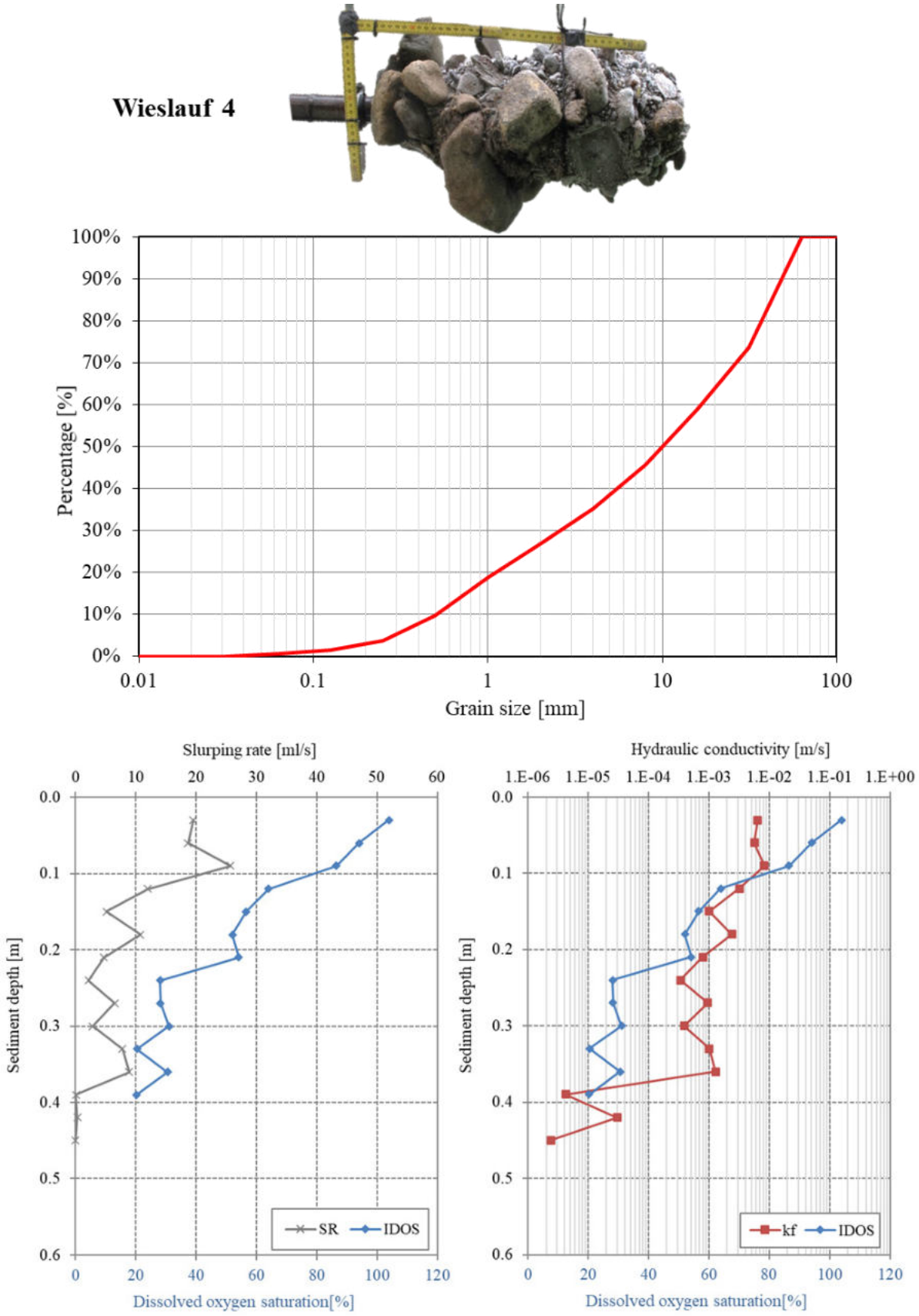

Appendix 2. 15: Results from Wieslauf 5 including image of sediment sample, cumulative sieve curve and vertical profiles from slurping rate, IDOS and kf.

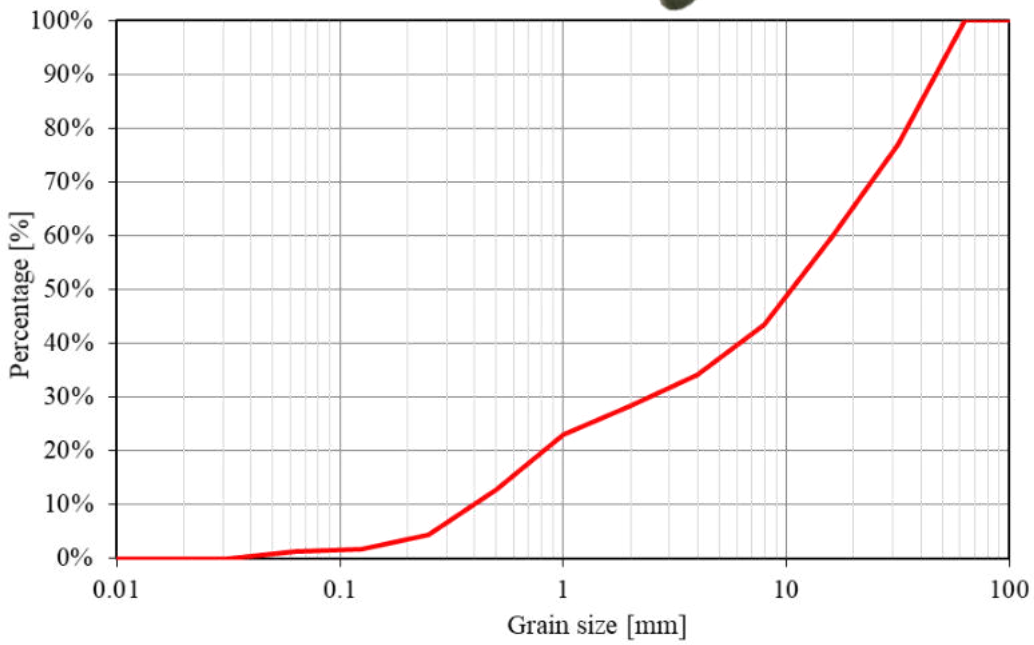

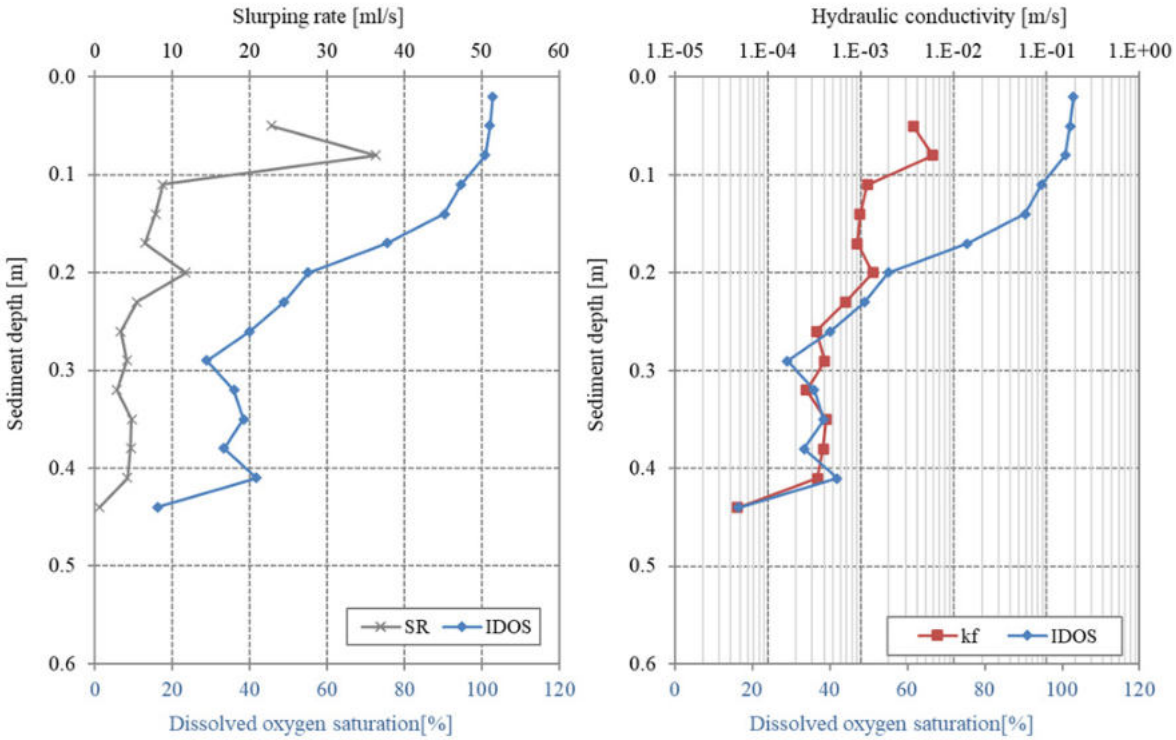

Appendix 2. 16: Results from Glems 1 including image of sediment sample, cumulative sieve curve and vertical profiles from slurping rate, IDOS and kf.

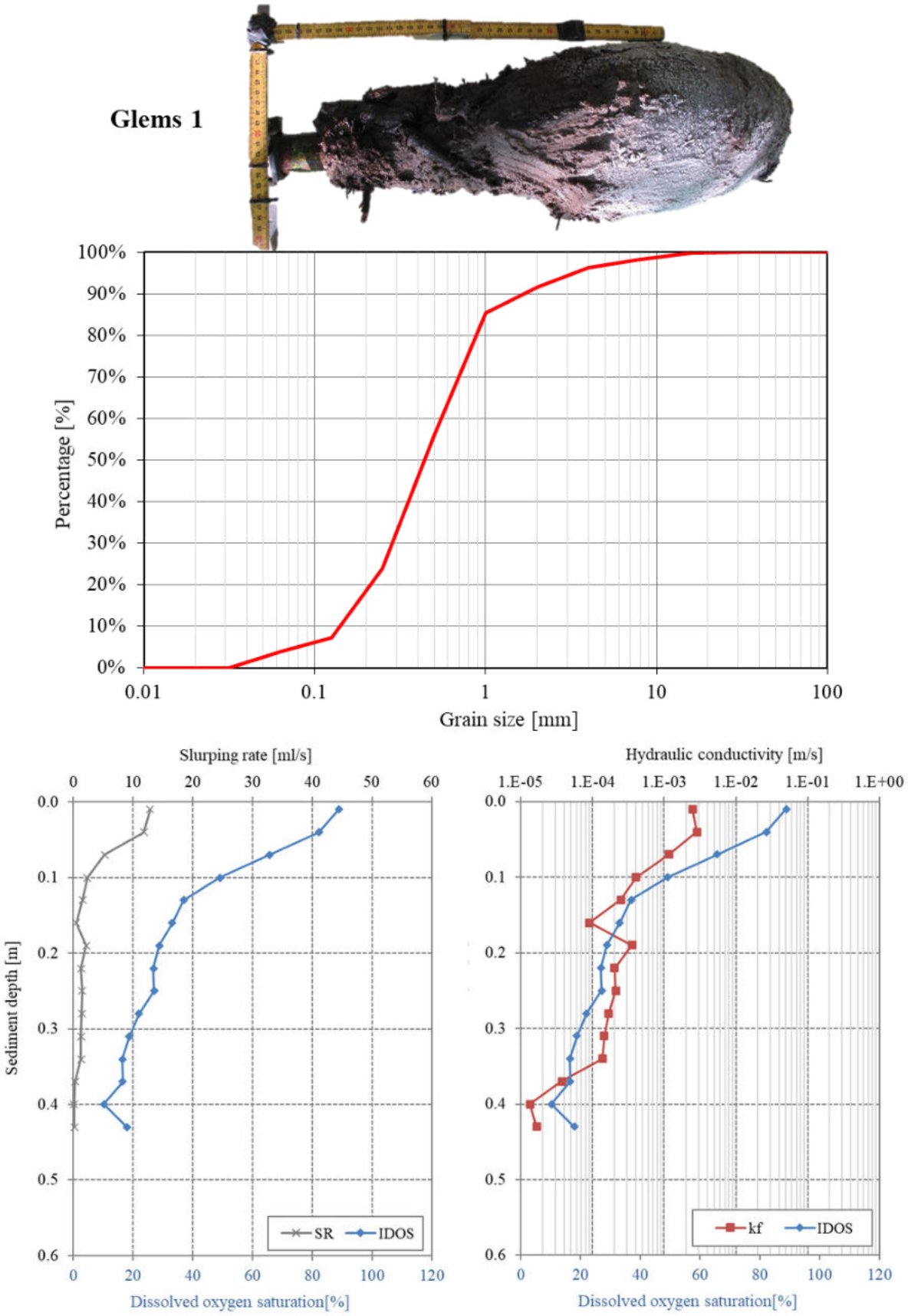

Appendix 2. 17: Results from Glems 2 including image of sediment sample, cumulative sieve curve and vertical profiles from slurping rate, IDOS and kf.

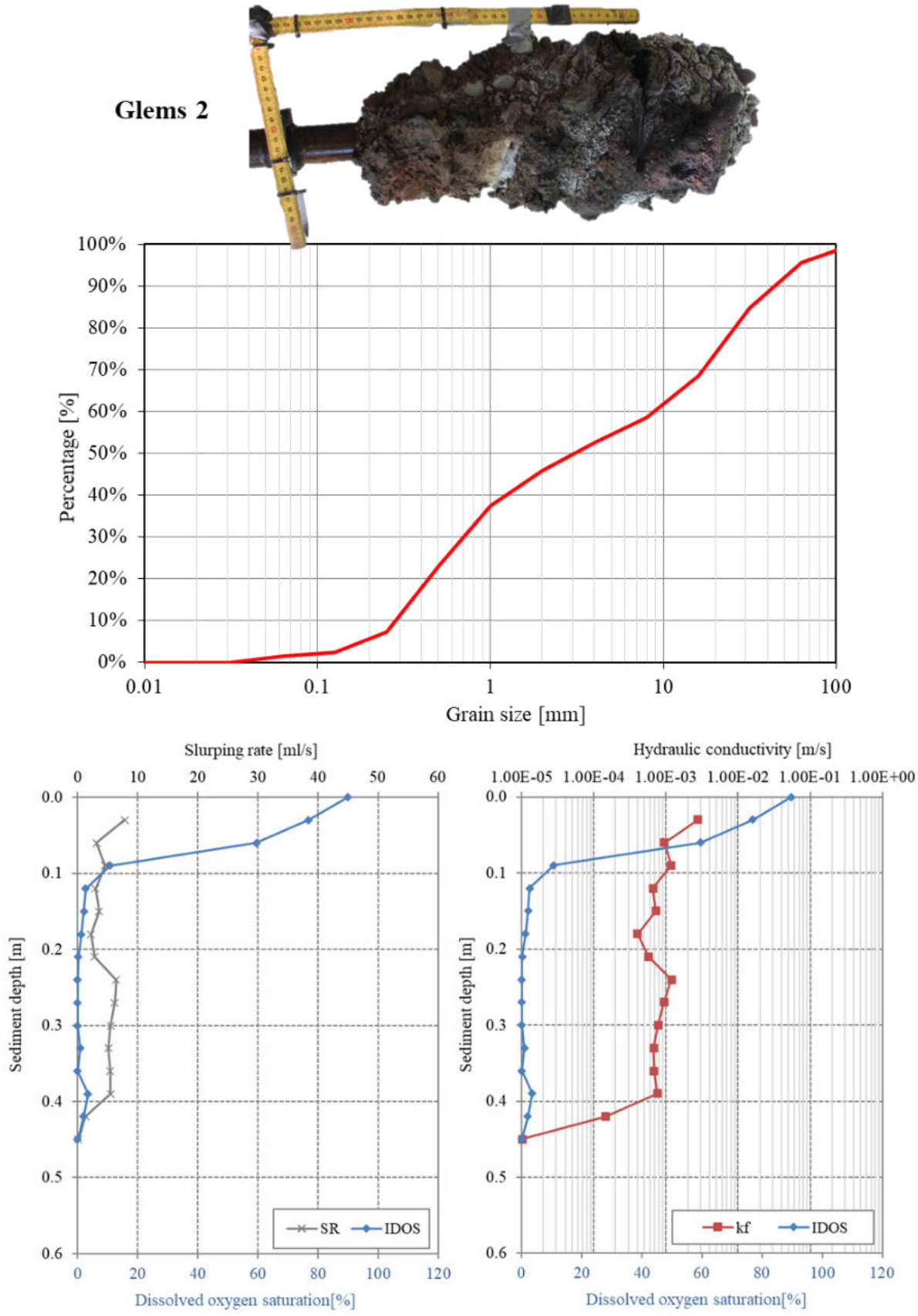

Appendix 2. 18: Results from Glems 3 including image of sediment sample, cumulative sieve curve and vertical profiles from slurping rate, IDOS and kf.

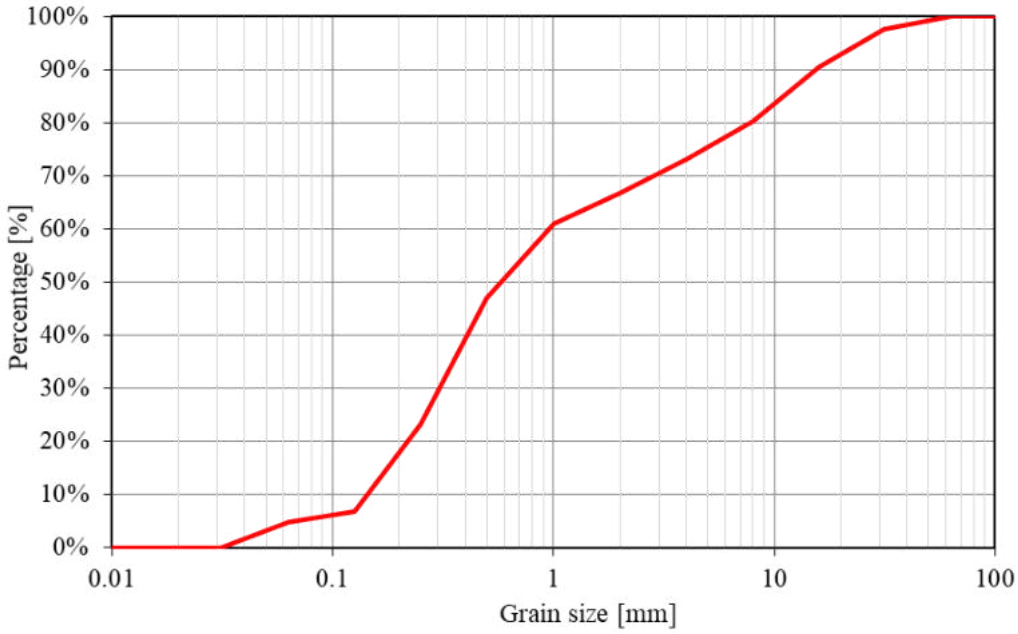

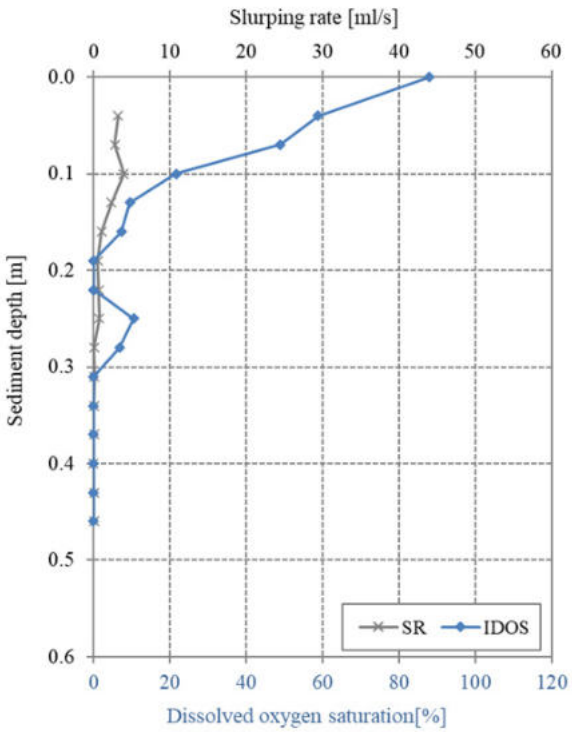

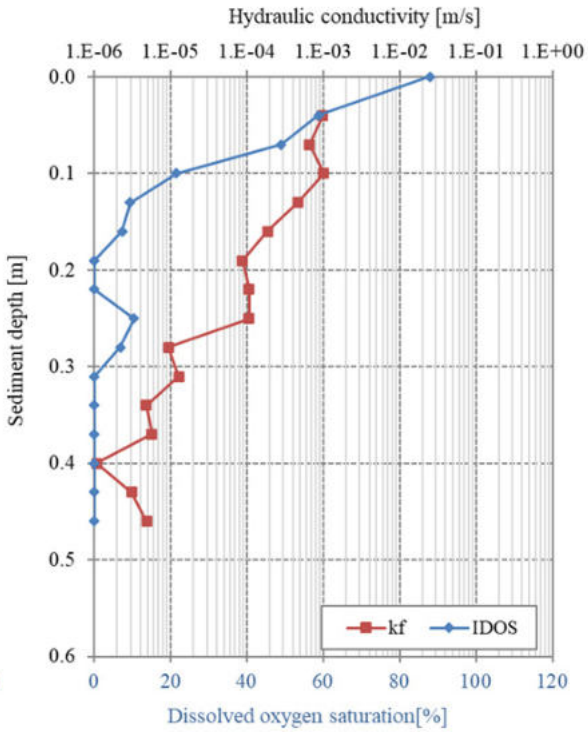

Appendix 2. 19: Results from Glems 4 including image of sediment sample, cumulative sieve curve and vertical profiles from slurping rate, IDOS and kf.

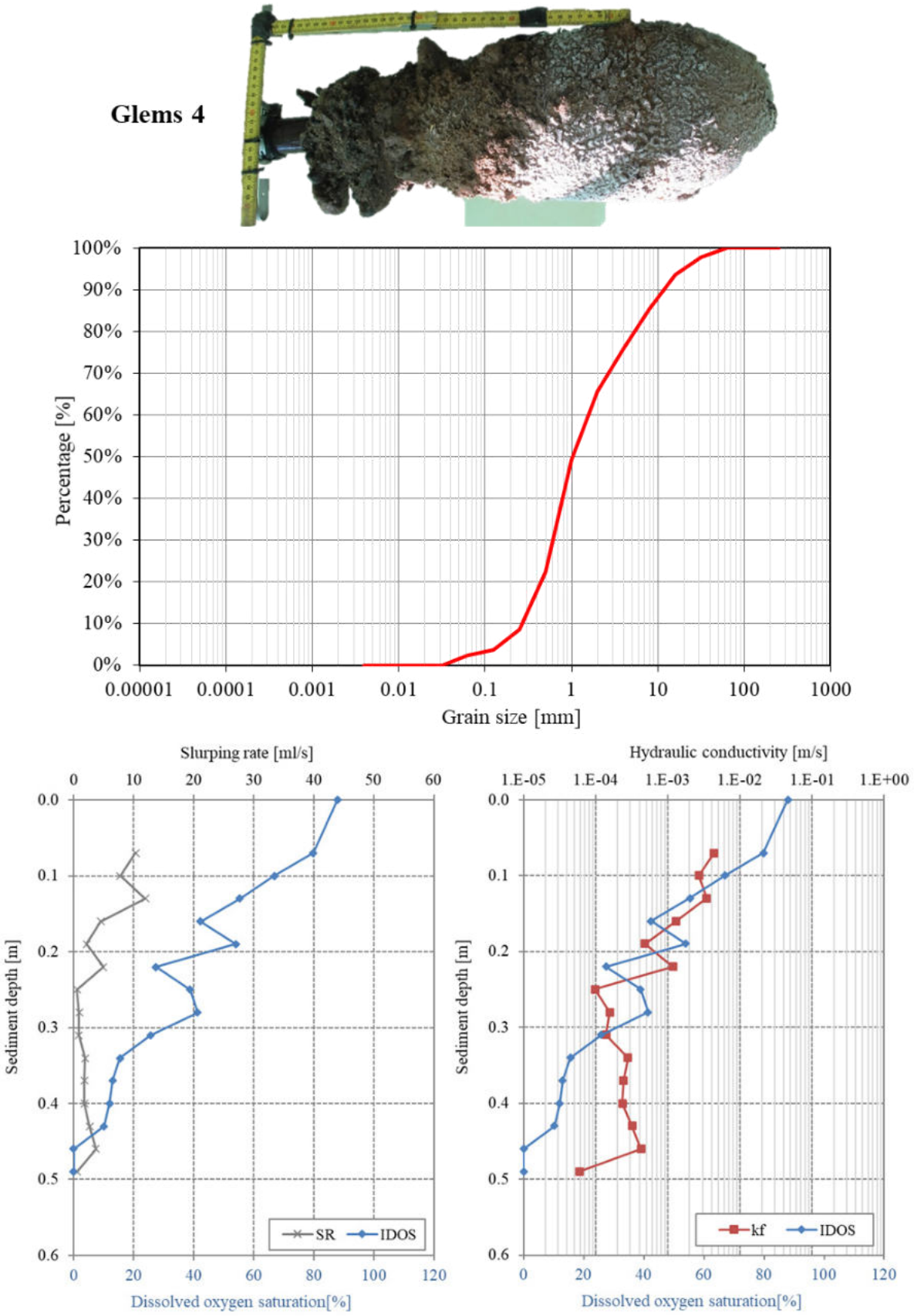

Appendix 2. 20: Results from Glems 5 including image of sediment sample, cumulative sieve curve and vertical profiles from slurping rate, IDOS and kf.

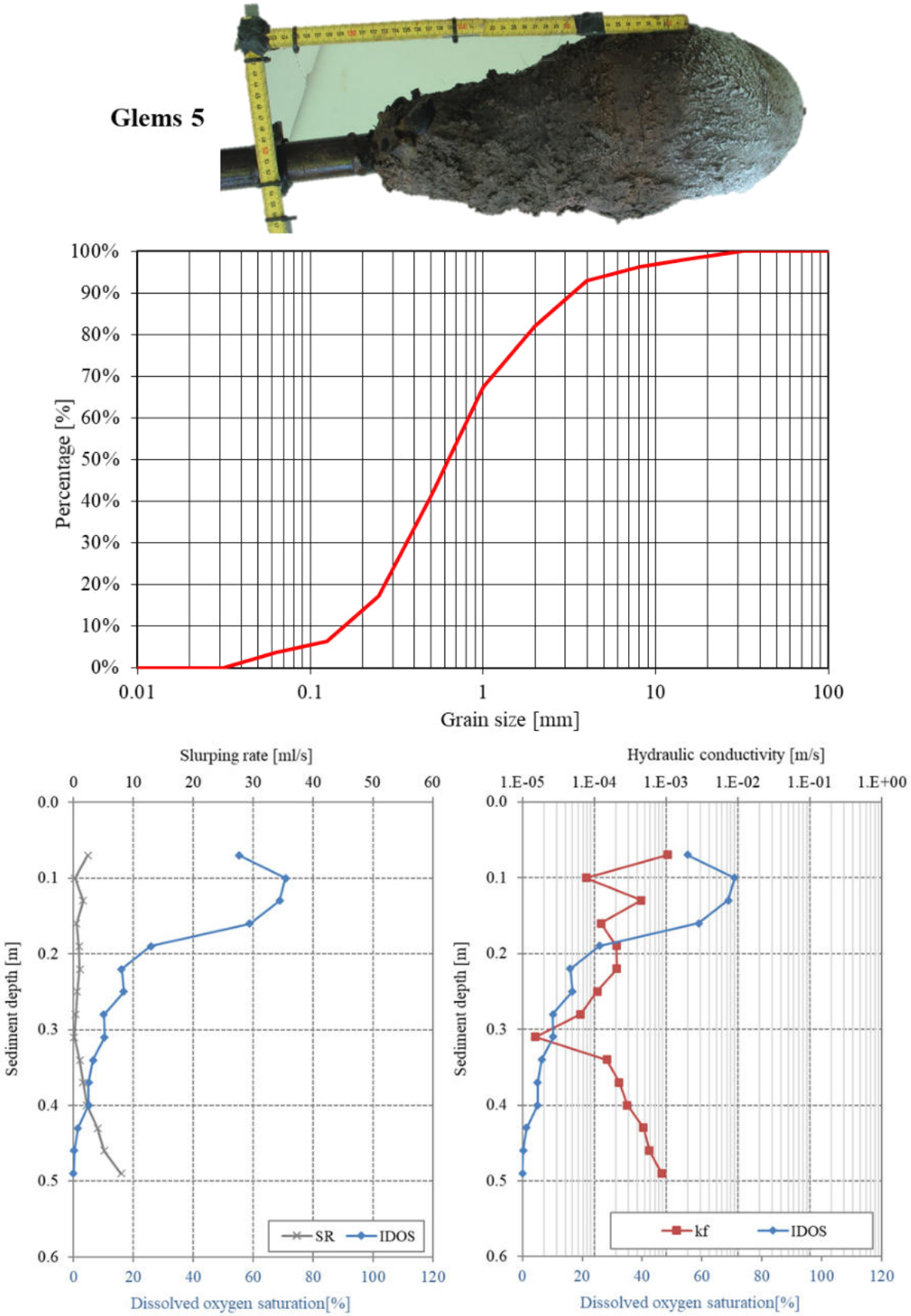

Appendix 2. 21: Results from Glems 6 including image of sediment sample, cumulative sieve curve and vertical profiles from slurping rate, IDOS and kf.

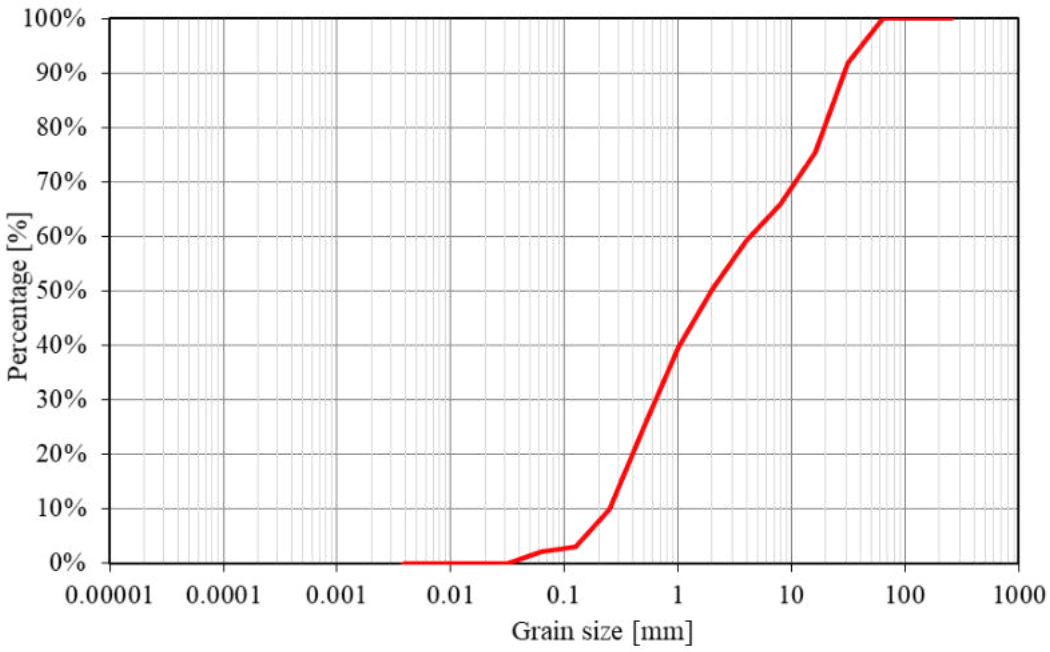

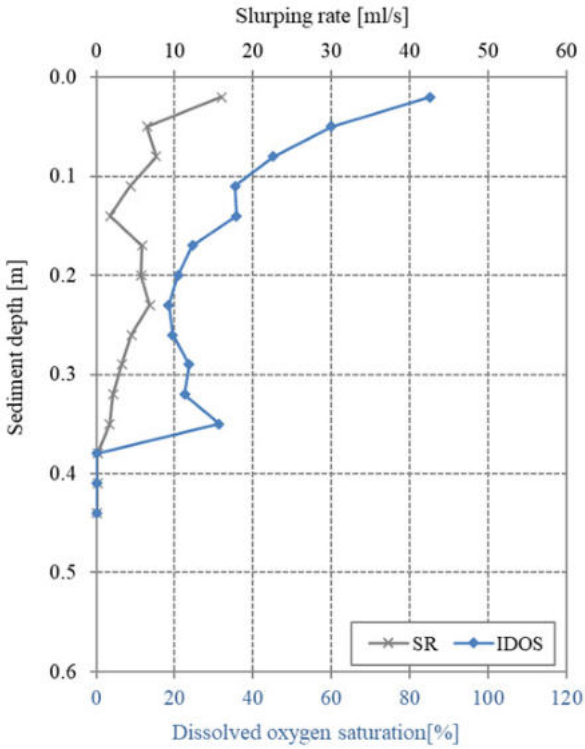

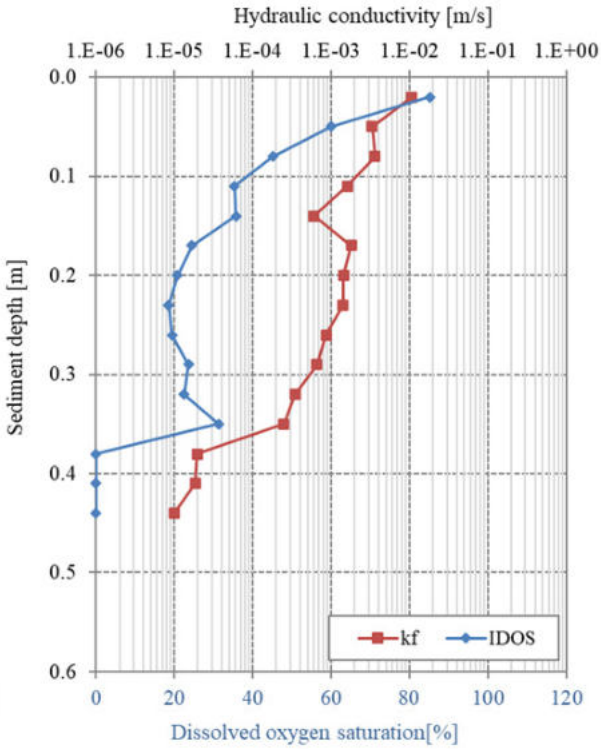

Appendix 2. 22: Results from Lein 1 including image of sediment sample, cumulative sieve curve and vertical profiles from slurping rate, IDOS and kf.

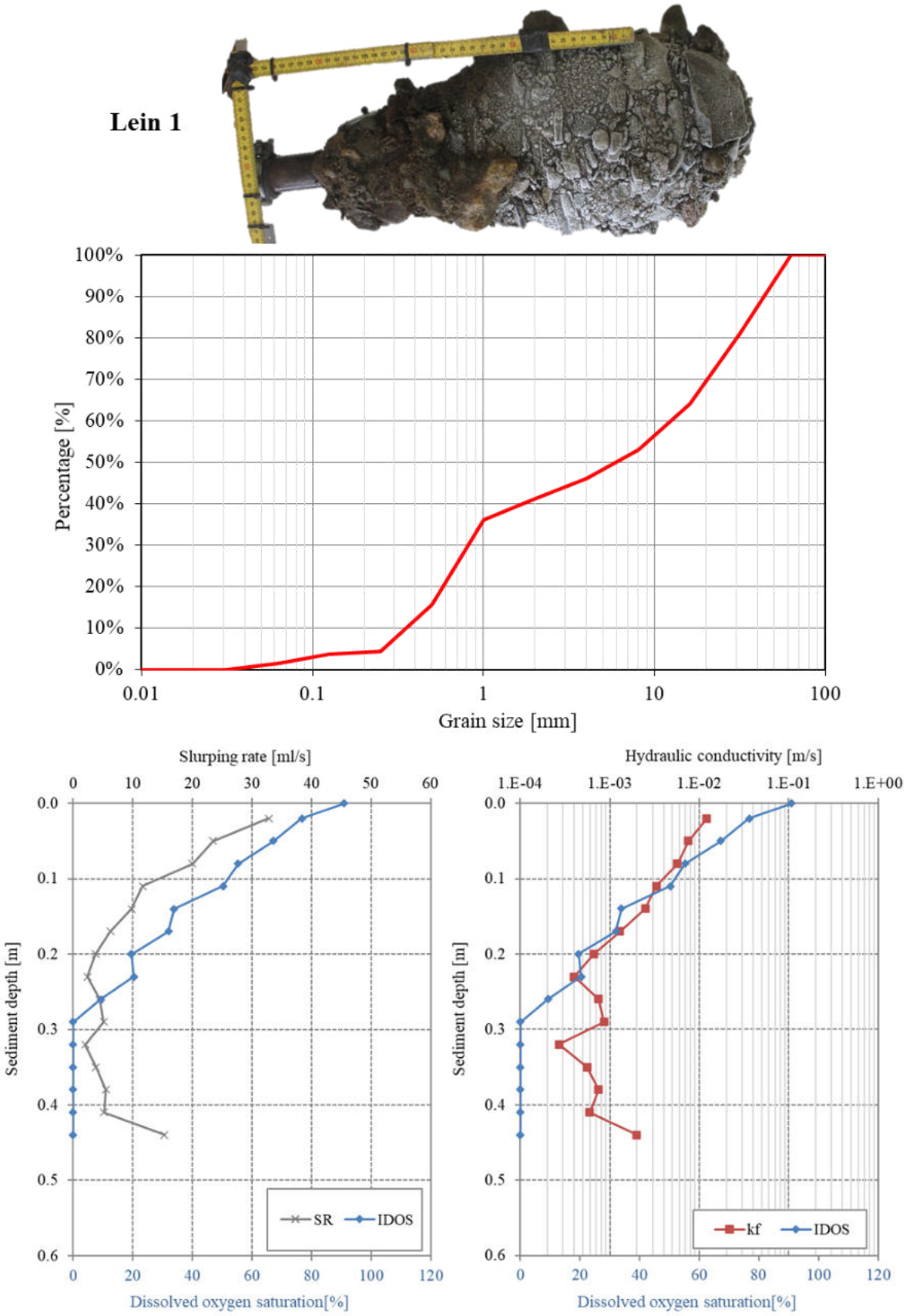

Appendix 2. 23: Results from Lein 2 including image of sediment sample, cumulative sieve curve and vertical profiles from slurping rate, IDOS and kf.

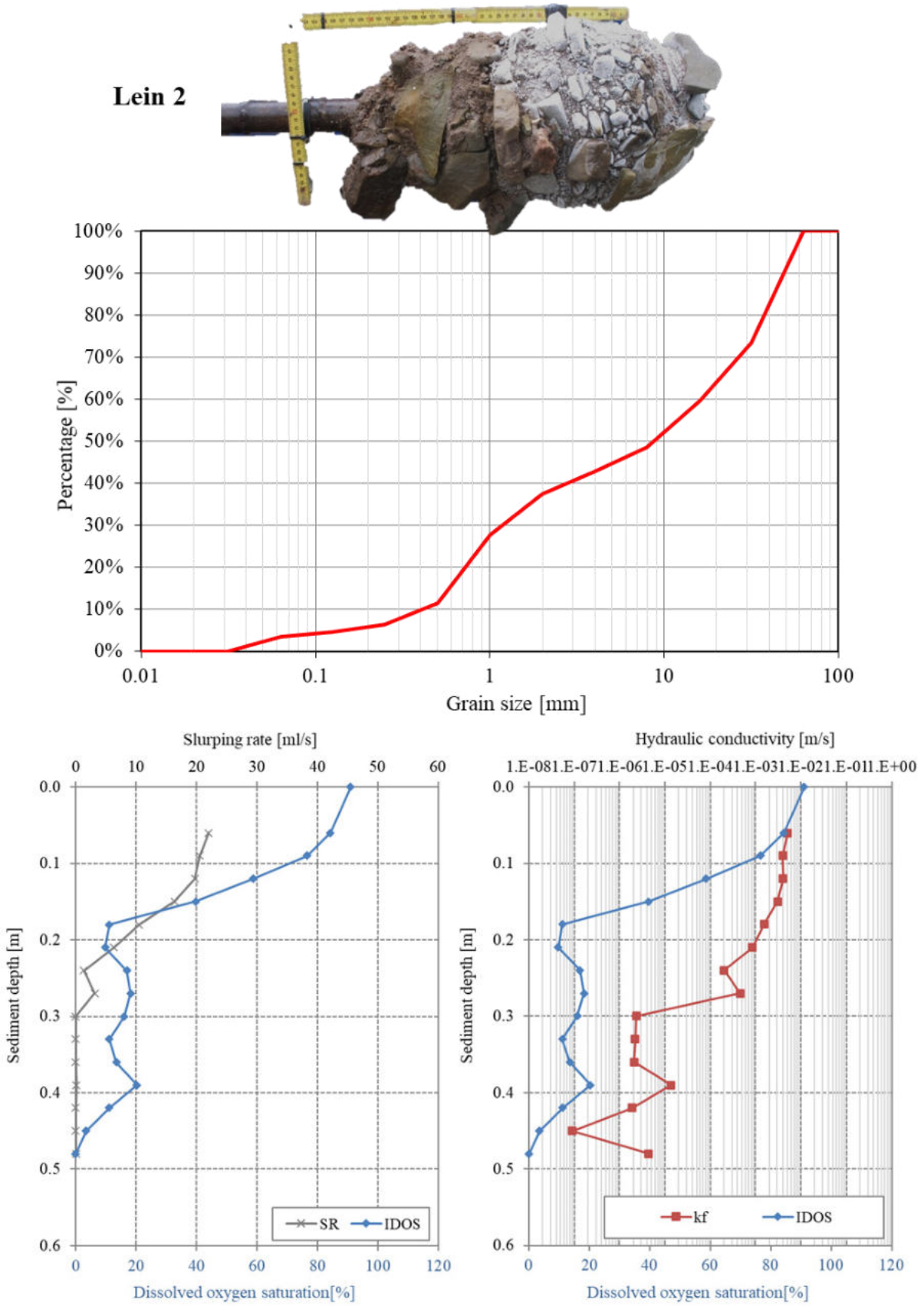

Appendix 2. 24: Results from Lein 3 including image of sediment sample, cumulative sieve curve and vertical profiles from slurping rate, IDOS and kf.

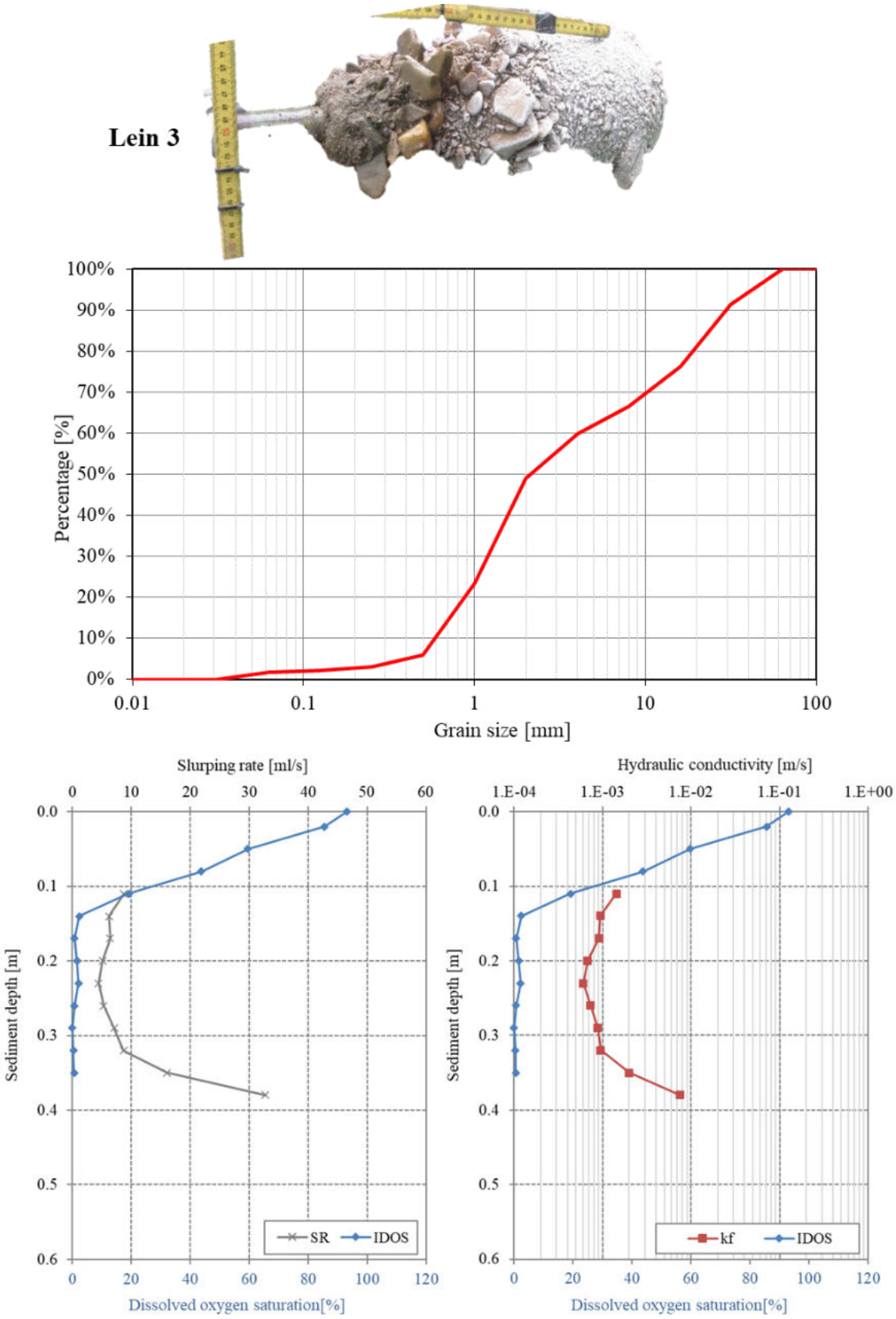

Appendix 2. 25: Results from Lein 4 including image of sediment sample, cumulative sieve curve and vertical profiles from slurping rate, IDOS and kf.

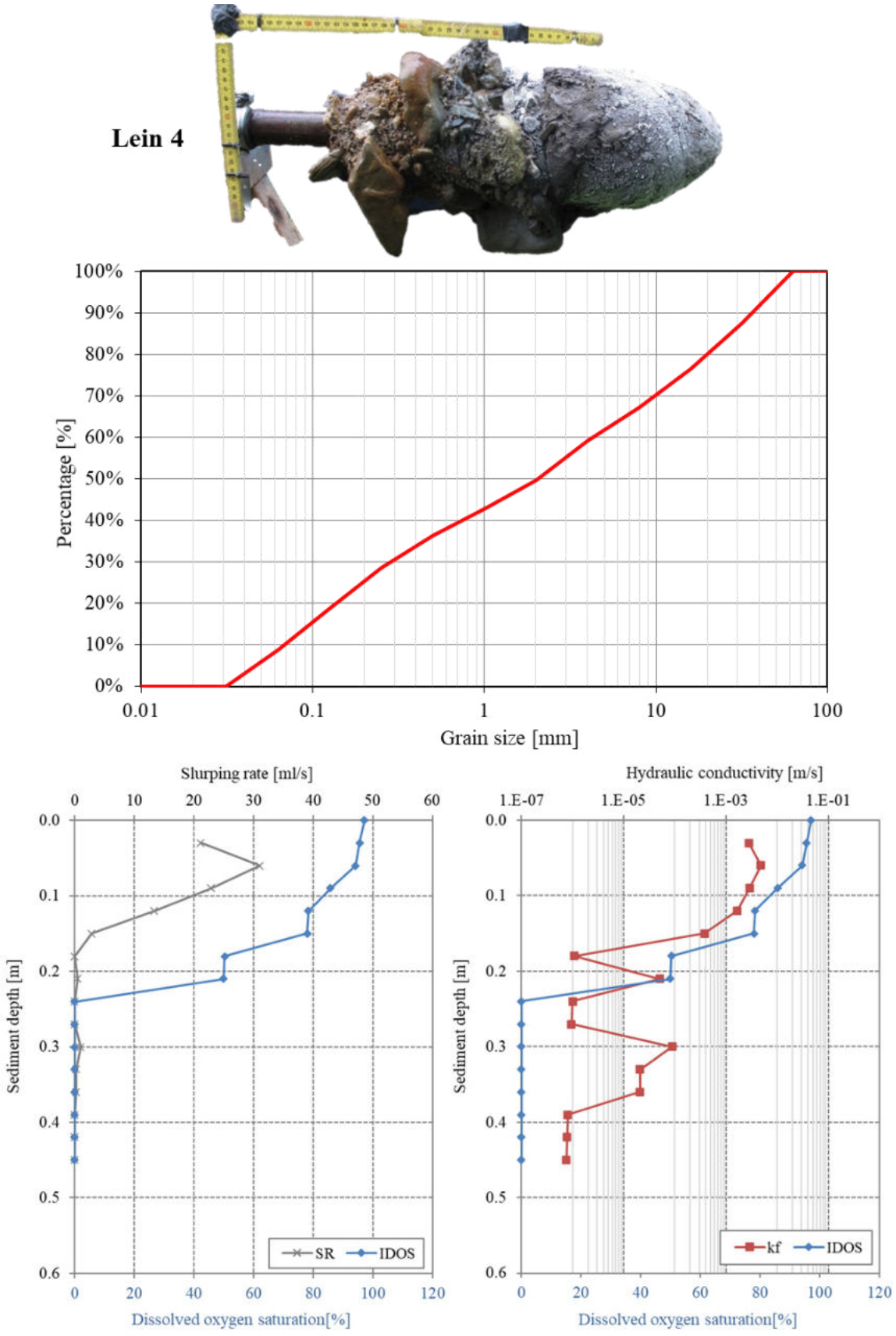

Appendix 2. 26. Results from Eyach 1 including image of sediment sample, cumulative sieve curve and vertical profiles from slurping rate, IDOS and kf.

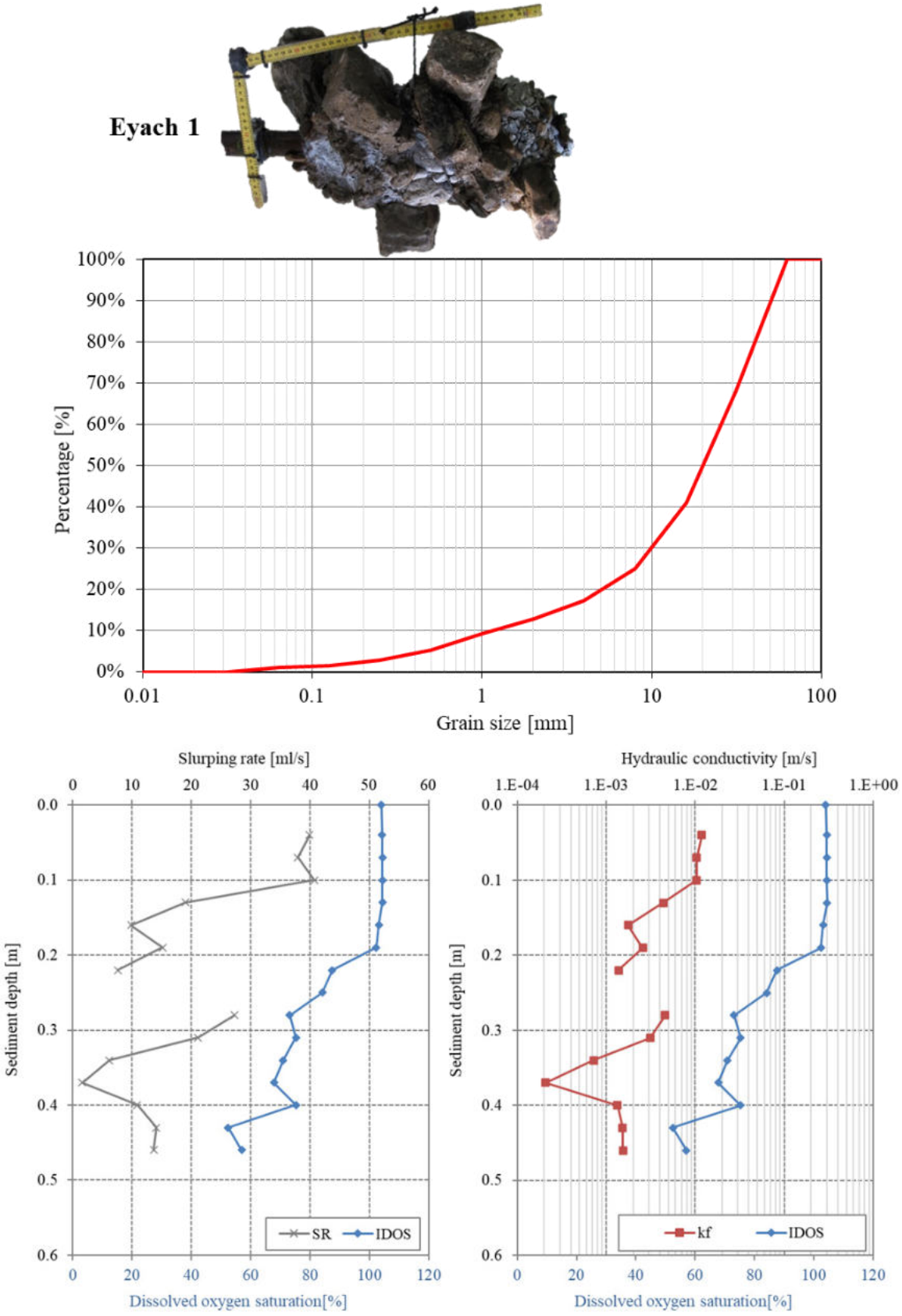

Appendix 2. 27: Results from Eyach 2 including image of sediment sample, cumulative sieve curve and vertical profiles from slurping rate, IDOS and kf.

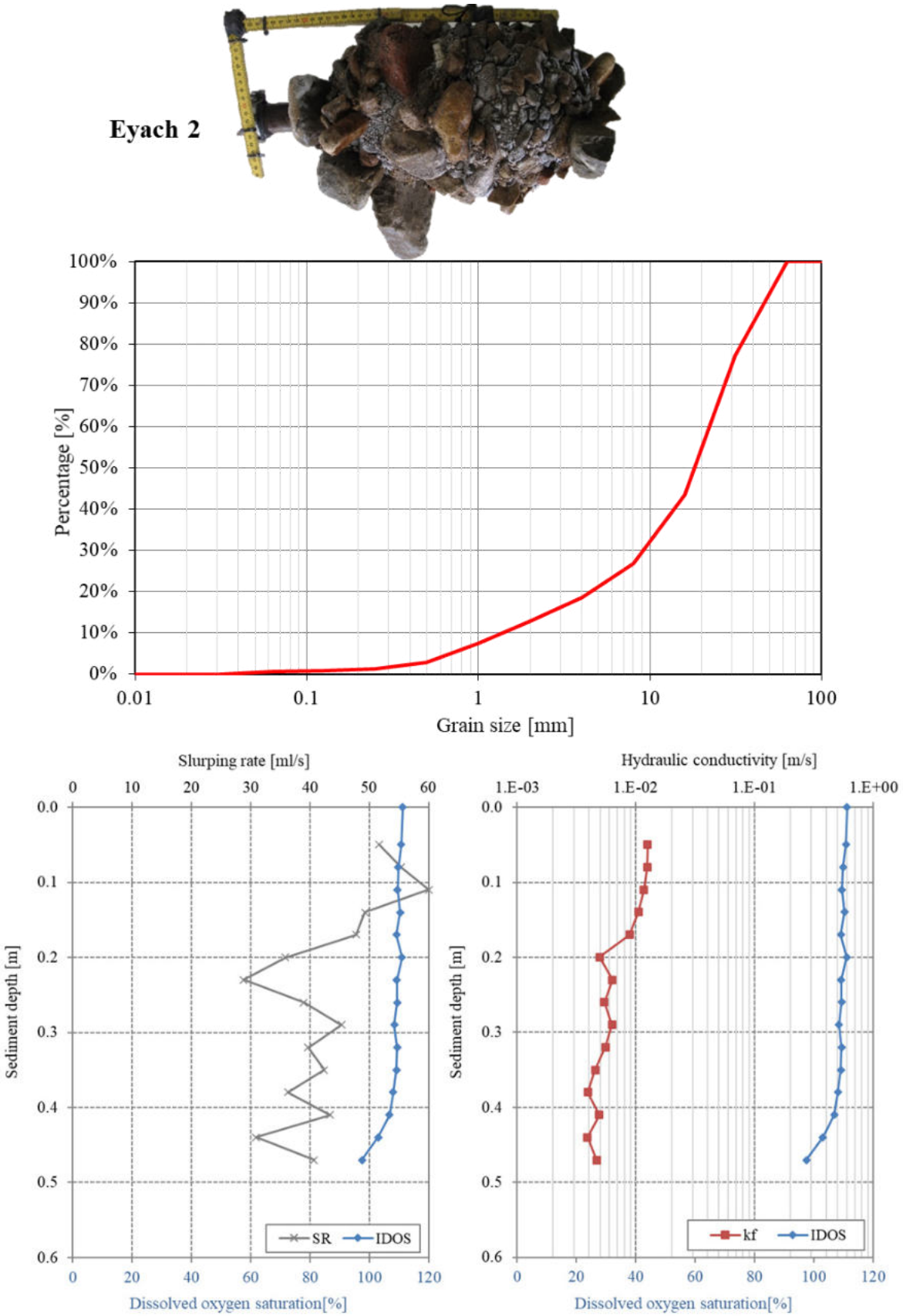

Appendix 2. 28: Results from Eyach 3 including image of sediment sample, cumulative sieve curve and vertical profiles from slurping rate, IDOS and kf.

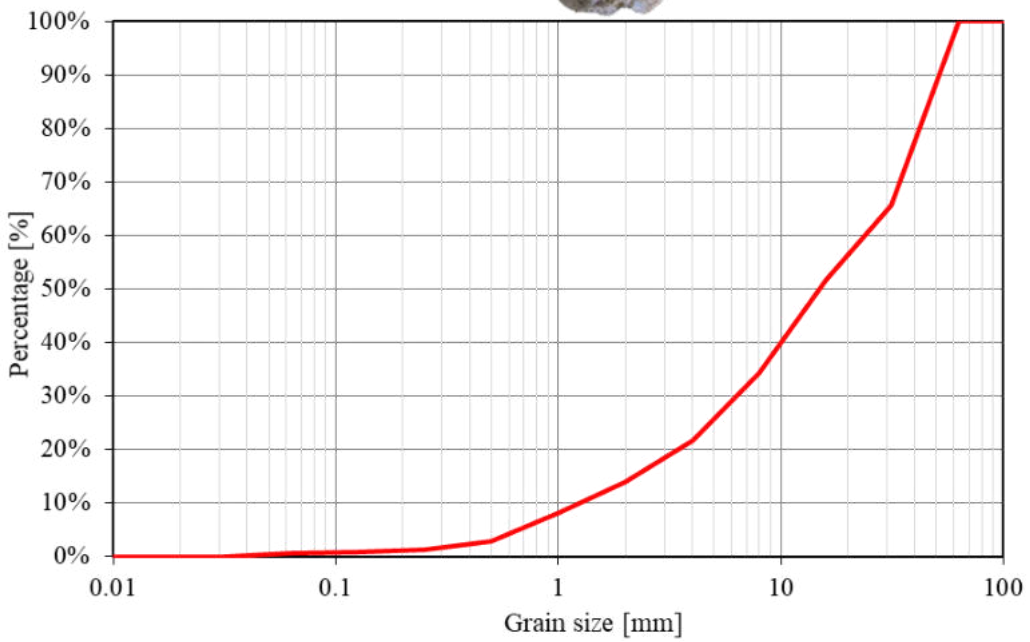

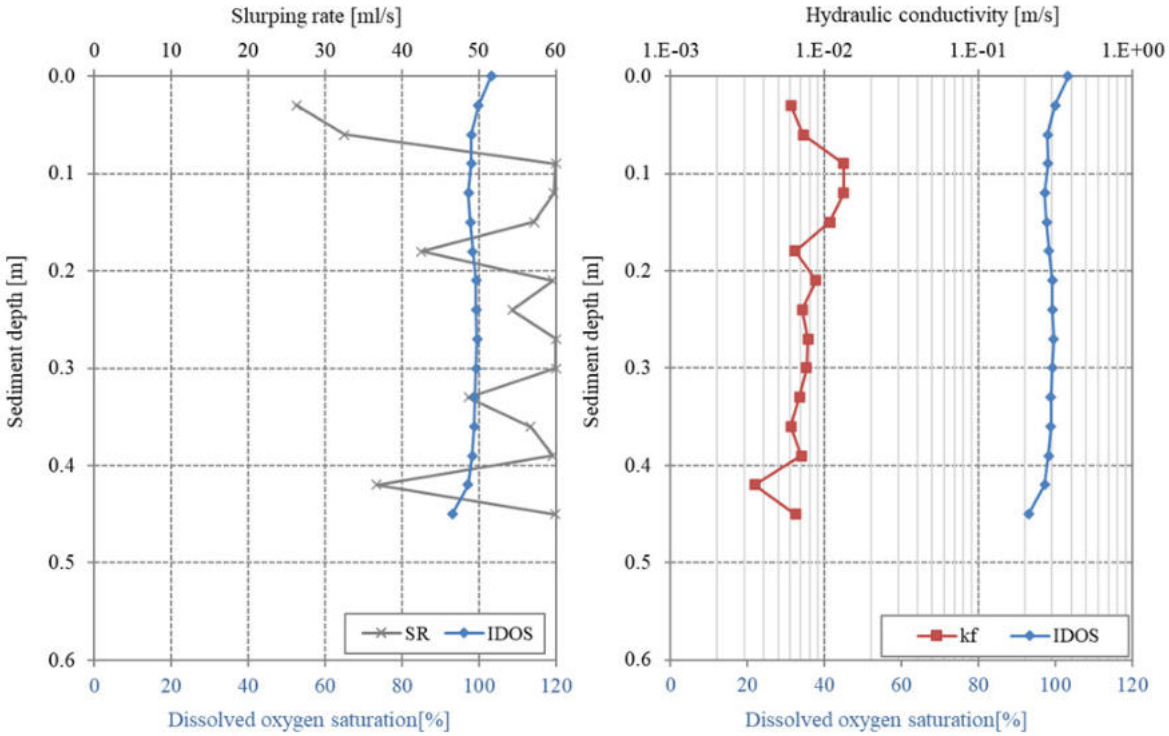

Appendix 2. 29: Results from Eyach 4 including image of sediment sample, cumulative sieve curve and vertical profiles from slurping rate, IDOS and kf.

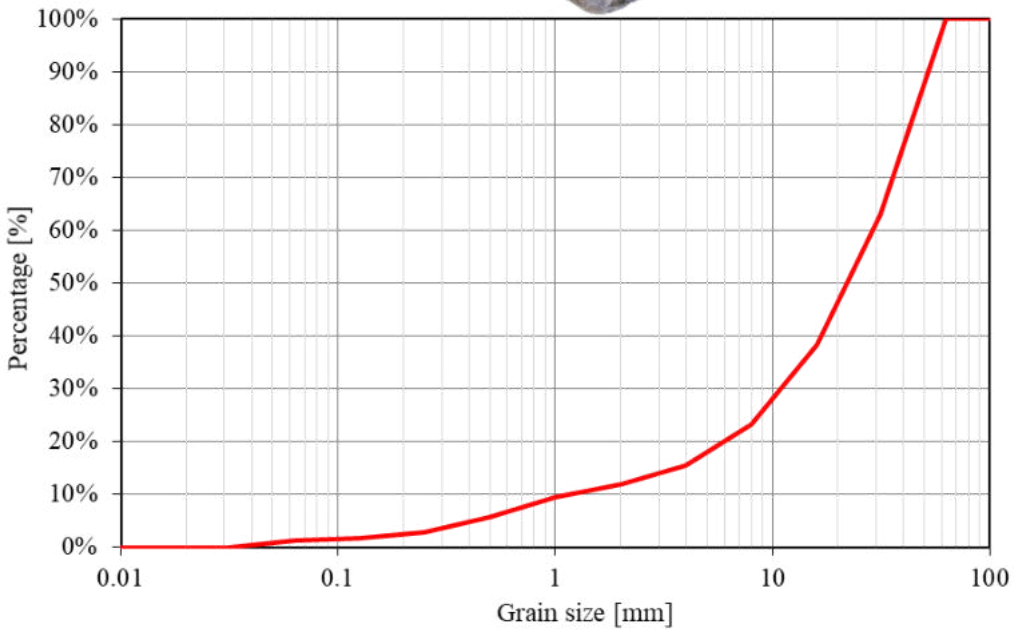

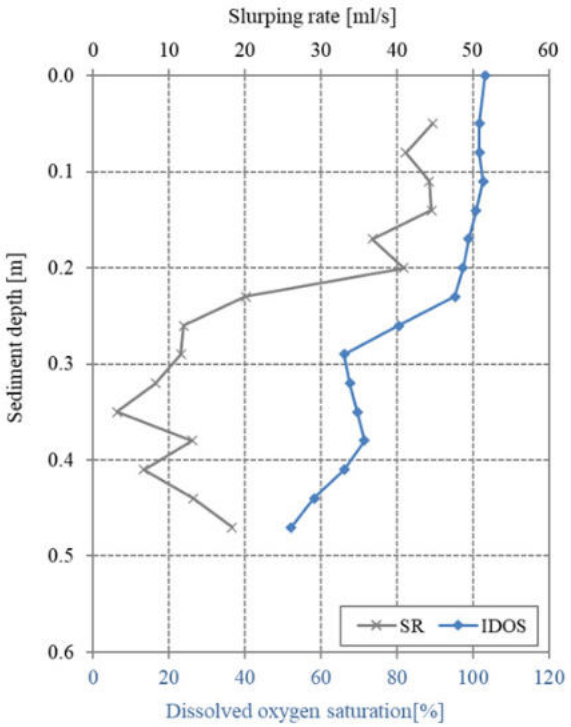

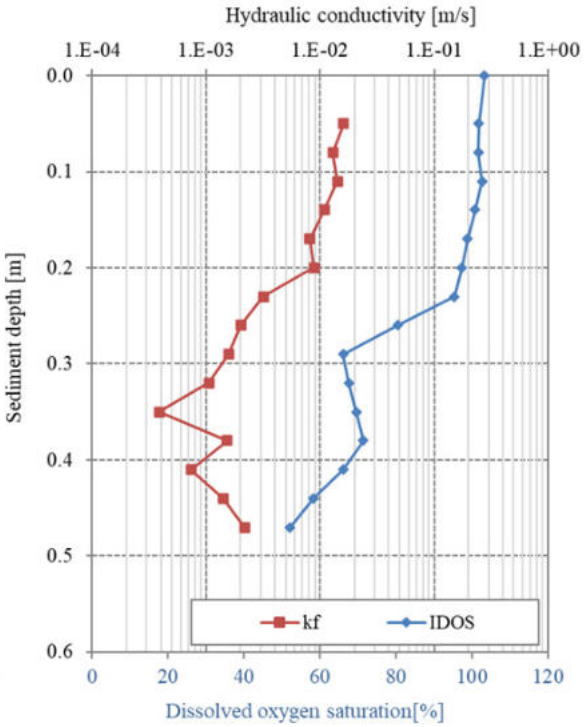

Appendix 2. 30: Results from Glatt 1 including image of sediment sample, cumulative sieve curve and vertical profiles from slurping rate, IDOS and kf.

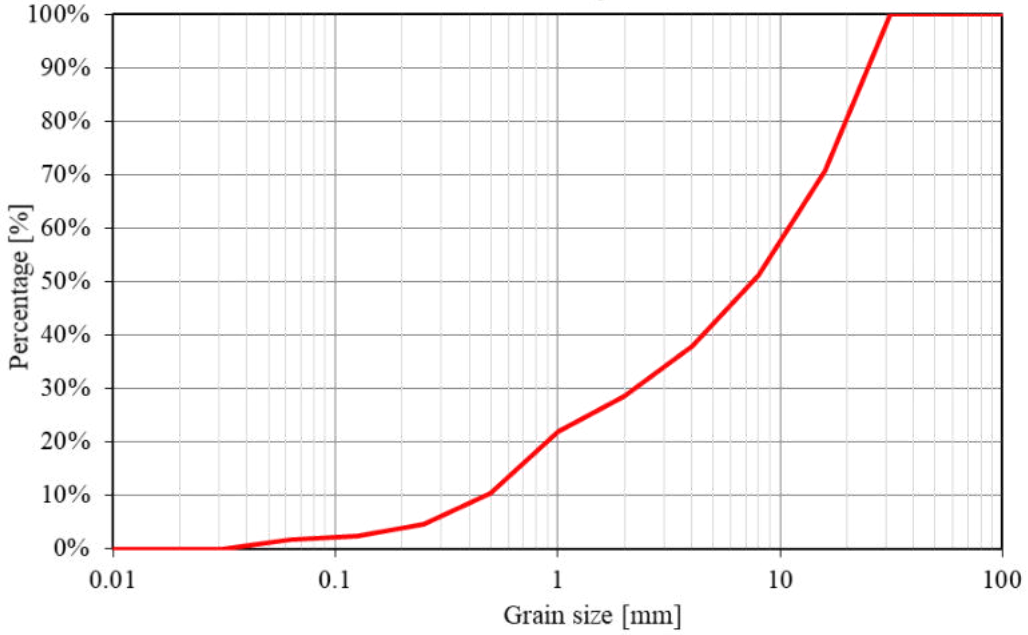

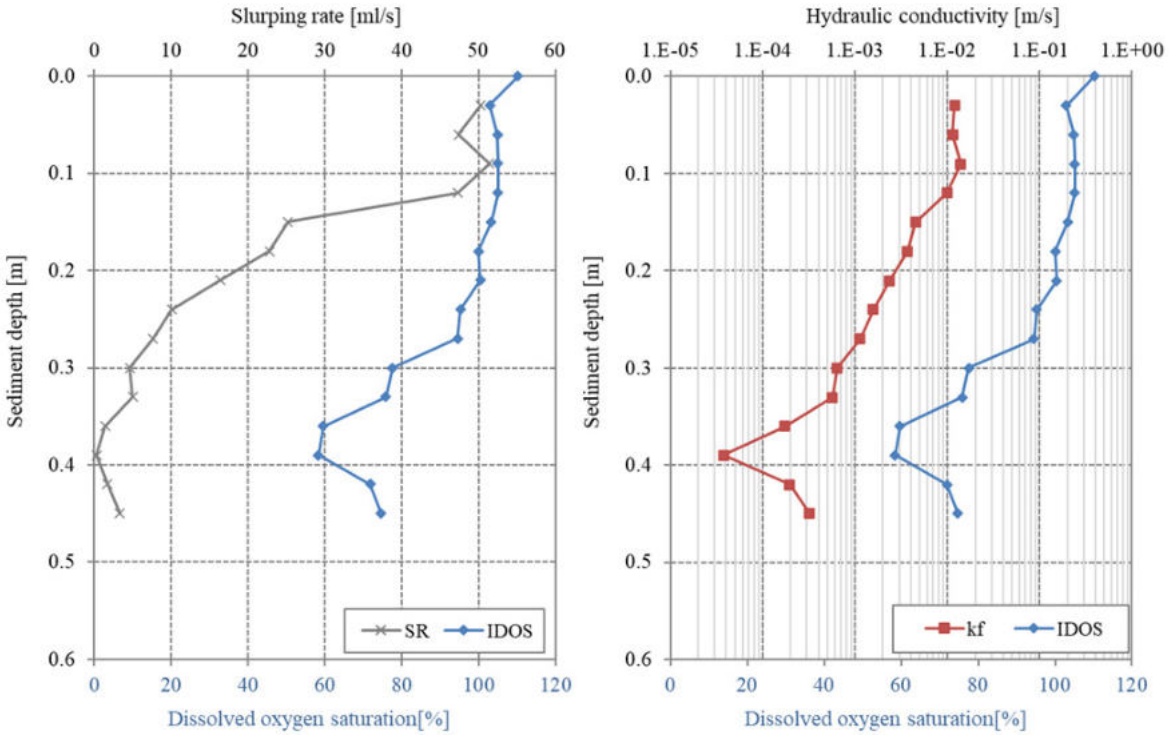

Appendix 2. 31: Results from Glatt 2 including image of sediment sample, cumulative sieve curve and vertical profiles from slurping rate, IDOS and kf.

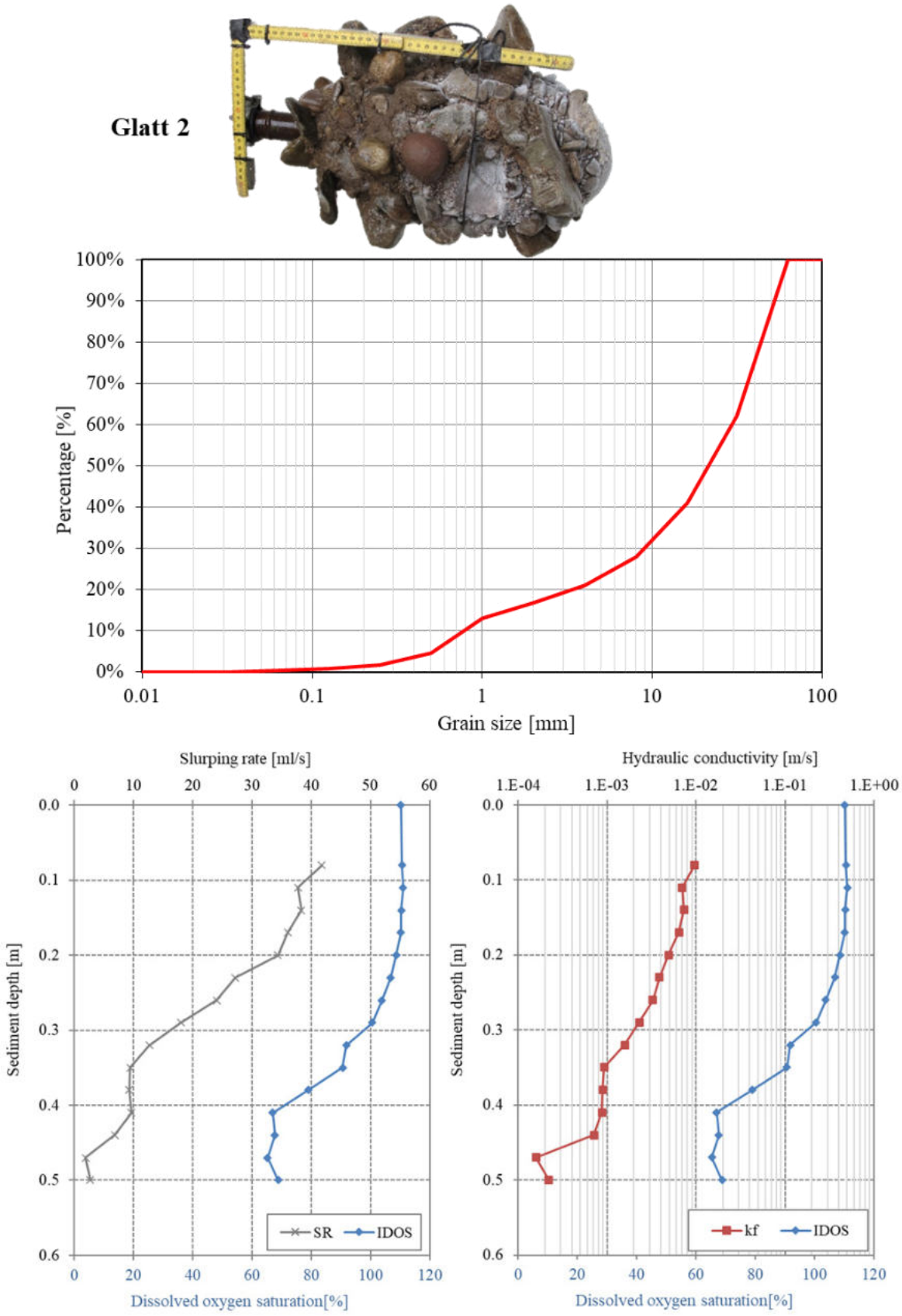

Appendix 2. 32: Results from Glatt 3 including image of sediment sample, cumulative sieve curve and vertical profiles from slurping rate, IDOS and kf.

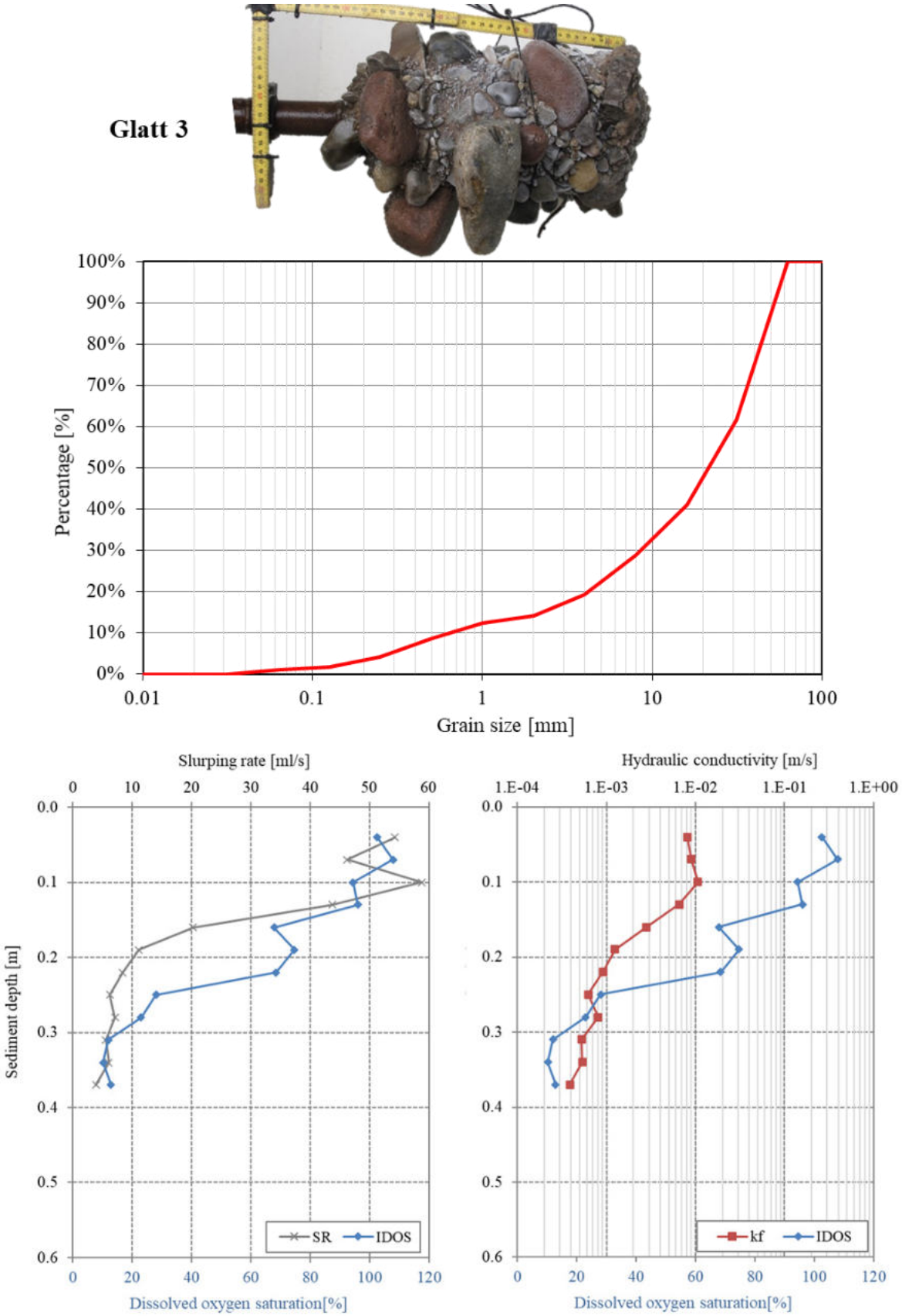

Appendix 2. 33: Results from Glatt 4 including image of sediment sample, cumulative sieve curve and vertical profiles from slurping rate, IDOS and kf.

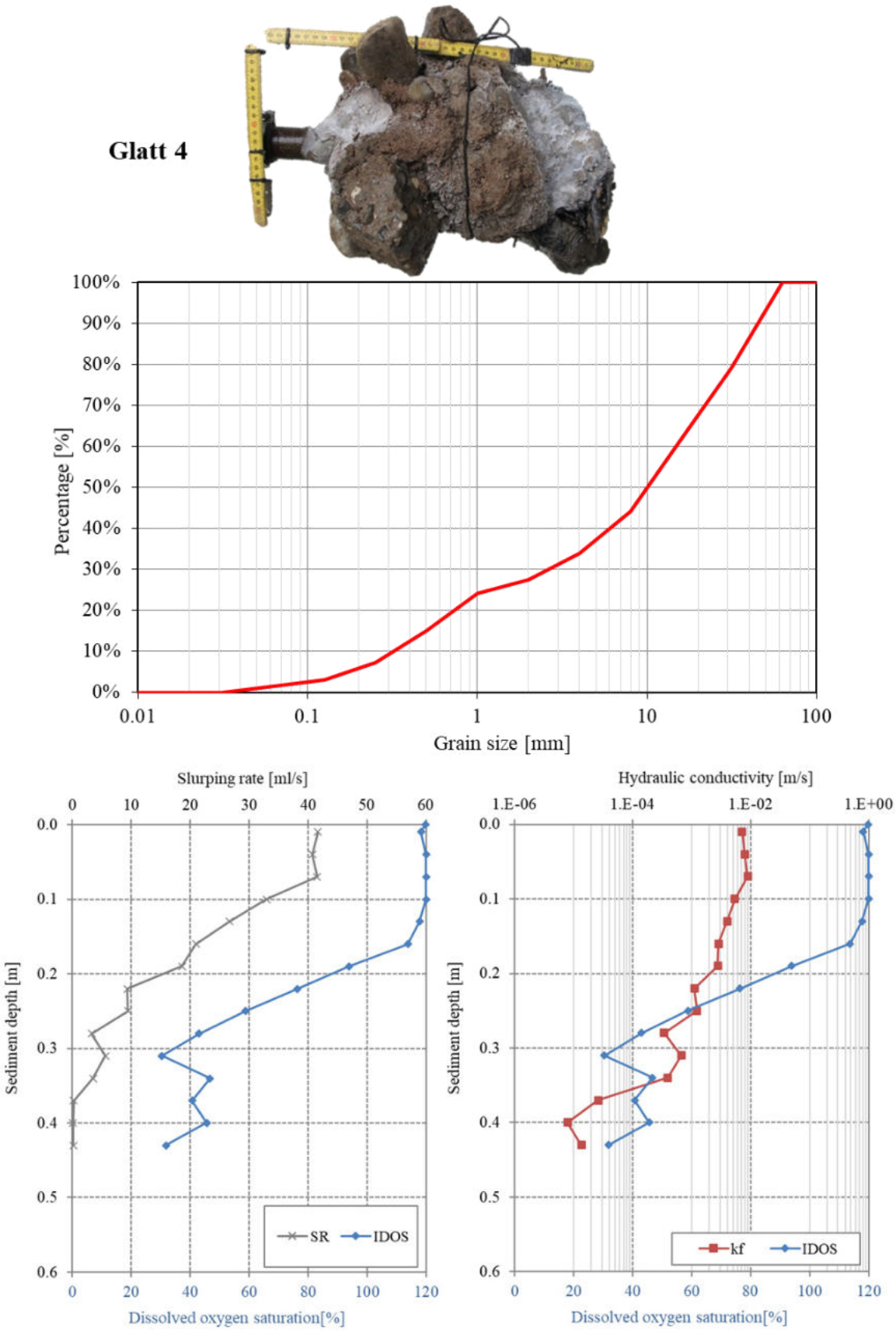

Appendix 2. 34: Results from Glatt 5 including image of sediment sample, cumulative sieve curve and vertical profiles from slurping rate, IDOS and kf.

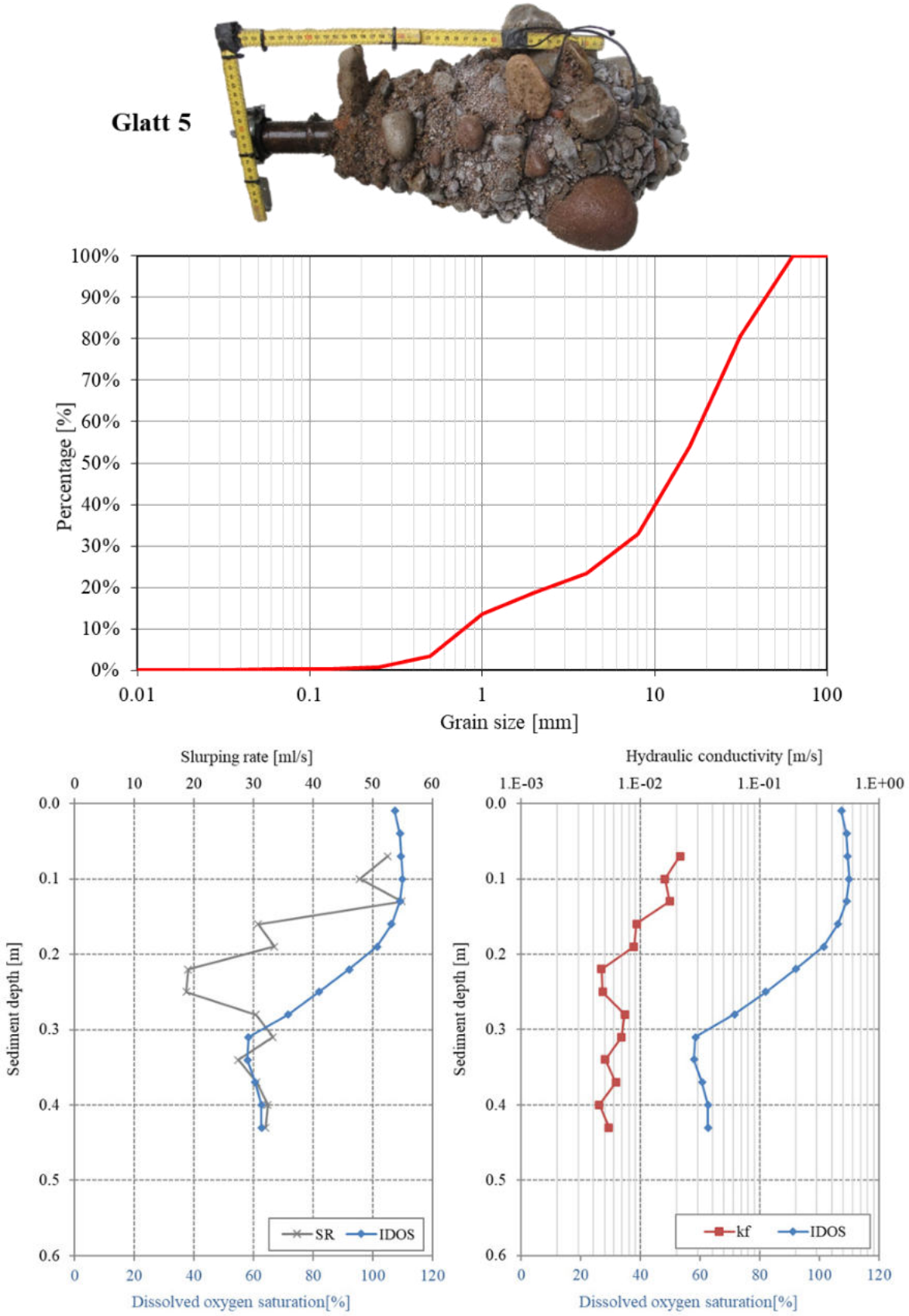

Appendix 2. 35: Results from Glatt 6 including image of sediment sample, cumulative sieve curve and vertical profiles from slurping rate, IDOS and kf.

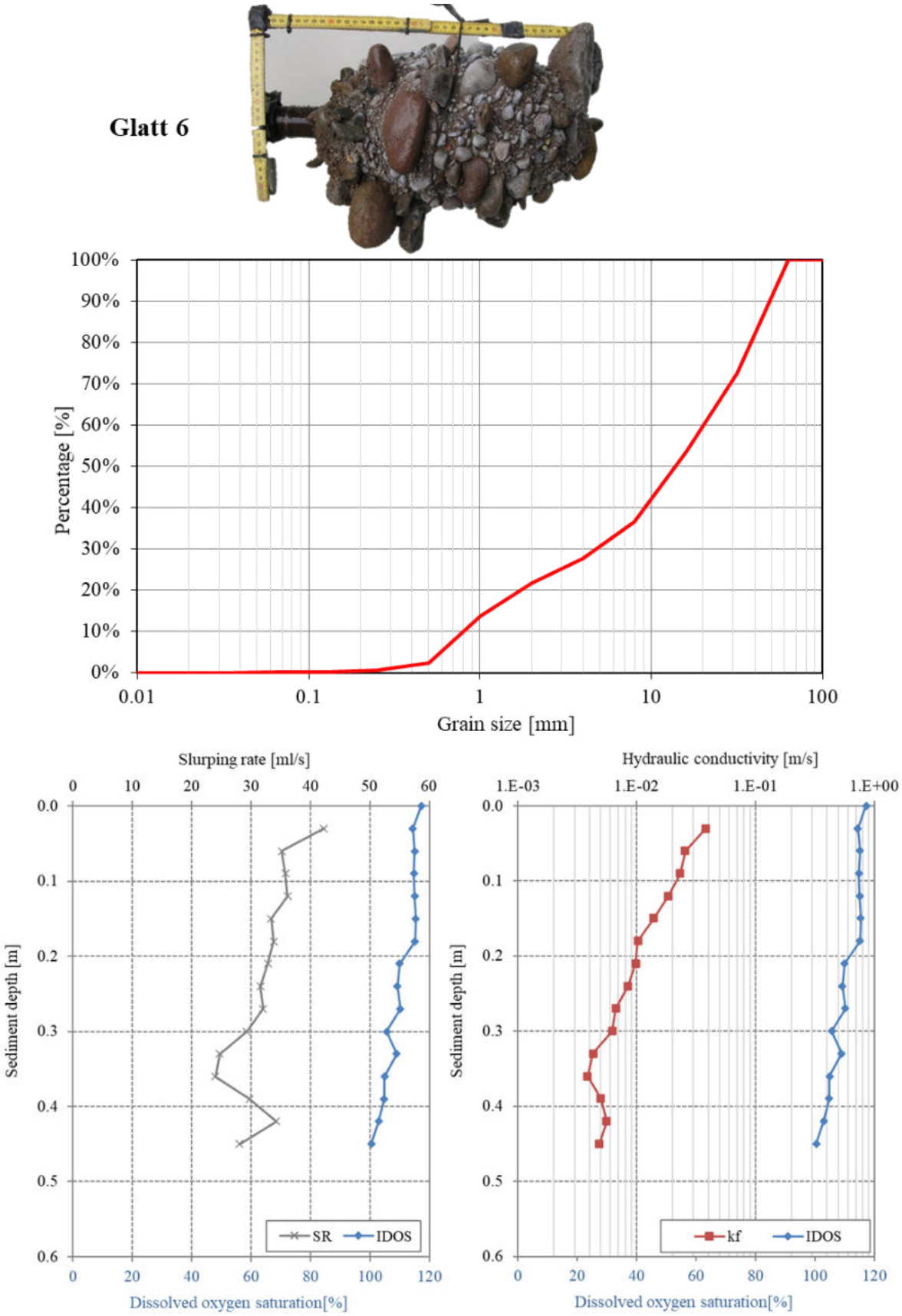

Appendix 2. 36: Results from Würm 1 including image of sediment sample, cumulative sieve curve and vertical profiles from slurping rate, IDOS and kf.

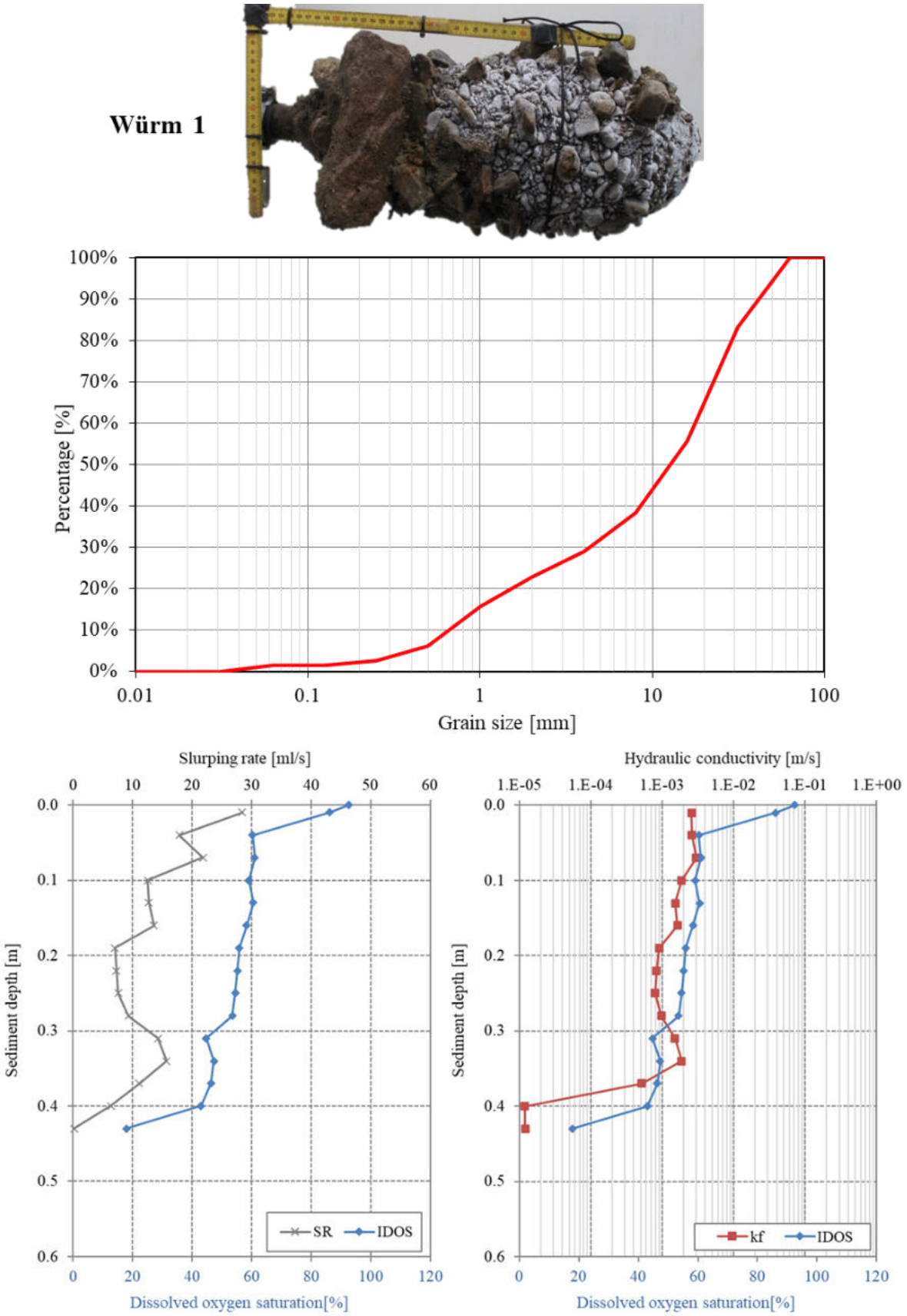

Appendix 2. 37: Results from Würm 2 including image of sediment sample, cumulative sieve curve and vertical profiles from slurping rate, IDOS and kf.

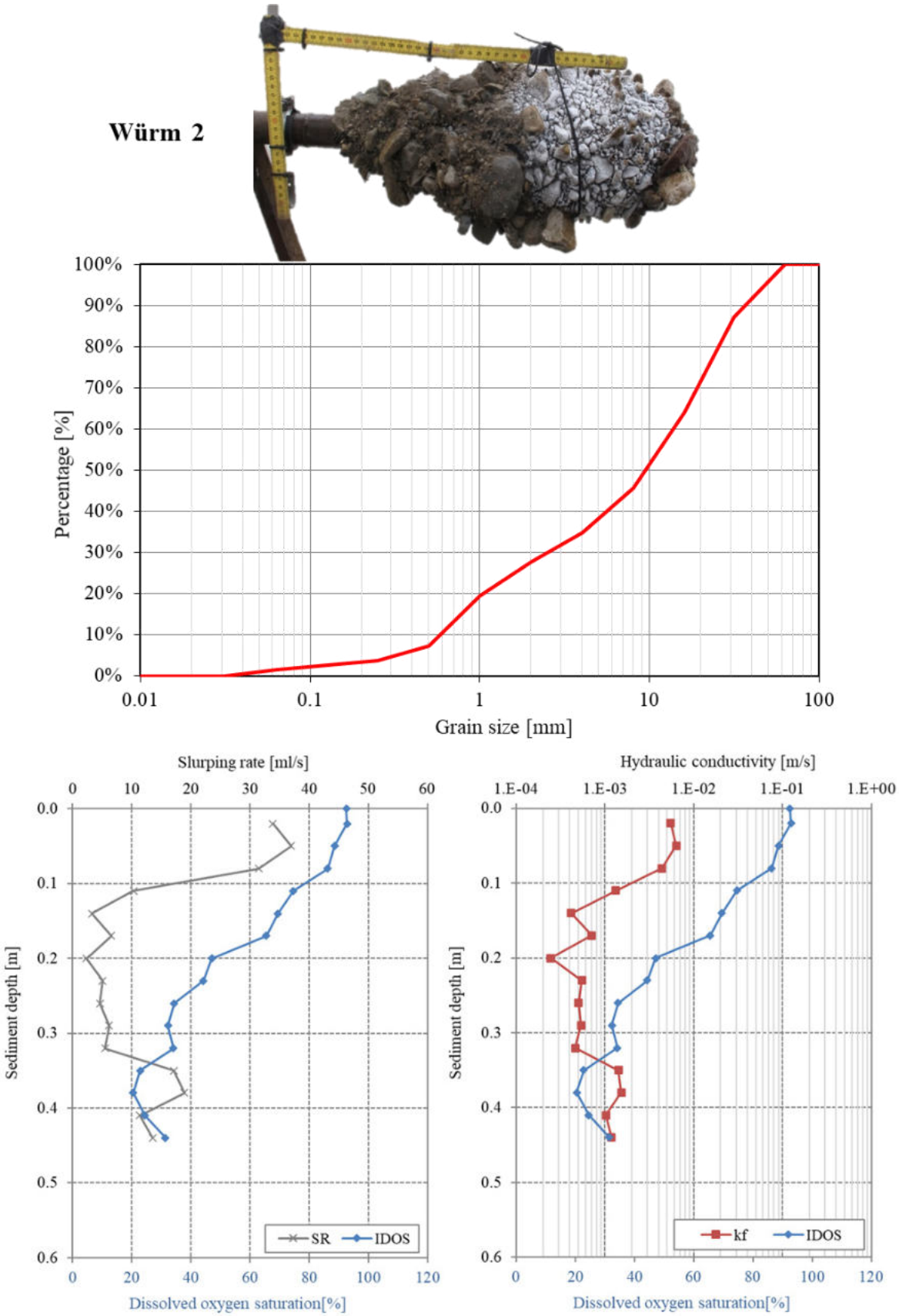

Appendix 2. 38: Results from Würm 3 including image of sediment sample, cumulative sieve curve and vertical profiles from slurping rate, IDOS and kf.

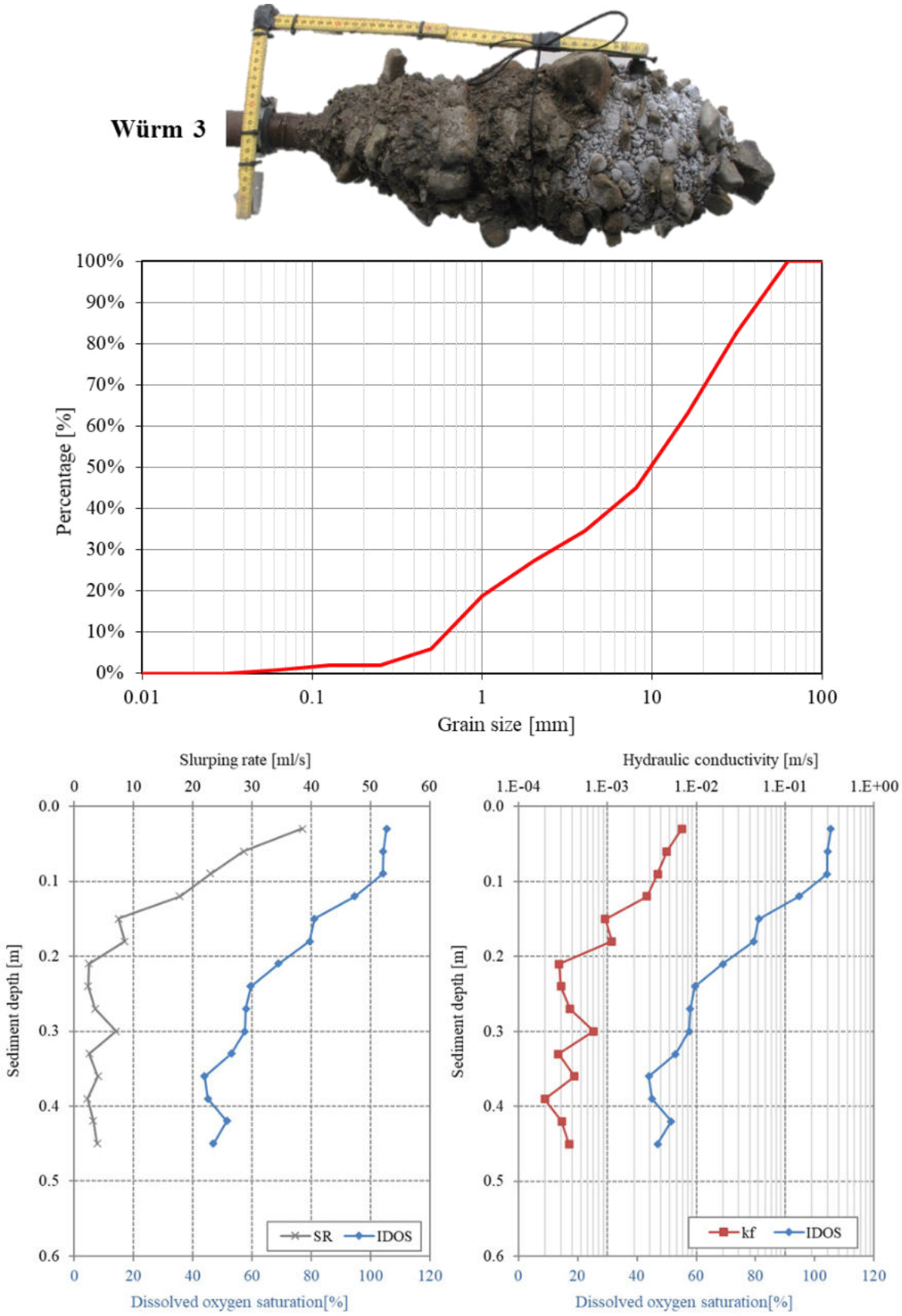

Appendix 2. 39: Results from Würm 4 including image of sediment sample, cumulative sieve curve and vertical profiles from slurping rate, IDOS and kf.

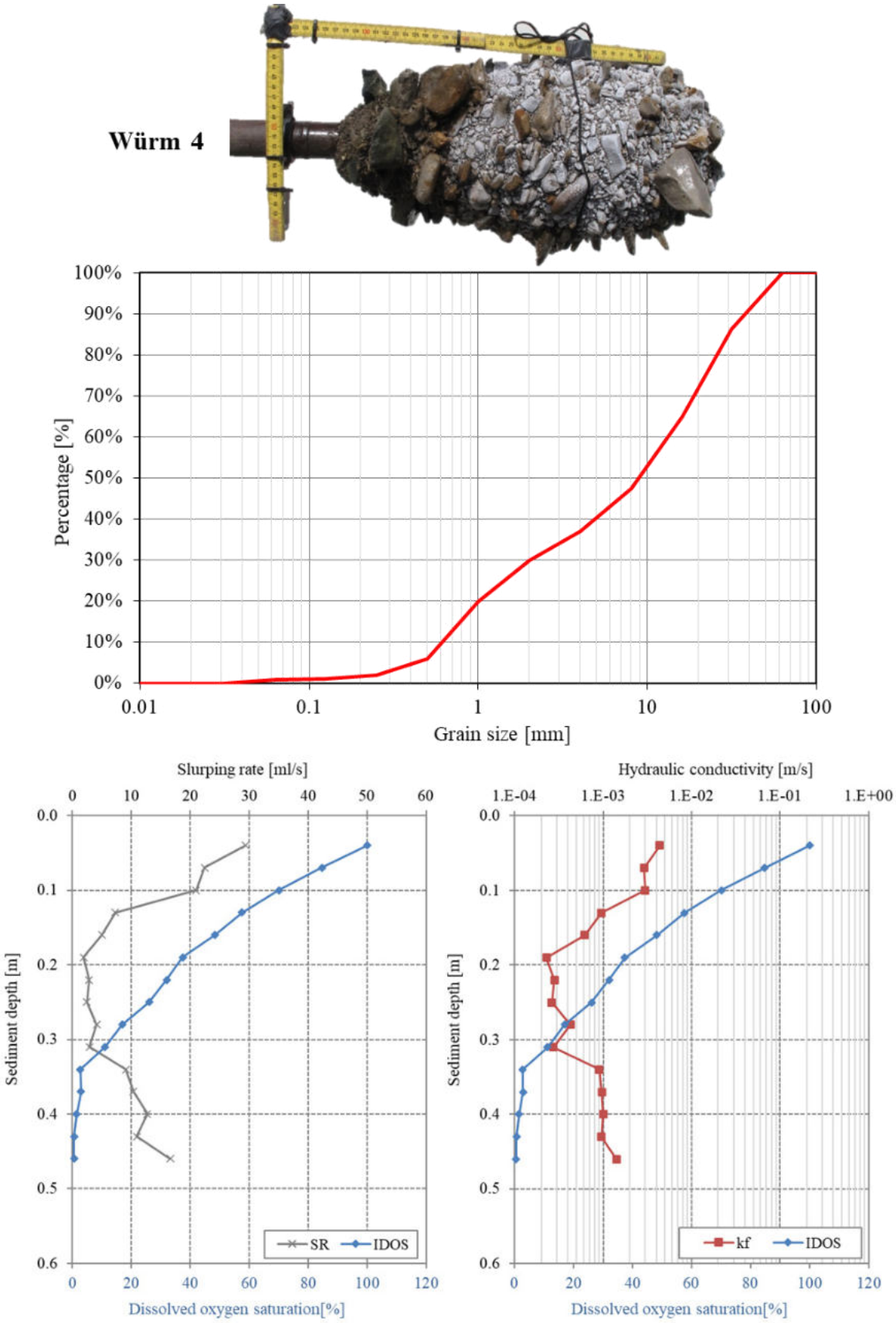

Appendix 2. 40: Results from Würm 5 including image of sediment sample, cumulative sieve curve and vertical profiles from slurping rate, IDOS and kf.

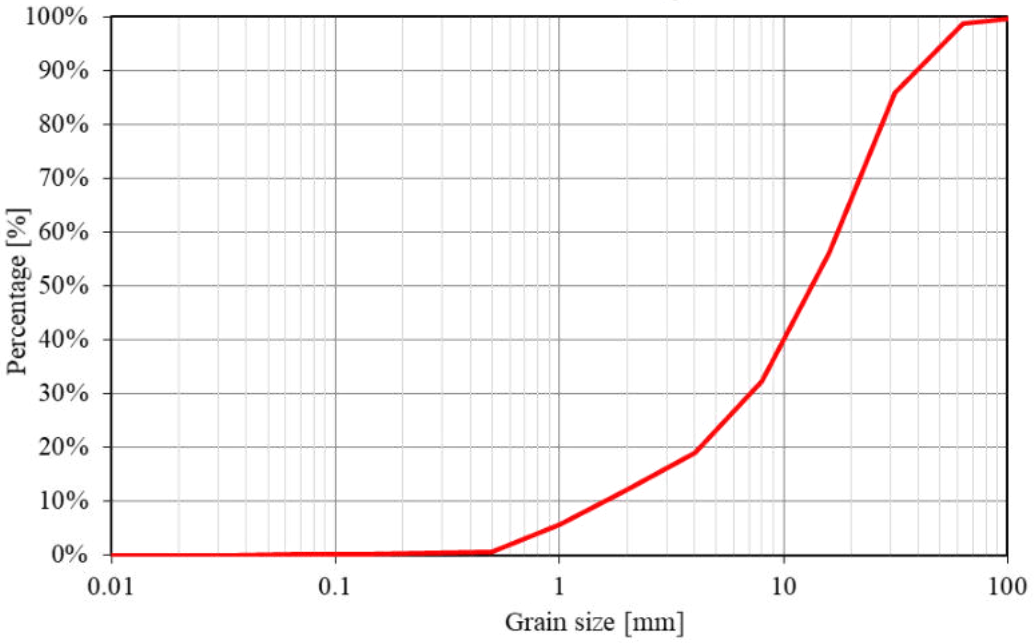

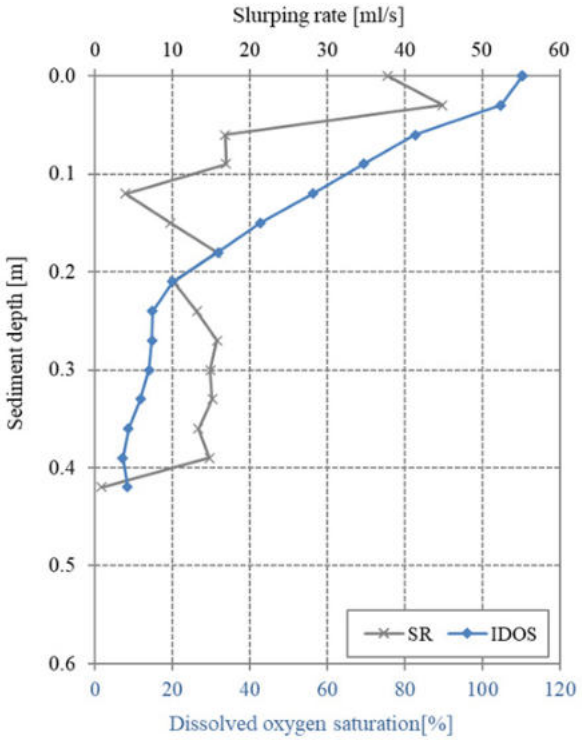

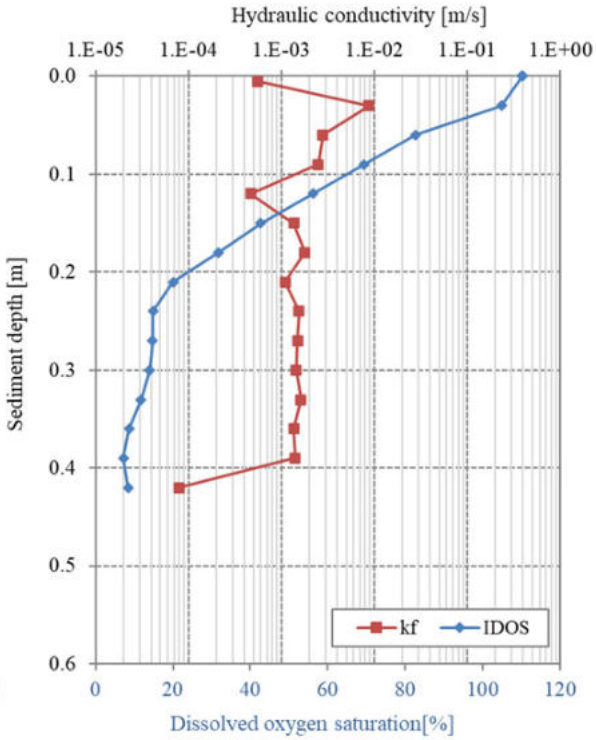

Appendix 2. 41: Results from Würm 6 including image of sediment sample, cumulative sieve curve and vertical profiles from slurping rate, IDOS and kf.

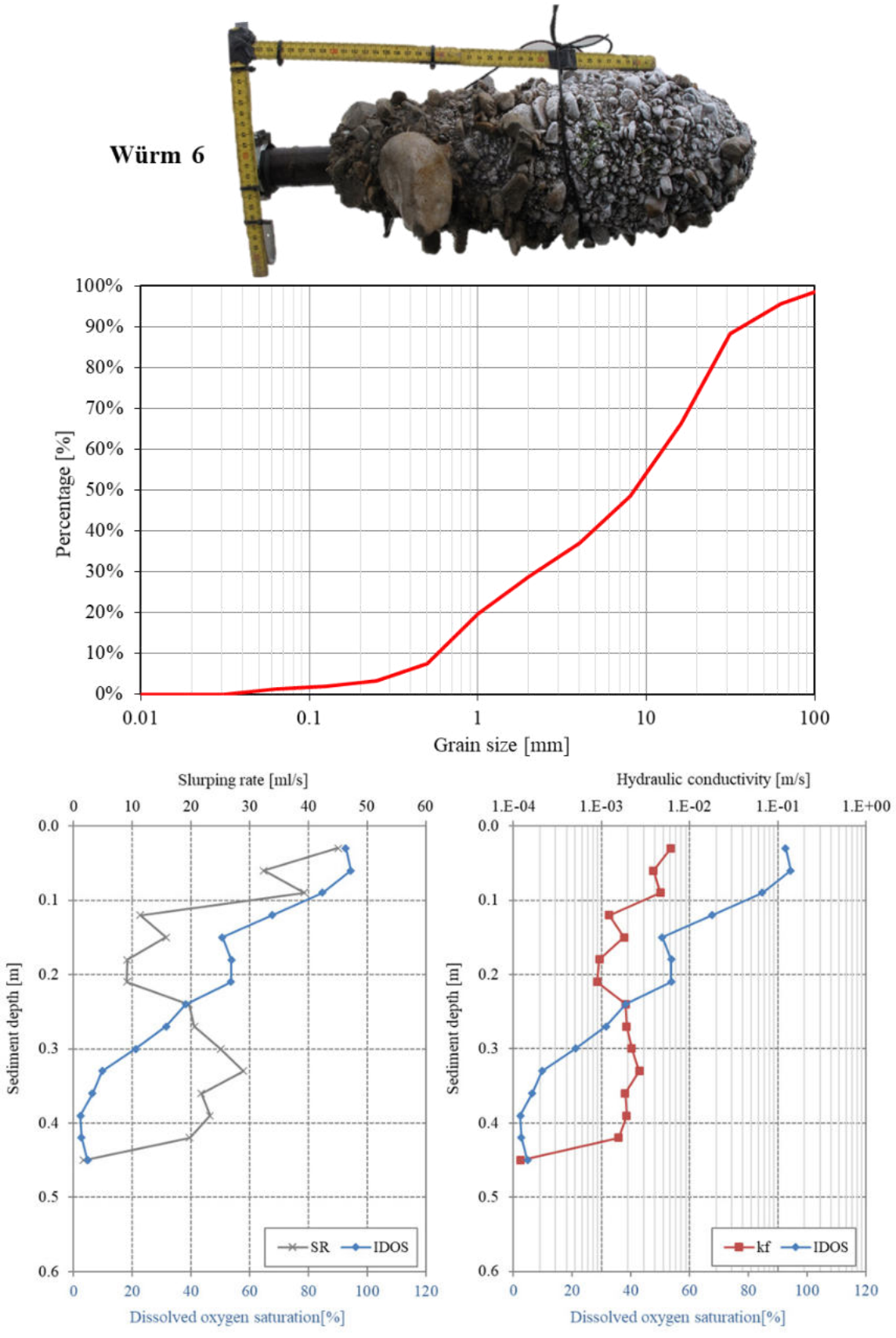

Appendix 3 – Correlation between parameters based on multi-parameter approach

Appendix 3. 1: River specific relation between k_f and IDOS.

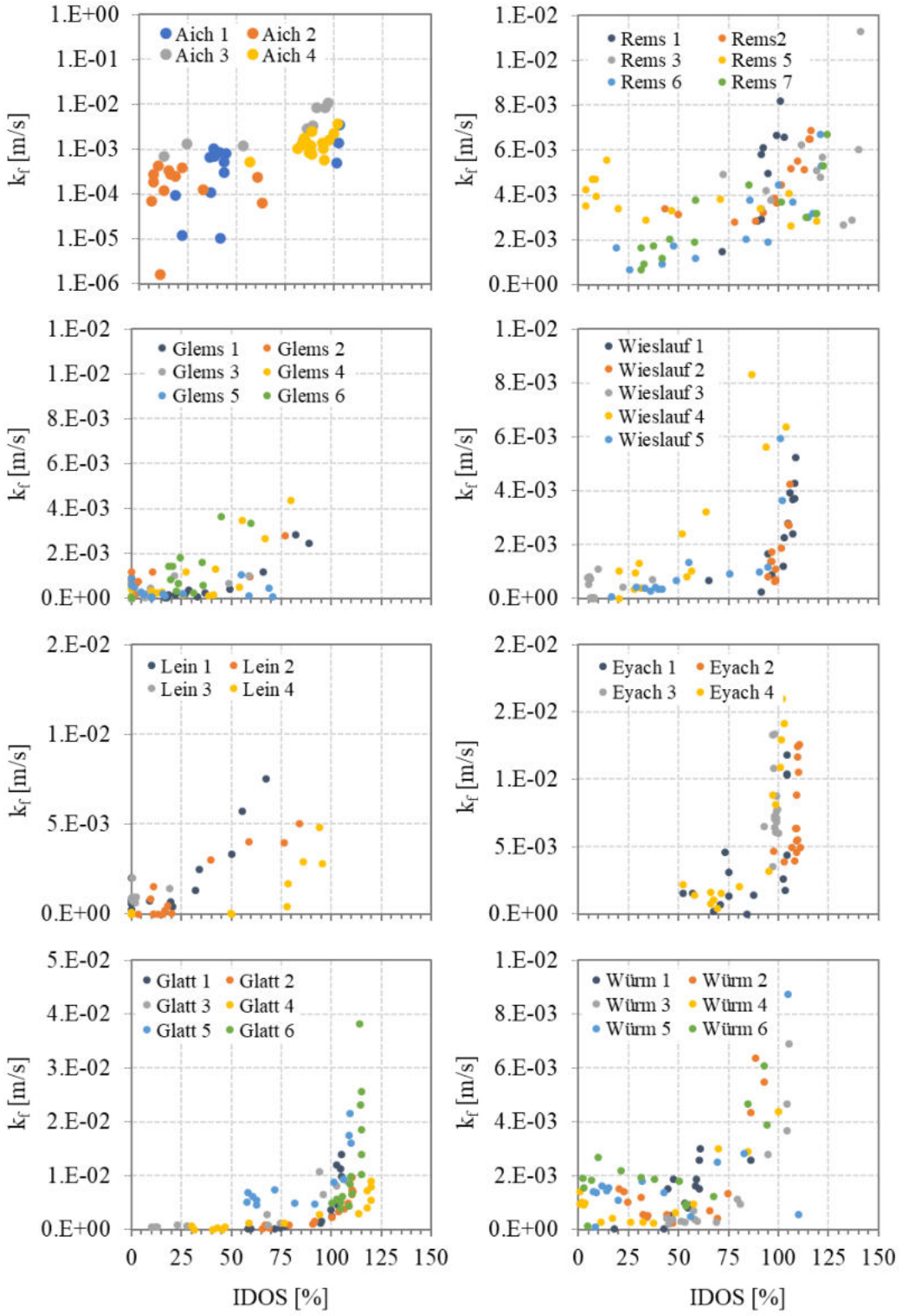

Appendix 3. 2: River specific relation between k_f and n.

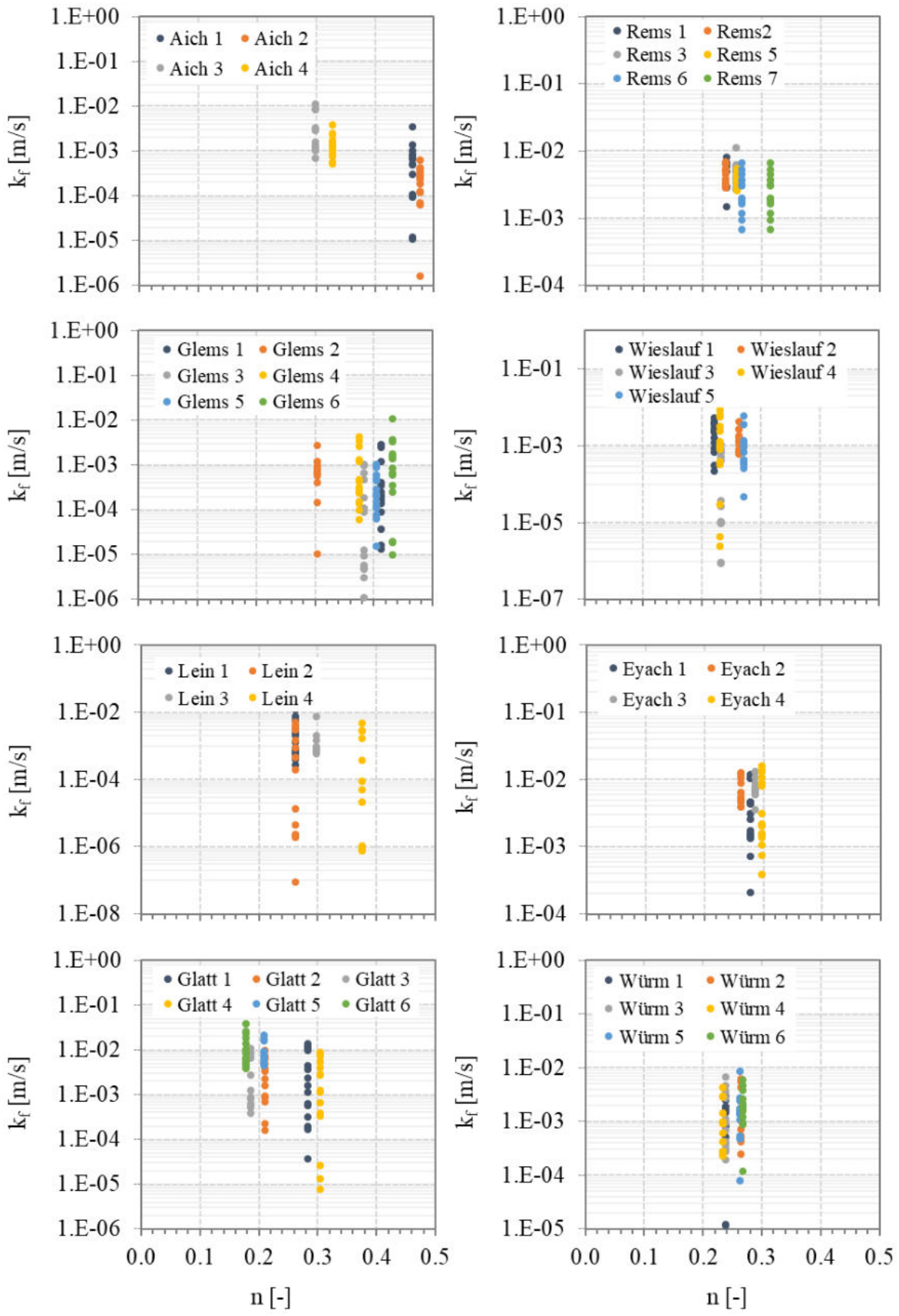

Appendix 3. 3: River specific relation between k_f and σ_g.

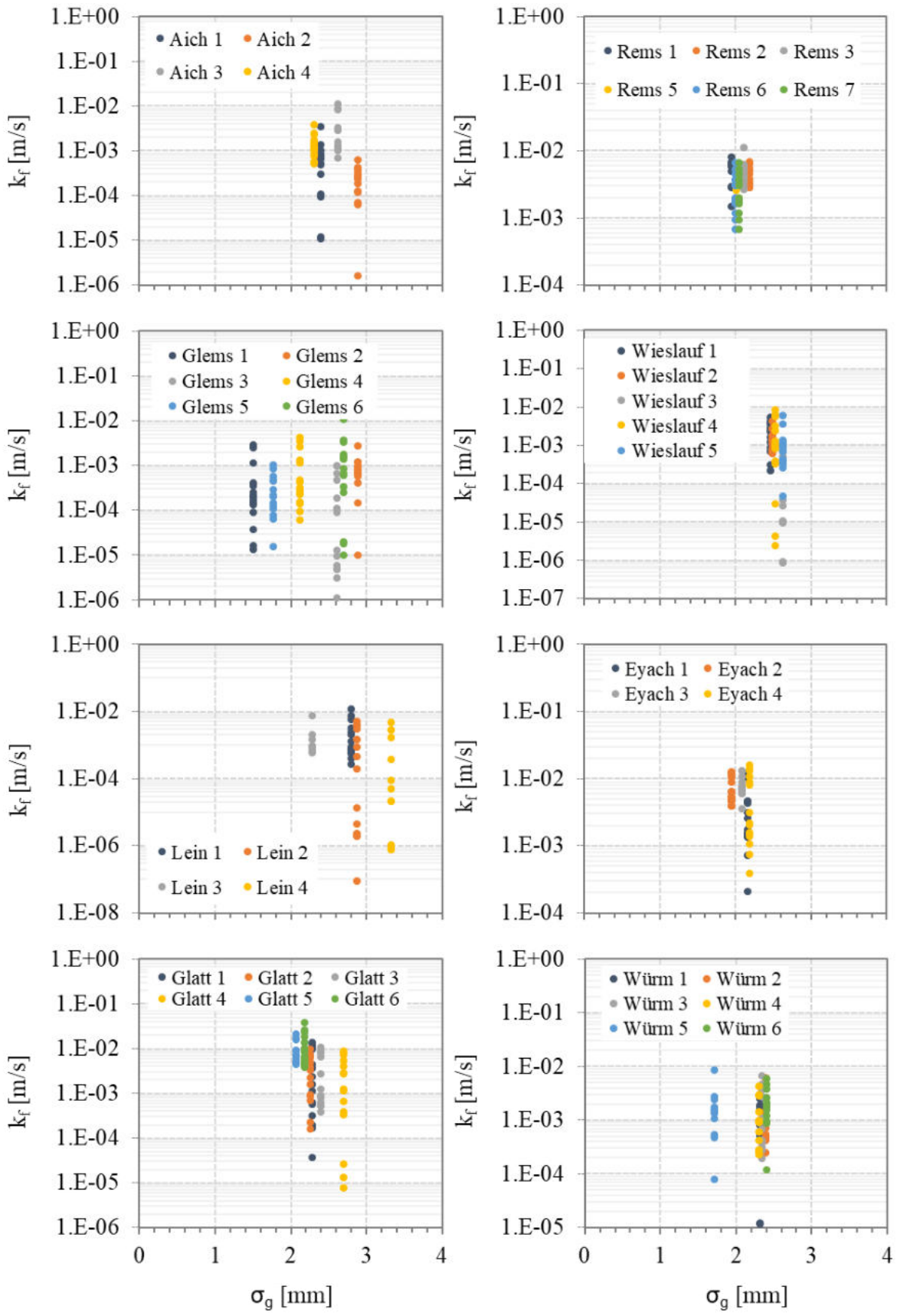

Appendix 3. 4: River specific relation between k_f and FSA<0.5 mm.

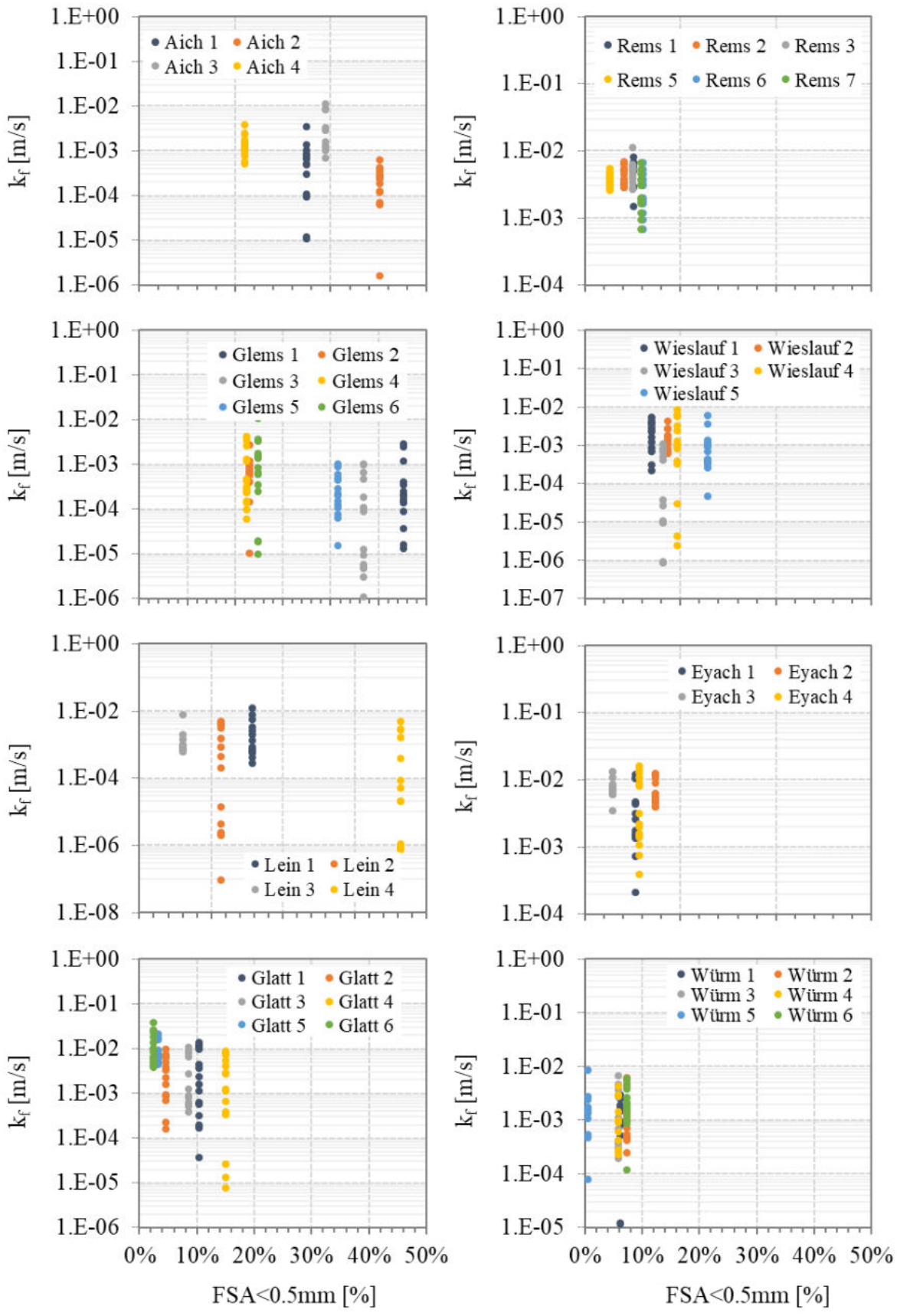

Appendix 3. 5: River specific relation between IDOS and *n*.

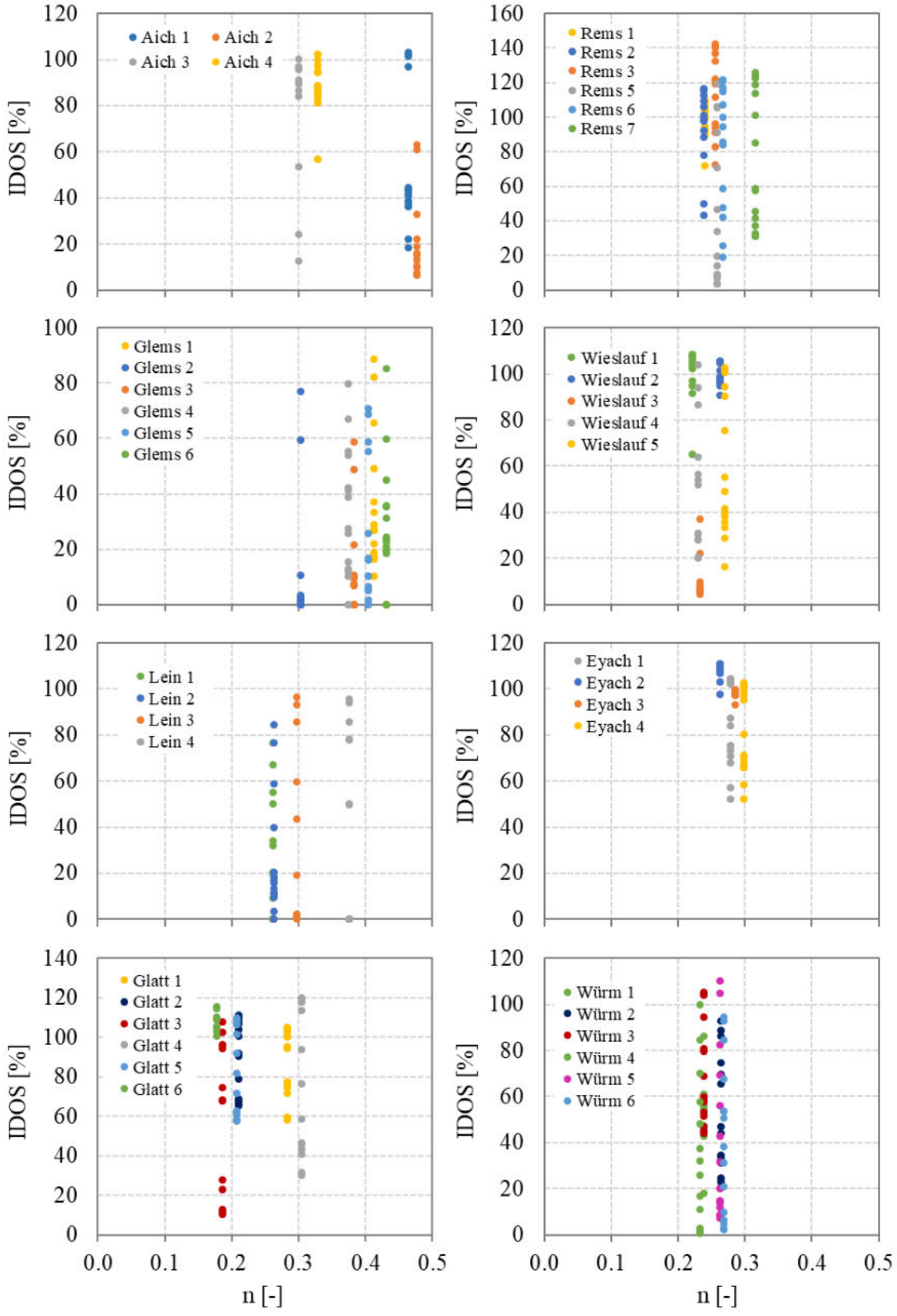

Appendix 3. 6: River specific relation between IDOS and FSA<0.5 mm

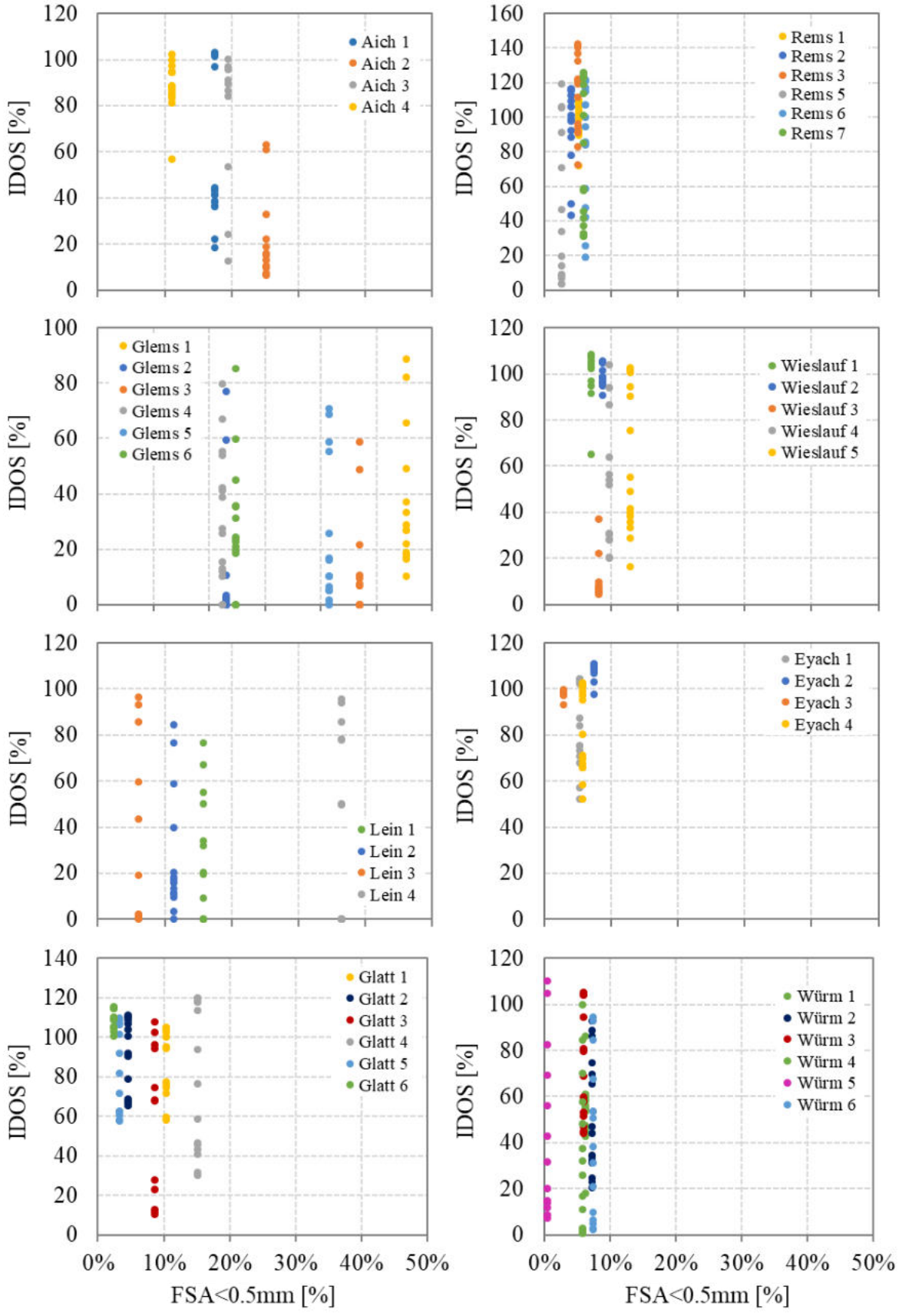

Appendix 3. 7: River specific relation between IDOS and σ_g.

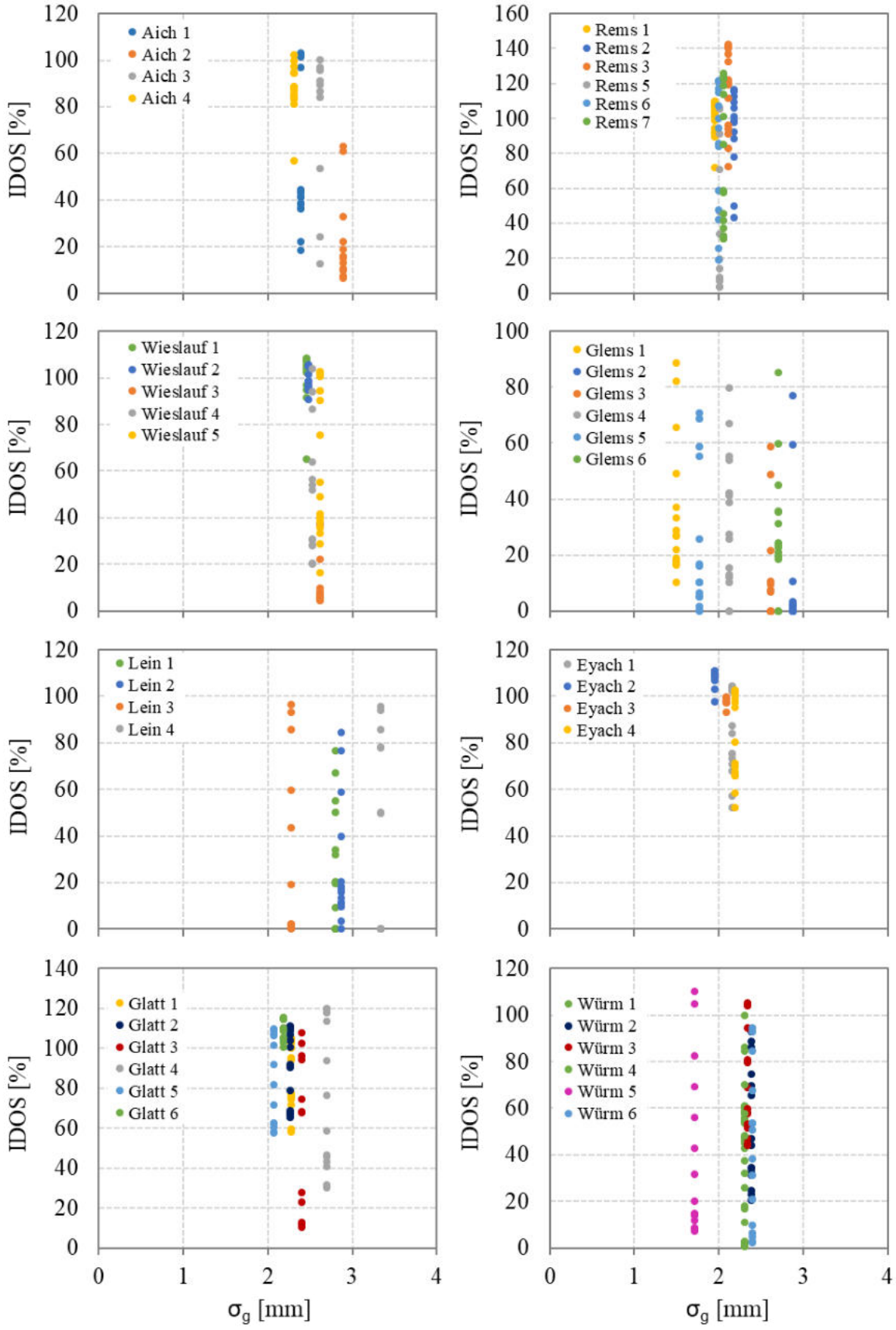

Appendix 3. 8: Relation between k_f and IDOS sorted into different classes of porosity.

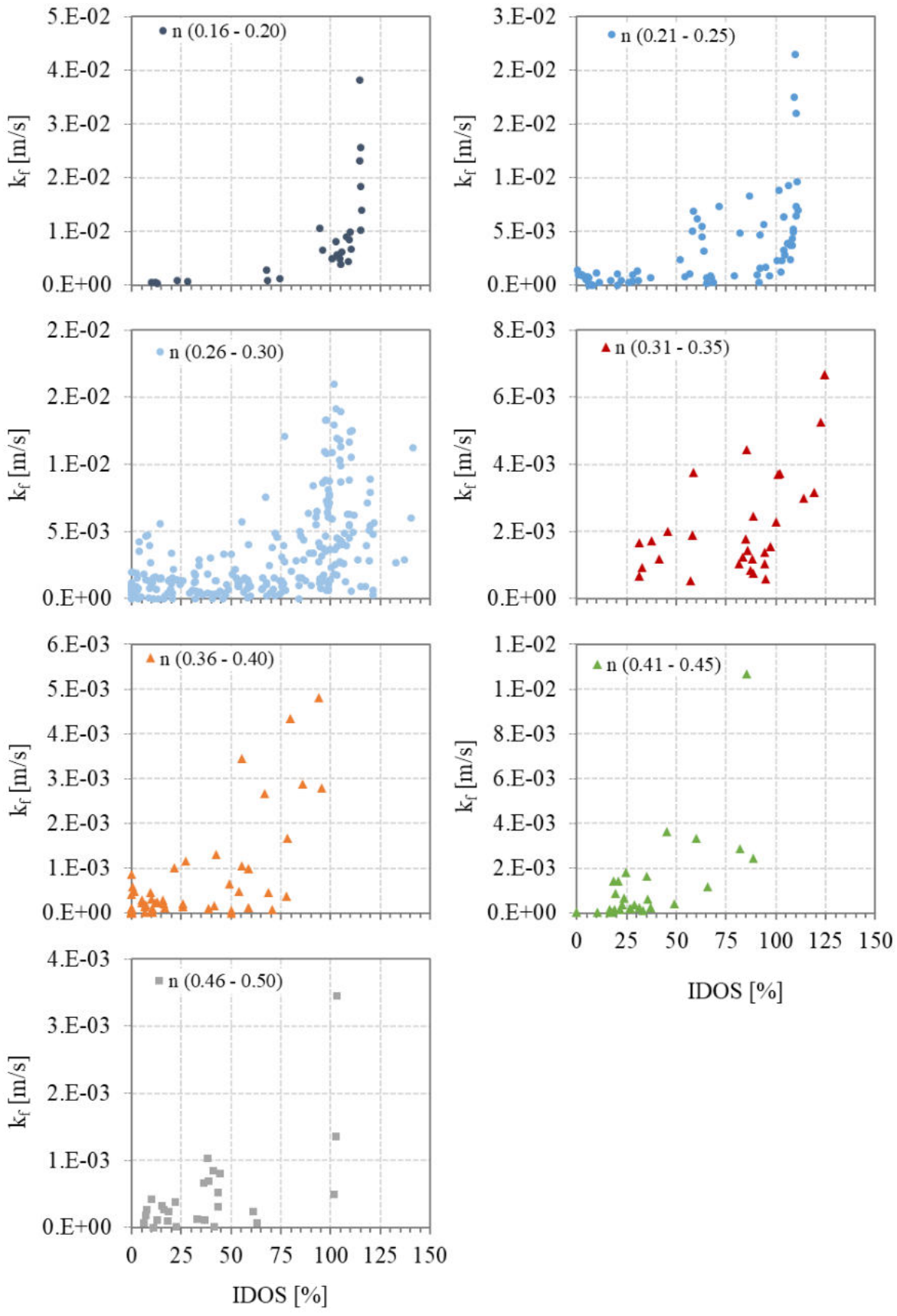

Appendix 3. 9: Relation between k_f and FSA<0.5 mm sorted into different classes of porosity

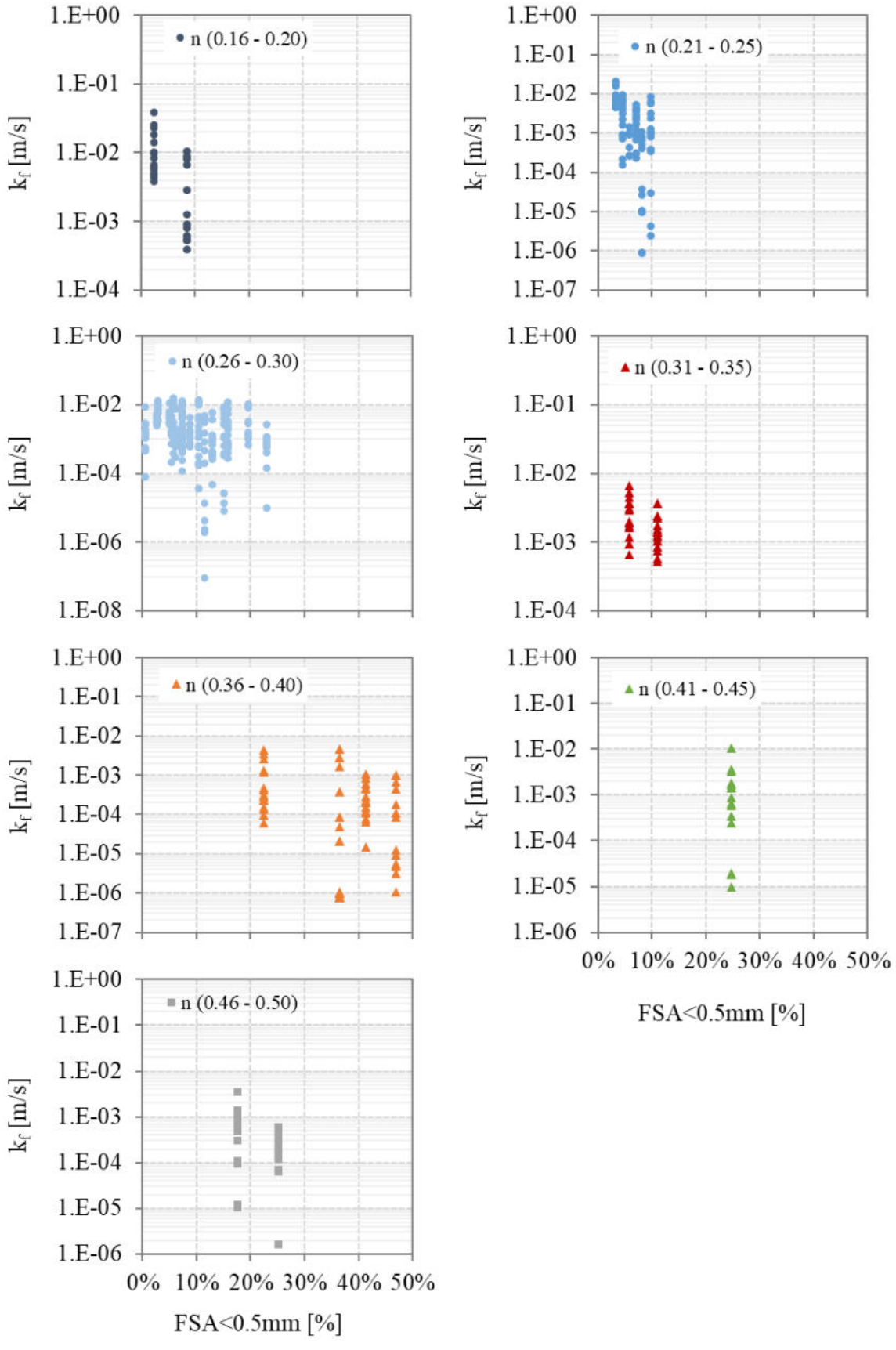

Appendix 3. 10: Relation between k_f and σ_g sorted into different classes of porosity.

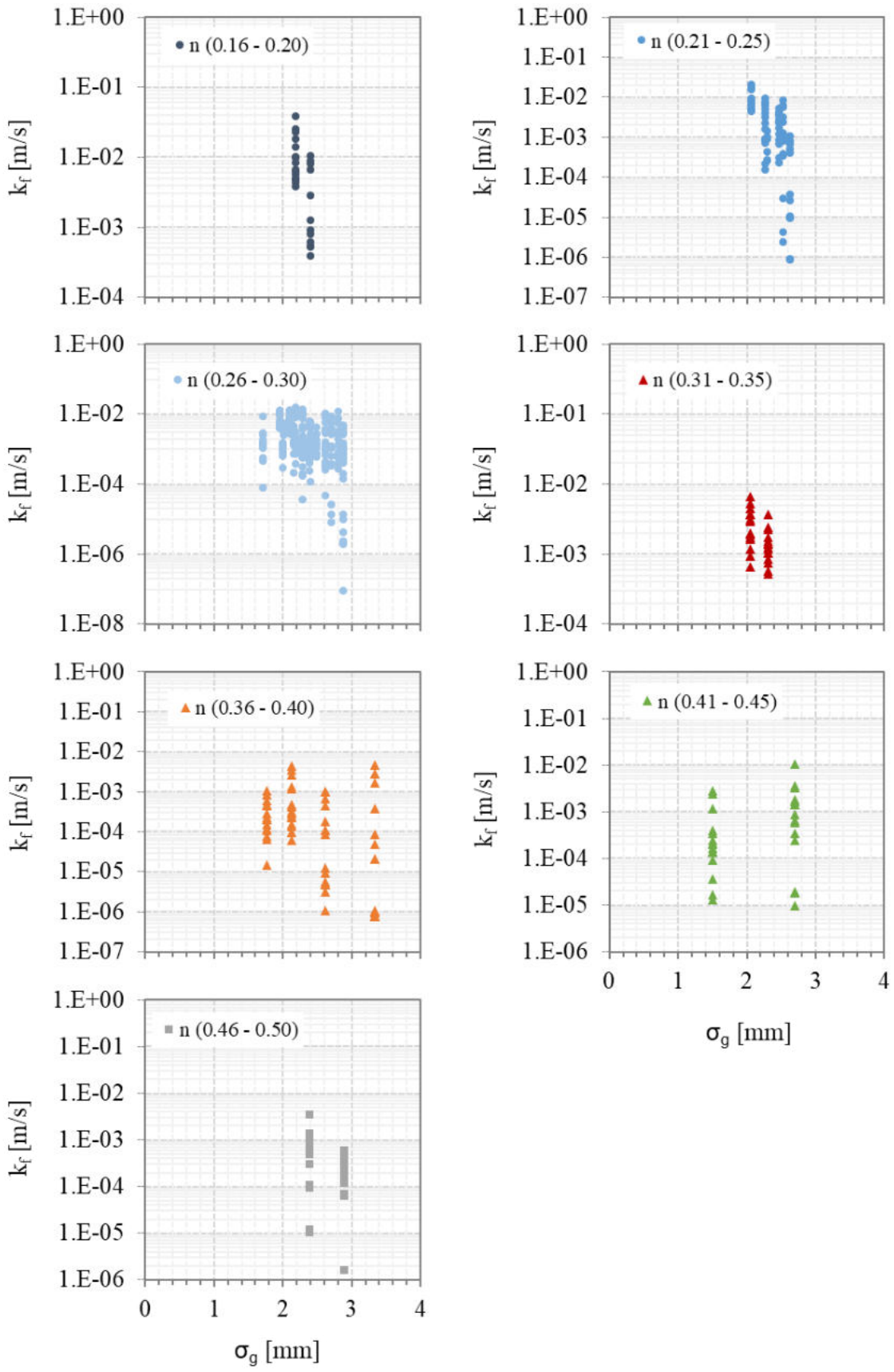

Institut für Wasser- und Umweltsystemmodellierung
Universität Stuttgart

Pfaffenwaldring 61
70569 Stuttgart (Vaihingen)
Telefon (0711) 685 - 60156
Telefax (0711) 685 - 51073
E-Mail: iws@iws.uni-stuttgart.de
http://www.iws.uni-stuttgart.de

Verzeichnis der Mitteilungshefte

1 Röhnisch, Arthur: *Die Bemühungen um eine Wasserbauliche Versuchsanstalt an der Technischen Hochschule Stuttgart*, und
Fattah Abouleid, Abdel: *Beitrag zur Berechnung einer in lockeren Sand gerammten, zweifach verankerten Spundwand*, 1963

2 Marotz, Günter: *Beitrag zur Frage der Standfestigkeit von dichten Asphaltbelägen im Großwasserbau*, 1964

3 Gurr, Siegfried: *Beitrag zur Berechnung zusammengesetzter ebener Flächentrag-werke unter besonderer Berücksichtigung ebener Stauwände, mit Hilfe von Rand-wert- und Lastwertmatrizen*, 1965

4 Plica, Peter: *Ein Beitrag zur Anwendung von Schalenkonstruktionen im Stahlwasserbau*, und
Petrikat, Kurt: *Möglichkeiten und Grenzen des wasserbaulichen Versuchswesens*, 1966

5 Plate, Erich: *Beitrag zur Bestimmung der Windgeschwindigkeitsverteilung in der durch eine Wand gestörten bodennahen Luftschicht*, und
Röhnisch, Arthur; Marotz, Günter: *Neue Baustoffe und Bauausführungen für den Schutz der Böschungen und der Sohle von Kanälen, Flüssen und Häfen; Gestehungskosten und jeweilige Vorteile*, sowie
Unny, T.E.: *Schwingungsuntersuchungen am Kegelstrahlschieber*, 1967

6 Seiler, Erich: *Die Ermittlung des Anlagenwertes der bundeseigenen Binnenschiffahrtsstraßen und Talsperren und des Anteils der Binnenschiffahrt an diesem Wert*, 1967

7 *Sonderheft anläßlich des 65. Geburtstages von Prof. Arthur Röhnisch mit Beiträgen von* Benk, Dieter; Breitling, J.; Gurr, Siegfried; Haberhauer, Robert; Honekamp, Hermann; Kuz, Klaus Dieter; Marotz, Günter; Mayer-Vorfelder, Hans-Jörg; Miller, Rudolf; Plate, Erich J.; Radomski, Helge; Schwarz, Helmut; Vollmer, Ernst; Wildenhahn, Eberhard; 1967

8 Jumikis, Alfred: *Beitrag zur experimentellen Untersuchung des Wassernachschubs in einem gefrierenden Boden und die Beurteilung der Ergebnisse*, 1968

9 Marotz, Günter: *Technische Grundlagen einer Wasserspeicherung im natürlichen Untergrund*, 1968

10 Radomski, Helge: *Untersuchungen über den Einfluß der Querschnittsform wellenförmiger Spundwände auf die statischen und rammtechnischen Eigenschaften*, 1968

11 Schwarz, Helmut: *Die Grenztragfähigkeit des Baugrundes bei Einwirkung vertikal gezogener Ankerplatten als zweidimensionales Bruchproblem*, 1969

12 Erbel, Klaus: *Ein Beitrag zur Untersuchung der Metamorphose von Mittelgebirgsschneedecken unter besonderer Berücksichtigung eines Verfahrens zur Bestimmung der thermischen Schneequalität*, 1969

13 Westhaus, Karl-Heinz: *Der Strukturwandel in der Binnenschiffahrt und sein Einfluß auf den Ausbau der Binnenschiffskanäle*, 1969

14 Mayer-Vorfelder, Hans-Jörg: *Ein Beitrag zur Berechnung des Erdwiderstandes unter Ansatz der logarithmischen Spirale als Gleitflächenfunktion*, 1970

15 Schulz, Manfred: *Berechnung des räumlichen Erddruckes auf die Wandung kreiszylindrischer Körper*, 1970

16 Mobasseri, Manoutschehr: *Die Rippenstützmauer. Konstruktion und Grenzen ihrer Standsicherheit*, 1970

17 Benk, Dieter: *Ein Beitrag zum Betrieb und zur Bemessung von Hochwasserrückhaltebecken*, 1970

18 Gàl, Attila: *Bestimmung der mitschwingenden Wassermasse bei überströmten Fischbauchklappen mit kreiszylindrischem Staublech*, 1971, vergriffen

19 Kuz, Klaus Dieter: *Ein Beitrag zur Frage des Einsetzens von Kavitationserscheinungen in einer Düsenströmung bei Berücksichtigung der im Wasser gelösten Gase*, 1971, vergriffen

20 Schaak, Hartmut: *Verteilleitungen von Wasserkraftanlagen*, 1971

21 *Sonderheft zur Eröffnung der neuen Versuchsanstalt des Instituts für Wasserbau der Universität Stuttgart mit Beiträgen von* Brombach, Hansjörg; Dirksen, Wolfram; Gàl, Attila; Gerlach, Reinhard; Giesecke, Jürgen; Holthoff, Franz-Josef; Kuz, Klaus Dieter; Marotz, Günter; Minor, Hans-Erwin; Petrikat, Kurt; Röhnisch, Arthur; Rueff, Helge; Schwarz, Helmut; Vollmer, Ernst; Wildenhahn, Eberhard; 1972

22 Wang, Chung-su: *Ein Beitrag zur Berechnung der Schwingungen an Kegelstrahlschiebern*, 1972

23 Mayer-Vorfelder, Hans-Jörg: *Erdwiderstandsbeiwerte nach dem Ohde-Variationsverfahren*, 1972

24 Minor, Hans-Erwin: *Beitrag zur Bestimmung der Schwingungsanfachungsfunktionen überströmter Stauklappen*, 1972, vergriffen

25 Brombach, Hansjörg: *Untersuchung strömungsmechanischer Elemente (Fluidik) und die Möglichkeit der Anwendung von Wirbelkammerelementen im Wasserbau*, 1972, vergriffen

26 Wildenhahn, Eberhard: *Beitrag zur Berechnung von Horizontalfilterbrunnen*, 1972

27 Steinlein, Helmut: *Die Eliminierung der Schwebstoffe aus Flußwasser zum Zweck der unterirdischen Wasserspeicherung, gezeigt am Beispiel der Iller*, 1972

28 Holthoff, Franz Josef: *Die Überwindung großer Hubhöhen in der Binnenschiffahrt durch Schwimmerhebewerke*, 1973

29 Röder, Karl: *Einwirkungen aus Baugrundbewegungen auf trog- und kastenförmige Konstruktionen des Wasser- und Tunnelbaues*, 1973

30 Kretschmer, Heinz: *Die Bemessung von Bogenstaumauern in Abhängigkeit von der Talform*, 1973

31 Honekamp, Hermann: *Beitrag zur Berechnung der Montage von Unterwasserpipelines*, 1973

32 Giesecke, Jürgen: *Die Wirbelkammertriode als neuartiges Steuerorgan im Wasserbau*, und Brombach, Hansjörg: *Entwicklung, Bauformen, Wirkungsweise und Steuereigenschaften von Wirbelkammerverstärkern*, 1974

33 Rueff, Helge: *Untersuchung der schwingungserregenden Kräfte an zwei hintereinander angeordneten Tiefschützen unter besonderer Berücksichtigung von Kavitation*, 1974

34 Röhnisch, Arthur: *Einpreßversuche mit Zementmörtel für Spannbeton - Vergleich der Ergebnisse von Modellversuchen mit Ausführungen in Hüllwellrohren*, 1975

35 *Sonderheft anläßlich des 65. Geburtstages von Prof. Dr.-Ing. Kurt Petrikat mit Beiträgen von*: Brombach, Hansjörg; Erbel, Klaus; Flinspach, Dieter; Fischer jr., Richard; Gàl, Attila; Gerlach, Reinhard; Giesecke, Jürgen; Haberhauer, Robert; Hafner Edzard; Hausenblas, Bernhard; Horlacher, Hans-Burkhard; Hutarew, Andreas; Knoll, Manfred; Krummet, Ralph; Marotz, Günter; Merkle, Theodor; Miller, Christoph; Minor, Hans-Erwin; Neumayer, Hans; Rao, Syamala; Rath, Paul; Rueff, Helge; Ruppert, Jürgen; Schwarz, Wolfgang; Topal-Gökceli, Mehmet; Vollmer, Ernst; Wang, Chung-su; Weber, Hans-Georg; 1975

36 Berger, Jochum: *Beitrag zur Berechnung des Spannungszustandes in rotationssymmetrisch belasteten Kugelschalen veränderlicher Wandstärke unter Gas- und Flüssigkeitsdruck durch Integration schwach singulärer Differentialgleichungen*, 1975

37 Dirksen, Wolfram: *Berechnung instationärer Abflußvorgänge in gestauten Gerinnen mittels Differenzenverfahren und die Anwendung auf Hochwasserrückhaltebecken*, 1976

38 Horlacher, Hans-Burkhard: *Berechnung instationärer Temperatur- und Wärmespannungsfelder in langen mehrschichtigen Hohlzylindern*, 1976

39 Hafner, Edzard: *Untersuchung der hydrodynamischen Kräfte auf Baukörper im Tiefwasserbereich des Meeres*, 1977, ISBN 3-921694-39-6

40 Ruppert, Jürgen: *Über den Axialwirbelkammerverstärker für den Einsatz im Wasserbau*, 1977, ISBN 3-921694-40-X

41 Hutarew, Andreas: *Beitrag zur Beeinflußbarkeit des Sauerstoffgehalts in Fließgewässern an Abstürzen und Wehren*, 1977, ISBN 3-921694-41-8, vergriffen

42 Miller, Christoph: *Ein Beitrag zur Bestimmung der schwingungserregenden Kräfte an unterströmten Wehren*, 1977, ISBN 3-921694-42-6

43 Schwarz, Wolfgang: *Druckstoßberechnung unter Berücksichtigung der Radial- und Längsverschiebungen der Rohrwandung*, 1978, ISBN 3-921694-43-4

44 Kinzelbach, Wolfgang: *Numerische Untersuchungen über den optimalen Einsatz variabler Kühlsysteme einer Kraftwerkskette am Beispiel Oberrhein*, 1978, ISBN 3-921694-44-2

45 Barczewski, Baldur: *Neue Meßmethoden für Wasser-Luftgemische und deren Anwendung auf zweiphasige Auftriebsstrahlen*, 1979, ISBN 3-921694-45-0

46 Neumayer, Hans: *Untersuchung der Strömungsvorgänge in radialen Wirbelkammerverstärkern*, 1979, ISBN 3-921694-46-9

47 Elalfy, Youssef-Elhassan: *Untersuchung der Strömungsvorgänge in Wirbelkammerdioden und -drosseln*, 1979, ISBN 3-921694-47-7

48 Brombach, Hansjörg: *Automatisierung der Bewirtschaftung von Wasserspeichern*, 1981, ISBN 3-921694-48-5

49 Geldner, Peter: *Deterministische und stochastische Methoden zur Bestimmung der*

Selbstdichtung von Gewässern, 1981, ISBN 3-921694-49-3, *vergriffen*

50 Mehlhorn, Hans: *Temperaturveränderungen im Grundwasser durch Brauchwassereinleitungen*, 1982, ISBN 3-921694-50-7, *vergriffen*

51 Hafner, Edzard: *Rohrleitungen und Behälter im Meer*, 1983, ISBN 3-921694-51-5

52 Rinnert, Bernd: *Hydrodynamische Dispersion in porösen Medien: Einfluß von Dichteunterschieden auf die Vertikalvermischung in horizontaler Strömung*, 1983, ISBN 3-921694-52-3, *vergriffen*

53 Lindner, Wulf: *Steuerung von Grundwasserentnahmen unter Einhaltung ökologischer Kriterien*, 1983, ISBN 3-921694-53-1, *vergriffen*

54 Herr, Michael; Herzer, Jörg; Kinzelbach, Wolfgang; Kobus, Helmut; Rinnert, Bernd: *Methoden zur rechnerischen Erfassung und hydraulischen Sanierung von Grundwasserkontaminationen*, 1983, ISBN 3-921694-54-X

55 Schmitt, Paul: *Wege zur Automatisierung der Niederschlagsermittlung*, 1984, ISBN 3-921694-55-8, *vergriffen*

56 Müller, Peter: *Transport und selektive Sedimentation von Schwebstoffen bei gestautem Abfluß*, 1985, ISBN 3-921694-56-6

57 El-Qawasmeh, Fuad: *Möglichkeiten und Grenzen der Tropfbewässerung unter besonderer Berücksichtigung der Verstopfungsanfälligkeit der Tropfelemente*, 1985, ISBN 3-921694-57-4, *vergriffen*

58 Kirchenbaur, Klaus: *Mikroprozessorgesteuerte Erfassung instationärer Druckfelder am Beispiel seegangsbelasteter Baukörper*, 1985, ISBN 3-921694-58-2

59 Kobus, Helmut (Hrsg.): *Modellierung des großräumigen Wärme- und Schadstofftransports im Grundwasser*, Tätigkeitsbericht 1984/85 (DFG-Forschergruppe an den Universitäten Hohenheim, Karlsruhe und Stuttgart), 1985, ISBN 3-921694-59-0, *vergriffen*

60 Spitz, Karlheinz: *Dispersion in porösen Medien: Einfluß von Inhomogenitäten und Dichteunterschieden*, 1985, ISBN 3-921694-60-4, *vergriffen*

61 Kobus, Helmut: *An Introduction to Air-Water Flows in Hydraulics*, 1985, ISBN 3-921694-61-2

62 Kaleris, Vassilios: *Erfassung des Austausches von Oberflächen- und Grundwasser in horizontalebenen Grundwassermodellen*, 1986, ISBN 3-921694-62-0

63 Herr, Michael: *Grundlagen der hydraulischen Sanierung verunreinigter Porengrundwasserleiter*, 1987, ISBN 3-921694-63-9

64 Marx, Walter: *Berechnung von Temperatur und Spannung in Massenbeton infolge Hydratation*, 1987, ISBN 3-921694-64-7

65 Koschitzky, Hans-Peter: *Dimensionierungskonzept für Sohlbelüfter in Schußrinnen zur Vermeidung von Kavitationsschäden*, 1987, ISBN 3-921694-65-5

66 Kobus, Helmut (Hrsg.): *Modellierung des großräumigen Wärme- und Schadstofftransports im Grundwasser*, Tätigkeitsbericht 1986/87 (DFG-Forschergruppe an den Universitäten Hohenheim, Karlsruhe und Stuttgart) 1987, ISBN 3-921694-66-3

67 Söll, Thomas: *Berechnungsverfahren zur Abschätzung anthropogener Temperaturanomalien im Grundwasser*, 1988, ISBN 3-921694-67-1

68 Dittrich, Andreas; Westrich, Bernd: *Bodenseeufererosion, Bestandsaufnahme und Bewertung*, 1988, ISBN 3-921694-68-X, *vergriffen*

69 Huwe, Bernd; van der Ploeg, Rienk R.: *Modelle zur Simulation des Stickstoffhaushaltes von Standorten mit unterschiedlicher landwirtschaftlicher Nutzung*, 1988, ISBN 3-921694-69-8, *vergriffen*

70 Stephan, Karl: *Integration elliptischer Funktionen*, 1988, ISBN 3-921694-70-1

71 Kobus, Helmut; Zilliox, Lothaire (Hrsg.): *Nitratbelastung des Grundwassers, Auswirkungen der Landwirtschaft auf die Grundwasser- und Rohwasserbeschaffenheit und Maßnahmen zum Schutz des Grundwassers*. Vorträge des deutsch-französischen Kolloquiums am 6. Oktober 1988, Universitäten Stuttgart und Louis Pasteur Strasbourg (Vorträge in deutsch oder französisch, Kurzfassungen zweisprachig), 1988, ISBN 3-921694-71-X

72 Soyeaux, Renald: *Unterströmung von Stauanlagen auf klüftigem Untergrund unter Berücksichtigung laminarer und turbulenter Fließzustände*,1991, ISBN 3-921694-72-8

73 Kohane, Roberto: *Berechnungsmethoden für Hochwasserabfluß in Fließgewässern mit überströmten Vorländern*, 1991, ISBN 3-921694-73-6

74 Hassinger, Reinhard: *Beitrag zur Hydraulik und Bemessung von Blocksteinrampen in flexibler Bauweise*, 1991, ISBN 3-921694-74-4, *vergriffen*

75 Schäfer, Gerhard: *Einfluß von Schichtenstrukturen und lokalen Einlagerungen auf die Längsdispersion in Porengrundwasserleitern*, 1991, ISBN 3-921694-75-2

76 Giesecke, Jürgen: *Vorträge, Wasserwirtschaft in stark besiedelten Regionen; Umweltforschung mit Schwerpunkt Wasserwirtschaft*, 1991, ISBN 3-921694-76-0

77 Huwe, Bernd: *Deterministische und stochastische Ansätze zur Modellierung des Stickstoffhaushalts landwirtschaftlich genutzter Flächen auf unterschiedlichem Skalenniveau*, 1992, ISBN 3-921694-77-9, *vergriffen*

78 Rommel, Michael: *Verwendung von Kluftdaten zur realitätsnahen Generierung von Kluftnetzen mit anschließender laminar-turbulenter Strömungsberechnung*, 1993, ISBN 3-92 1694-78-7

79 Marschall, Paul: *Die Ermittlung lokaler Stofffrachten im Grundwasser mit Hilfe von Einbohrloch-Meßverfahren*, 1993, ISBN 3-921694-79-5, *vergriffen*

80 Ptak, Thomas: *Stofftransport in heterogenen Porenaquiferen: Felduntersuchungen und stochastische Modellierung*, 1993, ISBN 3-921694-80-9, *vergriffen*

81 Haakh, Frieder: *Transientes Strömungsverhalten in Wirbelkammern,* 1993, ISBN 3-921694-81-7

82 Kobus, Helmut; Cirpka, Olaf; Barczewski, Baldur; Koschitzky, Hans-Peter: *Versuchseinrichtung zur Grundwasser- und Altlastensanierung VEGAS, Konzeption und Programmrahmen*, 1993, ISBN 3-921694-82-5

83 Zang, Weidong: *Optimaler Echtzeit-Betrieb eines Speichers mit aktueller Abflußregenerierung*, 1994, ISBN 3-921694-83-3, *vergriffen*

84 Franke, Hans-Jörg: *Stochastische Modellierung eines flächenhaften Stoffeintrages und Transports in Grundwasser am Beispiel der Pflanzenschutzmittelproblematik*, 1995, ISBN 3-921694-84-1

85 Lang, Ulrich: *Simulation regionaler Strömungs- und Transportvorgänge in Karstaquiferen mit Hilfe des Doppelkontinuum-Ansatzes: Methodenentwicklung und Parameteridentifikation*, 1995, ISBN 3-921694-85-X, *vergriffen*

86 Helmig, Rainer: *Einführung in die Numerischen Methoden der Hydromechanik*, 1996, ISBN 3-921694-86-8, *vergriffen*

87 Cirpka, Olaf: *CONTRACT: A Numerical Tool for Contaminant Transport and Chemical Transformations - Theory and Program Documentation -*, 1996, ISBN 3-921694-87-6

88 Haberlandt, Uwe: *Stochastische Synthese und Regionalisierung des Niederschlages für Schmutzfrachtberechnungen*, 1996, ISBN 3-921694-88-4

89 Croisé, Jean: *Extraktion von flüchtigen Chemikalien aus natürlichen Lockergesteinen mittels erzwungener Luftströmung*, 1996, ISBN 3-921694-89-2, *vergriffen*

90 Jorde, Klaus: *Ökologisch begründete, dynamische Mindestwasserregelungen bei Ausleitungskraftwerken*, 1997, ISBN 3-921694-90-6, *vergriffen*

91 Helmig, Rainer: *Gekoppelte Strömungs- und Transportprozesse im Untergrund - Ein Beitrag zur Hydrosystemmodellierung-*, 1998, ISBN 3-921694-91-4, *vergriffen*

92 Emmert, Martin: *Numerische Modellierung nichtisothermer Gas-Wasser Systeme in porösen Medien,* 1997, ISBN 3-921694-92-2

93 Kern, Ulrich: *Transport von Schweb- und Schadstoffen in staugeregelten Fließgewässern am Beispiel des Neckars*, 1997, ISBN 3-921694-93-0, *vergriffen*

94 Förster, Georg: *Druckstoßdämpfung durch große Luftblasen in Hochpunkten von Rohrleitungen 1997*, ISBN 3-921694-94-9

95 Cirpka, Olaf: *Numerische Methoden zur Simulation des reaktiven Mehrkomponententransports im Grundwasser*, 1997, ISBN 3-921694-95-7, *vergriffen*

96 Färber, Arne: *Wärmetransport in der ungesättigten Bodenzone: Entwicklung einer thermischen In-situ-Sanierungstechnologie*, 1997, ISBN 3-921694-96-5

97 Betz, Christoph: *Wasserdampfdestillation von Schadstoffen im porösen Medium: Entwicklung einer thermischen In-situ-Sanierungstechnologie*, 1998, SBN 3-921694-97-3

98 Xu, Yichun: *Numerical Modeling of Suspended Sediment Transport in Rivers*, 1998, ISBN 3-921694-98-1, *vergriffen*

99 Wüst, Wolfgang: *Geochemische Untersuchungen zur Sanierung CKW-kontaminierter Aquifere mit Fe(0)-Reaktionswänden,* 2000, ISBN 3-933761-02-2

100 Sheta, Hussam: *Simulation von Mehrphasenvorgängen in porösen Medien unter Einbeziehung von Hysterese-Effekten*, 2000, ISBN 3-933761-03-4

101 Ayros, Edwin: *Regionalisierung extremer Abflüsse auf der Grundlage statistischer Verfahren*, 2000, ISBN 3-933761-04-2, *vergriffen*

102 Huber, Ralf: *Compositional Multiphase Flow and Transport in Heterogeneous Porous Media*, 2000, ISBN 3-933761-05-0

103 Braun, Christopherus: *Ein Upscaling-Verfahren für Mehrphasenströmungen in porösen Medien*, 2000, ISBN 3-933761-06-9

104 Hofmann, Bernd: *Entwicklung eines rechnergestützten Managementsystems zur Beurteilung von Grundwasserschadensfällen*, 2000, ISBN 3-933761-07-7

105 Class, Holger: *Theorie und numerische Modellierung nichtisothermer Mehrphasenprozesse in NAPL-kontaminierten porösen Medien,* 2001, ISBN 3-933761-08-5

106 Schmidt, Reinhard: *Wasserdampf- und Heißluftinjektion zur thermischen Sanierung kontaminierter Standorte*, 2001, ISBN 3-933761-09-3

107 Josef, Reinhold: *Schadstoffextraktion mit hydraulischen Sanierungsverfahren unter Anwendung von grenzflächenaktiven Stoffen*, 2001, ISBN 3-933761-10-7

108 Schneider, Matthias: *Habitat- und Abflussmodellierung für Fließgewässer mit unscharfen Berechnungsansätzen*, 2001, ISBN 3-933761-11-5

109 Rathgeb, Andreas: *Hydrodynamische Bemessungsgrundlagen für Lockerdeckwerke an überströmbaren Erddämmen*, 2001, ISBN 3-933761-12-3

110 Lang, Stefan: *Parallele numerische Simulation instätionärer Probleme mit adaptiven Methoden auf unstrukturierten Gittern*, 2001, ISBN 3-933761-13-1

111 Appt, Jochen; Stumpp Simone: *Die Bodensee-Messkampagne 2001, IWS/CWR Lake Constance Measurement Program 2001*, 2002, ISBN 3-933761-14-X

112 Heimerl, Stephan: *Systematische Beurteilung von Wasserkraftprojekten,* 2002, ISBN 3-933761-15-8, *vergriffen*

113 Iqbal, Amin: *On the Management and Salinity Control of Drip Irrigation,* 2002, ISBN 3-933761-16-6

114 Silberhorn-Hemminger, Annette: *Modellierung von Kluftaquifersystemen: Geostatistische Analyse und deterministisch-stochastische Kluftgenerierung,* 2002, ISBN 3-933761-17-4

115 Winkler, Angela: *Prozesse des Wärme- und Stofftransports bei der In-situ-Sanierung mit festen Wärmequellen,* 2003, ISBN 3-933761-18-2

116 Marx, Walter: *Wasserkraft, Bewässerung, Umwelt - Planungs- und Bewertungsschwerpunkte der Wasserbewirtschaftung,* 2003, ISBN 3-933761-19-0

117 Hinkelmann, Reinhard: *Efficient Numerical Methods and Information-Processing Techniques in Environment Water,* 2003, ISBN 3-933761-20-4

118 Samaniego-Eguiguren, Luis Eduardo: *Hydrological Consequences of Land Use / Land Cover and Climatic Changes in Mesoscale Catchments*, 2003, ISBN 3-933761-21-2

119 Neunhäuserer, Lina: *Diskretisierungsansätze zur Modellierung von Strömungs- und Transportprozessen in geklüftet-porösen Medien*, 2003, ISBN 3-933761-22-0

120 Paul, Maren: *Simulation of Two-Phase Flow in Heterogeneous Poros Media with Adaptive*

Methods, 2003, ISBN 3-933761-23-9

121 Ehret, Uwe: *Rainfall and Flood Nowcasting in Small Catchments using Weather Radar*, 2003, ISBN 3-933761-24-7

122 Haag, Ingo: *Der Sauerstoffhaushalt staugeregelter Flüsse am Beispiel des Neckars - Analysen, Experimente, Simulationen -,* 2003, ISBN 3-933761-25-5

123 Appt, Jochen: *Analysis of Basin-Scale Internal Waves in Upper Lake Constance,* 2003, ISBN 3-933761-26-3

124 Hrsg.: Schrenk, Volker; Batereau, Katrin; Barczewski, Baldur; Weber, Karolin und Koschitzky, Hans-Peter: *Symposium Ressource Fläche und VEGAS - Statuskolloquium 2003, 30. September und 1. Oktober 2003,* 2003, ISBN 3-933761-27-1

125 Omar Khalil Ouda: *Optimisation of Agricultural Water Use: A Decision Support System for the Gaza Strip,* 2003, ISBN 3-933761-28-0

126 Batereau, Katrin: *Sensorbasierte Bodenluftmessung zur Vor-Ort-Erkundung von Schadensherden im Untergrund*, 2004, ISBN 3-933761-29-8

127 Witt, Oliver: *Erosionsstabilität von Gewässersedimenten mit Auswirkung auf den Stofftransport bei Hochwasser am Beispiel ausgewählter Stauhaltungen des Oberrheins*, 2004, ISBN 3-933761-30-1

128 Jakobs, Hartmut: *Simulation nicht-isothermer Gas-Wasser-Prozesse in komplexen Kluft-Matrix-Systemen*, 2004, ISBN 3-933761-31-X

129 Li, Chen-Chien: *Deterministisch-stochastisches Berechnungskonzept zur Beurteilung der Auswirkungen erosiver Hochwasserereignisse in Flussstauhaltungen,* 2004, ISBN 3-933761-32-8

130 Reichenberger, Volker; Helmig, Rainer; Jakobs, Hartmut; Bastian, Peter; Niessner, Jennifer: *Complex Gas-Water Processes in Discrete Fracture-Matrix Systems: Up-scaling, Mass-Conservative Discretization and Efficient Multilevel Solution,* 2004, ISBN 3-933761-33-6

131 Hrsg.: Barczewski, Baldur; Koschitzky, Hans-Peter; Weber, Karolin; Wege, Ralf: *VEGAS - Statuskolloquium 2004,* Tagungsband zur Veranstaltung am 05. Oktober 2004 an der Universität Stuttgart, Campus Stuttgart-Vaihingen, 2004, ISBN 3-933761-34-4

132 Asie, Kemal Jabir: *Finite Volume Models for Multiphase Multicomponent Flow through Porous Media*. 2005, ISBN 3-933761-35-2

133 Jacoub, George: *Development of a 2-D Numerical Module for Particulate Contaminant Transport in Flood Retention Reservoirs and Impounded Rivers,* 2004, ISBN 3-933761-36-0

134 Nowak, Wolfgang: *Geostatistical Methods for the Identification of Flow and Transport Parameters in the Subsurface,* 2005, ISBN 3-933761-37-9

135 Süß, Mia: *Analysis of the influence of structures and boundaries on flow and transport processes in fractured porous media*, 2005, ISBN 3-933761-38-7

136 Jose, Surabhin Chackiath: *Experimental Investigations on Longitudinal Dispersive Mixing in Heterogeneous Aquifers,* 2005, ISBN: 3-933761-39-5

137 Filiz, Fulya: *Linking Large-Scale Meteorological Conditions to Floods in Mesoscale Catchments,* 2005, ISBN 3-933761-40-9

138 Qin, Minghao: *Wirklichkeitsnahe und recheneffiziente Ermittlung von Temperatur und Spannungen bei großen RCC-Staumauern*, 2005, ISBN 3-933761-41-7

139 Kobayashi, Kenichiro: *Optimization Methods for Multiphase Systems in the Subsurface - Application to Methane Migration in Coal Mining Areas*, 2005, ISBN 3-933761-42-5

140 Rahman, Md. Arifur: *Experimental Investigations on Transverse Dispersive Mixing in Heterogeneous Porous Media,* 2005, ISBN 3-933761-43-3

141 Schrenk, Volker: *Ökobilanzen zur Bewertung von Altlastensanierungsmaßnahmen,* 2005, ISBN 3-933761-44-1

142 Hundecha, Hirpa Yeshewatesfa: *Regionalization of Parameters of a Conceptual Rainfall-Runoff Model*, 2005, ISBN: 3-933761-45-X

143 Wege, Ralf: *Untersuchungs- und Überwachungsmethoden für die Beurteilung natürlicher Selbstreinigungsprozesse im Grundwasser,* 2005, ISBN 3-933761-46-8

144 Breiting, Thomas: *Techniken und Methoden der Hydroinformatik - Modellierung von komplexen Hydrosystemen im Untergrund*, 2006, ISBN 3-933761-47-6

145 Hrsg.: Braun, Jürgen; Koschitzky, Hans-Peter; Müller, Martin: *Ressource Untergrund: 10 Jahre VEGAS: Forschung und Technologieentwicklung zum Schutz von Grundwasser und Boden,* Tagungsband zur Veranstaltung am 28. und 29. September 2005 an der Universität Stuttgart, Campus Stuttgart-Vaihingen, 2005, ISBN 3-933761-48-4

146 Rojanschi, Vlad: *Abflusskonzentration in mesoskaligen Einzugsgebieten unter Berücksichtigung des Sickerraumes,* 2006, ISBN 3-933761-49-2

147 Winkler, Nina Simone: *Optimierung der Steuerung von Hochwasserrückhaltebeckensystemen,* 2006, ISBN 3-933761-50-6

148 Wolf, Jens: *Räumlich differenzierte Modellierung der Grundwasserströmung alluvialer Aquifere für mesoskalige Einzugsgebiete*, 2006, ISBN: 3-933761-51-4

149 Kohler, Beate: *Externe Effekte der Laufwasserkraftnutzung*, 2006, ISBN 3-933761-52-2

150 Hrsg.: Braun, Jürgen; Koschitzky, Hans-Peter; Stuhrmann, Matthias: *VEGAS-Statuskolloquium 2006,* Tagungsband zur Veranstaltung am 28. September 2006 an der Universität Stuttgart, Campus Stuttgart-Vaihingen, 2006, ISBN 3-933761-53-0

151 Niessner, Jennifer: *Multi-Scale Modeling of Multi-Phase - Multi-Component Processes in Heterogeneous Porous Media*, 2006, ISBN 3-933761-54-9

152 Fischer, Markus: *Beanspruchung eingeerdeter Rohrleitungen infolge Austrocknung bindiger Böden,* 2006, ISBN 3-933761-55-7

153 Schneck, Alexander: *Optimierung der Grundwasserbewirtschaftung unter Berücksichtigung der Belange der Wasserversorgung, der Landwirtschaft und des Naturschutzes*, 2006, ISBN 3-933761-56-5

154 Das, Tapash: *The Impact of Spatial Variability of Precipitation on the Predictive Uncertainty of Hydrological Models,* 2006, ISBN 3-33761-57-3

155 Bielinski, Andreas: *Numerical Simulation of CO_2 sequestration in geological formations*, 2007, ISBN 3-933761-58-1

156 Mödinger, Jens: *Entwicklung eines Bewertungs- und Entscheidungsunterstützungssystems für eine nachhaltige regionale Grundwasserbewirtschaftung*, 2006, ISBN 3-933761-60-3

157 Manthey, Sabine: *Two-phase flow processes with dynamic effects in porous media - parameter estimation and simulation,* 2007, ISBN 3-933761-61-1

158 Pozos Estrada, Oscar: *Investigation on the Effects of Entrained Air in Pipelines,* 2007, ISBN 3-933761-62-X

159 Ochs, Steffen Oliver: *Steam injection into saturated porous media – process analysis including experimental and numerical investigations*, 2007, ISBN 3-933761-63-8

160 Marx, Andreas: *Einsatz gekoppelter Modelle und Wetterradar zur Abschätzung von Niederschlagsintensitäten und zur Abflussvorhersage, 2007,* ISBN 3-933761-64-6

161 Hartmann, Gabriele Maria: *Investigation of Evapotranspiration Concepts in Hydrological Modelling for Climate Change Impact Assessment*, 2007, ISBN 3-933761-65-4

162 Kebede Gurmessa, Tesfaye: *Numerical Investigation on Flow and Transport Characteristics to Improve Long-Term Simulation of Reservoir Sedimentation*, 2007, ISBN 3-933761-66-2

163 Trifković, Aleksandar: *Multi-objective and Risk-based Modelling Methodology for Planning, Design and Operation of Water Supply Systems*, 2007, ISBN 3-933761-67-0

164 Götzinger, Jens: *Distributed Conceptual Hydrological Modelling - Simulation of Climate, Land Use Change Impact and Uncertainty Analysis*, 2007, ISBN 3-933761-68-9

165 Hrsg.: Braun, Jürgen; Koschitzky, Hans-Peter; Stuhrmann, Matthias: *VEGAS – Kolloquium 2007,* Tagungsband zur Veranstaltung am 26. September 2007 an der Universität Stuttgart, Campus Stuttgart-Vaihingen, 2007, ISBN 3-933761-69-7

166 Freeman, Beau: *Modernization Criteria Assessment for Water Resources Planning; Klamath Irrigation Project, U.S.*, 2008, ISBN 3-933761-70-0

167 Dreher, Thomas: *Selektive Sedimentation von Feinstschwebstoffen in Wechselwirkung mit wandnahen turbulenten Strömungsbedingungen*, 2008, ISBN 3-933761-71-9

168 Yang, Wei: *Discrete-Continuous Downscaling Model for Generating Daily Precipitation Time Series*, 2008, ISBN 3-933761-72-7

169 Kopecki, Ianina: *Calculational Approach to FST-Hemispheres for Multiparametrical Benthos Habitat Modelling,* 2008*,* ISBN 3-933761-73-5

170 Brommundt, Jürgen: *Stochastische Generierung räumlich zusammenhängender Niederschlagszeitreihen*, 2008, ISBN 3-933761-74-3

171 Papafotiou, *Alexandros: Numerical Investigations of the Role of Hysteresis in Heterogeneous Two-Phase Flow Systems*, 2008, ISBN 3-933761-75-1

172 He, Yi: *Application of a Non-Parametric Classification Scheme to Catchment Hydrology*, 2008, ISBN 978-3-933761-76-7

173 Wagner, Sven: *Water Balance in a Poorly Gauged Basin in West Africa Using Atmospheric Modelling and Remote Sensing Information*, 2008, ISBN 978-3-933761-77-4

174 Hrsg.: Braun, Jürgen; Koschitzky, Hans-Peter; Stuhrmann, Matthias; Schrenk, Volker: *VEGAS-Kolloquium 2008 Ressource Fläche III*, Tagungsband zur Veranstaltung am 01. Oktober 2008 an der Universität Stuttgart, Campus Stuttgart-Vaihingen, 2008, ISBN 978-3-933761-78-1

175 Patil, Sachin: *Regionalization of an Event Based Nash Cascade Model for Flood Predictions in Ungauged Basins*, 2008, ISBN 978-3-933761-79-8

176 Assteerawatt, Anongnart: *Flow and Transport Modelling of Fractured Aquifers based on a Geostatistical Approach,* 2008, ISBN 978-3-933761-80-4

177 Karnahl, Joachim Alexander: *2D numerische Modellierung von multifraktionalem Schwebstoff- und Schadstofftransport in Flüssen*, 2008, ISBN 978-3-933761-81-1

178 Hiester, Uwe: *Technologieentwicklung zur In-situ-Sanierung der ungesättigten Bodenzone mit festen Wärmequellen,* 2009, ISBN 978-3-933761-82-8

179 Laux, Patrick: *Statistical Modeling of Precipitation for Agricultural Planning in the Volta Basin of West Africa,* 2009, ISBN 978-3-933761-83-5

180 Ehsan, Saqib: *Evaluation of Life Safety Risks Related to Severe Flooding,* 2009, ISBN 978-3-933761-84-2

181 Prohaska, Sandra: *Development and Application of a 1D Multi-Strip Fine Sediment Transport Model for Regulated Rivers,* 2009, ISBN 978-3-933761-85-9

182 Kopp, Andreas: *Evaluation of CO_2 Injection Processes in Geological Formations for Site Screening,* 2009, ISBN 978-3-933761-86-6

183 Ebigbo, Anozie: *Modelling of biofilm growth and its influence on CO_2 and water (two-phase) flow in porous media,* 2009, ISBN 978-3-933761-87-3

184 Freiboth, Sandra: *A phenomenological model for the numerical simulation of multiphase multicomponent processes considering structural alterations of porous media*, 2009, ISBN 978-3-933761-88-0

185 Zöllner, Frank: *Implementierung und Anwendung netzfreier Methoden im Konstruktiven Wasserbau und in der Hydromechanik*, 2009, ISBN 978-3-933761-89-7

186 Vasin, Milos: *Influence of the soil structure and property contrast on flow and transport in the unsaturated zone*, 2010, ISBN 978-3-933761-90-3

187 Li, Jing: *Application of Copulas as a New Geostatistical Tool*, 2010, ISBN 978-3-933761-91-0

188 AghaKouchak, Amir: *Simulation of Remotely Sensed Rainfall Fields Using Copulas*, 2010, ISBN 978-3-933761-92-7

189 Thapa, Pawan Kumar: *Physically-based spatially distributed rainfall runoff modelling for soil erosion estimation*, 2010, ISBN 978-3-933761-93-4

190 Wurms, Sven: *Numerische Modellierung der Sedimentationsprozesse in Retentionsanla-*

gen zur Steuerung von Stoffströmen bei extremen Hochwasserabflussereignissen, 2011, ISBN 978-3-933761-94-1

191 Merkel, Uwe: *Unsicherheitsanalyse hydraulischer Einwirkungen auf Hochwasserschutzdeiche und Steigerung der Leistungsfähigkeit durch adaptive Strömungsmodellierung*, 2011, ISBN 978-3-933761-95-8

192 Fritz, Jochen: *A Decoupled Model for Compositional Non-Isothermal Multiphase Flow in Porous Media and Multiphysics Approaches for Two-Phase Flow*, 2010, ISBN 978-3-933761-96-5

193 Weber, Karolin (Hrsg.): *12. Treffen junger WissenschaftlerInnen an Wasserbauinstituten*, 2010, ISBN 978-3-933761-97-2

194 Bliefernicht, Jan-Geert: *Probability Forecasts of Daily Areal Precipitation for Small River Basins,* 2011, ISBN 978-3-933761-98-9

195 Hrsg.: Koschitzky, Hans-Peter; Braun, Jürgen: *VEGAS-Kolloquium 2010 In-situ-Sanierung - Stand und Entwicklung Nano und ISCO -,* Tagungsband zur Veranstaltung am 07. Oktober 2010 an der Universität Stuttgart, Campus Stuttgart-Vaihingen*,* 2010*,* ISBN 978-3-933761-99-6

196 Gafurov, Abror: *Water Balance Modeling Using Remote Sensing Information - Focus on Central Asia,* 2010, ISBN 978-3-942036-00-9

197 Mackenberg, Sylvia: *Die Quellstärke in der Sickerwasserprognose: Möglichkeiten und Grenzen von Labor- und Freilanduntersuchungen,* 2010, ISBN 978-3-942036-01-6

198 Singh, Shailesh Kumar: *Robust Parameter Estimation in Gauged and Ungauged Basins,* 2010, ISBN 978-3-942036-02-3

199 Doğan, Mehmet Onur: *Coupling of porous media flow with pipe flow,* 2011, ISBN 978-3-942036-03-0

200 Liu, Min: *Study of Topographic Effects on Hydrological Patterns and the Implication on Hydrological Modeling and Data Interpolation,* 2011, ISBN 978-3-942036-04-7

201 Geleta, Habtamu Itefa: *Watershed Sediment Yield Modeling for Data Scarce Areas,* 2011, ISBN 978-3-942036-05-4

202 Franke, Jörg: *Einfluss der Überwachung auf die Versagenswahrscheinlichkeit von Staustufen,* 2011, ISBN 978-3-942036-06-1

203 Bakimchandra, Oinam: *Integrated Fuzzy-GIS approach for assessing regional soil erosion risks,* 2011, ISBN 978-3-942036-07-8

204 Alam, Muhammad Mahboob: *Statistical Downscaling of Extremes of Precipitation in Mesoscale Catchments from Different RCMs and Their Effects on Local Hydrology,* 2011, ISBN 978-3-942036-08-5

205 Hrsg.: Koschitzky, Hans-Peter; Braun, Jürgen: *VEGAS-Kolloquium 2011 Flache Geothermie - Perspektiven und Risiken,* Tagungsband zur Veranstaltung am 06. Oktober 2011 an der Universität Stuttgart, Campus Stuttgart-Vaihingen*,* 2011*,* ISBN 978-3-933761-09-2

206 Haslauer, Claus: *Analysis of Real-World Spatial Dependence of Subsurface Hydraulic Properties Using Copulas with a Focus on Solute Transport Behaviour,* 2011, ISBN 978-3-942036-10-8

207 Dung, Nguyen Viet: *Multi-objective automatic calibration of hydrodynamic models – development of the concept and an application in the Mekong Delta,* 2011, ISBN 978-3-942036-11-5

208 Hung, Nguyen Nghia: *Sediment dynamics in the floodplain of the Mekong Delta, Vietnam,* 2011, ISBN 978-3-942036-12-2

209 Kuhlmann, Anna: *Influence of soil structure and root water uptake on flow in the unsaturated zone,* 2012, ISBN 978-3-942036-13-9

210 Tuhtan, Jeffrey Andrew: *Including the Second Law Inequality in Aquatic Ecodynamics: A Modeling Approach for Alpine Rivers Impacted by Hydropeaking,* 2012, ISBN 978-3-942036-14-6

211 Tolossa, Habtamu: *Sediment Transport Computation Using a Data-Driven Adaptive Neu-*

ro-Fuzzy Modelling Approach, 2012, ISBN 978-3-942036-15-3

212 Tatomir, Alexandru-Bodgan: *From Discrete to Continuum Concepts of Flow in Fractured Porous Media,* 2012, ISBN 978-3-942036-16-0

213 Erbertseder, Karin: *A Multi-Scale Model for Describing Cancer-Therapeutic Transport in the Human Lung,* 2012, ISBN 978-3-942036-17-7

214 Noack, Markus: *Modelling Approach for Interstitial Sediment Dynamics and Reproduction of Gravel Spawning Fish,* 2012, ISBN 978-3-942036-18-4

215 De Boer, Cjestmir Volkert: *Transport of Nano Sized Zero Valent Iron Colloids during Injection into the Subsurface*, 2012, ISBN 978-3-942036-19-1

216 Pfaff, Thomas: *Processing and Analysis of Weather Radar Data for Use in Hydrology*, 2013, ISBN 978-3-942036-20-7

217 Lebrenz, Hans-Henning: *Addressing the Input Uncertainty for Hydrological Modeling by a New Geostatistical Method*, 2013, ISBN 978-3-942036-21-4

218 Darcis, Melanie Yvonne: *Coupling Models of Different Complexity for the Simulation of CO_2 Storage in Deep Saline Aquifers*, 2013, ISBN 978-3-942036-22-1

219 Beck, Ferdinand: *Generation of Spatially Correlated Synthetic Rainfall Time Series in High Temporal Resolution - A Data Driven Approach*, 2013, ISBN 978-3-942036-23-8

220 Guthke, Philipp: *Non-multi-Gaussian spatial structures: Process-driven natural genesis, manifestation, modeling approaches, and influences on dependent processes*, 2013, ISBN 978-3-942036-24-5

221 Walter, Lena: *Uncertainty studies and risk assessment for CO_2 storage in geological formations*, 2013, ISBN 978-3-942036-25-2

222 Wolff, Markus: *Multi-scale modeling of two-phase flow in porous media including capillary pressure effects,* 2013, ISBN 978-3-942036-26-9

223 Mosthaf, Klaus Roland: *Modeling and analysis of coupled porous-medium and free flow with application to evaporation processes,* 2014, ISBN 978-3-942036-27-6

224 Leube, Philipp Christoph: *Methods for Physically-Based Model Reduction in Time: Analysis, Comparison of Methods and Application*, 2013, ISBN 978-3-942036-28-3

225 Rodríguez Fernández, Jhan Ignacio: *High Order Interactions among environmental variables: Diagnostics and initial steps towards modeling*, 2013, ISBN 978-3-942036-29-0

226 Eder, Maria Magdalena: *Climate Sensitivity of a Large Lake*, 2013, ISBN 978-3-942036-30-6

227 Greiner, Philipp: *Alkoholinjektion zur In-situ-Sanierung von CKW Schadensherden in Grundwasserleitern: Charakterisierung der relevanten Prozesse auf unterschiedlichen Skalen*, 2014, ISBN 978-3-942036-31-3

228 Lauser, Andreas: *Theory and Numerical Applications of Compositional Multi-Phase Flow in Porous Media*, 2014, ISBN 978-3-942036-32-0

229 Enzenhöfer, Rainer: *Risk Quantification and Management in Water Production and Supply Systems*, 2014, ISBN 978-3-942036-33-7

230 Faigle, Benjamin: *Adaptive modelling of compositional multi-phase flow with capillary pressure*, 2014, ISBN 978-3-942036-34-4

231 Oladyshkin, Sergey: *Efficient modeling of environmental systems in the face of complexity and uncertainty*, 2014, ISBN 978-3-942036-35-1

232 Sugimoto, Takayuki: *Copula based Stochastic Analysis of Discharge Time Series*, 2014, ISBN 978-3-942036-36-8

233 Koch, Jonas: *Simulation, Identification and Characterization of Contaminant Source Architectures in the Subsurface*, 2014, ISBN 978-3-942036-37-5

234 Zhang, Jin: *Investigations on Urban River Regulation and Ecological Rehabilitation Measures, Case of Shenzhen in China*, 2014, ISBN 978-3-942036-38-2

235 Siebel, Rüdiger: *Experimentelle Untersuchungen zur hydrodynamischen Belastung und Standsicherheit von Deckwerken an überströmbaren Erddämmen,* 2014, ISBN 978-3-942036-39-9

236 Baber, Katherina: *Coupling free flow and flow in porous media in biological and technical applications: From a simple to a complex interface description,* 2014, ISBN 978-3-942036-40-5

237 Nuske, Klaus Philipp: *Beyond Local Equilibrium — Relaxing local equilibrium assumptions in multiphase flow in porous media,* 2014, ISBN 978-3-942036-41-2

238 Geiges, Andreas: *Efficient concepts for optimal experimental design in nonlinear environmental systems*, 2014, ISBN 978-3-942036-42-9

239 Schwenck, Nicolas: *An XFEM-Based Model for Fluid Flow in Fractured Porous Media*, 2014, ISBN 978-3-942036-43-6

240 Chamorro Chávez, Alejandro: *Stochastic and hydrological modelling for climate change prediction in the Lima region, Peru*, 2015, ISBN 978-3-942036-44-3

241 Yulizar: *Investigation of Changes in Hydro-Meteorological Time Series Using a Depth-Based Approach*, 2015, ISBN 978-3-942036-45-0

242 Kretschmer, Nicole: *Impacts of the existing water allocation scheme on the Limarí watershed – Chile, an integrative approach*, 2015, ISBN 978-3-942036-46-7

243 Kramer, Matthias: *Luftbedarf von Freistrahlturbinen im Gegendruckbetrieb*, 2015, ISBN 978-3-942036-47-4

244 Hommel, Johannes: *Modeling biogeochemical and mass transport processes in the subsurface: Investigation of microbially induced calcite precipitation*, 2016, ISBN 978-3-942036-48-1

245 Germer, Kai: *Wasserinfiltration in die ungesättigte Zone eines makroporösen Hanges und deren Einfluss auf die Hangstabilität*, 2016, ISBN 978-3-942036-49-8

246 Hörning, Sebastian: *Process-oriented modeling of spatial random fields using copulas*, 2016, ISBN 978-3-942036-50-4

247 Jambhekar, Vishal: *Numerical modeling and analysis of evaporative salinization in a coupled free-flow porous-media system,* 2016, ISBN 978-3-942036-51-1

248 Huang, Yingchun: *Study on the spatial and temporal transferability of conceptual hydrological models*, 2016, ISBN 978-3-942036-52-8

249 Kleinknecht, Simon Matthias: *Migration and retention of a heavy NAPL vapor and remediation of the unsaturated zone*, 2016, ISBN 978-3-942036-53-5

250 Kwakye, Stephen Oppong: *Study on the effects of climate change on the hydrology of the West African sub-region*, 2016, ISBN 978-3-942036-54-2

251 Kissinger, Alexander: *Basin-Scale Site Screening and Investigation of Possible Impacts of CO_2 Storage on Subsurface Hydrosystems*, 2016, ISBN 978-3-942036-55-9

252 Müller, Thomas: *Generation of a Realistic Temporal Structure of Synthetic Precipitation Time Series for Sewer Applications*, 2017, ISBN 978-3-942036-56-6

253 Grüninger, Christoph: *Numerical Coupling of Navier-Stokes and Darcy Flow for Soil-Water Evaporation*, 2017, ISBN 978-3-942036-57-3

254 Suroso: *Asymmetric Dependence Based Spatial Copula Models: Empirical Investigations and Consequences on Precipitation Fields*, 2017, ISBN 978-3-942036-58-0

255 Müller, Thomas; Mosthaf, Tobias; Gunzenhauser, Sarah; Seidel, Jochen; Bárdossy, András: *Grundlagenbericht Niederschlags-Simulator (NiedSim3)*, 2017, ISBN 978-3-942036-59-7

256 Mosthaf, Tobias: *New Concepts for Regionalizing Temporal Distributions of Precipitation and for its Application in Spatial Rainfall Simulation,* 2017, ISBN 978-3-942036-60-3

257 Fenrich, Eva Katrin: *Entwicklung eines ökologisch-ökonomischen Vernetzungsmodells für Wasserkraftanlagen und Mehrzweckspeicher,* 2018, ISBN 978-3-942036-61-0

258 Schmidt, Holger: *Microbial stabilization of lotic fine sediments*, 2018, ISBN 978-3-942036-62-7

259 Fetzer, Thomas: *Coupled Free and Porous-Medium Flow Processes Affected by Turbulence and Roughness – Models, Concepts and Analysis*, 2018, ISBN 978-3-942036-63-4

260 Schröder, Hans Christoph: *Large-scale High Head Pico Hydropower Potential Assessment*, 2018, ISBN 978-3-942036-64-1

261 Bode, Felix: *Early-Warning Monitoring Systems for Improved Drinking Water Resource Protection*, 2018, ISBN 978-3-942036-65-8

262 Gebler, Tobias: *Statistische Auswertung von simulierten Talsperrenüberwachungsdaten zur Identifikation von Schadensprozessen an Gewichtsstaumauern*, 2018, ISBN 978-3-942036-66-5

263 Harten, Matthias von: *Analyse des Zuppinger-Wasserrades – Hydraulische Optimierungen unter Berücksichtigung ökologischer Aspekte*, 2018, ISBN 978-3-942036-67-2

264 Yan, Jieru: *Nonlinear estimation of short time precipitation using weather radar and surface observations*, 2018, ISBN 978-3-942036-68-9

265 Beck, Martin: *Conceptual approaches for the analysis of coupled hydraulic and geomechanical processes*, 2019, ISBN 978-3-942036-69-6

266 Haas, Jannik: *Optimal planning of hydropower and energy storage technologies for fully renewable power systems*, 2019, ISBN 978-3-942036-70-2

267 Schneider, Martin: *Nonlinear Finite Volume Schemes for Complex Flow Processes and Challenging Grids*, 2019, ISBN 978-3-942036-71-9

268 Most, Sebastian Christopher: *Analysis and Simulation of Anomalous Transport in Porous Media*, 2019, ISBN 978-3-942036-72-6

269 Buchta, Rocco: *Entwicklung eines Ziel- und Bewertungssystems zur Schaffung nachhaltiger naturnaher Strukturen in großen sandgeprägten Flüssen des norddeutschen Tieflandes*, 2019, ISBN 978-3-942036-73-3

270 Thom, Moritz: *Towards a Better Understanding of the Biostabilization Mechanisms of Sediment Beds*, 2019, ISBN 978-3-942036-74-0

271 Stolz, Daniel: *Die Nullspannungstemperatur in Gewichtsstaumauern unter Berücksichtigung der Festigkeitsentwicklung des Betons*, 2019, ISBN 978-3-942036-75-7

272 Rodriguez Pretelin, Abelardo: *Integrating transient flow conditions into groundwater well protection*, 2020, ISBN: 978-3-942036-76-4

273 Weishaupt, Kilian: *Model Concepts for Coupling Free Flow with Porous Medium Flow at the Pore-Network Scale: From Single-Phase Flow to Compositional Non-Isothermal Two-Phase Flow*, 2020, ISBN: 978-3-942036-77-1

274 Koch, Timo: *Mixed-dimension models for flow and transport processes in porous media with embedded tubular network systems*, 2020, ISBN: 978-3-942036-78-8

275 Gläser, Dennis: *Discrete fracture modeling of multi-phase flow and deformation in fractured poroelastic media*, 2020, ISBN: 978-3-942036-79-5

276 Seitz, Lydia: Development of new methods to apply a multi-parameter approach – A first step towards the determination of colmation, 2020, ISBN: 978-3-942036-80-1

Die Mitteilungshefte ab der Nr. 134 (Jg. 2005) stehen als pdf-Datei über die Homepage des Instituts: www.iws.uni-stuttgart.de zur Verfügung.